GeoForschungsZentrum Potsdam GFZ
Fernerkundung

Qualitative and Quantitative Analyses of Lake Baikal's Surface-Waters Using Ocean Colour Satellite Data (SeaWiFS)

Dissertation
zur Erlangung des akademischen Grades
"doctor rerum naturalium"
(Dr. rer. nat.)
in der Wissenschaftsdisziplin „Geowissenschaftliche Fernerkundung"

eingereicht an der
Mathematisch-Naturwissenschaftlichen Fakultät
der Universität Potsdam

von
Birgit Heim

Potsdam, den 27.06.2005

ABSTRACT

One of the most difficult issues when dealing with optical water remote-sensing is its acceptance as a useful application for environmental research. This problem is, on the one hand, concerned with the optical complexity and variability of the investigated natural media, and therefore the question arises as to the plausibility of the parameters derived from remote-sensing techniques. Detailed knowledge about the regional bio- and chemico-optical properties is required for such studies, however such information is seldom available for the sites of interest. On the other hand, the primary advantage of remote-sensing information, which is the provision of a spatial overview, may not be exploited fully by the disciplines that would benefit most from such information. It is often seen in a variety of disciplines that scientists have been primarily trained to look at discrete data-sets, and therefore have no experience of incorporating information dealing with spatial heterogeneity.

In this thesis, the opportunity was made available to assess the potential of Ocean Colour data to provide spatial and seasonal information about the surface waters of Lake Baikal (Siberia). While discrete limnological field data is available, the spatial extension of Lake Baikal is enormous (ca. 600 km), while the field data is limited to selected sites and expedition time windows. Therefore, this remote-sensing investigation aimed to support a multi-disciplinary limnological investigation within the framework of the paleoclimate EU-project 'High Resolution CONTINENTal Paleoclimate Record in Lake Baikal, Siberia (CONTINENT)' using spatial and seasonal information from the SeaWiFS satellite (NASA). From this, the SeaWiFS study evolved to become the first efficient bio-optical satellite study of Lake Baikal.

During the course of three years, field work including spectral field measurements and water sampling, was carried out at Lake Baikal in Southern Siberia, and at the Mecklenburg and Brandenburg lake districts in Germany. The first step in processing the SeaWiFS satellite data involved adapting the SeaDAS (NASA) atmospheric-correction processing to match as close as possible the specific conditions of Lake Baikal. Next, various Chl-*a* algorithms were tested on the atmospherically-corrected optimized SeaWiFS data-set (years 2001 to 2002), comparing the CONTINENT pigment ground-truth data with the Chl-*a* concentrations derived from the satellite data. This showed the high performance of the global Chl-*a* products OC2 and OC4 for the oligotrophic, transparent waters (bio-optical Case 1) of Lake Baikal. However, considerable Chl-*a* overestimation prevailed in bio-optical Case 2 areas for the case of discharge events. High-organic terrigenous input into Lake Baikal could be traced and information extracted using the SeaWiFS spectral data. Suspended Particulate Matter (SPM) was quantified by the regression of the SeaDAS attenuation coefficient as the optical parameter with SPM field data.

Finally, the Chl-*a* and terrigenous input maps derived from the remote sensing data were used to assist with analyzing the relationships between the various discrete data obtained during the CONTINENT field work. Hence, plausible spatial and seasonal information describing autochthonous and allochthonous material in Lake Baikal could be provided by satellite data.

Lake Baikal, with its bio-optical complexity and its different areas of Case 1 and Case 2 waters, is a very interesting case study for Ocean Colour analyses. Proposals for future Ocean Colour studies of Lake Baikal are discussed, including which bio-optical parameters for analytical models still need to be clarified by field investigations.

LIST OF TABLES

LIST OF FIGURES

LIST OF FREQUENTLY USED SYMBOLS

A Albedo

a absorption coefficient [m^{-1}]

bb backscattering coefficient [m^{-1}]

c beam attenuation coefficient [m^{-1}]

Chl-*a* chlorophyll a concentration [$\mu g\ l^{-1}$]

δ isotopic delta value

$\varepsilon^{(i,j)}$ theoretical single-scattering aerosol reflectance ratio, bands *i:j*

$\varepsilon^{(7,8)}$ imposed multiple-scattering aerosol reflectance ratio, bands *7:8,*

E(λ) spectral irradiance [$W\ m^{-2}\ nm^{-1}$]. Frequently used variants are:

- $E_{up}(\lambda)$ upwelling irradiance
- $E_{down}(\lambda)$ downwelling irradiance
- $E_{sol}(\lambda)$ exo-atmospheric solar irradiance

K490 diffuse attenuation coefficient at 490 nm in m^{-1}

L(λ) spectral radiance [$W\ m^{-2}\ nm^{-1}\ sr^{-1}$]. Frequently used variants are:

- $L_{up}(\lambda)$ upwelling radiance
- $L_{down}(\lambda)$ downwelling radiance
- $L_{sky}(\lambda)$ sky radiance
- $L_{glint}(\lambda)$ sun glint radiance

n number

OD optical density (= Absorbance)

r_{aw} directly reflected at the air-water interface (≈ Fresnel reflectance)

r_{wa} directly (internally) reflected at the water-air interface

r^2 R-square/coefficient of determination

R(λ) spectral reflectance. Frequently used variants are:

- $R_{TOA}(\lambda)$ top-of-atmosphere reflectance
- $R_{RS}(\lambda)$ remote sensing reflectance [sr^{-1}]
- $R_{vol}(\lambda)$ water volume reflectance
- R(λ) surface reflectance

S exponential slope value

Q angular distribution factor [sr]

LIST OF FREQUENTLY USED ACRONYMS

ASD	Analytical Spectral Device
ATSR	Along Track Scanning Radiometer
AVHRR	Advanced Very High Resolution Radiometer
cDOM	coloured Dissolved Organic /Matter
CNES	Centre Nationale d'Etudes spatiales (France)
CZSC	Coastal Zone Scanner
CONTINENT	High Resolution CONTINENTal Paleoclimate Record in Lake Baikal
DEM	Digital Elevation Model
DLR	Deutsches Zentrum für Luft- und Raumfahrt
DOC	Dissolved Organic Carbon
ENVI	Environment for Visualizing Images, software
ERDAS	Earth Resources Data Analysis System Imagine, software
ESA	European Space Agency
GER	Geophysical and Environmental Research field spectrometer
HPLC	High Performance Liquid Chromatography
HRPT	High Resolution Picture Transmission
IFOV	Instantaneous Field of View
L 1A	Level 1A satellite data, unprocessed satellite data
L 1B	Level 1B satellite data, calibrated radiances
MERIS	Medium Resolution Imaging Spectrometer
MODIS	MODderate resolution Imaging Spectrometer
NASA	National Aeronautics and Space Administration (U.S.A)
NASDA	National Space Development Agency (Japan)
NIR	near-infrared
RGB	Red Green Blue composite
SAR	Synthetic Apertur Radar
SeaDAS	SeaWiFS Data Analysis System
SeaWiFS	Sea-viewing Wide Field-of-view Sensor
SISCAL	Satellite-based Information System on Coastal Areas and Lakes Server
SPM	Suspended Particulate Matter
TM/ETM+	Thematic Mapper/Enhanced Thematic Mapper
USGS	United States Geological Survey
UTM	Universal Transversal Mercator
WGS84	World Geodetic System (1984)
WFD 2000	Water framework Directive (2000)

1 INTRODUCTION

Elevatis nihil celatur „aus der Höhe verheimlicht sich nichts“ *Corpus Caesarianum, 47 v. Chr.*

1.1 APPLICATIONS IN REMOTE-SENSING

Satellite and airborne scanner data enables the mapping of bio- and geochemical, and physical parameters of the atmosphere, land surface and surface waters. Imaging remote-sensing data provides information about ecological parameters within their spatial context. It is especially important that for highly dynamic and heterogeneous marine and limnic hydrographic environments, seasonal and spatial information is obtained. Optical remote-sensing methods have been established to monitor the phytoplankton in the world oceans for biological, hydrophysical and biochemical studies. Ocean Colour data is therefore able to provide phytoplankton estimates to assess the marine bio-geochemical carbon cycle, and yields instantaneous information on phytoplankton patches during research cruises. In addition, remote-sensing methods are in development to monitor the phytoplankton productivity of coastal and inland water bodies to investigate their trophic and economical state. Higher-level remote-sensing products are planned to support the environmental surveillance of river outlets and coastal dynamics.

This study shows the potential of optical satellite data to deliver representative information about limnological parameters for the European project ‘High Resolution CONTINENTal Paleoclimate Record in Lake Baikal, Siberia (CONTINENT)’ (2001 - 2004).

The subject of study, the unique Lake Baikal, is a complex oligotrophic fresh-water system, spanning from 51°29’ - 55°46’ N to 103°43’ - 109°56’ E, a length of four geographic latitudes. The SeaWiFS Ocean Colour sensor enabled the monitoring of two summer periods (2001, 2002) and one spring season (2002) of Lake Baikal. Multidisciplinary CONTINENT cruises provided the essential ground-truth on limnological parameters. Therefore, the aim of this study is to explore relevant synoptical information on the autochthonous (remote-sensing parameter: chlorophyll a (Chl-*a*) and allochthonous material (remote-sensing parameter: terrigenous Suspended Particulate Matter (SPM)) in Lake Baikal.

1.2 STATE OF WATER-REMOTE SENSING STUDIES

The SeaWiFS study presented here evolved to become the first thoroughly bio-optical study of Lake Baikal using satellite data in the optical visible wavelength range.

There are a large number of water remote-sensing studies of Lake Baikal undertaken by Russian scientists, using the physical information of water surface temperature from the High Resolution Radiometer (AVHRR) and from the Along Track Scanning Radiometer (ATSR) [*Gitel'zon et al.,* 1991; *Bolgrien at al.*, 1992, *Evans et al.,* 1992; *Bolgrien at al.*, 1995; *Semowski et al.*, 1998; *Semowski et al.*, 2001]. These studies investigated physical surface hydraulics and recognized, for example, the thermal spring bar along the eastern coast of Lake Baikal (*Llewellyn*, unpublished data from Leicester University, in *Imberger*, [1998]). Furthermore, radar data-sets (ERS-1) have been used to study surface water circulation in Lake Baikal [*Semowski et al.,* 1999a]. Optical remote-sensing studies at Lake Baikal have so far concentrated on lake ice cover and ice types using AVHRR data [*Mogilev et al.*, 1999; *Semowski et al.*, 2000] and ATSR satellite data [Lawrence et al., 2000].

Semowski [1999b] was the first to conduct a preliminary bio-optical remote-sensing analysis using AVHRR satellite data over the visible wavelength range. His study was limited by the low spectral and radiometric potential of the broad AVHRR bands and the high transparency of Lake Baikal. Owing to these technical limitations, and to a land-surface adapted atmospheric-correction approach [pers., Mogilev, Irkutsk State University, Russia], the study did not result in an applicable remote-sensing Chl-*a* algorithm.

These remote-sensing studies have been oriented towards understanding the horizontal hydraulics of Lake Baikal, rather then investigating the biological processes. One reason is that the method for Ocean Colour analyses of transparent fresh-water bodies is still under development. Bio-optical water remote-sensing investigations have its origin within atmospheric-oceanographic investigations. The first Ocean Colour sensor, the CZSC (Coastal Zone Scanner), was launched in 1978. The sensor had a high spectral and radiometric resolution in the blue to green wavelength ranges, with a spatial resolution of 1 km^2. The CZCS mission provided invaluable information (between 1978 to 1986) about a large variety of biological processes and ocean-circulation patterns [*Gregg and Conkright*, 2001; *Harris et al.*, 1993; *Yentsch,* 1993; *Yoder et al.,* 1993].

The scientific success of the CZCS mission induced a new series of improved Ocean Colour sensors. The new generation of Ocean Colour missions started in 1996 with the German MOS mission (German Space Agency (DLR)) [*Zimmermann and Neumann*, 1997], and the Japanese OCTS mission (NASDA) together with the French sensor POLDER (CNES), both on board the ADEOS spacecraft. Regrettably, the ADEOS mission operated only until June 1997. MOS was designed as a technology demonstrator and operated with a small swath width over a limited geographic coverage. Nevertheless, automatic processing of MOS data provided the demonstrator 'Chl-*a* map of the Baltic Sea' (produced in 1998 at the DLR data center). In 1997, NASA launched the successful SeaWiFS mission. MODIS (NASA) on board Terra (1998) and the second MODIS instrument on board Aqua (2002) followed the SeaWiFS mission. In 2002, ESA launched the powerful Ocean Colour Instrument MERIS (Medium Resolution Imaging Spectrometer). The value of the data of the highly performing Ocean Colour sensors providing global daily Ocean Colour information is described in [e.g., *Barnes et al.*, 1998; *Doerffer et al.*, 1999; *Rast and Bezy,* 1999].

To obtain information on phytoplankton, algorithms for its main pigment Chl-*a* were developed for marine oligotrophic pelagic waters [*Morel and Gordon*, 1980; *Gordon and Morel*, 1983; *Stumpf and Tyler*, 1988]. These 'Case 1 waters' [*Jerlov*, 1978] are specified such that the only optically relevant component is the phytoplankton. In 1997, the SeaWiFS Bio-optical Algorithm Mini-Workshop (SeaBAM) [*Firestone and Hooker*, 1998] assembled a global marine ground-truth data-

set of concomitant Chl-*a* and reflectance measurements. O'Reilly et al. [1998] established from this data-set the ocean chlorophyll-2-band (OC2) and ocean chlorophyll-4-band (OC4) algorithms.

The characteristics of coastal and inland waters do not match the bio-optical classification of 'Case 1' water type. These optically more complex waters are termed 'Case 2 waters' [*Jerlov*, 1978] where the visible water constituents, existing of: i) Chl-*a*, ii) Suspended Particulate Matter (SPM), and iii) coloured Dissolved Organic Matter (cDOM), stem from different sources and are not necessarily correlated. For remote-sensing investigations of Case 2 waters, experimental algorithms for the calculation of Chl-*a* and SPM concentrations may be based on the linear regression of spectral features according to global data-sets [*O'Reilley et al.*, 1998] or regional campaigns [*Tassan*, 1994; *Kahru and Mitchell*, 1999; *Froidefond et al.,* 1999; *Froidefond et al.,* 2002]. However, the visible water constituents optically interfere with each other, and their functional relationship with the water-leaving reflectances is no longer linear for the wide range of concentrations encountered. Also problematic are the regionally different settings in terms of phytoplankton composition, SPM composition, and the organic loading of the water bodies. To develop useful applications, the bio-optical parameters for coastal waters needed to be clarified. The on-site monitoring of these parameters was the scope of the EU-Project COASTlOOC [*Babin,* 2000], and the German MERIS Application and Regional Products (MAPP) Project [*http://auc.dfd.dlr.de/mapp/MAPP/*].

Advanced analytical techniques have been increasingly applied to separate the optically interfering and uncorrelated water constituents in Case 2 waters. Non-linear regression techniques such as neural networks were developed for multi-variable analyses. For land classification studies, neural networks are generally trained empirically on real data-sets [e.g., *Segel,* 1996; *Kamp et al.*, 1997]. In the case of marine and fresh-waters, this approach may be hampered by the limited and inhomogeneous distribution of real data-sets. Radiative transfer simulations offer the opportunity to provide synthetic training data with a dense and homogeneous distribution of the relevant parameters, requiring a reflectance model and specific bio-optical parameters. One of the first attempts at radiative transfer modelling used matrix-operator theory and succeeded in calculating the concentrations of SPM, Chl-a and cDOM from CZCS data [*Fischer and Doerffer*, 1987]. In Fell and Fischer [2001], the radiative transfer computer code 'Matrix Operator Model' (MOMO) simulates radiative transfer in a coupled atmosphere-ocean system. Heege and Fischer [2004] used basal partitions of MOMO to construct the Modular Inversion Program (MIP) that includes modules for the calculation of aerosol types and concentrations, for the correction of sun glitter radiances, and for the atmospheric correction of airborne sensor data. Based on MIP, Heege [2000], Heege and Fischer [2004] successfully produced Chl-*a* and SPM maps of Lake Constance (Germany) from airborne scanner data. Schroeder and Fischer [2002] extended the performance of the Inverse Modelling method for the abundance of absorbing aerosols, and for Case 2 waters [*Schroeder and Fischer*, 2003]. Schroeder [2003] defined the input and output conditions for MERIS Case 2 products by using MOMO for modelling the synthetic data-set within the framework of the Neural Algorithms for Ocean Colour (NAOC) project [*http://www.ipsl.jussieu.fr/ NAOC/*].

Ocean Colour investigations on freshwater bodies have, up until recently, been rarely carried out due to the limited spatial resolution of the majority of operating Ocean Colour sensors. However, MERIS full resolution (FR) data that has recently become available, offers a high spatial resolution (maximal 0.3 km^2 for sub-satellite pixels). There is also now a choice of routinely processed Chl-*a* and SPM MERIS standard products. For limnological applications, the DLR plans to install an automatic processing of regional case II water products for FR MERIS data for Lake Constance (Germany).

The optical information from SeaWiFS satellite data has been used within the interdisciplinary research project EEGLE (Episodic Events-Great Lakes Experiment Understanding the Historical

Magnitude of Spring Turbidity Plumes in Southern Lake Michigan) [*http://www.glerl.noaa.gov/eegle*], where Chen et al. [2004] qualitatively inferred the spatial distribution of the highly reflective recurrent coastal resuspension plume in the American Lake Michigan from the Ocean Colour data.

In this study, the interdisciplinary paleoclimate CONTINENT project [*http://continent.gfz-potsdam.de*] has provided a valuable opportunity to incorporate Ocean Colour information into freshwater-related limnological research being undertaken at Lake Baikal, in the centre of the Asian landmass.

1.3 THE CONTINENT PALEOCLIMATE PROJECT

The study of past climate variability supports the evaluation and prediction of future climate changes. Attempts to assess the impact of various climatic parameters require a highly resolved record of ecological proxy data that are, for example, absent in lacustrine sediments. Lake Baikal is in fact the deepest (1600 m) and oldest lake on Earth due to its formation within subsiding continental rift basins. Its lacustrine sediments are 8 to 10 km thick and date back to the Middle Eocene [*Hutchinson et al.*, 1992; *Scholz et al.,* 1993]. These sediments provide a highly informative paleoclimate archive: the lake's high-latitude location makes it sensitive to long-term changes in insolation patterns and to climatic short-term changes associated with shifts in the Siberian high- and Asiatic low-pressure monsoon systems [e.g., *Dodson and Lui*, 1995].

Bio-stratigraphical studies over Pleistocene and Holocene timescales have interpreted variations in paleoclimatic proxies of Baikal sediments as being indicative of climatic changes [*Colman et al.*, 1995; *Mackay et al.*, 1998]. The climatic reconstructions have been based on mainly biotic paleoclimatic proxies, such as diatoms [*Granina et al.*, 1992; *Grachev et al.*, 1998; *Mackay et al.*, 1998; *Karabanov et al.*, 2000; *Bangs et al.*, 2000], pollen and spores [*Demske et al.*, 2000], and δ^{13}C in organic carbon [*Prokopenko et al.*, 1999]. Abiotic parameters, in particular clay minerals, have also been used [*Williams et al.*, 1997; *Solotchina et al.*, 2002]. A recent important coring project in Lake Baikal has been the Baikal Drilling Project (BDP) from 1996 to 1998, where several scientific boreholes were drilled on the subaquatic '*Academician Ridge'* in Lake Baikal [e.g., *Members BDP*, 1997; *http://icdp.gfz-potsdam.de*]. Two of the cores penetrated over 190 m into the sediments, and recovered sediments more than 5 Ma old at the base of the cores [*Williams et al.*, 1997].

The European paleoclimate project CONTINENT [5th Framework, Global Change, Climate and Biodiversity, EVK2-2000-00057] is based on earlier collaborative paleoclimate and environmental projects that started in 1995 under the auspices of Baikal International Centre for Ecological Research (BICER) [*Flower et al.*, 1998]. From 2001 to 2004, the multi-disciplinary CONTINENT project team examined the biotic and abiotic environmental responses of the high-continental Baikal region to climatic changes during the late Quaternary period covering the Holocene and the Eemian interglacials, and the Weichsel and Saale glacials (i.e., approximately the last 180 ka). In order to interpret the biogenic and silico-clastic sediment records more comprehensively, present-day climatically sensitive proxies have been investigated by field cruises, and by sequential sediment trap data.

However, bio-limnological and geochemical field data is always restricted to discrete spatial information and to expedition time windows. In addition, the sequential sediment trap data, despite yielding seasonal data, is only from the bottom of the photic layer downwards, and is restricted in recording pelagic conditions. Therefore, despite the high-quality discrete CONTINENT data, large-scale and seasonal information is lacking.

1.4 AIMS OF THIS STUDY

The research questions formulated in this study using satellite data of the Sea viewing Wide Field of view Sensor (SeaWiFS) are the following:

Does SeaWiFS data of Lake Baikal show the distribution of allochthonous material (i.e., silico-clastic and dissolved organic fluvial input) in the upper-lake water layer, and can terrigenous SPM be quantified?

Does SeaWiFS data of Lake Baikal show the distribution of autochthonous material (i.e., phytoplankton) using the photosynthesis pigment Chl-*a* as a proxy, and can Chl-*a* be quantified?

Will it be possible to trace the seasonal behaviour of the autochthonous and allochthonous material?

Will the information provided by satellite data reflect the autochthonous and allochthonous influences on the three selected project sites of CONTINENT?

The results of this study are summarized in "Variation in Lake Baikal's phytoplankton distribution and fluvial input assessed by SeaWiFS satellite data" [*Heim et al.*, 2005], which is included under §5.4.

2 FUNDAMENTALS OF WATER REMOTE-SENSING

2.1 OPTICAL PROPERTIES OF NATURAL WATERS

The concentration and composition of phytoplankton, coloured Dissolved Organic Matter (cDOM), and the Suspended Particulate Matter (SPM) composition are the main factors that influence the optical properties of natural waters [*Prieur and Sathyendranath*, 1981], producing the apparent water colour [*Effler and Auer*, 1987]. A comprehensive study of the absorption and scattering properties of the main visible water constituents has been given in Gordon and Morel [1983]. They conclude that the water-leaving remote-sensing signal is mainly a function of:

- Absorption by phytoplankton pigments and detritus, where the photosynthesis pigment Chl-*a* is of major importance
- Backscattering by SPM
- Absorption by cDOM
- Fluorescence by cDOM and the phytoplankton pigment groups of billiproteins and chlorophylls (unlike absorption, fluorescence is directly linked to the physiological state of the photosynthetic system)
- Scattering by water molecules at short wavelengths and Raman scattering at intermediate wavelengths

Bacteria, viruses and colloids are assumed to contribute only to the backscatter coefficient [*Morel et al.*, 1993; *Stramski and Kiefer*, 1991]. Micro- to macro-zooplankton, even highly abundant in natural waters, is considered to have minor or no optical influences.

Bio-optical water types can be differentiated, for example clear waters with little dissolved and suspended substances, biologically productive waters, or waters with heavy sediment or organic-matter loading. Therefore, the optical properties of natural waters are assumed to be indicative of limnological and marine processes [*Thomson and Jerome*, 1975; *Smith and Baker*, 1978]. The main optical influences depending on phytoplankton composition, SPM, cDOM and pure water, and the bio-optical classification into Case 1 and Case 2 waters are here explained.

2.1.1 Optical Effect of Phytoplankton Pigments

Phytoplankton determines the bulk optical properties by the absorption behaviour of its pigments. There are three groups of pigments, the lipophilic groups of chlorophylls and carotenoids, and the hydrophilic group of biliproteins. Chlorophylls and carotenoids are always present in micro- and macro algae. The main photosynthetic pigment is Chl-*a*, the chlorophylls b, c and d are antenna pigments and coexist in species-specific variations. All chlorophylls absorb in the short blue-wavelength range, and Chl-*a* considerably in the red-wavelength range. The group of carotenoids is composed of a variety of pigments that serve as antenna pigments or protect the organism, and absorb in the blue-to-green wavelength range. The antenna pigment group of phycobilins is bound to phycobiliproteins and includes red pigments (e.g., phycoerythrin, phycoerythrocyanin) and blue pigments (e.g., phycocyanin).

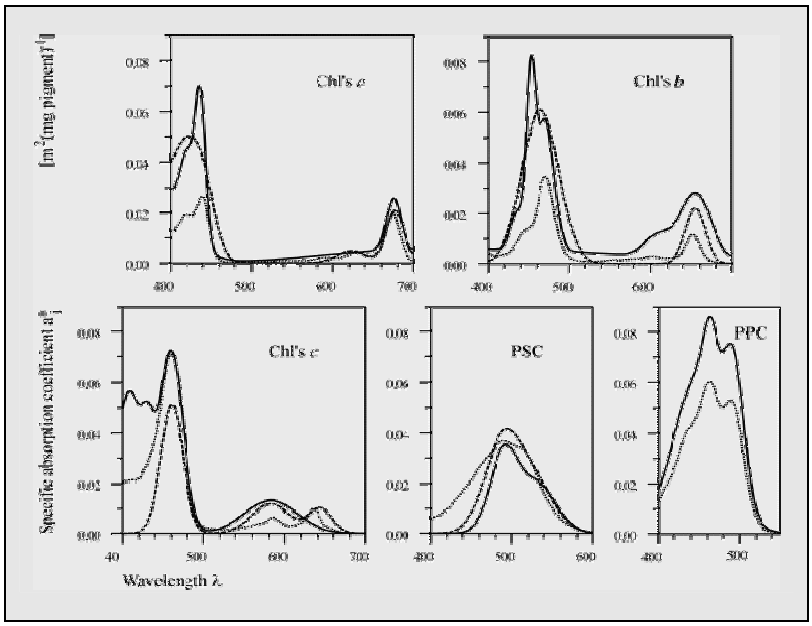

Figure 2.1: Modelled in-vivo specific absorption spectra of major phytoplankton pigment groups: Chl's *a*, Chl's *b*, Chl's *c*, photosynthetic carotenoids (PSC), photoprotective carotenoids (PPC). Woźniak et al. [1998] (solid lines), Hoepffner and Sathyendranath [1991] (dashed lines), Bidigare et al. [1990] (dotted lines). Source: Woźniak et al. [1998].

Due to species-specific pigment composition, there is a wide variety of absorption spectra for phytoplankton [e.g., *Morel et al.*, 1993; *Bricaud et al.*, 1995]. In addition, shape and magnitude of the specific phytoplankton absorption of one phytoplankton species may vary depending on irradiance and effects of stress (due to changes in nutrients, temperature, salinity, pH). The main variations in spectral shape occur in the blue to green wavelength range, where the accessory pigments show the maximum absorption (e.g., Figure 2.1).

Pigments within phytoplankton cells occur *in vivo* in chloroplast organelles, the thylakoids (with the exception for cyanobacteria). Thus, the absorption capacity depends on the packing set-up of the thylakoids [e.g., *Morel and Bricaud*, 1981; *Kohl and Nicklisch*, 1988]. Examples of the specific absorption coefficient of phytoplankton at 440 nm, $a^*_{phyto}(440)$, are presented in Table 2.1. Generally, for specific temperature-nutrient regimes, the spectral shape of absorption spectra may be generalized, such as in Fischer and Fell [1999], where for temperate regions, an averaged specific absorption coefficient spectra, $a^*_{phyto}(\lambda) = A_{phyto}(\lambda)[\text{Chl-}a]^{Bphyto(\lambda)}$, is defined according to the extensive research work of Bricaud et al. [1991, 1995].

The phytoplankton scattering varies according to cell and colony sizes and shows lower backscattering probability with increasing cell size [Sathyendranath, 1995]. Various parameterisations of the spectral backscattering coefficient as a function of the Chl-*a* concentration have been proposed by Gordon et al. [1988], Morel [1988], Haltrin and Kattawar [1991], Fischer and Fell [1999]. The IOCCG [2003] followed the simple approximation of Morel [1980] to relate phytoplankton backscattering at a reference wavelength to Chl-*a* concentration and described $bb_{phyto}(550) = 0.12\ [\text{Chl-}a]^{0.63}$. A definition of the phase function of the backscattering probability of phytoplankton is given by the San Diego harbour function (San Diego Harbour Stn. 2040) [*Petzold*, 1972]. Recently, a new phase function for Case 1 marine particles has been modelled by Zhang et al. [2003] using the SeaBAM data-set (§1.2).

Table 2.1: Specific absorption coefficients of phytoplankton at 440 nm, $a^*_{phyto}(440)$. Various sources.

Sources	a^*_{phyto} (440) [$m^2\ mg^{-1}$]	Water types
Suzuki et al. [1998], North-western Pacific, May 1997	0.082 to 0.022 0.019 to 0.009 0.040 to 0.003	Marine warm water stations Marine cold water stations Marine mixed water conditions
Bricaud et al. [1995] global investigations	0.18 to 0.01	Marine waters, different types
Gege [1994] Lake Constance (Germany)	0.034 (inverted reflectance measurements)	Mesotrophic freshwater stations
Heege [2001]; Heege and Fischer [2004] Lake Constance (Germany)	0.038 ± 0.01 (combined data-sets from Tilzer, Gege, Hartig and Heege)	Mesotrophic freshwater stations

2.1.2 Optical Effect of Suspended Particulate Matter (SPM)

The SPM term incorporates the whole pool of suspended particulates, including organic and inorganic material. In this sense, the phytoplankton cells and colonies and detritus are included and may dominate, as in Case 1 waters [*Bricaud et al.*, 1983; *Bricaud and Stramsky,* 1990; *Carder et al.,* 1991; *Roessler et al.,* 1989], or as in eutrophic to hypertrophic inland waters. On the other hand, if the SPM sources are fluvial input, coastal erosion, or resuspension events in shallow waters, SPM will be mainly composed of inorganic or non-living organic material. The composition of inorganic SPM is dependent upon the lithology of the catchment areas and coastal banks. Additionally, climatic conditions have an impact on various factors such as clay mineralogy, secondary mineralization and other geochemical processes. The wide range of minerogenic SPM incorporates amorphous and crystal particles of mainly silica-oxides, alumo-, iron-, and mangan-oxides and -hydroxides, clays, and calcite or dolomite.

In moderate to high latitudes, a small-sized silt to fine-sized clay fraction generally dominates the background fluvial input. The fine-size fraction is surface active and generally occurs coagulated with humic acids (Figure 2.2) due to cationic, anionic, and ligandic exchanges, and hydrophobic interactions [*Hedges,* 1977; *Rengasamy,* 1987]. However, these organo-mineralogic macroflocs are difficult to study by sampling and are predominately known from filmed submerged observations [*Eisma et al.*, 1983; *Wells and Kim,* 1989].

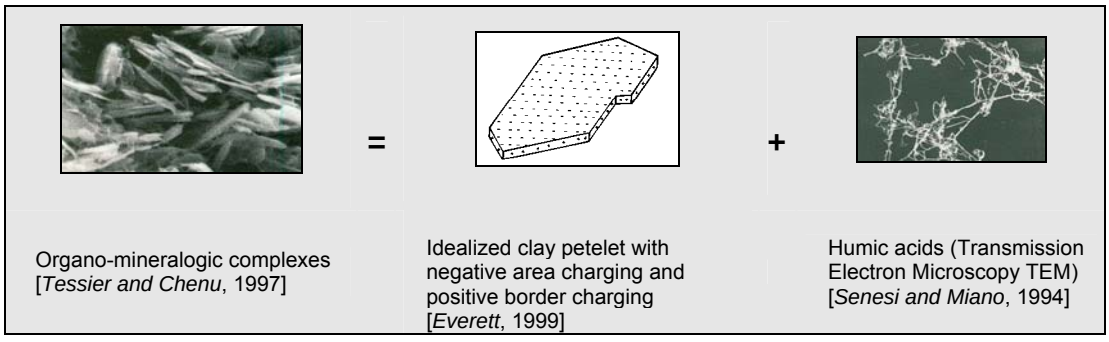

Figure 2.2: Naturally agglomerated organo-mineralogic complexes.

Therefore, depending upon the season and the local hydrodynamics, there may be a wide particle-size distribution of SPM, and distinctive seasonally variable coatings (for a summary see McCave [1984], and Eisma [1986]). For example, Babin et al. [2003] investigated COASTlOOC data (§ 1.2) where the contribution of nonalgal particles to absorption was significant in all coastal regions. Their investigations showed that specific backscattering coefficients exhibited markedly differing values in coastal waters (0.5 $m^2\ g^{-1}$) compared to pelagic Atlantic waters (1 $m^2\ g^{-1}$). And so, still to date, the optical specification in regional studies is very problematic, and there are only few published values for SPM absorption and backscattering cross-section spectra [e.g., *Bukata et al.,* 1991; *Babin et al.,* 2003].

2.1.3 Optical Effect of Coloured Dissolved Organic Matter (cDOM)

"Gelbstoff" as an important aquatic group was first introduced by Kalle [1937, 1949]. In limnological literature, this complex group is also called gilvin, while in remote-sensing terms, it is known as yellow substance [*Bricaud et al.,* 1981], aquatic humus [*Dekker*, 1993] and cDOM [*Schwarz et al.,* 2002]. Fulvic and humic acids in varying attributions constitute the main part of cDOM and represent the coloured fraction of Dissolved Organic Carbon (DOC) in natural waters [*Theng*, 1987]. These complex dissolved organic substances are autochthonous, originating from decaying phytoplankton biomass, and allochthonous, coming from river input and coastal erosion.

Their common optical behaviour is that they strongly absorb in the ultraviolet to blue wavelength region, causing the yellowish to brownish colours in organic-rich waters. Bio-optical bleaching processes of cDOM in the water surface layer due to photo-oxidation may occur, changing the optical behaviour over time [*Kieber et al.,* 1990]. The numerous narrow absorption bands of this complex organic group in the short wavelength region cannot be recorded separately by passive optical spectrometric methods. cDOM absorption is therefore described by the following exponential equation: $a_{cDOM}(\lambda) = a_{cDOM}(\lambda_0) \exp [- S (\lambda - \lambda_0)]$ [*Bricaud et al.,* 1981]. Specific Absorption Coefficients, SAC at reference wavelengths (e.g., SAC254, SAC400, SAC440), and the exponential Slope gradient, S, are measurable parameters. The exponent S generally lies between 0.01 - 0.02 [*Kirk,* 1976; *Babin et al.,* 2003].

The term dissolved is defined operationally, by filtrating the filtrate either through a 0.2 or a 0.45 µm pore-size cellulose filter. Colloids, ranging in size from 0.001 to 1 µm, are therefore partly included in the dissolved component, and partly in the particulate fraction. This further complicates any study undertaken, since the measured cDOM absorption, and even the spectral characteristics, has a dependence on the filter pore-size chosen during a specific investigation. Table 2.2 lists examples of S values from different aquatic sources.

Larger organic complexes that do not pass through the filter will accumulate on it and may contribute to the detritus fraction. All material on the filter, after the destruction (by acidification or bleaching) of phytoplankton cells (inclusive of Chl-*a* pigments), is referred to as *detritus* [*Tassan and Ferrari*, 1995]. This *detritus* absorption shows a similar, ideally exponential absorption curve as the dissolved fraction cDOM, however with lower S values between 0.007 and 0.015 [*Kirk*, 1976; *Babin et al.*, 2003; *Roesler et al.*, 1989].

Siegel et al. [2003] described how the *detritus* absorption contributed to the *cDOM* absorption of ca. 25 % in coastal waters and ca. 15 % in pelagic waters of the Baltic Sea. 'YSBPA' (Yellow Substance and Bleached Particle Absorption) is for example a MERIS level-2 product (§1.2) that accounts for the additional optical influence of *detritus*, representing the sum of absorption of cDOM and of detritus (in terms of the bleached particle absorption), both measured at 442 nm.

Table 2.2 : Averaged Slope S values of cDOM from different sources.

Reference	S	Wavelength range	Source
Bricaud et al. [1981]	0.014	375 - 500	Marine
Dekker [1993]	0.015	400 - 600	Eutrophic lakes (N)
Bukata et al. [1995]	0.016	-	Lake Ontario (USA)
Heege [2000], Heege and Fischer [2004]	0.018	360 - 480	Lake Constance (G)

2.1.4 Optical Effect of Pure Water

Smith and Baker [1981] and Pope and Fry [1997] provide absorption spectra of pure water derived from laboratory investigations. Ocean Optic Protocols propose the absorption spectra of Sogandares and Fry [1997] for wavelengths between 340 nm and 380 nm, Pope and Fry [1997] for wavelengths between 380 nm and 700 nm, and Smith and Baker [1981] for wavelengths between 700 nm and 800 nm. Buiteveld et al. [1994] investigated the temperature dependant water absorption properties. Morel [1974] provides spectral values of the pure water volume scattering coefficient at specific temperatures and salinity, and the phase function.

2.1.5 Bio-optical Classification/ Case 1 and Case 2 Waters

i) Case 1 waters are defined as waters in which the autochthonous material (phytoplankton and its detritus, cDOM from degraded phytoplankton) controls the optical properties [*Morel and Prieur*, 1977; *Gordon and Morel*, 1983]. Even if the detritus-to-Chl-*a* ratio, accessory pigments-to-Chl-*a* ratio, and the cDOM-to-Chl-*a* ratio vary [*Wozniak et al.*, 1992], it is useful to express Case 1 waters as a function of Chl-*a* [*Gordon and Morel*, 1983; *Morel and Maritorena*, 2001; *Mobley and Sundman*, 2000]. Case 1 waters are expected in pelagic marine waters, even though the Chl-*a* concentration may range from low values (0.02 µg l^{-1}) in ultra-oligotrophic waters up to high values (5-20 µg l^{-1}) in upwelling areas.

ii) Case 2 waters occur as coastal and inland waters with a complex bio-optical setting. In cases of allochthonous sources, such as fluvial input, coastal erosion, and resuspension events, the different groups of optically-visible water constituents (phytoplankton and its detritus, minerogenic SPM, terrigenous cDOM) are generally uncorrelated.

Figure 2.3 explains the classification of Case 2 waters according a triangular diagram. The three vertices are denoted as Chl for chlorophylls, as Y for 'yellow substance', and as S for Sediments (minerogenic SPM). The upper tip represents Chl-*a* dominated waters (i.e., Case 1 waters). The centre of the triangle represents Case 2 waters with various mixtures of optically visible substances. The yellow substance dominated waters are predominantly absorbing, whereas sediment dominated Case 2 waters are strongly scattering with high reflectances. Sauberer [1962], Jerlov [1968], Smith et al. [1973], and Thomson and Jerome [1975] used measurements of water colour (expressed as the dominant wavelength) to separate optical water types and for lake classification, relating water colour to the dominant water constituents.

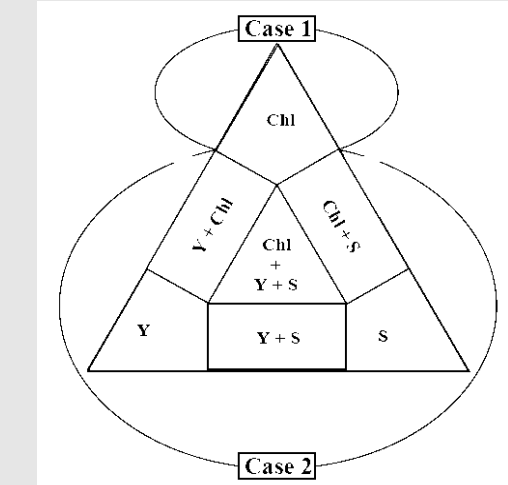

Figure 2.3: Triangular diagram, adapted from Prieur and Sathyendranath [1981], describing the classification of Case 1 and Case 2 waters.

2.2 THE UNDERWATER LIGHT-FIELD

In contrast to spectral investigations of solid-surface materials, natural waters limit the wavelength range of investigation to between 400 to 850 nm, due to the sharply increasing absorption of pure water at longer wavelengths (§2.1.4). Preisendorfer [1981], Austin [1974], Jerlov [1976], and Kirk [1981, 1983] explored the physical basis for the underwater-light field and defined Inherent and Apparent Optical Properties (IOPs and AOPs). Apparent Optical Properties (AOPs), such as spectral reflectances and the apparent water colour (the dominant wavelength) are directly measurable. Inherent Optical Properties (IOPs) are defined to be independent of the ambient light field and are not directly measurable in the field. All parameters of bio-optical models can be referred back to the IOPs that theoretically express the bulk optical properties of natural waters in terms of: i) the absorption coefficients, ii) the backscattering coefficients of the visible water constituents, and iii) the phase function, which describes the angular behaviour of scattering processes.

By adding the optical coefficients, the bio-optical frame can be adapted to specific cases [*Bukata et al.*, 1995; *Carder et al.*, 1991; *Doerffer et al.*, 2002; *Fischer and Fell*, 1999; *Prieur and Sathyendranath*, 1981; *Roesler et al.,* 1989]:

$$a(\lambda) = a_{\text{water}}(\lambda) + a_{\text{phyto}}(\lambda) + a_{\text{detritus}}(\lambda) + a_{\text{cDOM}}(\lambda) \tag{2.1}$$

$$bb(\lambda) = bb_{\text{water}}(\lambda) + bb_{\text{phyto}}(\lambda) + bb_{\text{detritus}}(\lambda) \tag{2.2}$$

where the terms used above are defined as

a_{water} is the absorption, bb_{water} is the backscattering coefficient due to pure water,

a_{phyto} is the absorption, bb_{phyto} is the backscattering coefficient due to phytoplankton,

a_{detritus} is the absorption, bb_{detritus} is the backscattering coefficient due to detritus,

a_{cDOM} is the absorption coefficient due to *cDOM.*

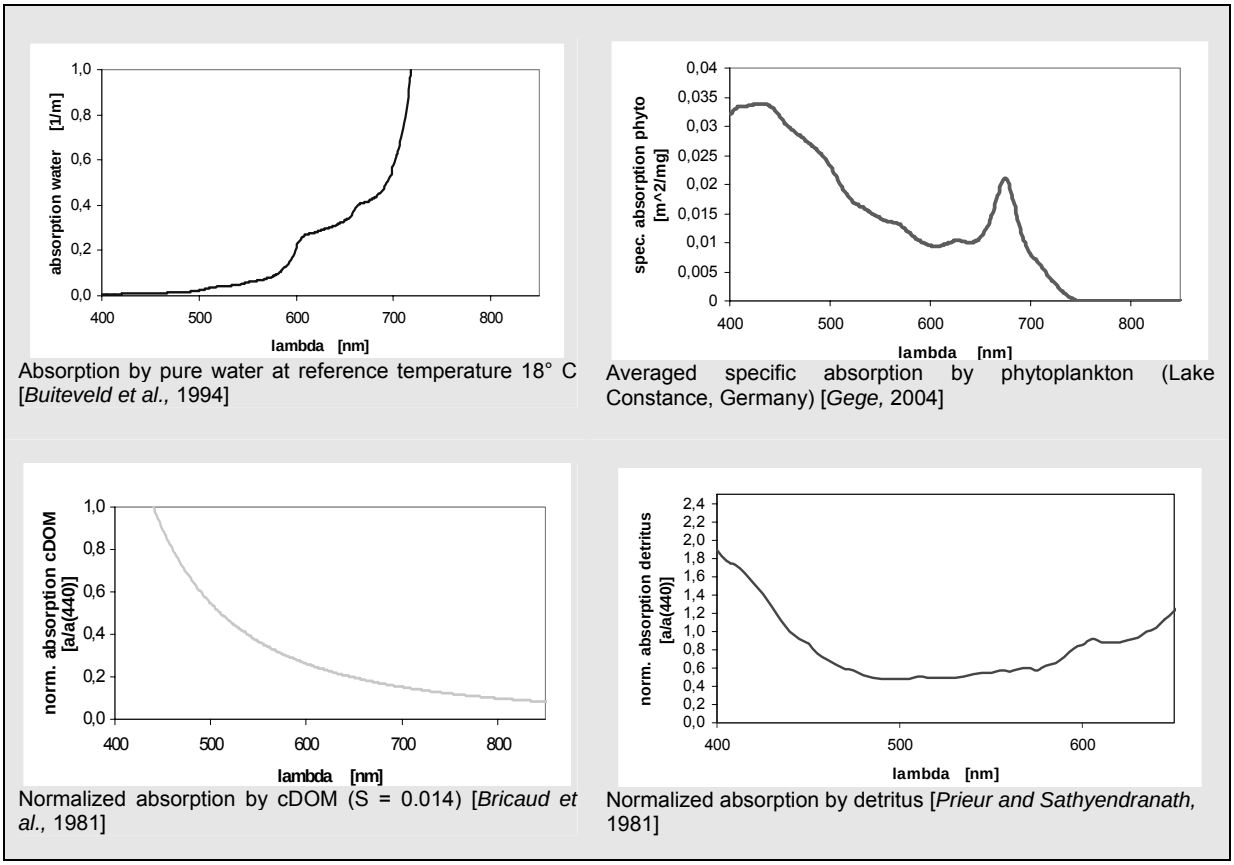

Absorption by pure water at reference temperature 18° C [*Buiteveld et al.,* 1994]

Averaged specific absorption by phytoplankton (Lake Constance, Germany) [*Gege,* 2004]

Normalized absorption by cDOM (S = 0.014) [*Bricaud et al.,* 1981]

Normalized absorption by detritus [*Prieur and Sathyendranath,* 1981]

Figure 2.4: Examples of absorption coefficient spectra for bio-optical modelling.

If IOPs are referred back to the concentrations, the specific coefficients are defined as coefficients per unit concentration, from absorption, *a*, and from backscattering, *bb*.

$$a^*(\lambda) = a(\lambda) \times C^{-1} \qquad [\mathrm{m^2\ mg^{-1}}]$$

$$bb^*(\lambda) = bb(\lambda) \times C^{-1} \qquad [\mathrm{m^2\ mg^{-1}}] \qquad (\mathrm{C} = \text{concentration})$$

The absorption of bulk water can in this case be parameterised using:

$$a(\lambda) = a_{\mathrm{water}}(\lambda) + a^*_{phyto}(\lambda) \times C + a^*_{\mathrm{det}\,ritus}(\lambda) \times C + a^*_{cDOM}(\lambda) \times C \qquad (2.3)$$

As an example, Figure 2.4 shows the spectral-absorption coefficients that may be the input parameters for equation 2.1. In this case, $a^*_{\mathrm{phyto}}(\lambda)$ and $a^*_{\mathrm{detritus}}(\lambda)$ are related per unit Chl-*a* concentration [mg m^{-3} (=µg l^{-1})], i.e. in [m^2 mg Chl-*a*$^{-1}$]. In the case of $a^*_{\mathrm{cDOM}}(\lambda)$ the absorption coefficient [m^{-1}] per unit is normalized to 440 nm [a/a(440)], similarly, $a^*_{\mathrm{detritus}}(\lambda)$ is normalized [a/a(440)].

Analytical approaches exist to obtain models of the reflectance (the ratio of reflected flux to incident flux) [*Gordon et al.,* 1988; *Zaneveld*, 1982; *Haltrin and Kattawar*, 1993]. A common analytical expression that relates in natural waters the hemispherical reflectance *R* to the total-absorption coefficient *a* and the total back scattering coefficient *bb*, was adapted by Gordon and Brown [1973]:

$$R = f \times \frac{bb}{a + bb} \tag{2.4}$$

Where *a* is the sum of the absorption coefficients, *bb* is the sum of the backscattering coefficients, and f is an empirical factor dependent upon solar-zenith angle and volume-scattering function of the water body. Morel and Prieur [1977] defined f = 0.33, while in Morel and Gentili [1993], f is defined to be in the range 0.3 to 0.5.

The fundamental radiometric property is the radiance, $L(\theta,\varphi,\lambda)$ (in units of W m^{-2} sr^{-1}), described as the radiant power in a specified zenith, θ, and azimuth, φ, direction per unit solid angle, per unit area, normal to the incident beam at a given wavelength. The various irradiances are derived by weighted integration of the radiance field over defined solid angles. In water, the downwelling irradiance, $E_{down}(\lambda)$ (in units of W m^{-2}), and upwelling irradiance, $E_{up}(\lambda)$, are given as the cosine-weighted integration of the $L(\theta,\varphi,\lambda)$ distribution over the upper (downwelling) and lower (upwelling) hemispheres, respectively. In order to relate the irradiance to radiance, a commonly introduced factor is the angular distribution factor, Q (in units of sr). Q, the ratio of $E(\lambda)$ to $L(\theta,\varphi,\lambda)$, results for the case of perfect diffuse conditions in the factor π [*Morel and Gentili,* 1993]. In natural waters, Q is dependent on the solar-zenith angle and particle-size distribution of the water constituents, and hence on the phase function, and will therefore deviate from the ideal case. Commonly, Q falls within a wide range of possible values, from 2 to 7 [*Tyler*, 1960; *Bukata et al.*, 1988; *Kirk,* 1983; *Gordon and Morel,* 1983], introducing here a factor of uncertainty. Dekker [1993] and Mueller and Austin [1992] refereed Q with the value 5, Fell modeled Q = 4.4 (at 708 nm) by using MOMO (§1.2) [1999]. Olbert [2000] used MOMO to calculate Q, for the case of a cloud-free sky dependant upon the recording scanning geometry and the wavelength range, while Heege [2000] calculated Q with respect to differing concentrations of water constituents.

For remote sensing applications, measurements of $L(\theta,\varphi,\lambda)$ and $E(\lambda)$ taken in water must be related to remotely sensed above-water $L(\theta,\varphi,\lambda)$. The index of refraction, n, is an IOP and is dependent on salinity and weakly on temperature and pressure [*Austin and Halikas*, 1976]. Most definitions of the transfer of the water-air interface have assumed nadir-viewing geometry. However, most remote sensing instruments view the ocean surface at angles removed from nadir. Furthermore, the Fresnel scattering of the directly reflected skylight component from the ocean surface upward, r_{aw}, is a strong function of illumination and viewing geometry. Mobley [1987] implies the Cox and Munk function [1956] to model ranges of r_{aw}, depending on sky and sea conditions. According to the Ocean Optic Protocols [2000] in which Mobley's calculations [1987] have been considered, the recommended measurement angles for lowest back-reflecting probability for above-water measurements are for θ = 40° (sensor zenith) and φ = 135° (azimuth towards the sun).

Volume Reflectance. The dimensionless bulk water reflectance, $R(z,\lambda)$, is defined by the ratio of E_{up} to E_{down}, both measured at the same distinct water depth, z. The required reflectance for remote sensing studies, the volume reflectance, $R_{vol}(0\text{-},\lambda)$, is defined directly at the subsurface (0-):

$$R_{vol}(0-,\lambda) = \frac{E_{up}(0-,\lambda)}{E_{down}(0-,\lambda)} \tag{2.5}$$

There are physical restrictions on the measurement of $E_{up}(\lambda)$ and $E_{down}(\lambda)$ directly beneath the subsurface (0-). In water, the irradiance at a particular depth, $E(z,\lambda)$, is a function of the intensity at the surface, $E(0\text{-},\lambda)$, and to the exponent of the negative-extinction coefficient, *K*, at the depth, z, (assumed constant over the interval 0- to z):

$$E(0-) = E(z) \times e^{Kz} \tag{2.6}$$

Remote Sensing Reflectance. This widely used reflectance for water remote sensing studies is defined as the ratio of the water-leaving radiance, $L_w(0+,\lambda)$, to $E_{down}(0+,\lambda)$, directly at the water surface (0+):

$$R_{RS}(0+,\lambda) = \frac{L_w(0+,\lambda)}{E_{down}(0+,\lambda)} \qquad [\mathrm{sr}^{-1}] \tag{2.7}$$

$R_{RS}(0+,\lambda)$ can, on one hand, be deduced from underwater measurements. In this case, $L_w(0+,\lambda)$ is calculated according to Austin (1974) from the nadir-looking $L_{up}(0-,\lambda)$ as:

$$L_w(0+,\lambda) = \left(\frac{1-r_{wa}}{n^2}\right) L_{up}(0-,\lambda) \qquad [\mathrm{W\ m^{-2}\ nm^{-1}\ sr^{-1}}] \tag{2.8}$$

This formula takes into account that light is internally reflected at the water-air boundary, $(1 - r_{wa})$, where r is the Fresnel coefficient that accounts for nadir-viewing radiances for $r_{wa}0° = 0.021$. In addition, the upward radiant flux is confined to a different angle, where n is the relative index of refraction of water to air, being 1.333 for fresh-water.
Therefore, $R_{RS}(0+,\lambda)$:

$$R_{RS}(0+,\lambda) = \frac{0.55 L_{up}(0-,\lambda)}{E_{down}(0+,\lambda)} \qquad [\mathrm{sr}^{-1}] \tag{2.9}$$

On the other hand, deducing $R_{RS}(0+,\lambda)$ directly from above-water measurements is dependant on the definition of $R_{RS}(0+,\lambda)$. Owing to the fact that in cases of clear water, a considerable part of the $L_{up}(0+,\lambda)$ is composed of a directly reflected skylight component, it is not possible to measure only $L_w(0+,\lambda)$ by measurements above the water surface. The amount of directly back-reflected skylight at the air-water interface, r_{aw}, varies with sun-zenith angle and water surface state, but accounts for a theoretical minimum of $r_{aw}0° \approx 0.021$ for a flat surface, containing no information about the water constituents.
Therefore, $R_{RS}(0+,\lambda)$ can be derived as follows from above-water measurements:

$$R_{RS}(0+,\lambda) = \frac{L_{up}(0+,\lambda) - r_{aw} \times L_{sky}(\lambda)}{E_{down}(0+,\lambda)} \qquad [\mathrm{sr}^{-1}] \tag{2.10}$$

The quality of this calculation is highly dependant on sky and sea conditions. Preferable is homogenously clear or homogenously overcast sky [*Ocean Optic Protocols*, 2000]. The presence of clouds will spectrally interfere with this measurement, especially in the blue wavelength range, and introduces a large uncertainty for the correction of shipborne spectro-radiometric measurements.

Surface Reflectance and Albedo. The Surface Reflectance, $R(0+,\lambda)$, is defined as the ratio of $L_{up}(0+,\lambda)$ to $L_{down}(0+,\lambda)$. In fact, in studies of eutrophic to hypertrophic inland water bodies, the upwelling signal $L_{up}(0+,\lambda)$ may be directly taken without further correction, similar to spectro-radiometric measurements of solid-surface materials. In this special case of turbid water bodies, the recorded uncorrected upwelling signal is dominated by the spectral bulk water signal due to high concentrations of water constituents. Similar to the dimensionless Surface Reflectance, $R(0+,\lambda)$, the

Albedo, A(0+,λ), also incorporates the uncorrected upwelling signal, π L_{up}(0+,λ), or E_{up}(0+,λ), respectively:

$$R(0+,\lambda)=\frac{L_{up}(0+,\lambda)}{L_{down}(0+,\lambda)} \qquad A(0+,\lambda)=\frac{\pi\times L_{up}(0+,\lambda)}{E_{down}(0+,\lambda)} \tag{2.11 a,b}$$

2.3 ATMOSPHERIC CORRECTIONS

The signal that is recorded by an airborne or satellite sensor is spectro-radiometrically shaped by the following processes in the atmosphere and bulk water layer:

i) Significant scattering and absorption as the solar radiation passes through the atmospheric layer.

ii) The surface material interacts with the total radiation, i.e., with a combination of direct solar radiation and diffusely scattered sky radiation.

iii) The uprising signal is again attenuated in the atmosphere during its transfer towards the sensor, before it is recorded by a satellite sensor as the Top-Of-Atmosphere Radiance, L_{TOA}.

A compendium of spectroradiometrical processes in the atmosphere and the bulk water is shown in Figure 2.5. L_{TOA}(λ) is spectrally modified only to a minor extent owing to optically interactions of the bulk water of interest, however by major contributions owing to the scattering and absorption processes within the atmospheric layer.

The Top-Of-Atmosphere Reflectance, R_{TOA}(λ), is defined as:

$$R_{TOA}(\lambda)=\frac{\pi\times L_{TOA}(\lambda)}{E_{sol}(\lambda)\times\cos\theta} \tag{2.12}$$

where L_{TOA}(λ), is the radiance in a given solar and viewing geometry reaching the sensor, E_{sol}(λ) is the exo-atmospheric solar irradiance, and θ is the solar-zenith angle.

The radiative transfer is described as:

$$R_{TOA}(\lambda)=\left[\rho_r(\lambda)+\rho_a(\lambda)+\rho_{ra}(\lambda)+\mathrm{T}(\lambda)\times\rho_{gl}(\lambda)+t(\lambda)\rho_f(\lambda)+t(\lambda)\rho_w(\lambda)\right]\times t_g(\lambda) \tag{2.13}$$

where ρ_r is the Rayleigh reflectance resulting from multiple scattering by air molecules, ρ_a is the reflectance resulting from multiple scattering by aerosols, ρ_{ra} is the multiple interaction term between air molecules and aerosols, ρ_{gl} is the direct reflectance of solar rays from the sea surface to the sensor (sun glint) [*Deschamps et al.,* 1983], ρ_f represents the direct reflection from skylight at the air-water interface (§2.2), including the reflection from wave whitecaps [*Gordon and Wang*, 1994], and ρ_w is the water-leaving reflectance. The *t* term is the atmospheric diffuse transmittance and similarly, *T* is the direct transmittance [*Wang*, 1999]. The $t_g(\lambda)$ term represents the gaseous transmittance, which accounts for absorption due to ozone (O_3), oxygen (O_2), and water vapour (H_2O) within the spectral wavelength range that is usable for optical water remote sensing studies.

The scattering processes occur selectively and non-selectively, governed by particle diameter: molecules of gases (diameters of ca. 10^{-4} µm) selectively scatter in the ultraviolet and the shortwave spectrum, as it is termed Rayleigh scattering. It occurs with an effect proportional to the inverse 4th power of the wavelength ($I_{Rayleigh} \approx \lambda^{-4}$). Conditions that are constraints for Rayleigh scattering, i.e., that the wavelengths of the radiation are much smaller than the diameters of the particles (d « λ), are no longer present in case of aerosols. Aerosols are liquid and solid particles suspended in the atmosphere, such as dust, smoke, volcanic ash, or crystals of sea salt. If wavelength and particle diameter are approximately the same order of magnitude (e.g., particles of dust, water) (d ≥ λ), the

dependency of scattering intensity on wavelength diminishes and this is referred as Mie scattering ($(I_{Mie} \approx \lambda^{-q}$, $q < 4$). For cases of large aerosols (e.g., water droplets, pollen), the scattering processes are no longer selective and become independent of wavelength. Usually, the aerosol assemblage contains a wide range of particle sizes. The phase function of Mie scattering is complex, dominated by forward scattering.

An indication of aerosol-size distribution may be derived from optical satellite data by the use of the ratio of two Rayleigh corrected spectral bands. Theoretically, at the near-infrared bands, the water-leaving reflectances are negligible owing to strong absorption by water (§2.1.4), and therefore, the single-scattering band ratio, $\varepsilon(i_{NIR} / j_{NIR})$; (i < j), is used to indicate aerosol climatologies [*Gordon and Wang*, 1994; *Wang and Gordon*, 1994]. $\varepsilon(i,j) > 1$ is assumed to be indicative for an aerosol composition typically dominated by small particles (e.g., aerosol size distribution in urban and rural atmospheres). $\varepsilon(i,j) \approx 1$ refers to white-spectral behaviour that is caused by the dominance of relatively large particles (e.g., aerosol size distribution in marine atmospheres).

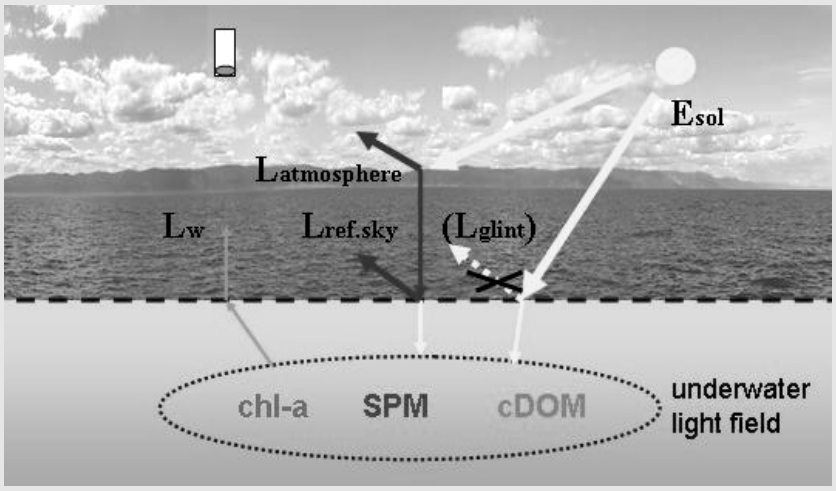

For the case where the direct sun glint, L_{glint}, can be avoided, the radiance reaching the sensor is composed of approx.:
92 to 98 % $L_{atmosphere}$
2 to 7 % $L_{ref.sky}$
0.1 to 1 % L_{water} (for the case of clear water bodies)

The underwater light field is modified by the optically visible water constituents Chl-*a*, SPM, and cDOM (§2.1).

Figure 2.5: Spectroradiometrical processes in the atmosphere and the bulk water.

3 LAKE BAIKAL AND ITS ENVIRONMENT

3.1 ECONOMIC AND ECOLOGICAL SETTING

Lake Baikal is situated very centrally in the Eurasian land mass. The geographic-economic Baikal region stretches from the southeastern section of Siberia in the Russian Federation towards Mongolia to the South (Figure 3.1). The local population comprises different ethnic groups, including Russians, Buryats, Evenks, and Sayats. In the Baikal region with its low and high mountain ranges, people have preferred to settle along the fertile river valleys. Farming here mainly consists of wheat and vegetables, notally potatoes, whereas nomadic sheep and cattle herding is more common in the South. Economic activities along the shore of Lake Baikal are dominated by forestry, fisheries, hunting and tourism.

Figure 3.1: Regional setting of Lake Baikal in Southern Siberia (RU)

The capital of the Irkutsk Oblast (Russian Federation), Irkutsk, is located at the Angara River, about 100 km from Lake Baikal. To the east, the lake forms a natural border with the Autonomous Buryat Republic (founded 1923). The capital of the Autonomous Buryat Republic, Ulan-Ude, is located at the junction of the Uda and Selenga rivers. All large settlements of the region are situated along the Trans-Siberian Railway, including industrial centres at the south coast of Lake Baikal (Baikal'sk, Slyudyanka, Selenginsk) and southwards to Mongolia (Gusinoozersk industrial centre).

Away from the railway lines, the vast boreal areas surrounding the Central and North basins of Lake Baikal are mainly unpopulated. This coniferous boreal forest - the taiga - is dominated by firs, pines and Siberian cedars. Southwards towards Mongolia, the taiga changes to temperate mixed and deciduous forest and to forest-steppe. The lake itself, the taiga, and the mountainous tundra of the Baikal region, have a high biodiversity. Approximately half of the plant and animal species found in these regions and in the lake are endemic.

The development of industry in the 1960s caused a sharp rise in pollution in Baikal's largest tributary, the Selenga River. Around the Baikal basin, sewage treatment of both domestic and industrial wastewaters was non-existent, or was of a very poor quality. These sources introduced nutrients, metal ions and derivatives of oil and petroleum directly into the lake, regionally exceeding global limits (i.e., limits set by the joint UN and WHO programme on the environment 1980). From the 1960s to 70s, pulp and paper mills went into operation along the South Basin in Baikal'sk and Selenginsk. Both mills caused considerable air pollution that had its impact on the taiga where the desiccation of trees could be observed. In addition, polluted waste-waters with high levels of dioxins and persistent organo-chlorines were dumped directly into the lake water, while solid waste was deposited on land. These human environmental impacts that have affected the southern part of Lake Baikal and its environment have been investigated in national and international programmes [*Russian 1998 Governmental Commission Report*, 1999; *Environmental Year Reports of Buryatia*, 1999, 2000; *UNESCO Annual Report*, 2000; *Selenga Conference Reports*, 2002; *Greenpeace Executive Summary*, 2003].

In 1996, Lake Baikal was designated a World Heritage Site and placed under the Protected Areas Program [*UNESCO list*, 2004]. The paper and pulp production complex at Selenginsk has been converted to a closed water-cycle system. Along the Selenga River, waste-water treatment plants have been installed.

Tarasova [1998] stated that Lake Baikal is under a much greater threat from chemical pollution (mainly organo-chlorines and dioxins) than from eutrophication. Future prognoses for eutrophication in Lake Baikal are discussed by Goldman [1993], Goldman et al. [1996] and Popovskaya [2000]. These sources see indications of eutrophication on a local scale around the Selenga delta and the coastal bays in the South Basin. However, Popovskaya [2000] concludes that eutrophication for the oligotrophic waters of Lake Baikal seems to be unlikely due to the enormous size of the water body.

3.2 GEOLOGICAL SETTING

The Baikal rift system is one of the world's biggest active continental rifting zones. After the initial collision of India with Eurasia during Paleocene-Early Eocene, resulting in the Himalayan orogenesis, India has continued to converge northwards, and this further induced strong post-collisional deformation in Central and Southeast Asia [*Cobbold and Davy*, 1988]. The Baikal rift development started in the Eocene/Lower Oligocene along reactivated ancient tectonic structures [e.g., *Zonenshain and Savestin*, 1981].

The central part of the Baikal rift is occupied by the Barguzin and the Baikal depression, the latter containing Lake Baikal. The basin topography of Lake Baikal is distinguished by three deep half-graben rift segments (900 to 1600 m deep) that are separated by inter-basinal high-relief ridges (200 to 400 m deep). The South Basin and the Central Basin are the two oldest and most deeply subsided segments. Sedimentation may have started as early as the Palaeocene to Early Eocene [*Logachev*, 1993]. Average (and maximum) water depths in the three main basins are today 843 (1414) m,

854 (1637) m, and 576 (989) m in the South, Central, and North basins, respectively [*Shimaraev et al.,* 1994; *Wong et al.,* 1991]. Table 3.1 lists the main morphometric data for the Baikal Basin. All basins are asymmetric in structure: the eastern walls have gradients of 6-15°, while the western fault slopes can be as steep as 45°.

The western mountain ranges bordering Lake Baikal are the Primorsky and Baikalsky ranges, with a maximum height of 2680 metres. On the eastern shore, Baikal is fringed by the Barguzinsky and Ulan-Burgasy ranges, while to the south and south-east there is the Khamar-Daban range, of which the highest summit (Munku-Sardyk) reaches an elevation of 3490 metres above sea level.

Table 3.1: Morphometric data of the Baikal Basin [*Wong et al.,* 1991]

Lake surface above sea level	456	m
N-S length of lake	636	km
Maximal width	80	km
Minimal width	25	km
Maximal depth	1620	m
Water volume	23000	km^3

3.3 CLIMATIC SETTING

The central Asian region is to a high degree isolated from oceanic influences, showing the highest degree of continentality in the world [*Lydolph*, 1977]. Southeastern Siberia itself is characterized by a subhumid boreal forest climate with four distinct seasons. Trans-Baikalian climate shows mean daily temperatures ranging from -50° C in January to 35° C in July. In winter, the region is dominated by a high-pressure system over Central Asia. Therefore, winters are long, cold and dry. In summer, the Siberian anticyclone is replaced by a low-pressure system centred over the Tibetian Plateau. This Asiatic monsoon low-pressure system is responsible for maximal precipitation and extensive cloud coverage during summer months.

Lake Baikal is large enough to influence air temperature over its open waters and beyond its shorelines. Thus, average winter air temperatures at the borders of Lake Baikal are -21° C, and average summer temperatures are only around 15° C [*Kozhova and Izmest'eva*, 1998]. Quickly changing air temperatures, heavy rainfall and frequent thunderstorms are typical features around Lake Baikal.

The precipitation pattern differs from north to south [*Atlas of World Water Balance*, 1979]. In the mountain ranges around Lake Baikal covered with taiga, mountain tundra and glaciers, the precipitation falls in the range of 400 to 500 mm a^{-1}. Southwards towards Mongolia, the Baikal watershed character changes towards a dryer climate with steppe vegetation, where the rates of precipitation decreases to a range of 300 to 400 mm a^{-1}.

For almost five months a year, Lake Baikal is covered with ice. There are distinct climatic variations from south to north, given Lake Baikal's large size and orientation. In the South Basin, ice decay begins in late March and is completed by mid May [*Verbolov et al.*, 1965], whereas in the North Basin, ice decay starts as late as May, and the basin is not ice-free until mid June [*Kozhov*, 1963].

3.4 LIMNOLOGICAL SETTING

Lake Baikal is the largest freshwater lake in the world by volume (Table 3.1). The average temperature of this huge water body is around 4° C, varying according to location and season. The lake surface temperature may reach between 8° to 10° C in August and up to 14° to 18° C along the coast, within bays and in the sub-basin Maloe More. Lake Baikal is classified as a dimictic type [*Kozhov*, 1963], with an intense vertical circulation and approximate isothermy in late spring and autumn. The considerable vertical exchanges of water masses support the high oxygen saturation in Lake Baikal. Summer stratification in the South and Central Basins is short (late July to August) with a thermocline of approximately 250 m and may even not develop in the North Basin [*Kozhova and Izmest'eva*, 1998]. During May through to June, the warming of coastal waters results in the development of thermal bars [*Shimaraev et al.,* 1994].

Figure 3.2 shows the prevailing winds and relative postions of cyclonic lake currents, which today have established. The bulk of information on currents in Lake Baikal has been obtained through systematic measurements with moored automatic current meters. General characteristics are the importance of wind driven surges and drift currents [*Fialkov*, 1983]. Permanent horizontal geostrophic currents are divided up into different fields according to the morphological form of Lake Baikal [*Kozhov*, 1963; *Shimaraev et al.*, 1994]. In June, a prominent physical phenomenon of large cold lakes, the thermal bar that separates pelagic from coastal waters in late spring and summer, develops along the eastern coast of the Central and the Southern Basin [*Shimaraev*, 1993].

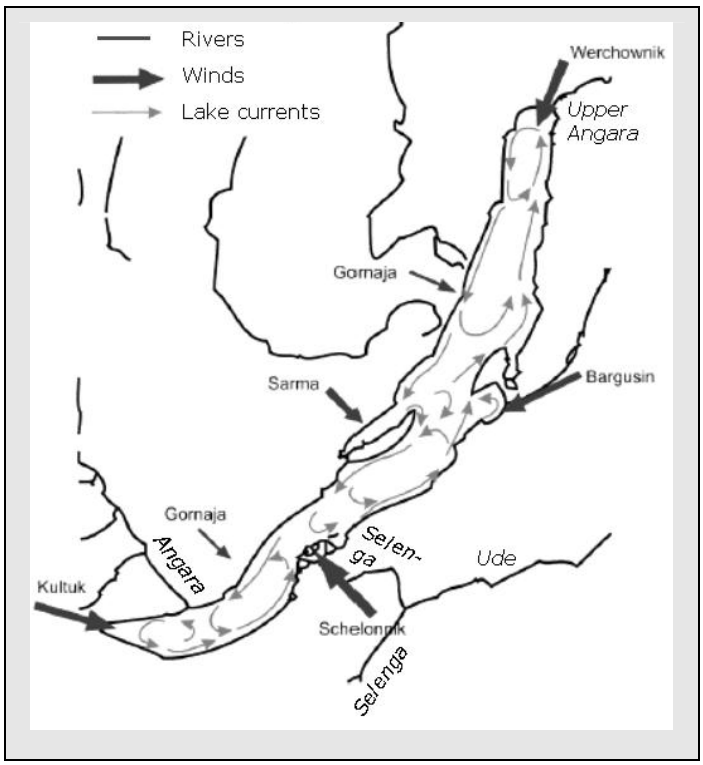

Figure 3.2: Prevailing wind systems about Lake Baikal [*Atlas of Baikal,* 1993] and the relative positions of cyclonic currents as proposed by Kozhov [1963].

Genkai-Kato [2000] classified the pelagial of Lake Baikal as oligotrophic ocean-like water, according his investigations and Russian long-time studies. The Irkutsk State University (SRIB) undertakes regular Chl-*a* monitoring (51°54'19.5'' N, 108°04'23.5'' E) around 2 km distance from the biological station Bolshye Koti (South Basin), where the depth at the site is 800 m. The samples are taken within a 1 to 4 week interval at various depths until 250 m depth. Chl-*a* analyses were carried out according to SCOR-UNESCO [1964].

These investigations and SRIB field expeditions show that Chl-*a* concentrations in pelagic waters range mainly between 0.5 and 1.2 µg l^{-1}. Within bays, and near the Selenga Delta, Chl-*a* may develop up to 5 µg l^{-1} in late summer [*Kozhova and Izmest'eva*, 1998].The main phytoplankton blooms (up to 10 µg l^{-1} Chl-*a*) develop in early spring (March to May), under transparent ice in turbulent waters, where the large-sized diatom species, *Aulacoseira baicalensins* (*Melosira baicalensis*), occurs periodically every third or fourth year in large quantities (so-called 'Melosira' years).

Spatial heterogeneity in Lake Baikal has been recorded by optical parameters, using fluorescence, attenuation coefficients and the Secchi depth [*Shimaraev et al.,* 1994]. Continuously conducted Secchi depth measurements revealed a specific optical property of Lake Baikal: its extremely high transparency. Secchi depth measurements in pelagic waters in Lake Baikal show values up to 40 m in June and still up to 20 m in late July when phytoplankton is more abundant [*Shimaraev et al.,* 1994]. On the one hand, the high transparency is due to Lake's Baikal oligotrophy. On the other, Lake Baikal is little influenced by resuspended sediments and coastal erosion, because its morphology is steep and the shores are dominated by rocky cliffs and shingle beaches. Table 3.2 shows for comparison the Secchi depth ranges from a number of clear fresh-water bodies.

Table 3.2: Attenuation coefficients and Secchi depths of the clearest fresh-water water bodies in the United States (sources: Makarewicz and Bertram [1993], Great Lakes Water Quality Board [1989]) and Lake Baikal (sources: Shimaraev et al. [1994] (**) and Sherstyankin [1975] (*)).

Lake	Attenuation coefficient [1 m^{-1}]	Secchi depth [m]	Description
Crater Lake (USA)	0.06 to 0.12	25 to 45	Clear, sky blue ultra-oligotrophic lake
Lake Tahoe (USA)	0.08 to 0.12	40	Clear, sky blue ultra-oligotrophic lake
Lake Superior (USA)	-	15 to 20	Most oligotrophic of the Laurentian Great Lakes
Lake Erie (USA)	0.20 to 1.20	-	Mesotrophic
Lake Baikal (RU)	0.06 to 0.20*	15 to 40**	Clear, sky blue ultra-oligotrophic lake

However, depending on the season, turbid surface water may also locally prevail. This is especially the case during the snow-melting season in May. The Selenga River is the largest tributary into the lake and has built up an enormous delta, the Selenga Delta, separating the South from the Central Basin. The Barguzin River discharges into Barguzin Bay in the Central Basin while the Upper Angara River feeds into Listvenichnyi Bay in the North Basin at the northernmost part (Figure 3.2), where for both bays relatively low Secchi depth measurements (approximately 15 m), at least for Lake Baikal, are reported in open waters [*Shimaraev et al.,* 1994].

4 OBSERVATIONS AND METHODOLOGY

4.1 OBSERVATIONS USED FOR AN OCEAN COLOUR STUDY AT LAKE BAIKAL

The observational data used for the presented Ocean Colour Study at Lake Baikal is composed of the following types of spectral data: the High Resolution Picture Transmission (HRPT) SeaWiFS satellite data and field-spectrometer measurements (GER1500, Geophysical & Environmental Research Corporation, New York, USA). Limnological ground-truth data from CONTINENT field investigations provide the data-sets to evaluate and validate the spectral methodology on the other hand. In addition, the accompanying investigations within the framework of this Ocean Colour study have been assisting the set-up of the Baikal Web-GIS on the public GFZ server domain (*http://continent.gfz-potsdam.de*) to visualize CONTINENT field data and to undertake areal quantification. Further investigations of field-spectrometer (GER1500 and FieldSpec ASD, Analytical Spectral Device, Boulder, USA) and laboratory spectrophotometer (Lambda19, Lambda950, Perkin Elmer, Boston, USA) measurement techniques have been undertaken within the framework of bio-optical investigations of the Brandenburg and Mecklenburg lake districts (Germany).

Table 4.1: Observational data of this Ocean Colour study.

	Observational data	**Type**	**Time frame**
Lake Baikal (RU)	Ocean Colour data	Top-of-Atmosphere Reflectances	June 2001 to December 2002
	GER1500 field-spectrometer data	Water Volume Reflectances, Remote Sensing Reflectances	CON01-2,-5, CON02-8, CON03-9
	NOVA60 spectroquant laboratory spectrometer data	cDOM	CON02-8, CON03-9
	Limnological ground-truth data	Pigments, phytoplankton composition, SPM, DOC	CON01-2,-5, CON02-8, CON03-9, + SRIB seasonal data
	GIS layers (point, vector, polygon)	Field samples, geology, pedology, river net, DEM, *etc* [e.g., *Heim et al.*, 2003]	-
	Observational data	**Type**	**Time frame**
Rheinsberg and Brandenburg lake districts (Germany)	GER1500 and ASD field-spectrometer data	Water Volume Reflectances, Surface Reflectances	August to October 2002, April to September 2003
	LAMBDA19 laboratory spectrometer data	CDOM, phytoplankton absorption	Spring/summer 2003 and 2004
	Limnological ground-truth data	Chl-*a*, phytoplankton composition, SPM, DOC	August to October 2002, April to September 2003

4.1.1 SeaWiFS Satellite Data

The Sea-viewing Wide Field-of-view Sensor (SeaWiFS) is on board the Orbimage2 satellite on a 705 km circular orbit with a revisit time of one to two days. The sensor consists of 8 bands at: 412, 443, 490, 510, 555, 670, 765, and 865 nm, each with band widths of 20 or 40 nm (Table 2 in Heim et al. [2005]). Incoming scene radiation from the atmosphere and earth's surface is continuously collected by a telescope and reflected onto a rotating half-angle mirror (Figure 4.1) Beam splitters separate the radiation into four wavelength intervals, of which the radiation is further separated through spectral filters into the required eight spectral SeaWiFS bands.

The advancing scanning device picks up radiation from a lateral ground distance of 1.1 km. Like this, the detectors image a two-dimensional, instantaneous Field-of-View (IFOV) that expresses the effective spatial instrument resolution. The spatial resolution in the Local Area Coverage (LAC) and HRPT mode is ≈ 1.1 km, and in the Global Area Coverage (GAC) mode it is 4 km. Swath widths are: LAC = 2801 km; GAC = 1502 km. For each band, the electronic IFOV results in a single digital number (DN), representing the picture element (pixel) of a SeaWiFS image.

SeaWiFS has been especially constructed to spectroradiometrically measure the low upwelling signal from water bodies: the outputs from four detectors within one band each are added to improve the signal-to-noise ratios. In addition, the optics are oriented to +20°, 0°, or -20° from nadir in the along-track direction to minimize the effects of sun glint on the data. The radiometric performance of SeaWiFS is still high, and there is no sign to date of uncorrected changes in the radiometric sensitivity in any of the instrument bands. The radiometric model for SeaWiFS is designed to incorporate the laboratory calibration of the instrument with on-orbit changes over time [*Barnes and Zalusk*, 2003]. In addition to the original calibration of the radiometer, solar and lunar measurements are made in orbit to monitor instrumental drift, along with comparisons with shipborne data and buoys to check the quality of the onboard calibration.

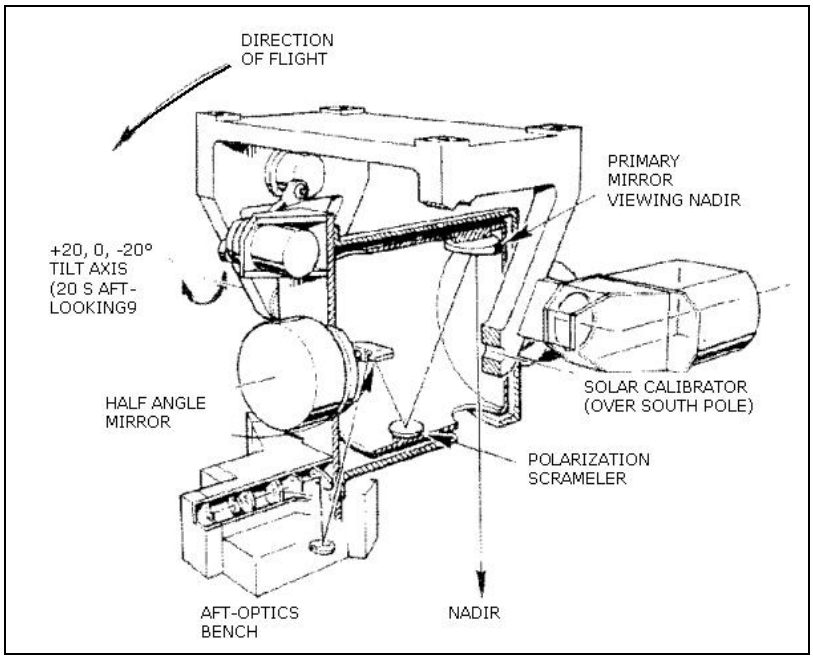

Figure 4.1: Schematic of the SeaWiFS scanner that scans from west to east.

From summer 2001 (2001/06/25) to winter 2002 (2002/12/31), the Ministry of Nature and the Environment in Ulaan Baatar, Mongolia, provided HRPT SeaWiFS data-sets for the CONTINENT project. Table 3 in Heim et al. [2005] gives an overview of the SeaWiFS data that was of adequate quality (radiometry, cloud cover, sensor zenith, season) to be processed as part of this study.

4.1.2 CONTINENT Field Investigations

The summer CONTINENT field work took place in July 2001, 2002 and 2003, when wind conditions across Lake Baikal were relatively moderate. However, the drawback for remote-sensing applications at Lake Baikal during this time is the problem of high cloud and fog coverage (§3.3).

The CONTINENT ship cruises on the Russian Research Vessel (RV) *'Vereshchagin'* covered the South, Central, and North basins (Figure 4.2). Geochemical and geological investigations (Table 4.1) were made on land within the catchment area of the Selenga River, where surface water was sampled from the Mongolian border, along the course of the Selenga River through to the Khamer Daban mountain range, towards the Selenga Delta (Figure 4.2).

The CONTINENT cruises were dedicated to coring activities, deploying and recovering mooring instrumentations and sediment traps. The bio-optical investigations were undertaken within the framework of the limnological and geochemical studies, without the specified technical equipment required according to the Ocean Optics Protocols [2000], as this was never part of the CONTINENT funding plan. GER1500 field-spectrometer measurements were performed at 10 stations above Selenga river surface waters, and at 15 to 20 stations in Lake Baikal in 2001, 2002 and 2003 [*Heim et al.,* 2003]. Another responsibility of the author was to establish a Suspended Particulate Matter (*SPM*) ground-truth data-set and to analyse for coloured Dissolved Organic Matter (*cDOM*).

All limnological parameters that are necessary for an Ocean Colour study or to support the interpretation are described in Table 4.2. An overview of the collaborating institutes and subcontractors is given in Table 1, Annex B. The most important data-set for remote-sensing ground-truth is represented by the pigment data-set that has been generated by Fietz (IGB, Germany) [*Fietz and Nicklisch*, 2004; *Heim et al.,* 2005]. To gain seasonal information, weekly phytoplankton sampling from May 2002 to June 2003 was conducted by SRIB, 2 km offshore from the Biological Station *Bolshye Koti* (South-West coast), [*Fietz et al.,* 2005].

In addition, monitoring data from 2001 to 2003 that has been processed at *Bolshye Koti* was processed by Kobanova and Ismest'eva and has been incorporated into the CONTINENT study by Straskrabova et al. [2005].

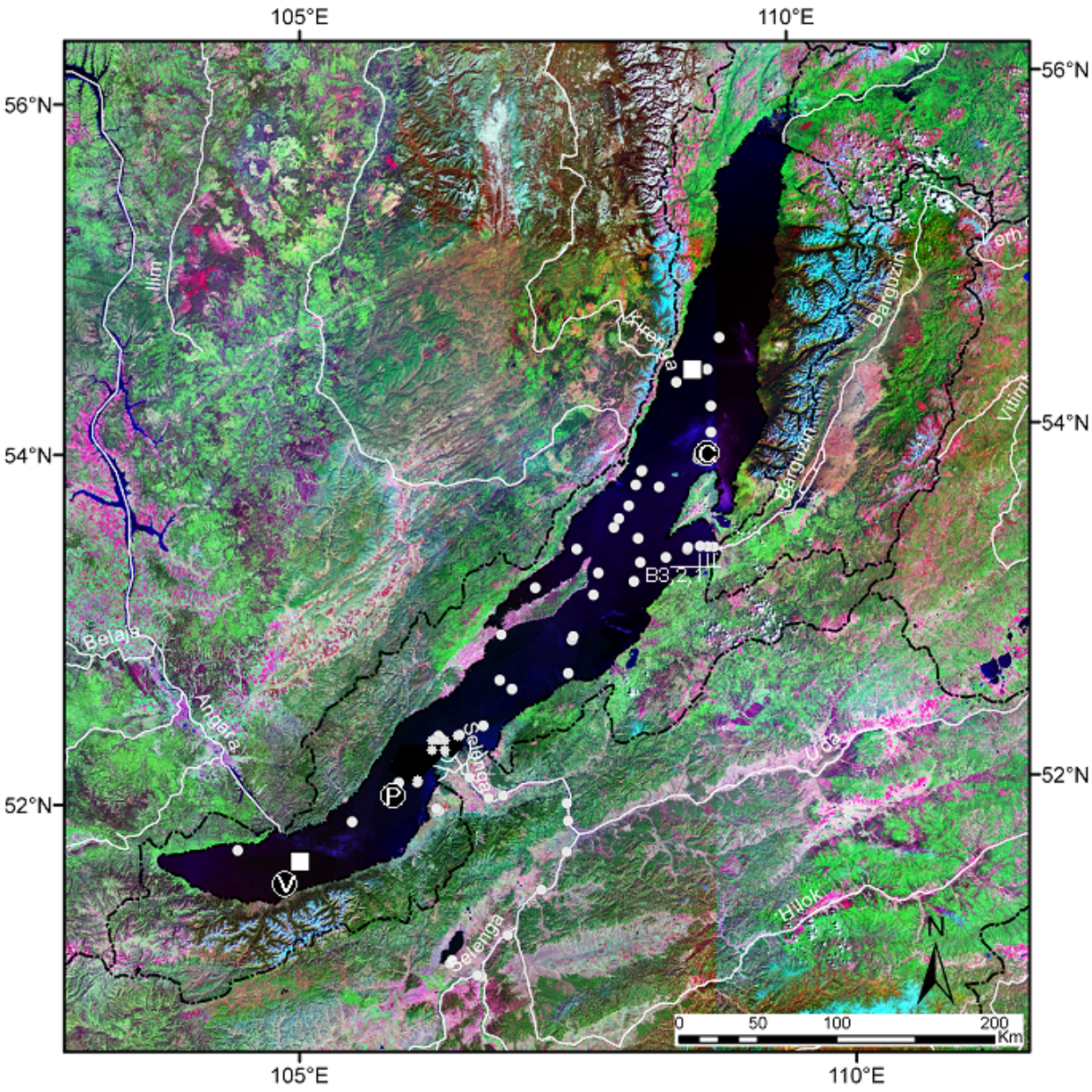

Figure 4.2: Landsat TM-MOSAIC RGB742 (UTM 48), source: Baikal Online-GIS: *http://dc108.gfz-potsdam.de/website/*. The satellite map shows the Lake Baikal area, the three CONTINENT coring sites (C = Continent, P = Posolsky, V = Vydrina), the sediment traps (squares), plus the stations where bio-optical data were collected in 2001, 2002, and 2003 (circles).
Additionally, note the transect sampling at B1, B2 and B3 in Barguzin Bay.

Table 4.2: CONTINENT cruise parameters (2001, 2002, 2003)

CONTINENT field expedition	Region (pref. visited)	Parameter	Method	Researcher (Institute)	Sampling depths (m)
CON01-2 2001 25/06 – 07/07	Selenga River catchment	SPM	Gravimetric method	Birgit Heim (GFZ)	0.5
		Mineralogy, geochemistry	X-ray Mass spectrometry	Nathalie Fagel (ULG)	0.5 , Bottom sediments
	Selenga River catchment	Spectro-radiometry	GER 1500 spectrometer	Birgit Heim (GFZ)	0.5
CON01-4 2001 15/07 – 25/07	Lake Baikal (South and Central basins)	Phytoplankton pigments Phytoplankton composition	HPLC Epifluorescence microscope	Susanne Fietz (IGB)	0.5, 5, 10, 30
	Lake Baikal (South Basin)	SPM	Gravimetric method	Birgit Heim (GFZ)	0.5, 5
	Lake Baikal (South Basin)	Spectro-radiometry	GER 1500 spectrometer	Birgit Heim (GFZ)	0.5, 3, 5
CON01-5 2001 26/07 – 04/08	Lake Baikal	Diatom taxa	Light microscope	UCL	Depth profiles
CON02-8 2002 05/07 – 015/07	Lake Baikal (Central and North Basin)	Phytoplankton pigments Phytoplankton composition	HPLC Epifluorescence microscope	Susanne Fietz (IGB)	5, 10, 30
	Lake Baikal (Central Basin)	DOC	0.2 µm filters HTCO	Rosell-Melé	5 , 10
	Lake Baikal (Central Basin)	SPM	Gravimetric method	Birgit Heim (GFZ)	5
	Lake Baikal (Central and North basins)	Spectro-fluoremetry	Moldaenke FluoroProbe	Andreas Niklisch (HU) Susanne Fietz (IGB)	Depth profiles
	Lake Baikal (Central Basin)	Spectro-radiometry	GER 1500 spectrometer	Birgit Heim (GFZ)	0.5, 5
	Lake Baikal (Central and North basins)	CTD	SeaBird sensor	LIN	Depth profiles
CON03-9 2003 04/07 – 014/07	Lake Baikal	Phytoplankton pigments Phytoplankton composition	HPLC Epifluorescence microscope	Susanne Fietz (IGB)	5, 10, 30
	Lake Baikal	Spectro-fluoremetry	Moldaenke fluoroprobe	Susanne Fietz (IGB)	Depth profiles, horiz. transects
	Lake Baikal	CTD	SeaBird sensor	LIN	Depth profiles
	Lake Baikal	SPM	Gravimetric method	Birgit Heim (GFZ)	5
	Lake Baikal	Spectro-radiometry	GER 1500 spectrometer	Birgit Heim (GFZ)	0.5, 5
	Lake Baikal	Primary production	Black and light glass flasks with bicarbonate	Vera Straskrabova (HBU)	5
	Lake Baikal	DOC	0.45 µm filters HTCO	Jacub Borovec (HBU)	5

4.1.3 Web Baikal Geographical Information System

Geographical Information Systems (GIS), specifically on-line GIS, are a tool to communicate in interdisciplinary projects, and to visualize and analyse project data. Therefore, the Baikal Web-GIS has been established on the public domain of the GFZ data centre [Heim et al., 2003].

The CONTINENT project data has been integrated (for example, the field sampling stations, the bathymetry, and lake sediment types) (*http://dc108.gfz-potsdam.de*). Then, various public available spatial data-sets from Southern Siberia and Mongolia were searched for (e.g., Geology, Pedology, Hydrology) and were made compatible for the Baikal GIS. Swiercz et al. [2003] and Swiercz [2004] contributed geographical and climatical spatial data-sets (e.g., Land Use, Precipitation), and the delineation of the lake and the main river catchment areas (Selenga-, Upper Angara-, and Barguzin) of Lake Baikal.

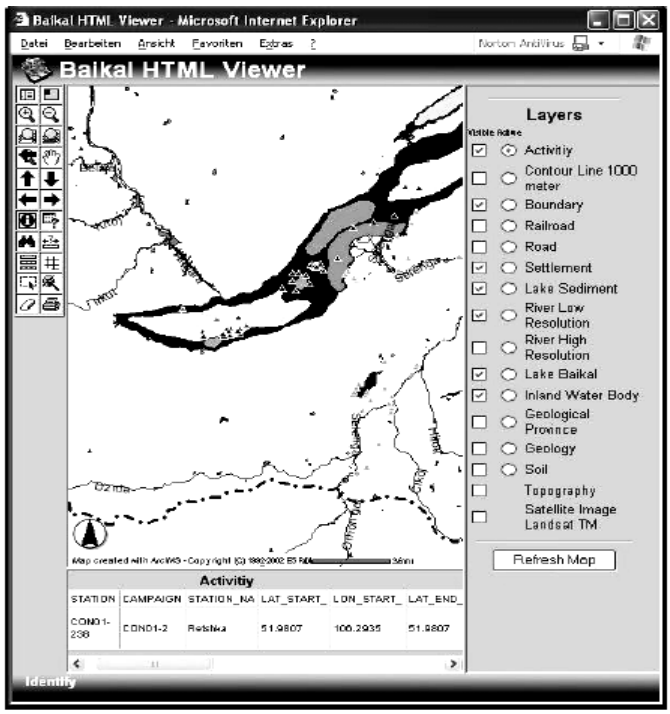

Figure 4.3: Snapshot of the CONTINENT Baikal Web-GIS, (*http://dc108.gfz-potsdam.de*).

4.1.4 Bio-optical Studies in the Brandenburg and Mecklenburg Lake Districts (Germany)

Within the framework of a principal investigation of hyperspectral and multiangle Compact High Resolution Imaging Spectrometer (CHRIS) sensor data onboard the ESA research platform Project for On Board Autonomy (PROBA) [*ESA Scientific Campaign Unit,* 1999], trophic parameters for water quality were investigated in the Brandenburg and Mecklenburg lake districts (Germany) [*Mannheim et al.,* 2004a; *Mannheim et al.*, 2004b]. During summer to autumn 2002, 2003, and 2004, field investigations with concomitant water sampling and field-spectrometer measurements took place on lakes covering a wide range of different trophic states.

The author organized the 2002 CHRIS-PROBA field campaigns and laboratory work, and was involved in coorganizing field work, planning sampling sites and assisting with the sampling and field-laboratory work in 2003. Ground-truth data collected were Chl-*a*, SPM, DOC, Secchi depth and field-spectrometer measurements. During these field campaigns, ground truth field techniques on water could be optimised such as field spectrometer measurements within the water body and instant sample handling for SPM and cDOM analyses. The author initiated laboratory spectroradiometrical measurements (Figure 4.4) of water filtrates and phytoplankton filters to extract lake specific values of cDOM and a_{phyto}.

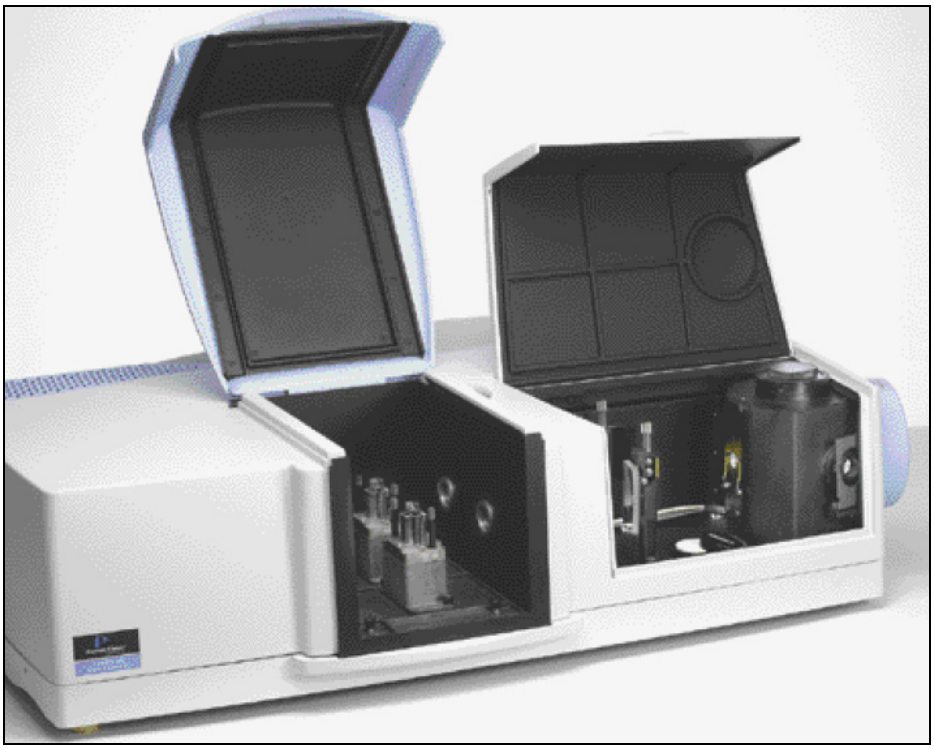

Figure 4.4: Universal Reflectance Accessory of the PerkinElmer Lambda950 UV/VIS/NIR spectrophotometer

4.2 METHODOLOGY OF OCEAN COLOUR DATA ANALYSES AND FIELD WORK

The Ocean Colour study undertaken for Lake Baikal involved the following activities that are discussed in detail:

i) Investigation of the regional characteristics of the atmospheric layer (§4.2.1, §5.1)

ii) Definition of the best-fit SeaDAS parameter set up for atmospheric correction of the HRPT SeaWiFS data of Lake Baikal (§4.2.1, §5.1, §6.1)

iii) Investigation of the regional Ocean Colour algorithms (arithmetic operations using spectral reflectance data of Lake Baikal and CONTINENT ground-truth data) (§4.2.2, §5.3.1, §6.4.1)

iv) Investigation of the standard Ocean Colour algorithms (global Chl-*a* algorithms + Chl-*a* and SPM algorithms from the literature) (§4.2.2, §5.3.1, §6.4.1)

v) Spectral characterization of field-spectrometer reflectances and atmospherical-corrected SeaWiFS reflectances (§5.2, §6.2, §6.3)

vi) Evaluation of the Chl-*a* and SPM products against the CONTINENT ground-truth data (§5.3.1, §5.3.2, §6.4.1, §6.4.2., §6.4.3)

vii) Calculation of the Chl-*a* and SPM maps from atmospheric-corrected SeaWiFS reflectances using the best performing algorithms (§6.4.1, §6.4.3)

viii) Observation of the regional spatial patterns of Lake Baikal (§6.5.2, §6.5.3)

ix) Observation of the seasonal dynamics of Lake Baikal (§6.5.1, §6.5.4, §6.5.7)

Table 4.3: Methodologies for an Ocean Colour study at Lake Baikal, Siberia.

Atmospheric correction	Regional characteristics	Atmospheric layer above Lake Baikal
	Best-fit parameter set-up	SeaDAS atmospheric correction
Ocean Colour algorithms	Investigation	Regional OC algorithms [Chl-*a*, SPM]
	Investigation	Standard OC algorithms [Chl-*a*, SPM]
	Evaluation	OC products [Chl-*a*, SPM]
Spectral characterization	Bio-optical specification Case 1, Case 2 waters	Field-spectrometer spectra; SeaWiFS spectra
Ocean Colour maps	Generation	Time series of maps [Chl-*a*, SPM]
	Observation	Spatial patterns [Chl-*a*, SPM]
	Observation	Seasonal dynamics [Chl-*a*, SPM]

4.2.1 Atmospheric Correction and Processing of SeaWiFS Satellite Data

The SeaWiFS Data Analysis System (SeaDAS) [*McClain et al.,* 2000] offers defined standard atmospheric-correction methods for the marine environment. The source code and documentation of SeaDAS (NASA) is freely available in the public domain (*http://seadas.gsfc.nasa.gov/*). SeaDAS is capable of determing the atmospheric correction of the Top-of-Atmosphere Radiance, L_{TOA}, from several Ocean Colour sensors, such as SeaWiFS, OCTS, MOS, OSMI, POLDER, and - since SeaDAS Version 4.5 and 4.6 -, MODIS AQUA and TERRA data (§1.2). By using the Multi-Sensor Level-1 to Level-2 (MSL12) processing code developed by the Sensor Intercomparison and Merger for Bio-optical and Interdisciplinary Oceanic Studies (SIMBIOS) project, SeaDAS provides user-friendly applications of calculating atmospheric and bio-optical parameters.

For the atmospheric correction, the radiative transfer [*Gordon and Wang*, 1994; *Gordon*, 1997] is described in a simplified form by :

$$R_{TOA}(\lambda) = \left[\rho_r(\lambda_1) + \rho_a(\lambda_1) + \rho_{ra}(\lambda_1) + t(\lambda_1)\rho_f(\lambda_1) + t(\lambda_1,\mu)\rho_w(\lambda_1)\right] \times t_g(\lambda_1) \qquad (4.1)$$

where λ_i is the centre wavelength for the SeaWiFS channel, and μ is the cosine of the satellite-viewing angle. As introduced in §2.2, ρ_r is the Rayleigh reflectance, ρ_a is the aerosol reflectance, ρ_{ra} is the multiple interaction term between air molecules and aerosols, ρ_f represents the direct reflection from skylight at the air-water interface, and ρ_w is the water-leaving reflectance. The *t*

term is the atmospheric diffuse transmittance, the t_g term represents the gaseous transmittance. Please note that the sunglint, ρ_g, can be omitted in equation (4.1) in contrast to equation (3.11), owing to the sensor's tilt of ± 20, avoiding sunglint.

Pre-calculated tables are provided for diffuse transmittance, $t(\lambda)$, by oxygen and ozone absorption. For the Rayleigh correction, SeaDAS offers pre-calculated Rayleigh-radiance tables that have been generated using the method developed by Gordon and Wang (1992) for various ocean-surface wind speeds. In this SeaWiFS study, specific barometric pressure values obtained from the Irkutsk meteorological station (469 m NN) *(http://meteo.infospace.ru/wcarch/html/e_day_stn.sht ?num =1808*) and corrected to the average lake level of Lake Baikal (456.5 m NN), were incorporated.

There are pre-calculated tables available for the Rayleigh-aerosol transmittance, and aerosol tables have been derived from radiative-transfer simulations that are based on aerosol models developed by Shettle and Fenn [1979]. The set-up of aerosol models (Table 4.4) represents atmospheric conditions over the world oceans. Oceanic and maritime aerosol models are characterized by relatively large particles, namely the sea-salt aerosols (diameter up to 10 µm). The coastal aerosol models are dominated by the rural aerosol component with an order-of-magnitude smaller particle-size distribution (≤ 0.5 µm). In addition, there is the choice in SeaDAS of the CZSC 'single scattering white aerosol model', and the 'band 7/8' model. By choosing the 'band 7/8' model, the single scattering ratio values of the Rayleigh-corrected reflectance in SeaWiFS band 7 against the Rayleigh-corrected reflectance in band 8, $\varepsilon^{(7,8)}$, are evaluated (§2.2). Unusually large epsilons, $\varepsilon > 1.4$, may be indicative of non-zero water-leaving radiances in the near-infrared.

Before SeaDAS4.4, the implementation of the Management Unit of the North Sea Mathematical Models (MUMM) turbid water correction [*Ruddick et al.*, 2000] into SeaDAS overcame the problems associated with unnaturally-large single-scattering aerosol-reflectance ratio values, ε, due to turbid waters [*Heim et al.,* 2004]. The MUMM tool fixed ε values for each data-set by selecting it manually (in scatter plots) from the group of lowest reflectances. In SeaDAS4.4, this problem can be fixed within the SeaDAS process itself.

Figure 4.5 visualizes the SeaDAS processing scheme used in this study: First, HRPT Level 1A data (Ulaan Baatar, Mongolia) was converted into Level 1B data, the L_{TOA} data, by using internal header information. The MSL12 processing code normalizes the nominal L_{TOA} values by nominal band solar irradiance E_{sol} values to calculate R_{TOA}. Automatical cloud masking is set by standard or flexible thresholds.

A correction removes the Fresnel effect in accordance with bidirectional factors [*Morel and Mueller,* 2002]. A bidirectionally shadowing factor for groups of wave facets is involved in all computations [*Gordon and Wang*, 1992]. SeaDAS has adopted the Frouin et al. [1996] results (with updates) for the spectral dependence of foam radiance and the results from Moore et al. [2000] for the magnitude of the whitecap contributions (assumed from high wind speeds > 8 ms^{-1}).

Table 4.4: SeaDAS aerosol models.

Model N°	Aerosol Model	Relative Humidity [%]	Symbol
1	**Oceanic**	**99**	O99
2-5	**Maritime**	**50, 70, 90, and 99**	M50 to M99
6-9	**Coastal**	**50, 70, 90, and 99**	C50 to C99
10-12	**Tropospheric**	**50, 90, and 99**	T50, T90, and T99

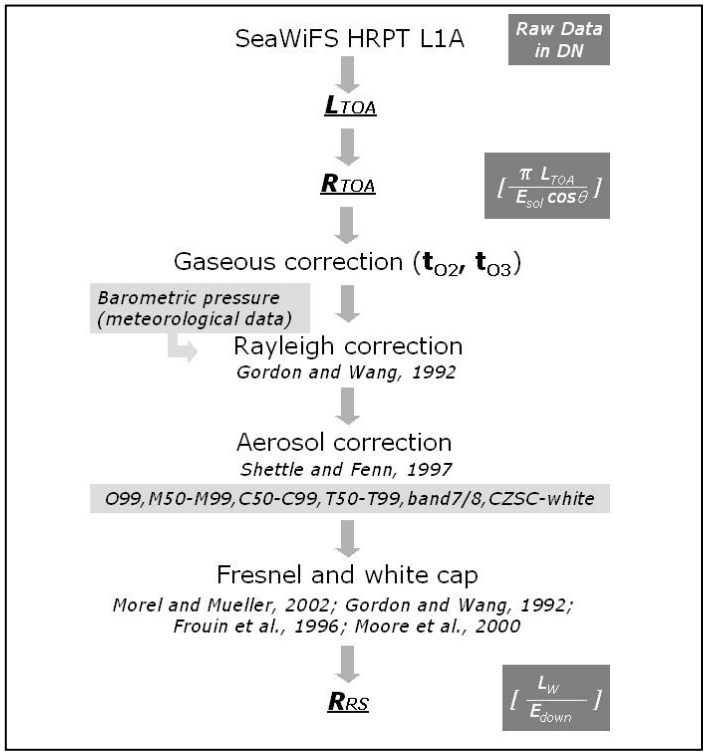

Figure 4.5 Flow chart of the SeaDAS processing applied in this study. Generally, the SeaDAS standard processing is performed choosing the 'band 7/8' model. The aerosol models, 099, M50 to M99, C50 to C99, T50 to T99, are explained in Table 4.4. *Radiance Top-of-Atmosphere* L_{TOA}; *Reflectance Top-of-Atmosphere* R_{TOA}; *Remote-sensing Reflectance* R_{RS}; *diffuse oxygen transmittance* t_{O2}; *diffuse ozone transmittance* t_{O3}.

To estimate disturbing factors for atmospheric correction required for the Baikal region, the presence of absorbing aerosols was investigated by analyzing the Total Ozone Mapping Spectrophotometer (TOMS) aerosol index (AI) climatologies for the dates of the assessed SeasWiFS acquisitions. In addition, available AErosol RObotic NETwork (AERONET) ground data from central Siberian stations were examined. AERONET data provides information about aerosol optical thickness (AOT), $\tau_a(\lambda)$, and on the Ångström coefficient α, indicating the particle size distribution. Stations were Tomsk (ca 1400 km from Lake Baikal), Krasnoyarsk (ca. 1100 km distance from Lake Baikal) and Irkutsk. The Irkutsk AERONET station (Institute of Solar-Terrestrial Physics, Irkutsk) has been established in 2003 in the Sayan Mountains and only provided two measurements (24 and 25 June) for the year 2003 and few days in January to March 2004.

Summary

Processing and analyses of HRPT SeaWiFS data for Lake Baikal have been established as follows: HRPT SeaWiFS Level 1A data was converted towards Level 1B L_{TOA} data, and atmospherically-corrected according to specific barometric pressure values and using the fixed SeaDAS aerosol models and the SeaDAS 'band 7/8' model.

Then, the atmospherically-corrected data-sets were successively georeferenced to Universal Transversal Mercator (UTM) projection, zone 48, World Geodetic System (WGS) 84, using internal header information. Lake Baikal stretches over three UTM zones (zone 47, 48, 49), whereby zone 48 is the central UTM zone. Further processing included enhanced georeferencing using the image analysing software IMAGINE® (ESRI) as follows: First, SeaWiFS master scenes with low cloud

cover were georeferenced to UTM projection, zone 48, WGS 84, according Tactical Pilotage Chart (TPC); Second, the SeaWiFS data-set was georeferenced image to image by using these SeaWiFS Master scenes.

Implementation and testing of algorithms (e.g., band-arithmetical operations) was conducted with the image analysing software ENVI® (RSI). Regions of Interest (ROI) were defined so as to calculate regionally averaged values. Ground-truth was linked to the new generated, high-level satellite products (Remote Sensing Reflectance (R_{RS}), diffuse attenuation coefficient at 490 nm (K490), chlorophyll (Chl-*a*), Suspended Particulate Matter (SPM). This was executed within SeaDAS by using the ship track mode with choices of scattergrams and data profiles.

4.2.2 Ocean Colour Algorithms

Ocean Colour – Attenuation Coefficient Algorithm

The beam-attenuation coefficient, *c*, is an inherent optical property (IOP) (§2.2), and incorporates absorbing, *a*, and scattering, *b*, processes, as defined by $c = a + b$ [*Kirk,* 1976]. On the other side, inside a water body, the attenuation coefficient is measured diffusely as an apparent optical property (AOP), and is then termed the diffuse attenuation coefficient, K. It quantitatively describes the rate at which the irradiance is attenuated in meters. The remote-sensing K_{down} is an averaged expression over the first irradiance attenuation depth.

O'Reilly et al [2000] defined SeaDAS Level 2 output K_{down} at 490 nm, K490, based on regression analyses from n = 319 samples. The K490 was tested on ground-truth data (n = 293) from the SeaBAM data-set (§1.2) and performed for K490 < 0.25 m^{-1} with an accuracy of ± 26 %, and for K490 > 0.25 m^{-1} with an accuracy of ± 48 %. The K40 algorithm is defined as:

$$K490 = Kw490 + 0.15645 \times (L_w490/ L_w555)^{-1.5401} \text{ in } [\ m^{-1}] \quad (4.2)$$

where Kw490 represents the value for pure water (0.016 m^{-1}), while the SeaWiFS input data is the normalized L_w value at 490 nm (band4) and 555 nm (band 5).

Ocean Colour - Chlorophyll Algorithms

The accuracy and utility of empirical algorithms are, naturally, highly dependent upon the quality and accuracy of the field data. The high-quality global OC2 and OC4 Chl-*a* algorithms have been established from the in-situ R_{RS} and Chl-*a* data of the SeaBAM ground-truth data-set (§1.2), globally covering a variety of oceanographic bio-optical provinces in different seasons. The first set of empirical coefficients for the 2-band OC2 and the 4-band OC4 algorithm is based on n = 919 observations [*O'Reilly et al.,* 1998]. The continuously growing and updated SeaBAM data-set shows presently the most equitable and dense distribution over the range of 0.03 to 3 µg l^{-1} Chl-*a*. The revised updates of the 4th OC algorithm version, the OC2v4 and OC4v4, are based on n = 2853 observations [*O'Reilly et al.,* 2000]. The OC2v4 and OC4v4 that are the current OC Chl-*a* algorithms are hereafter referred to as OC2 and OC4, respectively. The current OC2 uses a modified cubic polynomial equation, the current OC4 a fourth order polynomial (Table 4.5). These global band ratio *Chl-a* algorithms achieve accuracies of better than ± 35 % in Case 1 conditions [*O'Reilly et al.,* 2000].

As another example for empirical Chl-*a* algorithms based on large data-sets are the investigations of Iluz et al. [2003]. Iluz et al. [2003] summarized a set of best-fit functions of the reflectance ratio $R_{RS}443/R_{RS}555$ that have been used by different authors for studies in ultra-oligotrophic to oligotrophic waters (Table 4.5).

Table 4.5: Ocean Colour Chl-*a* algorithms. Various sources.

Source	x = Ri/Rj (R = L_{up}/E_{down})	Chl-*a* algorithm
A OC2v4 global Chl-*a* O'Reilly et al. [2000]	x = log10{R490/R555}	$10^{\wedge}\{0.319 - (-2.336x) + 0.879(x^2) - 0.135(x^3) - 0.071(x^4)\}$
B OC4v4 global Chl-*a* O'Reilly et al. [2000]	x = log10 {R443/R555}, {R490/R555}, {R512/R555} (maximal ratio: MAX)	$10^{\wedge}\{0.366 - (-3.067x\ \mathrm{MAX}) + 1.93(x\ \mathrm{MAX}^2) + 0.649(x\ \mathrm{MAX}^3) + 1.532(x\ \mathrm{MAX}^4)\}$
F Iluz et al. [2003], Gulf of Eilat [Red Sea], years 1994 + 1995 + 1996, all seasons	x = R443/R550	$0.7\ x^{-0.98}$
G Iluz et al. [2003], Gulf of Eilat [Red Sea], year 1996, all seasons,	x = R443/R550	$1.27\ x^{-1.38}$
H Gordon et al. *Case 1* [1983] [in Iluz et al., 2003]	x = R443/R550	$1.13\ x^{-1.71}$

Generally, empirical Chl-*a* algorithms may be calculated from Chl-*a* ground-truth data by regression, most commonly with ratio combinations of atmospherically-corrected reflectance data of the nearest acquisition dates. The number of observations from the CONTINENT ground-truth data-set that are of a suitable quality to establish an empirical algorithm in this study, are n = 6 for 2001, and n = 20 for 2002.

Ocean Colour - Suspended Matter Algorithms

A large number of coastal sediment algorithms have been proposed since the launch of CZCS and its Ocean Colour successors, for example in Tassan and Sturm [1986]. The accepted principle for standard SPM algorithms holds that for increasing concentrations of SPM, the reflectance increases in the visible and near infrared spectrum [*Tassan*, 1994; *Peters et al.,* 1999]. Commonly, SPM algorithms are derived by correlating the green reflectance maximum and the in situ SPM data-set, such as in Peters et al. [1999] and Binding et al. [2003], while the height of the reflectance maximum may be normalized by dividing band 8 (850 nm) [*Doxaran et al.,* 2002] or multiplying the band ratio value of band 3 against band 4 [*Chaiham et al.*, 2001].

An operable empirical coastal SPM algorithm [*Jørgensen*, 2000] is established in the SISCAL (n = 45, Danish waters and North Sea, SPM range from 0.5 to 8 mg l^{-1}), consisting of:

$$TSM = 0.5619 \times R_{vol}(555nm) + 0.0932 \qquad (4.3)$$

where TSM is the Total Suspended Matter (equivalent to SPM), and R_{vol} is here defined in [%].

For more turbid waters, the change in absolute reflectance height in the green wavelength range seems to plateau to match a logarithmic distribution [*Froidefond et al.,* 2002; *Stumpf and Pennock*, 1989; *Ritchie et al.,* 1990; *Moore et al.,* 1999]. Therefore, in terms of empirical SeaWiFS SPM algorithms, the red to green reflectance ratio band 5 (555 nm)/band 6 (650 nm) is expected to perform for SPM algorithms of highly turbid coastal waters (approx. above 10 mg l^{-1}), reflecting the shift of the maxima in the reflectance spectra from green to red with increasing SPM concentrations [*Mitchelson-Jacob*, 1999; *Froidefond et al.*, 2002]. Commonly, these empirical SPM algorithms, which are based on the principle of rising reflectances, originate from coastal areas of the Mediterranean, Atlantic Ocean, and the North Sea.

4.2.3 Field Spectroradiometer Measurements

Information about the under-water light field was spectrometrically acquired using GER1500 field-spectrometer measurements. The GER1500 is a portable field-spectrometer that can be used hand held. The spectroradiometer's spectral range covers the ultra violet (UV) to the near infrared (NIR) (350 nm to 1050 nm) with a spectral resolution of approx. 3 nm Full Width Half Maximum (FWHM) for 512 channels. The entrance optical options are bare fiber optic (22° Field of View (FOV)), connection optics with 4° and 8° FOV and cosine receptor (180° FOV).

For measurements of the underwater light field, the instrumentation consists of a combination of two GER1500 field-spectrometers, where one is connected to an 11 m fibre optic cable (Figure 4.6). The choice of different calibrated optics allows measurement of the downwelling irradiances and radiances E_{down}, L_{down}, and the upwelling irradiances and radiances, E_{up}, L_{up} (§2.2). The equipment requires only a few minutes to set up and allows simultaneous measurements of the signal inside the waterbody, and the downwelling signal above the water body. The field-spectrometer measurements were undertaken from board the RV 'Vereshchagin' (see also Figure 4.6). The bilge of the RV 'Vereshchagin' is within a 2 to 3 m distance to the sensor head, depending on depth and lake conditions. The bilge of the 'Vereshchagin' is orange-painted below the waterline.

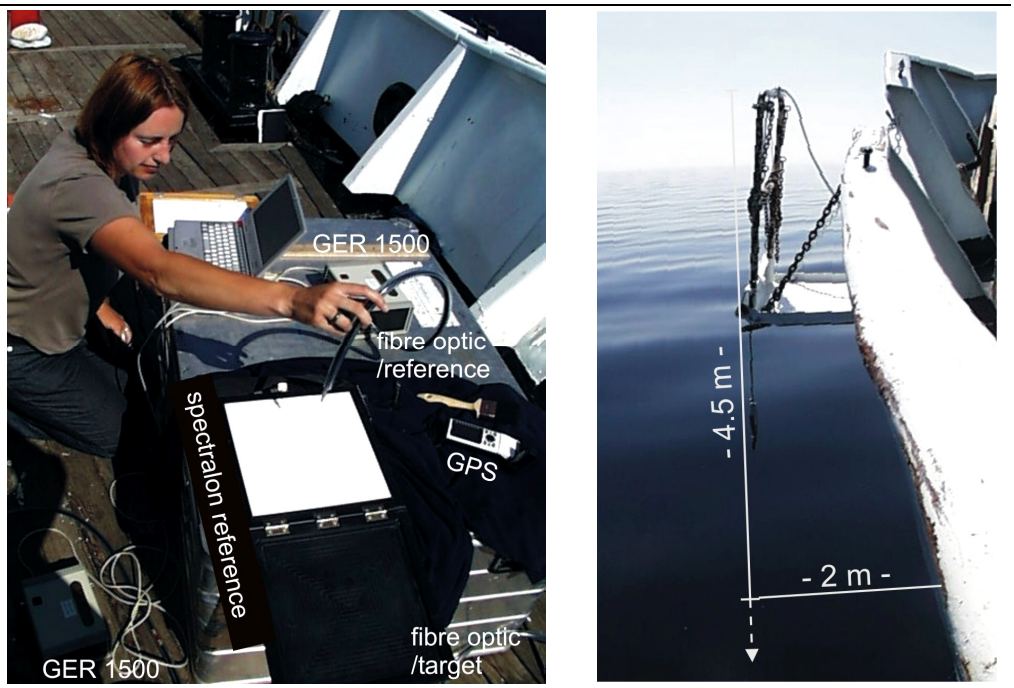

Figure 4.6: GER1500 measurement configuration on board the RV *'Vereshchagin'*.
The left photo shows the spectralon reference measurement of downwelling spectral solar radiances.
The right photo shows the lowering of the GER1500 fibre optic for underwater radiance measurements.

The drawback of this non-commercial GER1500 instrument arrangement is that is does not achieve the accuracy requirements as proposed in the Ocean Optic Protocols [2000]. It is not possible to deploy the sensor away from the ship, nor is it constructed to measure continuously and exactly at a given depth, nor concomitant measurements of E_{up} and E_{down} in same depths, as is the case for submersible spectroradiometer. Additionally, the 11 m fibre optic dramatically attenuates the recorded light. Despite these limitations on absolute reflectance measurements, the GER data are of value, providing information about spectral features of the underwater light field with a high-spectral resolution of 3 nm.

As outlined in the SIMBIOS Ocean Optic Protocols, uncertainties even in optimized spectroradiometric measurements are the perturbations of the in-water light field by the ship's movements [*Gordon*, 1985; *Smith and Baker*, 1986], shading by the sensor itself [*Gordon and Ding*, 1992], and the influence of ship's shadow [*Gordon*, 1985]. Surface waves may also cause temporal and spatial variations such as bright flashes and shadow-like features in E_{up} and L_{up} measurements [*Zaneveld et al.,* 2001]. The uncertainties for determining R_{RS} from above-water radiometric measurements are even more poorly understood, owing to difficulties in accurately removing the contribution of directly-reflected skylight [e.g., *Toole et al.,* 2000].

During CONTINENT cruises, on-board measurements at stations were made as follows:

$E_{down}(0+)$ was measured by using a cosine receptor. The repeated measurements (n = 10) took place on board the ship, preferably at the bow, avoiding spectral contamination by the substructure of the research vessel as best as possible (CON01-5, CON02-8, CON03-9).

$L_{down}(0+)$ was repeatedly measured (n = 10) from a 99 % reflective diffuse spectralon™ plaque by using a 20° fiber optic. The reference GER1500 instrument never recorded the water radiances, therefore there was no danger of target-sensor oversaturation due to the white 99 % reflective spectralon[1] (CON1-5, CON02-8).

Repeated measurements of the sky radiance, L_{sky}, (n = 10) were done using the fiber optic with a +40° degree angle to zenith, preferable 135° azimuth to the sun, according to the Ocean Optics Protocols [2000] (CON02-8).

Repeated measurements of $L_{up}(0+)$ above the water (n = 10) were done with the fiber optic with a -40° degree angle to zenith, preferable 135° azimuth to the sun, according to the Ocean Optics Protocols [2000]. The system was mounted in front of the ship to avoid possible signal contamination by oil, foam and the ship's wake (CON02-8).

Inside the water body, measurements at stations were made as follows:

$E_{up}(z-)$ at several depths z was repeatedly measured (n = 10) using a cosine receptor mounted on the 11 m fiber optic (CON01-2, CON01-5, CON02-8, CON03-9).

L_{up} (z-) was repeatedly measured (n = 10) with the bare 11 m fiber optic (CON01-2, CON01-5, CON02-8).

The underwater light field was measured within a depth range of 1 to 5 meters. Deeper measurements were not possible from the RV 'Vereshchagin' due to limitations of the 11 m fibre optic-cable. The field-spectrometer measurements were undertaken at as many sampling stations as possible. Tables 2a,b in Annex B give an overview of the locations and - often unfavourable - measurement conditions for the spectro-radiometrical field measurements.

[1] Therefore, there was no need to use a gray 10 % reflective spectralon plate (as proposed in Carder and Steward [1985], and Hooker et al. [1999]).

The recalculation of the field measurements are based on the principles described in §2.2.:

A . $R_{vol}(0-) = \frac{E_{up}(0-)}{E_{down}(0-)}$

1. E_{down} (0+) was corrected towards E_{down} (0-), by using [*Gordon et al.*, 1988a]:

$$E_{down}(0-) = 0.96 E_{down}(0+) \quad (4.4)$$

2. The vertical-upwelling diffuse attenuation coefficient, $K_{up}[z]$ was estimated within a depth interval spanning 4 meters (traditionally, Δ z is taken from a distance of approximately 2 to 4 m [*Smith and Baker*, 1983]):

$$K_{up}(z) = -\Delta E_{up}(z-) / E_{up}(z-)\Delta z \quad (4.5)$$

E_{up}(z-) and L_{up}(z-) had to be extrapolated towards the subsurface using equation (2.6).

B $R_{RS}(0+) = \frac{L_w(0+)}{E_{down}(0+)}$ [sr^{-1}]

R_{RS}(0+) was calculated using equation (2.9), where Q was assumed to be equal to 5 [*Mueller and Austin*, 1995], and the ratio between the below and above water radiance is assumed to equal 0.55 (§2.2). A difficult approach is to calculate R_{RS}(0+) from above water and sky radiance measurements using equation (2.10). The method had considerable limitations due to unfavourable weather conditions (Annex A, tables 2a,b).

4.2.4 CONTINENT Limnological Investigation

Water samples were taken on the first cruise in 2001 from subsurface (bucket sampling), from 0.5 m, 5 m, 10 m, and 30 m depths (Figure 4.7). The pigment analyses [pers., Fietz, 2002] indicated that bucket sampling from a moving ship at Lake Baikal was inaccurate. Concentrations of the 0.5 m sample in 2001 were generally conforming to concentrations at 5 m depth. Therefore, the sampling depths during the CONTINENT cruises 2002 and 2003 started from 5 m, and continued to 10 m, 30 m, plus additional depths, if the fluorescence-probe measurements that started in 2002, indicated phytoplankton subsurface maxima at these depths.

Pigments. Duplicate samples for HPLC-aided pigment determination were filtered on CON01-4 (2001), CON02-8 (2002), and CON03-9 (2003) on board the ship through glass-fiber GF/F filters (0.7 µm pore-size) (Whatman, Kent, UK) placed into 2 ml reaction vessels, and immediately freeze-dried and stored frozen in darkness. Chlorophylls, carotenoids, and their derivatives were extracted in organic solvents as described in Fietz [2005]. The separation, identification and quantification of pigments were performed according to Woitke et al. [1994] with a Waters HPLC system described by Fietz and Nicklisch [2004].

Phytoplankton. Nano- and microphytoplankton and autotrophic picoplankton were counted under light and epifluorescence microscopes [*Fietz and Nicklisch*, 2004}.

Primary Production Primary production was measured using black and light quartz glass flasks (130 ml) with added ^{14}C bicarbonate (described in Straskrabova et al. [1999]) on CON03-9 (July 2003) (Figure 4.7).

Upper left: Water sampling at Lake Baikal (S. Fietz, IGB) for Chl-*a* and SPM ground-truth on CON01-5 (July 2001)

Lower left: Differently shaded quartz glass flasks in container onboard ship on CON03-9 (July 2003) used for measurements of primary production (V. Straskrabova, HUB).

Right: Filtering in Gusinosersk (RU) (N. Fagel, F. Hauregard, ULG and B. Heim, GFZ) of fresh Selenga River water samples on CON01-2 (June 2001).

Figure 4.7: CONTINENT field work at Lake Baikal

Suspended Particulate Matter. The SPM analysis was undertaken by the author according to the recommendations of Strickland and Parsons (1972) using the gravimetric method. Fresh samples were filtered on the same day (Figure 4.7) during the CON01-2 (2001), CON01-5 (2001), CON02-8 (2002), and CON03-9 (2003) expeditions through predried (95° C for 2 h) and preweighed cellulose-acetate filters (0.45 µm pore-size). Additionally, distilled water was filtered through blank reference filters for each filtering series to account for the varying humidity and temperature conditions of filtering in the field. All filters were dried onboard for storage. Oven-dried (95° C for 2 h) sample filters and blank filters were reweighed at stable (temperature, humidity) laboratory conditions.

Dissolved Organic Matter. Samples were filtered through preburned cellulose-acetate filters (0.2 µm pore-size), and the filtrates were later analysed for DOC [pers., Rosell-Melé, CEA Barcelona, Spain] using the high temperature catalytic oxidation (HTCO) method. On CON03-9 in July 2003, samples were filtered through cellulose-acetate filters (0.45 µm pore-size), and the filtrates were later analysed for DOC by using HTCO [pers., Borovec, HUB, Budejovice, Czech Republic].

Coloured Dissolved Organic Matter. On CON02-8 in July 2002, absorbance, or Optical Density (OD), was measured on fresh samples after filtration through glass-fiber filters (0.7 µm pore-size), relative to pure water in a 5 cm cuvet, using the EAWAG Spectroquant NOVA60 (Merck). OD values were transformed into absorption, *a*, values [m^{-1}] by: 2.303 × OD / 0.05.

On CON03-9 in July 2003, samples were filtered through 0.45 µm pore-size cellulose acetate filters. OD could not be measured on fresh samples onboard, these samples were kept cooled and were measured from 254 to 400 nm relative to pure water in a 1 cm cuvet at the HUB laboratory [pers. Borovec, HUB, Budejovice, Czech Republic]. For these samples, OD is transformed into *a* [m^{-1}] by: 2.303 × OD / 0.01.

4.2.5 Spectro-radiometrical and Limnological Analyses at the Brandenburg and Mecklenburg Lake Districts (Germany)

Water Volume Reflectance was measured in 2002 and 2003, using the dual GER1500 field-spectrometer configuration (Figure 4.8) as described in §4.2.3.

Surface Reflectance was measured in 2003 and 2004 using an ASD as described in Mannheim et al. [2004a, 2004b].

Pigments. Samples for analysis of pigment concentration were directly filtered through glass-fiber GF/F filters (0.7 µm pore-size) (Whatman, Kent, UK). The filters were immediately frozen and kept in the dark until analysis. The photospectrometrical Chl-*a* analyses according DIN 38 412-L16 were carried out by the Institute for applied Freshwater Ecology (IaGB).

Dissolved Organic Matter. Samples were filtered through cellulose-acetate filters (0.45 µm pore-size). The filtrates were analysed at the IaGB for DOC using HTCO.

Coloured Dissolved Organic Matter. In 2003 and 2004, Absorptance, A, of fresh samples was measured after filtration through cellulose-acetate filters (0.45 µm pore-size), relative to pure water in a 5 cm cuvet, using a Lambda UV/VIS/NIR spectrophotometer with integrating sphere. (For these samples, A values were transformed into *a* [m^{-1}] by: A / 0.05).

Phytoplankton Absorption Coefficient. In 2003 and 2004, phytoplankton absorption was measured on fresh GF/F filters, relatively to a blank filter, according to the methods of Tassan and Ferrari [1995], using a Lambda UV/VIS/NIR spectrophotometer with integrating sphere (described in Mannheim [in prep]).

Suspended Particulate Matter. SPM concentrations were determined using the gravimetric method as described in §4.2.4.

Figure 4.8: Downwelling irradiance measurements at Lake Wannsee (Germany). These were undertaken simultaneously with an HYMAP airborne scanner overflight (July 2003).

4.2.6 GIS Processing and Analyses

The locations (latitude/longitude) of the sampling points were incorporated into the PANGAEA Network for Geological and Environmental Data (*http://www.pangaea.de*). For incorporation into the Baikal Online-GIS, the field stations coordinates were transformed into UTM projection, zone 48, WGS 84. As a result, field-sampling points can be overlain on thematic GIS layers, for example on the bathymetric information (source: University Gent (BE), *http://allserv.rug.ac.be/~jphenrie*) and on georectified Ocean Colour and Landsat satellite maps. This allows the vizualisation of data coverage and interpretation of CONTINENT field investigations (for example, Figure 4.2). The spatial information provided by the Baikal GIS supported paleolimnological investigations within the CONTINENT study (*Klump and Schneider*, 2004).

In addition, within the framework of provenance analyses, spatial GIS analyses were incorporated. Provenance analysis was carried out to trace back the pathways and origin of specific sediments. These source analyses usually involve analysing the mineralogy and geochemistry of both the sediment samples and rocks in the fluvial or aeolian catchment. In the CONTINENT study, source analysis was carried out by clay and bulk mineralogical and heavy mineral analyses from source rocks and sediments in the catchment area, and from the CONINENT sediment cores [*Fagel et al., in press*]. Using GIS analysis, the percentage of source rocks in the Lake Baikal catchment area can be extracted. First, digital stratigraphic geological data-sets (USGS) of Southern Siberia and Northern Mongolia were combined into one geological map layer and needed to be standardized in terms of stratigraphic attributions (Figure 4.9). This map layer had to be therefore corrected by the author in terms of the petrographic attributions according to the Russian geological maps of the area [*Jansin et al.,* 1989; *Kalinin and Moiseeva,* 1981; *Mac et al.,* 2001]. A second layer was produced where the stratigraphic groups were reassigned in terms of lithological parameters. Clipping the new lithological GIS-layer using the catchment delineation of Swierz [2004], the proportions of specific source rocks within the Lake Baikal catchment can be calculated.

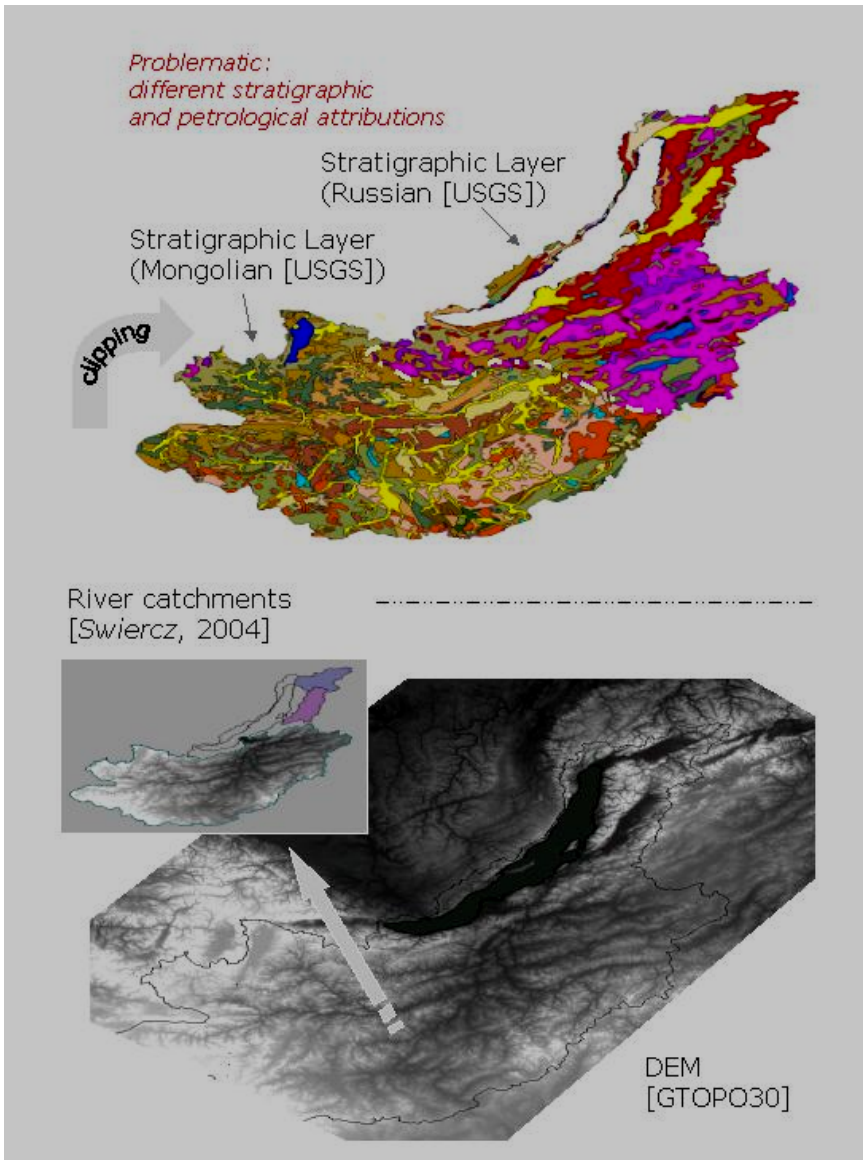

Figure 4.9: Modules of the Baikal GIS analysis. This graph shows the extracted river catchments (Selenga, Barguzin, Upper Angara) defined using a GTOPO30 DEM mosaic [*Swiercz*, 2004; *Swiercz et al.,* 2003]. This vector layer clips all the parameterized Baikal GIS layers for continuative catchment analyses. However, the geological mosaic polygon layer (source: USGS) required correction and attribute redefinitions (please note the differences between the different national data-sets).

5 RESULTS

5.1 ATMOSPHERIC CORRECTIONS

The problem of interfering absorbing aerosols have been present in the atmospheric layer above Lake Baikal for the respective SeaWiFS data-set, was addressed: Absorbing aerosols (e.g., iron-rich desert dust-like or soot) are not included in the SeaDAS atmospheric-correction process, but may, however, play an important role over central Asia, with the Gobi and Taklamakan deserts and the Chinese loess plateau being one of the main sources of mid-Asian absorbing aerosol events [*Seinfeld et al.,* 2004]. The latest outstanding massive dust storm over the Asian mainland occurred from 5 to 15 April 2001 [*Holden*, 2001; *USA National Air Quality and Emissions Trends Report*, 2003], and migrated eastwards towards the American continent. Generally, Asian dust events occur only in spring, after the break down of the Siberian high-pressure zone, moving eastwards [*Holden*, 2001] towards China and Thailand. Investigations of Total Ozone Mapping Spectrophotometer (TOMS) data from 2001 to 2002 confirmed that absorbing Aerosol Index (AI) dust events were not present in the Baikal area during the late spring and summer months of 2001 and 2002. Indicative TOMS AI values for absorbing aerosols at Lake Baikal were only found in June/July 2003, when extensive forest fires were persistent throughout summer 2003. Both outstanding events, the desert dust storm in spring 2001, and the extensive forest fires in this region in summer 2003 are not covered within the CONTINENT SeaWiFS data-set.

Zuev et al. [1996] have described, how the aerosol optical thickness above Siberia from 1992 to 1995 varied within one order of magnitude from 0.04 to 0.5 µm, within a mean value of about 0.2 µm. An interannual trend in aerosol optical thickness has been detected, and found to be caused by the volcanic eruption of Mt. Pinatubo (Philippines) in 1991. However, Zuev et al. [1998] found in further investigations with long-term LIDAR observations that volcanic-aerosol concentrations peaked in 1992, and then degraded to normal atmospheric background levels after 1995. Until recently, no major volcanic eruptions have occurred in Eastern Asia. Therefore, the assumed standard stratospheric aerosol component in SeaDAS is reasonable.

The discrepancy between the actual low-pressure values in July to the barometric air pressure calculated using a Digital Elevation Model (DEM) accounted in a variety of acquisition dates for approx. 10 mbar. Therefore, using the meteorological data-sets instead of the DEM barometric air pressure value, the SeaDAS processing was adapted to the continental air pressure oscillation in Southern Siberia. The results of SeaDAS atmospheric correction using the 'band7/8' model and the fixed SeaDAS aerosol models (§4.2.1) showed that the 'band7/8' model and the majority of fixed aerosol models completely failed during the processing. This was represented in large areas of no data values and error flags. In a lot of cases, the remaining areas of atmospherically-corrected reflectance data showed noise in the first spectral bands. In this study, the SeaDAS atmospheric-correction processes performed best with the choice of a spectrally-flat aerosol ($\varepsilon \approx 1$), i.e., with the option of SeaDAS model 1 (oceanic model), model 5 (maritime model, 99 % humidity) and the single scattering CZSC 'white aerosol' model. The SeaWiFS time series for 2001 and 2002 was subsequently processed using the fixed SeaDAS aerosol model 5.

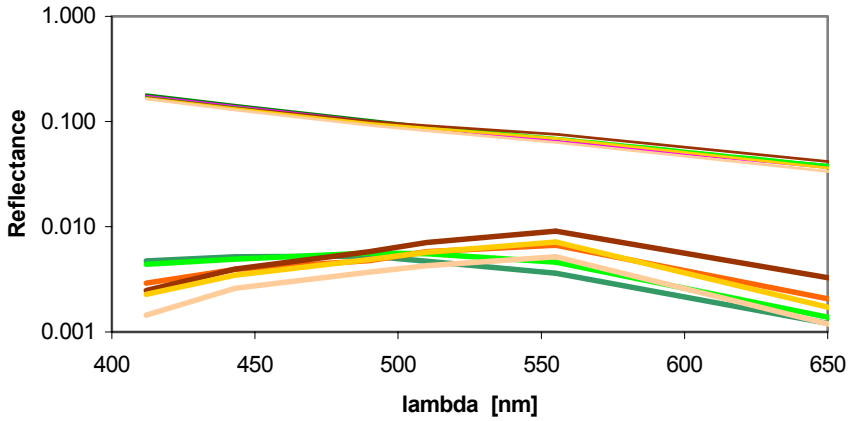

Figure 5.1: Lake Baikal, 2001/07/19; The R_{TOA} spectra [dimensionless] of different water pixels are represented by the upper group between 0.1 and 1 Reflectance, R. The lower group of spectra between 0.001 and 0.01 R are the R_{RS} [sr^{-1}] spectra from the same locations, however after the atmospheric correction process. The R spectra were extracted from locations in the North Basin (dark green), Central Basin (bright green) and from the vicinity of the Selenga delta (orange to brown colours).

Figure 5.1 shows the result of the optimized atmospheric correction exemplary on the 2001/07/19 SeaWiFS acquisition. Spectra have been extracted from the same locations (latitude/longitude), on one hand from the atmospherically uncorrected hemispherical SeaWiFS Top-of-Atmosphere reflectance data-set, R_{TOA}, and on the other hand from the atmospherically-corrected Remote Sensing Reflectance data-set, R_{RS}. The dominant proportion of the atmospheric signal within the R_{TOA} is obvious, in contrast to the weak contribution of the water leaving signals itself, here displayed as R_{RS} values.

5.2 SPECTRAL REFLECTANCE DATA

The combined pool of GER1500 field-spectrometer reflectance, R, spectra and atmospherically-corrected SeaWiFS R spectra from 2001 and 2002 provides a visual description of the optical specifications of the bio-optical provinces of Lake Baikal.

According to these R spectra, the spectral R peak (or the dominant wavelength) of the highly transparent waters of Lake Baikal is commonly located around SeaWiFS bands 3 (490nm) and 4 (510 nm). Figure 5.2 shows characteristic R_{RS} spectra of pelagic waters in Lake Baikal, where the reflectance maximum position (or the dominant wavelength) is always situated around 490 to 510 nm.

From the R spectra, it was also found that different R maximum positions that are placed at longer wavelength ranges around 550 nm occurred in July 2001 within wide areas of the South Basin. The same holds for HRPT SeaWiFS data-sets from May 2002, at which time there was high-energy fluvial input caused by snow and ice melting. For the remaining SeaWiFS acquisitions from 2001 to 2002, reflectance maximum positions at these longer wavelength ranges around 550 nm occurred in the vicinity of the Selenga Delta, in Barguzin Bay (e.g., Figure 3 in Heim et al. [2005]) and near local river outlets. In all these cases, the spectral-reflectance maximum position is shifted towards SeaWiFS band 5 (555 nm) (e.g. Figure 5.3).

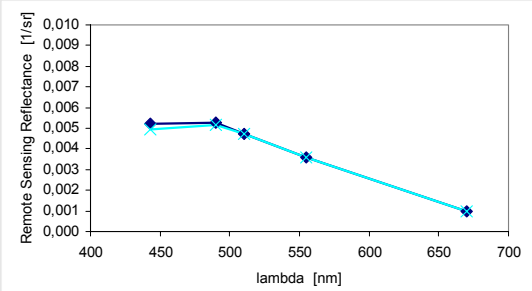

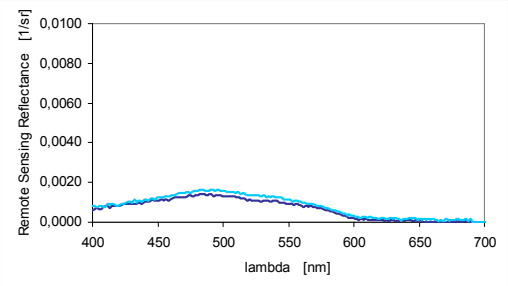

01/07/19 SeaWiFS R_{RS} Case 1

dark blue: North Basin

turquoise: Central Basin

GER1500 R_{RS} Case 1

dark blue: **CON01-7** (North Basin) **01/07/18**
0.2 mg l^{-1} *SPM*, 0.66 µ g l^{-1} Chl-*a*, 0.4 µg l^{-1} sum carotenoids; Chl-*a* contribution: diatoms (and Cryptophyta)

turquoise: **CON01-1** (Central Basin) **01/07/15**
0.5 mg l^{-1} *SPM*, 0.6 µg l^{-1} Chl-*a*, 027 µg l^{-1} sum carotenoids; Chl-*a* contribution: diatoms (and Cryptophyta)

Figure 5.2: SeaWiFS and GER1500 R_{RS} field spectra of clear pelagic Case 1 waters in Lake Baikal(July 2001) (same positions, different dates).

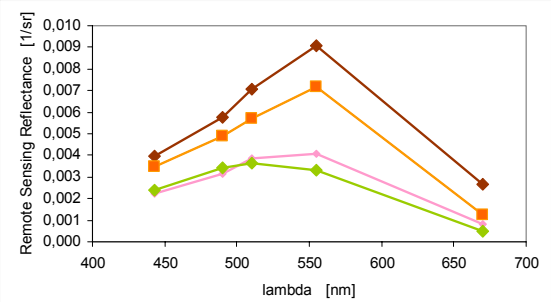

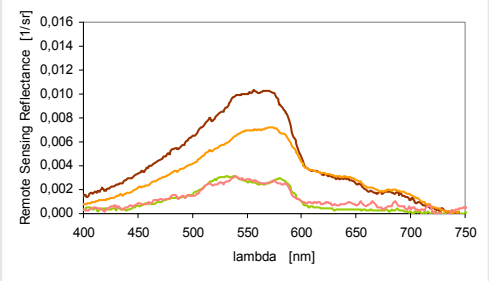

01/07/19 SeaWiFS R_{RS} Case 2

dark brown: Central Basin, Selenga influence
medium brown: Central Basin, Selenga influence
beige: South Basin (Posolsky)
olive green: South Basin

GER1500 R_{RS} Case 2

dark brown: **CON01-22** (Selenga II) **01/07/21**
GER1500 R_{RS}
3.8 mg l^{-1} *SPM*, 2.1 µg l^{-1} Chl-*a* , 1.0 µg l^{-1} sum carotenoids; Chl-*a* contribution: picocyanobacteria and diatoms, green algae, Cryptophyta

medium brown: **CON01-23** (Selenga III) **01/07/21**
2.6 mg l^{-1} *SPM*, 1.0 µg l^{-1} Chl-*a*, 0.65 µg l^{-1} sum carotenoids; Chl-*a* contribution: picocyanobacteria and diatoms, green algae

beige: **CON01-25** (Posolsky) **01/07/21**
2.6 µg l^{-1} Chl-*a*, 2.4 µ g l^{-1} sum carotenoids; Chl-*a* contribution: picocyanobacteria and diatoms, green algae

olive green: **CON01-27** (South Basin) **01/07/24**
2.4 µg l^{-1} Chl-*a*, 1.7 µg l^{-1} sum carotenoids; Chl-*a* contribution: picocyanobacteria

Figure 5.3: SeaWiFS and GER1500 R_{RS} field spectra of Case 2 wate in Lake Baikal (July 2001) (same positions, different dates).

A spectral shift in the R maximum position from SeaWiFS band 5 (555 nm) to band 6 (650 nm) has been observed in coastal waters (e.g., Mitchelson-Jacob 1999, Froidefond et al. 2002), however, only in cases of highly turbid waters with tens of mg l^{-1}. At lake Baikal, this spectral shift can only be noticed on SeaWiFS pixels very close to the coast and in Selenga Bay. However, these are largely land-contaminated pixels, and pixels including the bottom reflections from bay sediments. Therefore, only the spectral shift of the R maximum from SeaWiFS band 4 to SeaWiFS band 5 is examined in this work.

5.3 OCEAN COLOUR PRODUCTS OF LAKE BAIKAL

5.3.1 Ocean Colour Chlorophyll Data

The following Chl-*a* algorithms have been evaluated using phytoplankton-pigment ground-truth data [pers., Fietz, IGB, Germany]: Global multi-temporal Chl-*a* algorithms OC2 and OC4 (Table 4.5) Chl-*a* algorithms for oligotrophic waters (Table 4.5), and empirical Chl-*a* algorithms calculated from CONTINENT ground-truth data.

In this study, empirical Chl-*a* algorithms for Lake Baikal were calculated from the Case 1 *in-situ* Chl-*a* data-sets by using linear-regression calculations with atmospherically-corrected SeaWiFS R_{RS} data of the nearest acquisition dates (Table 5.1). As the in-situ reference, Chl-*a* concentrations of discrete samples of the respective sampling points have been averaged over a depth of 30 m. The ground-truth data for 2001 were taken from the storm-free period between 17/07 to 24/07 and compared with the cloud-free parts of SeaWiFS acquisitions on the 02/07, 04/07, 16/07, 18/07, 19/07 (19/07 is the only acquisition with less then 30 % cloud cover), 21/07, and 26/07. In 2002, there were foggy and high-rainfall weather conditions, especially in the North Basin region. The ground-truth was taken between 05/07 to 15/07, while the useable SeaWiFS acquisition dates are 02/07, 12/07, 13/07, 20/07, 22/07, 24/07, and 25/07. The evaluation ground-truth data-sets for 2001 and 2002 originate from a two-week time span around the SeaWiFS acquisition dates. Therefore, the accuracy of the evaluation data-set is limited.

Table 5.1: *Chl-a* algorithms, derived from the regression analysis of CON01-5 and CON02-8 Chl-*a* ground-truth data-sets.

source	x = Ri/Rj ($R = R_{RS} = L_{up}/E_{down}$)	Chl-*a* algorithm
C Empirical Chl-*a* this study, Lake Baikal (RU), July 2002	x = R490/R550	$1.94\ x^{-2.81}$
D Empirical Chl-*a* this study, Lake Baikal (RU), July 2001 + 2002	x = R490/R550	$1.43\ x^{-1.8}$
E Empirical Chl-*a* this study, Lake Baikal (RU), July 2002	x = R443/R550	$1.82\ x^{-2.47}$

However, fortunately, strong surface currents do not influence Lake Baikal, as is the case for tidally influenced marine coastal waters, hence the additional uncertainty that is expected to arise is limited.

The performance of empirical algorithms **C**, **D**, and **E** (Table 5.1) was evaluated using the combined data-set (2001 and 2002), and for the data from individual years. The determination coefficients (r^2) of the Chl-*a* measured and Chl-*a* calculated (using Chl-*a* algorithms **C** and **D** in Table 5.1) for the SeaWiFS data-sets in summer 2002 show the best results (r^2 = 0.7 to 0.74). This is, for example, demonstrated in Table 4 in Heim et al. [2005]. However, calculated Chl-*a* concentrations from empirical Chl-*a* algorithms strongly deviate from ground-truth data-sets if Case 1 areas of SeaWiFS data-sets of summer 2001, for example 07/19, were tested (r^2 = 0.55). The performance of the empirical algorithms strongly deviates when applied to the individual years.

The Chl-*a* algorithms for oligotrophic water bodies that are listed in Iluz et al. [2003], were applied to the atmospherically-corrected SeaWiFS data and compared with the in-situ Chl-*a* data-set. The coefficients of Gordon et al. [1983] performed best (Tables 4 and 6 in Heim et al. [2005]), while the other coefficients for Case 1 waters listed in Iluz et al. [2003] showed a very low performance and are not applicable for Lake Baikal.

The performance of the OC2 and OC4 Chl-*a* algorithms was tested in detail (Tables 5, 6a,b, 7a,b in Annex A, summary Tables 5a,b and Table 6 in Heim et al. 2005). Figure 5.4 shows the comparison of OC2 Chl-*a* of successive SeaWiFS acquisitions with CON02-8 in-situ samples for July 2002. The calculated OC2 and OC4 Chl-*a* concentrations are within an error of ± 32 % for July 2001, if only the cases of clear pelagic waters are considered, and within an error of ± 27 % for July 2002.

In summary, OC2 and OC4 Chl-*a* algorithms convincingly and robustly perform for the HRPT SeaWiFS data-sets of July 2001 and July 2002.

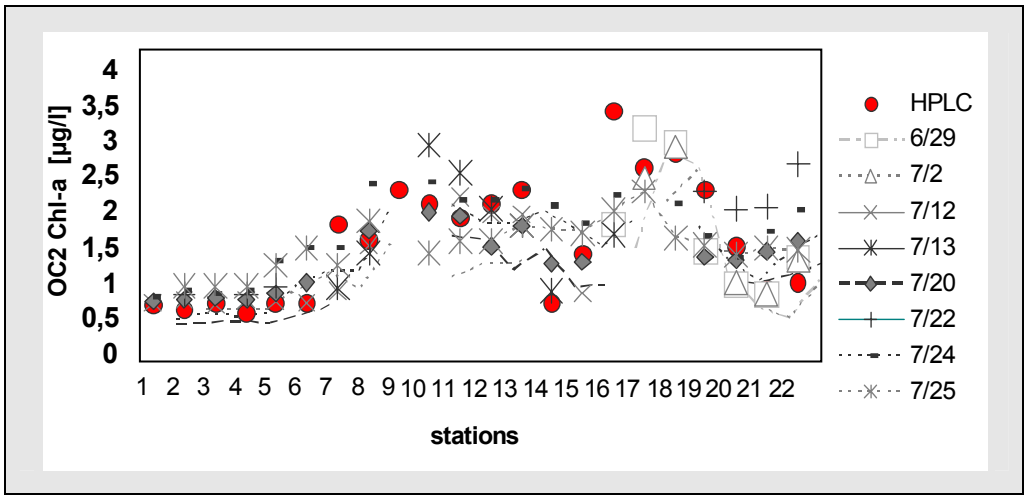

Figure 5.4: Comparison of OC2 Chl-*a* of successive SeaWiFS acquisitions with in-situ Chl-*a* [pers, Fietz, IGB, Germany] of CON02-8 (July 2002). The transect is drawn from North to South: Stations 1 to 5 North Basin, stations 6 to 16 Central Basin, including Barguzin Bay, and stations 17 to 22 along the Selenga Delta and in the South Basin.

5.3.2 Ocean Colour Suspended Particulate Matter Data

First, an established SPM algorithm was applied to the atmospherically-corrected SeaWiFS data, in this case the SISCAL SPM algorithm [Jørgensen, 2000], which is optimized as a coastal SPM type in the range of 0.5 to 8 mg l^{-1} (§2.1.2). For calculating SPM, the SeaWiFS $R_{RS}(555)$ were converted to subsurface hemispherical $R_{vol}(555)$ according the SISCAL technical report [2004][2]. When calculating this SPM product, which is correlated with the absolute R value, SPM concentrations in coastal waters around the Selenga delta are within the range of the CONTINENT SPM ground-truth data in July 2001 (n = 6, 0.8 to 5 mg l^{-1}). On the other hand, on calculated SPM maps from the July 2001 acquisitions, the fluvial input in Barguzin Bay is non-visible near the river inlet and shows unrealistic inverse grading, with the lowest calculated SPM concentrations towards the river inlet.

For preliminary investigations, SPM concentrations of Selenga River surface samples (CON01-02) have been correlated with $R_{vol}(555)$ to simulate a SeaWiFS SPM algorithm. In this case, the linear regression for Selenga River surface waters (n = 7), and a SPM range from 15 to 32 mg l^{-1} leads to

$$SPM = 0.9634 \times R_{vol}(555) + 11.92 \quad [\text{mg l}^{-1}] \tag{5.1}$$

Despite the exclusion of the two extrema (brownish-coloured surface waters (lower right in the left scattergram, Figure 5.5) from the construction of equation (5.1), the correlation coefficient is relatively low (r^2=0.6). Also due to high concentrations of absorbing water constituents in the Selenga River (phytoplankton, fulvic and humic acids), R values are lowered despite high concentrations of SPM, and therefore, the minimum-SPM value that can be calculated using equation 5.1 is only 6 mg l^{-1}.

In addition, the coastal SISCAL and the MUMM SPM algorithms [*SISCAL*, 2004] have been tested. Figure 5.6 shows the dependence of the calculated SPM concentrations on what SPM algorithm is chosen. The coastal SISCAL SPM algorithm has been originally constructed from relatively higher reflective SPM types, while the Selenga river water SPM type is dominated by absorbing organic material.

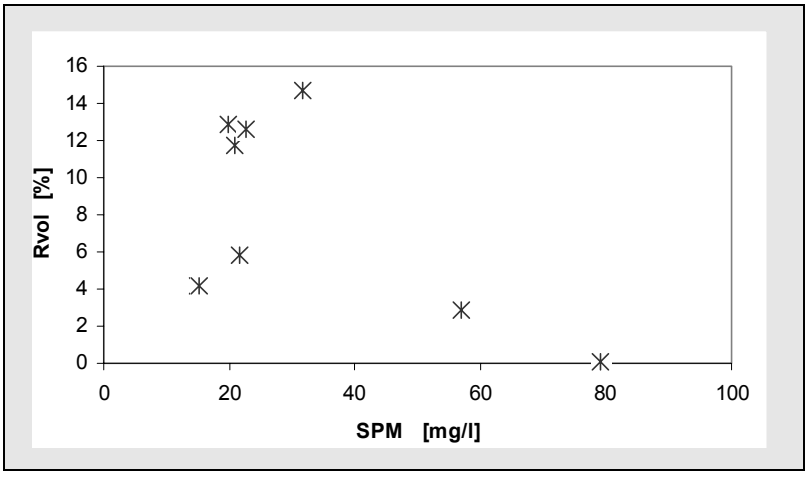

Figure 5.5: Scattergram of $R_{vol}(555)$ against SPM concentrations of the river surface samples (Selenga River, RU).

[2] $R_{vol}(0-,\lambda) = [R_{RS}(0+,\lambda)/0.56] \times Q$,

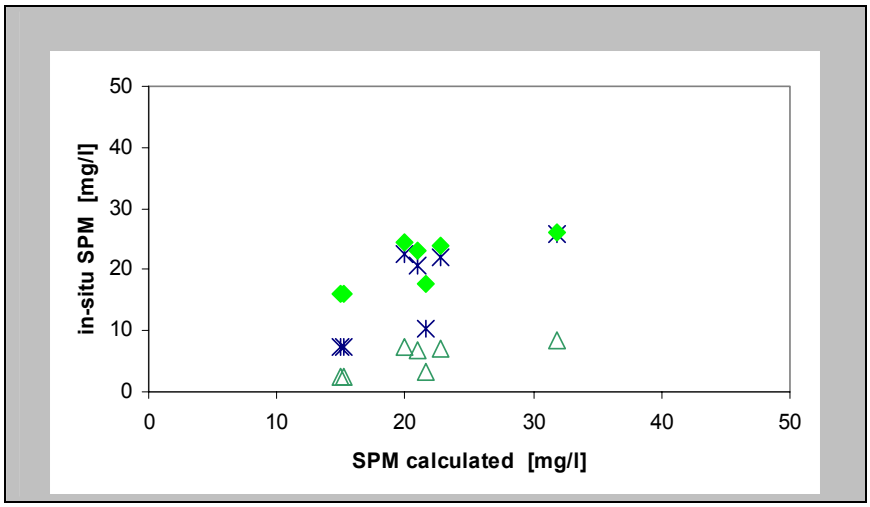

Figure 5.6: SPM concentrations, calculated using $R_{vol}(555)$ of Selenga stations (n = 6) for different SPM models: green squares represent the Selenga SPM algorithm (equation 5.1), blue stars represent the MUMM SPM equation [*SISCAL*, 2004]; and green triangles the SISCAL *SPM* equation [*Joergensen*, 2000; *SISCAL*, 2004].

To investigate the dilution of terrigenous input, Barguzin Bay was visited during the CON02-8 expedition in July 2002, and the Barguzin transect was established from East to West (B1, B2, B3 in Figure 4.2). Note, however, that the direct Barguzin outflow into Barguzin Bay is forced by on-shore currents to flow northwards, and the terrigenous signals quickly wear off along the CONTINENT transect. The sampling points Barguzin I, II, and III are discussed in detail in Heim et al. [2005]. The first visual investigation of the optical-water properties at Barguzin I (B1) (1 km from the Barguzin river inlet), demonstrated the influence of high-organic terrigenous material: The surface waters appeared very dark, the foamy wavecapes were brownish coloured, and the Secchi depths were only to one metre [pers., LIN, 2002]. The R_{vol} spectra at B1 in Figure 3 in Heim et al. (2005) confirms the extreme absorption in the blue and green wavelength range, and in turn, the very low R_{vol} (below 0.1 %), despite high SPM concentrations (3.9 mg l^{-1}). SPM Filters of the Barguzin transect are intensely brownish-yellowish in colour. The closer to the river inlet, the lower in turn is the overall reflectance, and the more the spectral maximum shifts towards longer wavelengths as the absorption activities due to humic substances are enhanced.

The Selenga transect that was also installed during CON02-8 (Selenga I, II, III,) at the south-west end of the Selenga Delta was less successful than the Barguzin transect (Barguzin I, II, III). Low SPM values indicated that during CON02-8, we did not detect one of the jet streams of the Selenga River output.

The author examined the SPM quantification by linearly linking the remote-sensing attenuation coefficient, K490 (§4.2.2), instead of the reflectance value with SPM lake ground-truth values. If the combined SPM data (n = 21, 2001 and 2002) was linked to SeaWiFS K490 data by linear regression, this leads to ($r^2 = 0.76$):

$$SPM = 16.158 \times \left(0.016 + 0.15645 \times \left(band4/band5\right)^{-1.5401}\right) - 1.1719 \text{ in [mg l}^{-1}\text{]} \qquad (5.2)$$

If only the SPM ground-truth data from 2001 (n = 6) is linked to SeaWiFS K490 data by linear regression, this leads to ($r^2 = 0.71$):

$$SPM = 17.437 \times \left(0.016 + 0.15645 \times \left(band4/band5\right)^{-1.5401}\right) - 1.4064 \text{ in [mg l}^{-1}\text{]} \qquad (5.3)$$

In Heim et al. [2005], different regression coefficients compared to equation (5.3) were given. These had been derived from a not-yet fully optimized atmospherically-corrected SeaWiFS data-set, where K490 values were slightly higher. Figure 4 in Heim et al. (2005) and Figure 5.7 present the results as concentrations of SPM [mg l^{-1}] of the 2001/07/19 acquisition. The calculated SPM concentrations correctly highlight the Selenga River and other local-river distributions with highest SPM concentrations near the river mouth.

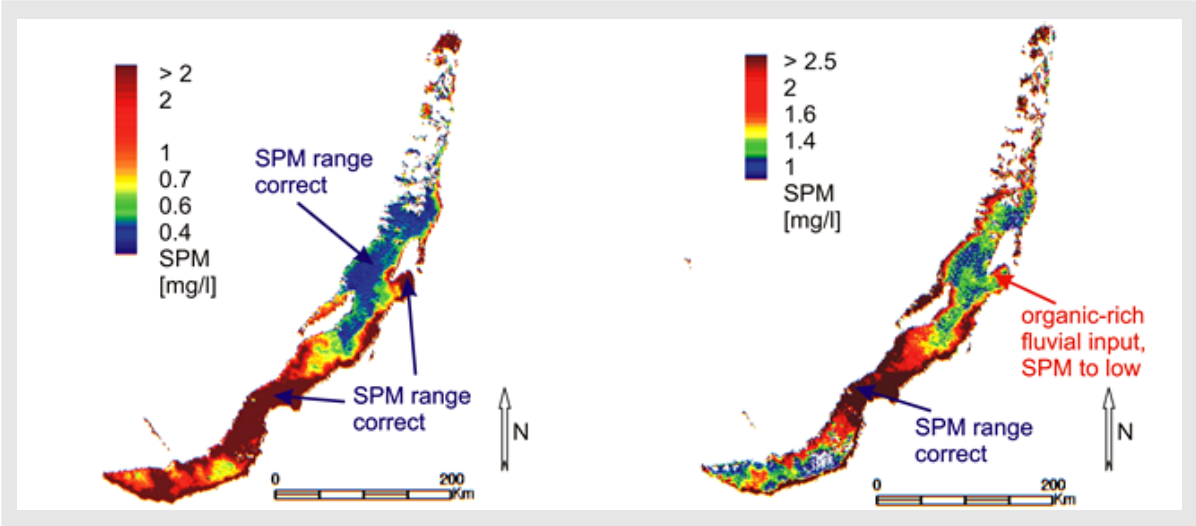

Figure 5.7: SPM concentrations [mg l^{-1}] (2001/07/19). Left: SPM algorithm using the SeaWiFS attenuation coefficient as an optical parameter (equation 5.3). right: SPM algorithm using the SISCAL SPM algorithm of Jørgensen [2000].

5.4 VARIATION IN LAKE BAIKAL'S PHYTOPLANKTON DISTRIBUTION AND FLUVIAL INPUT ASSESSED BY SEAWIFS SATELLTE DATA, HEIM B., OBERHAENSLI H., FIETZ S., KAUFMANN H. [2005]

Available online at www.sciencedirect.com
SCIENCE DIRECT®
Global and Planetary Change 46 (2005) 9–27
GLOBAL AND PLANETARY CHANGE
www.elsevier.com/locate/gloplacha

Variation in Lake Baikal's phytoplankton distribution and fluvial input assessed by SeaWiFS satellite data

Birgit Heim[a,*], Hedi Oberhaensli[a], Susanne Fietz[b], Hermann Kaufmann[a]

[a]GeoForschungsZentrum Potsdam GFZ, Telegrafenberg, 14473 Potsdam, Germany
[b]Leibniz Institute of Freshwater Ecology and Inland Fisheries, 12587 Berlin, Germany

Received 1 November 2004; accepted 1 November 2004

Abstract

The current behaviour of selected climate proxies in Lake Baikal was assessed by remote sensing analyses of 'Sea viewing Wide Field of view Sensor' (SeaWiFS) satellite data. Suitable proxies include optically visible water constituents such as phytoplankton, suspended terrigenous matter and yellow substance. These limnological parameters reflect the present-day climate bioproductivity and the river discharge in the catchment area.

A biological and geochemical ground truth data set for Lake Baikal was established with the help of members of the paleoclimate project 'high-resolution CONTINENTal paleoclimate record in Lake Baikal' (CONTINENT). For processing the SeaWiFS satellite data, the atmospheric correction was adapted to the case of Lake Baikal. Chlorophyll as a proxy for phytoplankton was quantified using global NASA ocean colour algorithms OC2 and OC4. In cases of no optical interferences by terrigenous input, the calculated chlorophyll concentrations in clear pelagic waters were within ±30% accuracy with the CONTINENT cruise data during the summers of 2001 and 2002. Within this range of accuracy, the SeaWiFS time series will be able to show the seasonal variations of chlorophyll of specified bio-optical provinces of Lake Baikal and of CONTINENT sites. In this study, the suspended matter as a proxy for the terrigenous input was calculated according to an empirical algorithm using ground truth data in the time frame of flooding events in summer 2001. The approach chosen correlates the suspended matter concentration with the remotely sensed parameter of 'attenuation coefficient' to account for the organic-rich terrigenous input that originates from the swampy watersheds.

Seasonal and spatial information that is provided by the analyses of the SeaWiFS satellite data will assist paleoclimate researchers to interpret the autochthonous and allochthonous influences at the CONTINENT coring sites.

Keywords: Lake Baikal; Remote sensing; SeaWiFS; Chlorophyll; Suspended matter

1. Introduction

Within the 'high-resolution CONTINENTal paleoclimate record in Lake Baikal' (CONTINENT) Proj-

* Corresponding author. Tel.: +49 331 288 1191; fax: +49 331 288 1192.
E-mail address: biggi.heim@web.de (B. Heim).

0921-8181/$ - see front matter © 2004 Elsevier B.V. All rights reserved.
doi:10.1016/j.gloplacha.2004.11.011

ect, funded by the European Union, sedimentary records from several locations in Lake Baikal are exploited for high-resolution paleoclimate studies. The record of the CONTINENT sediment cores (spanning potentially 150,000 years) at three sites within the lake (Charlet et al., 2005-this issue) and the multiproxy approach of the project provide unique opportunities to understand the Late Quaternary climate history of the Earth. However, in order to interpret the biogenic and silico-clastic records in the paleosediments more comprehensively, the present-day formation of these climate proxies within Lake Baikal needs to be investigated. The interdisciplinary approach allows the examination of the present-day bio-limnological and geochemical conditions of Lake Baikal, as well the processes occurring in the water column and the catchment. Sequential sediment trap data from the South and North Basins, as well as field data provide information on the lake's phytoplankton and bioproductivity, on the terrigenous input into the lake and on the geochemistry.

The goal of this study is to show the potential of high spectral resolution satellite data to map the phytoplankton distribution and the terrigenous input into Lake Baikal.

Previous investigations on water clarity and suspended matter using operational satellite data were carried out, e.g. by Bukata et al. (1974), Klemas et al. (1974), Munday (1974), Munday and Alfoeldi (1979), or Lillesand et al. (1983). They used Landsat-Multispectral Scanner (MSS) data, but their research was restricted to turbid, eutrophic lakes. The challenge then was to extract not only relative turbidity, but to estimate the main phytoplankton pigment (chlorophyll; (chl-*a*)) from the satellite data of the Landsat sensors MSS, TM, and ETM+ (Yacobi et al., 1995; Mayo et al., 1995). While these land-focused sensors provide high spatially resolved information, the limited radiometric and spectral resolution of these sensors in the visible wavelength range are not suitable for analysing clear water bodies. The average errors of chlorophyll derivation in the case of land-focused sensors are high for existing algorithms, from ± 10 up to ± 20 $\mu g\ l^{-1}$ chl-*a* (Burgess, 2003). In cases that use advanced techniques such as the spectral unmixing method in the Mecklenburg Lake district (Germany) (Thiemann and Kaufmann, 2000), the accuracy range is about ± 10 $\mu g\ l^{-1}$ chlorophyll.

Due to the limited spatial resolution (1 km^2 per pixel) of the first ocean colour sensor, the Coastal Zone Scanner (CZCS), launched in 1987 by NASA, water quality monitoring strategies for inland water bodies are mainly based on hyperspectral airborne scanner data. Hyperspectral approaches provide lake maps of water clarity, suspended matter concentration, chlorophyll, and dissolved organic carbon (DOC) concentration (Dekker, 1993; Heege, 2000; George and Malthus, 2001; Kallio et al., 2001; Keller, 2001; Koponen et al., 2002; Thiemann and Kaufmann, 2002; Kloiber et al., 2002). The chlorophyll algorithms for these generally eutrophic inland water bodies are principally based on the stable and significant reflectance features in the red and the near-infrared wavelengths. In contrast, the water-leaving radiances of clear water bodies are naturally restricted to the blue and the green wavelength range due to the reduced contribution of scattering processes on particles (i.e. phytoplankton, detritus, minerogenic particles). The red to near-infrared algorithms used for water quality investigations of eutrophic lake water bodies are therefore not applicable for clear water bodies, such as Lake Baikal.

The marine chlorophyll algorithm development for oligotrophic, pelagic waters (Morel and Gordon, 1980; Gordon and Morel, 1983; Stumpf and Tyler, 1988; Gitelson et al., 1994) is performed with radiometrically highly resolved ocean colour satellite data, supported by high spectral resolution in the blue and green spectral regions. The chlorophyll algorithms were designed for clear pelagic 'case 1 waters' (Jerlov, 1978), in which the phytoplankton is the main optically relevant component, and other water constituents such as suspended matter and yellow substances are low in concentration and directly correlated with the chlorophyll concentration. New powerful generations of high spectral resolution satellite sensors with a very high radiometric sensibility (SeaWiFS (NASA), MODIS (NASA), MERIS (ESA)) were launched in the late 1990s. Recent investigations (e.g. Moore et al., 1999; Ruddick et al., 2000; Koponen et al., 2002) focused on the optically more complex waters, 'case 2 waters' (Jerlov, 1978), in which the optically important water constituents may not be correlated, such as in coastal waters and semi-enclosed seas and large inland water bodies. So, while experimental

algorithms for the calculation of chlorophyll and suspended matter concentrations are based on linear regression of spectral features according to field measurements (Kahru and Mitchell, 1999; Froidefond et al., 1999, 2002), advanced techniques have been developed to separate the optically interfering and uncorrelated water constituents, such as analytical inverse modelling using neuronal network techniques (Doerffer and Fischer, 1994; Hoogenboom et al., 1998; Schiller and Doerffer, 1999; Heege and Fischer, 2004) and principal component inversion (Neumann et al., 1995; Krawczyk et al., 1996).

Perhaps one of the most important, yet complex tasks refers to the atmospheric correction of satellite data. Normally in the case of clear water body targets, more than 99% of the radiometric signal that is scanned by the satellite sensor originates solely from the atmospheric contribution and specular reflection of sky radiance at the air–water interface. Therefore, the quality of the extraction of limnological parameters from satellite data is highly dependant on the atmospheric correction process. Defined standard atmospheric correction methods exist for the marine environment such as in the 'SeaWiFS data analysis system' SeaDAS (McClain et al., 2000). Recently, Knobelspiesse et al. (2000) developed a tool within SeaDAS for atmospheric correction over inland water bodies (Lake Superior (USA)). Knobelspiesse et al. (2000) extrapolated atmospheric parameters that were calculated above clear water areas towards turbid lake areas. The atmospheric correction method proved to be successful in the green to red wavelength range (±5% for SeaWiFS bands 3–6), but still failed for the important blue wavelength range (SeaWiFS bands 1 and 2). An ocean colour data processing for continental inland water bodies, which will be used as satellite data standard processing (i.e. for MERIS data), was accomplished by Vidot and Santer (2003) using Lake Balaton (Hungary) and Lake Constance (Germany) as test sites.

For Lake Baikal, the first remote sensing studies used information from 'Advanced Very High Resolution Radiometer' (AVHRR) satellite data in the thermal wavelength range (3.6–3.9, 10.3–11.3, and 11.5–12.5 μm) (Gitel'zon et al., 1991; Bolgrien et al., 1992, 1995; Evans et al., 1992; Semovski et al., 1998, 2001) and radar data sets (ERS-1) for water body circulation studies (Semovski et al., 1999). For optical remote sensing studies of lake ice cover and ice types, AVHRR data (Mogilev and Semovski, 1999; Semovski et al., 2000) and satellite data of the 'Along Track Scanning Radiometer' (ATSR) (Lawrence et al., 2002) have been used. Physical investigations of optical properties of Lake Baikal by Russian authors (e.g. Sherstyankin, 1975), including the spectral composition of upwelling and downwelling irradiance, concentrated on studies of the underwater light field under ice and snow cover and on specific optical properties of deep water layers. Semovski (1999a) first conducted remote sensing studies of Lake Baikal's water constituents with satellite data in the visible wavelength range. His study on the visible bands of the AVHRR was limited by a land surface adapted atmospheric correction approach, which did not result in an applicable remote sensing chlorophyll algorithm. Instead, Semovski (1999b) was the first to define the bio-optical parameters for Lake Baikal to simulate the underwater light-field. This bio-optical model for Lake Baikal performs well in simulating the vertical optical structure, which was validated with in situ attenuation depth profiles of Sherstyankin in the South Basin of Lake Baikal (Semovski, 1999b). Semowski further concluded that bio-optical modelling in the South Basin of Lake Baikal has to account for its 'yellow substance' content.

'Yellow substance' is a limnological term that is applied to a variable mixture of different groups of absorbing and fluorescing water constituents, after the concept of 'Gelbstoff', first introduced by Kalle (1949). Humic, fulvic, and some hydrophilic acids are the main coloured constituents of dissolved organic carbons. However, the bio-optical properties of dissolved and particulate organic matter in the natural aquatic environment are not yet well understood (e.g. Yacobi et al., 2003).

This paper presents the first remote sensing study of Lake Baikal's surface waters using optical satellite data with high spectral resolution. The SeaWiFS satellite data show the seasonal distribution pattern and intensity of terrigenous input and the spatial and seasonal variations of phytoplankton. The results are then related to the autochthonous and allochthonous influences with regard to the coring sites

'Continent', 'Posolsky', and 'Vydrino' (Charlet et al., 2005-this issue).

2. Lake Baikal

Lake Baikal located in southeastern Siberia (51–56°N, 104–110°E) is the most voluminous inland water body on earth (Shimaraev et al., 1994). The lake is oligotrophic and has a mean chlorophyll pigment concentration in summer from about 0.5 to 2.5 μg l^{-1} chl-*a* (Kozhova and Izmesteva, 1998). Within bays, along the coast, and near the Selenga Delta, the water may carry up to 5 μg l^{-1} chl-*a* in late summer. Baikal water is extremely transparent, with Secchi depth measurements in pelagic waters showing values up to 40 m in June and still up to 20 m in July when phytoplankton is more abundant. The main phytoplankton blooms (up to 10 μg l^{-1} chl-*a*) develop in early spring in turbulent waters under the ice cover (Kozhova and Izmesteva, 1998). In the South Basin, the ice usually establishes in early January and breaks up in May, although the break-up time for the North Basin can be as late as in June.

River discharge and shore erosion, aeolic and ice transport result in a horizontally heterogeneous pattern of dissolved and particulate terrigenous matter in Lake Baikal. The Selenga River is the largest tributary into the lake and has built up an enormous delta region, separating the South from the Central Basin (Fig. 1). The Barguzin River discharges into the Central Basin while the Upper Angara River feeds into the very north of the North Basin. The seasonally controlled input of humic substances into the lake can be high, e.g. 200–500 μM C (2.4–6 mg l^{-1}) DOC, and 100 μM C (1.2 mg l^{-1}) particulate organic matter (POC) downstream from the Selenga and the Barguzin rivers (Yoshioka et al., 2002). During periods of high terrigenous input, Lake Baikal may be seasonally and locally assigned to 'case 2 waters' according to the classification of Jerlov (1978) due to the significant optical contribution of non-correlated terrestrial matter. The dissolved and particulate organic matter originates from swampy areas and bogs within the Lake Baikal watershed. Yoshioka et al. concluded that the main origin of DOC in Lake Baikal, even in pelagic waters, seems to be terrestrial because the $\delta^{13}C$ values of DOM in the lake and in the tributaries are comparable.

3. Materials and methods

3.1. Ground truth data

3.1.1. Field expedition

Data collection during field expeditions were planned to take place in June and July when wind conditions across Lake Baikal are moderate. However, these months have one draw back for remote sensing applications because of frequent cloudy, foggy, and rainy weather conditions. Despite weather limitations, a set of ground truth data has been collected during the CONTINENT ship cruises in summers 2001, 2002, and 2003 (Table 1) in the Southern, Central, and North Basins (Fig. 1). Special attention was paid to the lake regions most influenced by terrigenous matter input by establishing transects from the vicinity of the large tributaries, such as the Barguzin and the Selenga River inflows, into the pelagic regions of the lake. Investigations were also made in the catchment area of the Selenga river: surface water (from 0.5 m depth) was sampled from the Mongolian border along the course of the river through the Khamer Daban mountain range towards the Selenga Delta (Fig. 1).

Limnological parameters that are of interest for remote sensing studies were derived by analysis of phytoplankton composition and pigment concentration of chlorophylls and carotenoids, (Fietz and Nicklisch, 2004; Fietz et al., 2005-this issue), on DOC (personal communication, Rosell-Melé, 2003; personal communication, Borovec, 2004), and on suspended matter concentration. The water samples were taken from 1, 5, and 30 m depths, plus additional depths if the fluorescence probe measurements indicated phytoplankton subsurface maxima at these depths. The sampled waters were immediately filtered on board the ship for the pigment and the DOC analyses, and for the yellow substance absorption measurements. The samples for analysis of pigment concentration were filtered on 0.7-μm pore Whatman GF/F filters and were analysed using HPLC (Fietz and Nicklisch, 2004). Phytoplankton and autotrophic picoplankton were counted under light and epifluorescence microscopes (Fietz and Nicklisch, 2004). The

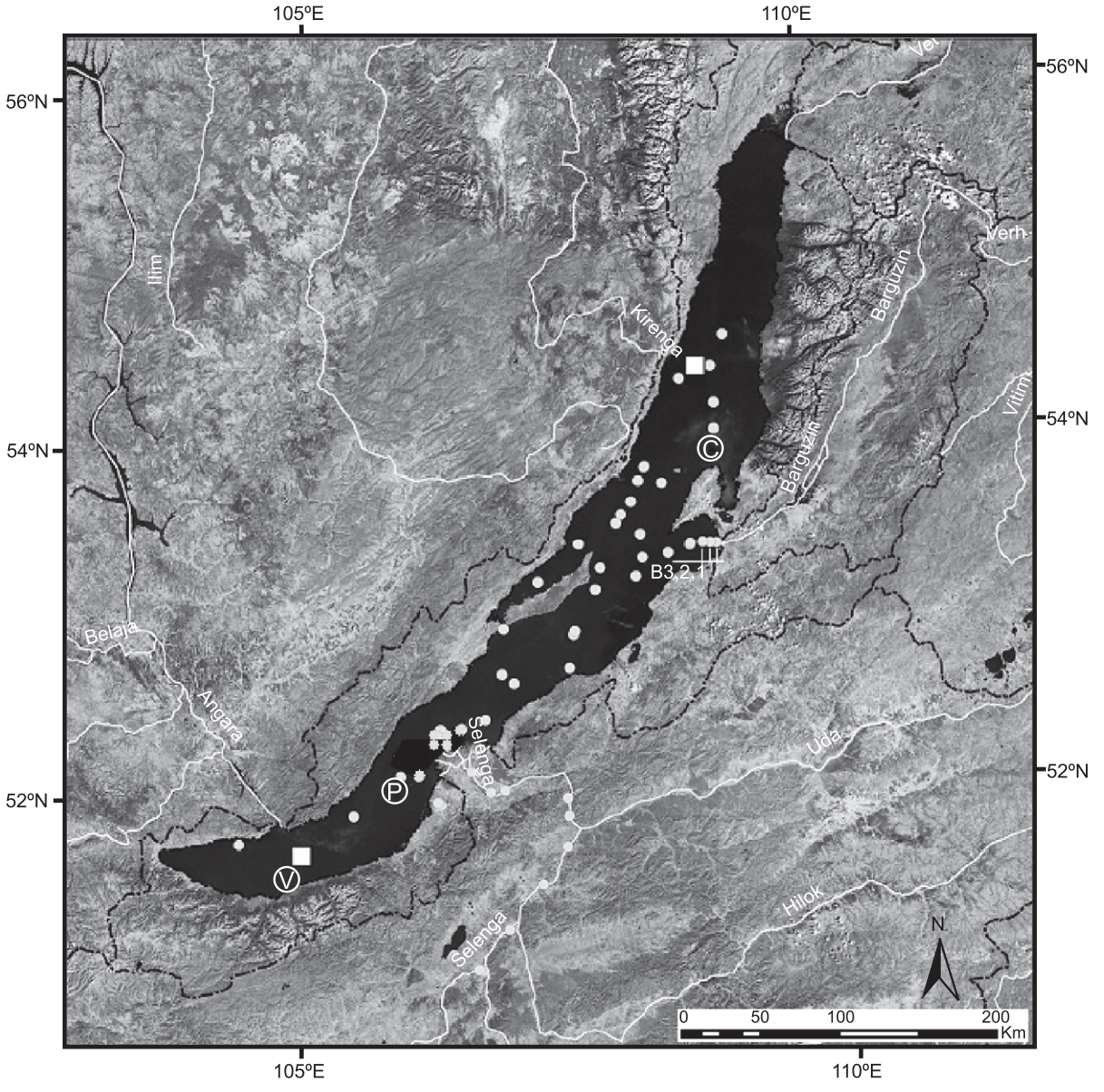

Fig. 1. Landsat TM-MOSAIC RGB742 (UTM 48), source: Baikal Online-GIS: http://dc108.gfz-potsdam.de/website/. The satellite map shows the Lake Baikal area, the three CONTINENT coring sites (C=Continent, P=Posolsky, V=Vydrino), the sediment traps (squares), plus the stations where bio-optical data were collected in 2001, 2002, and 2003 (circles). Additionally, note the transect sampling at B1, B2, B3, in Barguzin Bay.

samples that were filtered on a 0.2-μm pore cellulose acetate filters were analysed for DOC (personal communication, Rosell-Melé, 2003) using the high-temperature catalytic oxidation method. Suspended particulate matter (SPM) concentration was determined using the gravimetric method: the samples were filtered on board ship on preweighed, predried (95 °C) cellulose acetate filters and dried before storage. Yellow substance absorption was measured relatively to pure water after filtration through 0.7-μm pore Whatmann glass fibre filters in a 5-cm cuvet, using a Spectroquant NOVA60 (Merck).

Information on the underwater light field was acquired spectrometrically using field spectrometer

Table 1
Value span of ground truth data sets (CONTINENT field expeditions in 2001, 2002, and 2003)

	Years	*n*	Mean	Min	Max
Chl-*a* [μg l^{-1}], all samples	2001, 2002, 2003	214	1.42	0.29	4.87
Chl-*a* [μg l^{-1}], type: pelagial	2001, 2002, 2003	142	1.07	0.29	3.5
SPM [mg l^{-1}], type: pelagial	2001, 2002, 2003	24	0.8	0.2	1.6
SPM [mg l^{-1}], type: fluvial input	2001	6	2.8	0.5	5.1

measurements (GER 1500, Geophysical and Environmental Research Corporation, New York, USA) that were performed at approximately 25 stations during each ship cruise in 2001, 2002, and 2003 (Heim et al., 2003). The underwater light field was measured within a depth range of 1–5 m based on the Smith and Baker (1983) method; simultaneously, the downwelling incident irradiances $E_{\mathrm{down}}(\lambda)[0+]$ were measured onboard ship. These irradiance values were transferred below the water surface after Gordon et al. (1988a) using:

$$E_{\mathrm{down}}(\lambda)[0-] = E_{\mathrm{down}}(\lambda)[0+]*0.96 \quad (1)$$

where the retrieved water volume reflectance, $R_{\mathrm{vol}}(\lambda)$, is the diffuse reflectance $E_{\mathrm{up}}(\lambda)[0-]/E_{\mathrm{down}}(\lambda)[0-]$ directly at the air–water interface. Another standard parameter, the remote sensing reflectance, $R_{\mathrm{RS}}(\lambda)$, was calculated by:

$$R_{\mathrm{RS}}(\lambda)[0+] = \left(E_{\mathrm{up}}(\lambda)[0-]*0.52/E_{\mathrm{down}}(\lambda)[0+]\right)/Q \quad (2)$$

where Q (the ratio between upwelling radiance and upwelling irradiance) is assumed to be equal to 5 (Mueller and Austin, 1995), and the ratio between below and above water radiance is assumed to be equal to 0.52 (Gordon et al., 1988a).

3.1.2. Geo-biolimnological data set

Fietz and Nicklisch (2004) assessed phytoplankton pigment composition of the water samples and phytoplankton assemblages for unstratified and stratified conditions. Chlorophyll concentrations in the pelagial waters ranged from 0.3 to 3.5 μg l^{-1} chl-*a*, with average concentrations for the central part of the North Basin of 0.4–0.7 μg l^{-1} chl-*a*, for the Central Basin of around 0.8 μg l^{-1} chl-*a*, for the South Basin of around 1.2 μg l^{-1} chl-*a*, and for the areas influenced by the Selenga input to around 2 μg l^{-1} chl-*a*. The dominant groups incorporated Bacillariophyceae plus Chrysophyceae, Chlorophyta, cyanobacterial picoplankton, and Eustigmatophyceae (Fietz et al., 2005-this issue). This phytoplankton composition varied within the Lake Baikal water body depending on latitude (Fietz and Nicklisch, 2004). As the remote sensing reference, chl-*a* values of each sampling point have been averaged over a depth up to 30 m, equivalent to the extent of Secchi depths in Lake Baikal.

The Selenga River carried a mean suspended matter load of approximately 15 mg l^{-1} along its course in June/July 2001, while up to ca. 22 mg l^{-1} SPM river load reached the Selenga Delta area. Data collected during the 2001 ship cruise exhibited the widest SPM concentration range due to flooding events in the Lake Baikal area and served as the calibration database for the SPM algorithm development. SPM concentrations in 2001 varied from 0.2 mg l^{-1} for the central region of the North Basin, to average concentrations from 0.4 to 1 mg l^{-1} for the Central and the South Basins and up to 5 mg l^{-1} around the shallow waters of the Selenga Delta. In summer 2002 and 2003, the hydrological conditions were unexceptional (unlike the flooding which occurred in summer 2001) and there was no influence of terrigenous input in the pelagic areas. Table 1 gives an overview of the range of chlorophyll and SPM measured during the CONTINENT Cruises 2001 and 2002.

In summer 2002, DOC measurements (0.2-μm filter pore size) for the pelagic waters showed values lower than 0.5 mg l^{-1} for the Northern and Central Basins in 2002, but were up to 2 mg l^{-1} DOC in several regions of the South Basin (personal communication, Rosell-Melé, 2003). In July 2003, DOC concentrations were on average 1.2–1.4 mg l^{-1} (0.4 μm filter pore size) in the pelagial waters of the Southern and the Central Basin (personal communication, Borovec, 2004). The yellow substance absorption

measurements of the cruise in 2002 served as an estimate of the absorption at 440 nm. However, the quality of the spectral laboratory measurements on board the ship was not good enough to evaluate slope and exponent values.

3.2. Satellite data

3.2.1. SeaWiFS

The SeaWiFS instrument is on board the Orbimage2 satellite on a 705-km circular orbit with a revisit time of 1–2 days. The optical scanner records the reflected radiances from the atmosphere and the earth's surface in eight spectral bands (Table 2). The transmitted High Resolution Picture Transmission (HRPT) satellite data have a spatial resolution of a nominal pixel size of 1.3 km^2 at nadir. From June 2001, the SeaWiFS receiving station in Ulaanbaatar (Mongolia) provided us with HRPT data of SeaWiFS, which were processed using the SeaDAS (NASA) software (McClain et al., 2000). The HRPT Level 1A (unprocessed) SeaWiFS data from Ulaanbaatar were transferred to Level 1B (radiometrically converted) products, the reflectances at the top of the atmosphere, R_{toa}. Table 2 gives an overview on the SeaWiFS acquisition data that were used in this study.

3.2.2. Atmospheric correction

The radiances measured at the sensor are typically an order of magnitude larger than the water-leaving radiances carrying the optical information of the upper water column. This is due to the scattering of solar radiation and reflected radiation by air molecules, aerosols, and by the lake's surface itself. The removal of these atmospheric and surface effects is called atmospheric correction. The reflectances R_{TOA} have at first to be corrected for the atmospheric molecular contribution of Rayleigh scattering (Young, 1981; Gordon et al., 1988b) and the ozone and oxygen absorption. Then, Mie scattering by specific aerosol assemblages and the multiple scattering between aerosols and air molecules have to be corrected according to established aerosol climatologies. With this kind of atmospheric correction, new geophysical output parameters of Level 2, the remote sensing reflectances R_{RS}, are produced, and in the case of water remote sensing, these are the water-leaving reflectances. Without a highly accurate atmospheric correction, it is not possible to derive chlorophyll and suspended matter values within realistic concentration ranges in the case of clear water bodies. This problem is well known, especially over inland and coastal water bodies (e.g. Ruddick et al., 2000; Jørgensen, 2000, 2004) due to complex atmospheric composition and areas of non-zero water-leaving radiances in the near-infrared.

The average barometric pressure values of the respective summer months were applied, to account for the continental air pressure oscillation in Southern Siberia. Changes in air pressure are related to changes in concentration of air molecules (nitrogen, oxygen, etc.). The discrepancy between the actual low-pressure values in July to the barometric pressure calculated using a digital elevation model (approximately 10 mbar) accounts, e.g. for -0.05 W m^{-2} nm^{-1} sr^{-1} in the Rayleigh radiances in SeaWiFS band 1 (412 nm).

The atmosphere over Lake Baikal is very transparent with low aerosol concentrations over the Central and the North Basins (van Molderen et al., 1996). The volume fraction of large biogenic aerosols (>2 μm) covers ca. 30% in the summer aerosol assemblage (Matthias-Maser et al., 2000). The atmospheric processes of cyclonic and anticyclonic air circulation force upwelling in the centre of the lake basins, and this in turn is accompanied by wide areas of high humidity (90%), humidifying of aerosols, or even by advective fogs (Balin et al., 2003). The

Table 2
Sensor characteristics of SeaWiFS onboard SeaSTAR (NASA): HRPT format

Mission (launch)	SeaWiFS (1997)
Resolution [km] (area coverage format)	1.1 (HRPT)
Swath [km] (area coverage format)	2801 (HRPT)
Visible band numbers	1, 2, 3, 4, 5, 6
Central visible wavelengths [nm]	412, 443, 490, 510, 555, 670
NIR band numbers	7,8
Central NIR wavelengths [nm]	765, 865
Orbit node (inclination)	12:00 noon+20 min (descending)
Orbit type (height [km])	Sunsynchronous (705)
Onboard calibration	Solar diffuser, lunar imaging

atmospheric conditions do not reflect standard continental atmospheric conditions, which generally have a low humidity and relatively high amount of small sized aerosols.

The results of SeaDAS standard atmospheric correction were tested on HRPT SeaWiFS summer data of 2001 and 2002 using different aerosol models. The ratio of two Rayleigh corrected spectral bands (i/j) is indicative for the aerosol composition. This is termed the ratio $\epsilon^{(i,j)}$ of single-scattering aerosol reflectances. In SeaDAS, the ratio $\epsilon^{(7,8)}$ of the Rayleigh-corrected reflectance in SeaWiFS band 7 against the Rayleigh-corrected reflectance in band 8 is used to choose the aerosol model. An ϵ value of approximately 1 refers to a so-called white spectral behaviour which is caused by relatively large particles (e.g. aerosol size distribution in marine atmospheres). Large epsilons point at an aerosol composition typically with a dominance of small particles (e.g. aerosol size distribution in urban and rural atmospheres). Unusual large epsilons (ϵ>1.35) may be indicative of non-zero water-leaving radiances in the near-infrared (e.g. Ruddick et al., 2000) and can be excluded since the development of SeaDAS version 4.4. The majority of SeaDAS aerosol models (coastal with different humidities; tropospheric, etc.) failed during the processing, which corrects for the Mie scattering. The SeaWiFS data in this study could be successfully processed with the parameter choice of ϵ around 1, representing an atmosphere containing large particles (Table 3).

3.2.3. Satellite data analyses

The atmospherically corrected satellite data were geo-referenced with the software ERDAS Imagine (ESRI). Image processing included spectral analyses, which were conducted with the image analysing software ENVI (RSI). Furthermore, using mathematical combinations of the atmospherically corrected visible SeaWiFS bands (b1, b2, b3, b4, b5, b6), it was possible to combine their multi-spectral information on an experimental basis with field data, respectively, with global ground truth data sets as described below.

The phytoplankton's main photosynthetic pigment, chl-*a*, is generally estimated in oligotrophic water by its absorption maximum in the blue wavelength region around 440 nm (Williams et al., 1986). Additionally, the phytoplankton pigment groups of carotenoids and phycobillins vary the spectral shape of the radiances leaving water. Therefore, chlorophyll algorithms that are suitable for oligotrophic waters also take into account the spectral green range, using different ratio algorithms. In oligotrophic waters, there is no water-leaving signal in the red and near-infrared region, which could be evaluated for chlorophyll quantification. This is, why we have proceeded with marine algorithms for oligotrophic systems, and not with the common red/near-infrared algorithms for limnic and coastal systems. Phytoplankton composition and its pigment configuration and morphology are variable on a regional and seasonal scale, which is a major reason for discrepancies in chlorophyll calculation (Williams et al., 1986).

The best known and globally used NASA chlorophyll algorithms OC2 and OC4 (O'Reilly et al., 1998, 2000) have been established by linear regression analyses between the logarithm of chlorophyll concentration (global ground truth data set) and the logarithm of the ratio of two bands in the blue–green spectral range (Table 4). These global band ratio algorithms achieve accuracies of ±35% in case 1 conditions (O'Reilly et al., 2000). Iluz et al. (2003) list a set of best-fit functions of the reflectance ratio

Table 3
HRPT SeaWiFS acquisitions and dates of CONTINENT cruises

	April	May	June	July	August	September
HRPT 2001			25, 27, 30	2, 4, 16, 18, 19, 21, 26, 30	6, 7, 8, 20, 25, 28, 29, 31	7, 17, 28
(<30% clouds)			(25)	(19)	(6, 8, 28)	
Cruise 2001				15–25		
HRPT 2002	30	6, 8, 9, 10, 12, 14, 18, 22, 23, 25	11, 12, 14, 22, 29	2, 12, 13, 20, 22, 24, 25, 26	1, 2, 6, 9, 11, 17, 24, 30	1, 7
(<30% clouds)	(30)	(6, 8, 14, 23, 25)		(20, 24, 25, 26)	(9)	
Cruise 2002				5–15		

Table 4
Comparison of the best-fit chl-*a* algorithms tested in this study

Source	x=Ri/Rj ($R=L_{up}/E_{down}$)	Chl-*a* algorithm	r^2
A			
OC2 global chl-*a*, O'Reilly et al. (2000)	x=log10{R490/R555}	$10^{\{0.319-(-2.336x)+0.879(x^2)-0.135(x^3)-0.071\ (x^4)\}}$	0.74
B			
OC4 global chl-*a*, O'Reilly et al. (2000)	x=log10{R443/R555}, {R490/R555}, {R512/R555} (max ratio: MAX)	$10^{\{0.366-(-3.067x\mathrm{MAX})+1.93(x\mathrm{MAX}^2)+0.649(x\mathrm{MAX}^3)+1.532\ (x\mathrm{MAX}^4)\}}$	0.74
C			
Empirical chl-*a*, this study, Lake Baikal (RU), July 2002	x=R490/R550	$1.94x^{-2.81}$	0.73
D			
Empirical chl-*a*, this study, Lake Baikal (RU), July 2001+2002	x=R490/R550	$1.43x^{-1.8}$	0.72
E			
Empirical chl-*a* this study, Lake Baikal (RU), July 2002	x=R443/R550	$1.82x^{-2.47}$	0.73
F			
Iluz et al. (2003), Gulf of Eilat (Red Sea), years 1994+1995+1996, all seasons	x=R443/R550	$0.7x^{-0.98}$	0.74
G			
Iluz et al. (2003), Gulf of Eilat (Red Sea), year 1996, all seasons	x=R443/R550	$1.27x^{-1.38}$	0.74
H			
Gordon and Morel case 1 (1983) (in Iluz et al., 2003)	x=R443/R550	$1.13x^{-1.71}$	0.74

This table shows the parameters of chl-*a* algorithm, and as an example, the performance using atmospherically corrected SeaWiFS data from 2002/07/20. In each case, the determination coefficient (r^2) of chl-*a* measured (ground truth data set of Lake Baikal in 2002) and chl-*a* calculated from 2002/07/20 is specified. Values of measured chlorophyll are the mean concentrations of all samples from 5 to 30 m at one sampling point.

$R_{Rs}443/R_{Rs}555$ that have been used by different authors for studies in oligotrophic waters. Their own empirical coefficients in their SeaWiFS satellite data investigations of the oligotrophic Gulf of Eilat (Red Sea) showed different values each year during three successive years. We calculated chlorophyll concentrations using OC2 and OC4 chlorophyll algorithms. Additionally, we tested coefficients for 11 ratio algorithms from several sources, which are described in Iluz et al. (2003) as well as a ratio algorithm derived from the ground truth data set in 2002 (n=12) (Table 4).

The physically accepted principle for standard empirical SPM algorithms (e.g. Tassan, 1994; Peters et al., 1999) holds that for increasing concentrations of suspended matter the reflectance increases in the visible and near-infrared spectrum. Commonly, SPM algorithms are derived from a linear regression between the peak of the water-leaving reflectances and the in situ SPM data set (e.g. Jørgensen, 2000; Binding et al., 2003), while the height of the peak may be normalized using band 8 (850 nm) (Doxaran et al., 2002). In terms of empirical algorithms, the red to

green reflectance ratio band 5 (555 nm)/band 6 (650 nm) is expected to perform for SPM algorithms, reflecting the shift of the peak in the reflectance spectra from green to red with increasing SPM concentrations (Mitchelson-Jacob, 1999, Froidefond et al., 2002). The reason is that the change in height of the water-leaving reflectance in the green wavelength range plateaus to match a logarithmic distribution above a given turbidity (e.g. in case of SPM higher than 5 mg l^{-1} (Froidefond et al., 2002) while similar results were also found by Stumpf and Pennock (1989), Ritchie et al. (1990), and Moore et al. (1999). Above this turbidity threshold, the height of reflectances, first in the red, then in the near-infrared wavelength range, rises with increasing SPM concentrations. Commonly, all these empirical SPM algorithms, which are based on the principle of rising reflectances in field spectrometer measurements and satellite data, originate from coastal areas of the Mediterranean, Atlantic Ocean, and the North Sea.

There still exists a large uncertainty from the optical properties of the in situ state of suspended matter (due in part to a lack of detailed field observations to derive accurate parameterizations of processes such as flocculation, re-suspension, etc.). Results of investigations in optical turbidity measurements include findings that optical variations (of measurements of attenuation, scattering, reflection) depend not only on the concentration, but significantly as well on the shape, size, and composition of suspended particles (Gippel, 1988; Clifford et al., 1995) as on the coloured dissolved matter content (Malcolm, 1985). Therefore, the optical relationships may be assessed in situ as trends of different water bodies (e.g. Novo et al., 1989; Packman et al., 1999).

In this study, we involved the optical parameter 'diffuse attenuation coefficient' as a sensible optical coefficient, which combines the absorbing and scattering processes (Kirk, 1976). The algorithm of the diffuse attenuation coefficient at 490 nm (K490) is based on calculations on empirical coefficients from a global data set (O'Reilly et al., 2000):

$$\mathrm{K490} = Kw490 + 0.15645 \times ([\text{band 4}]/[\text{band 5}])^{-1.5401} \text{in} [m^{-1}] \quad (3)$$

where Kw490 is the diffuse attenuation coefficient for pure water, while the SeaWiFS band input data band 4 (510 nm) and band 5 (555 nm) are the atmospherically corrected water-leaving radiances. This remotely sensed parameter was related to a limited set of CONTINENT ground truth samples representing terrigenous influence.

4. Results

4.1. SeaWiFS data analyses

4.1.1. Quantitative results

Lake Baikal is not influenced by strong surface currents, as is the case for marine coastal waters. Therefore, we used the ground truth data set of chlorophyll and suspended matter concentrations that originate from a storm-free cruising period between 17/07/2001 and 24/07/2001 as the validation data set for the cloud-free parts of SeaWiFS acquisitions on the 02/07, 04/07, 16/07, 18/07, 19/07 (19/07 as the only acquisition with less then 30% cloud cover), 21/07, and 26/07/2001. In 2002, despite foggy and high rainfall weather conditions, the ground truth data between 05/07 and 15/07/2002 were used to evaluate the cloud-free parts of the SeaWiFS acquisition dates 02/07, 12/07, 13/07, 20/07, 22/07, 24/07, and 25/07/2002.

The self-established empirical chlorophyll algorithm (n=12) of the SeaWiFS data set from 2002 (r^2=0.86) seems not to be suitable for the data sets in 2001 (r^2=0.55), and is therefore not examined any further. One possible reason are significant differences in horizontal phytoplankton distribution (Fietz and Nicklisch, 2004), considering that the large water body of Lake Baikal stretches over three latitudes and therefore is regionally influenced by different meteorological and hydrophysical factors. Additionally, factors influencing the quality of OC2 and OC4 algorithms such as the carotinoid/chlorophyll ratio varied within the bio-optical provinces of Lake Baikal and showed a different average value for summer 2003 compared to the summers 2001 and 2002.

Therefore, a global chl-a algorithm, which is based on a large ground truth data set, was considered to be more robust and more suitable for this study. The results in Tables 5a, 5b and 6 show the best collective performance for OC2 and OC4 chlorophyll algorithms

Table 5a
Comparison between chl-*a* measured and chl-*a* calculated from SeaWiFS data in July 2001

2001	HPLC	OC4 07/16-26	OC4 07/19	OC2 07/16-26	OC2 07/19
n chl-*a*, all	12	4	12	4	12
n chl-*a*, case 1		4	8	4	8
Mean [μg l^{-1}]	1.7	1.7	2.6	1.5	2.4
Median [μg l^{-1}]	1.2	1.0	1.9	1.0	1.8
S.D. [μg l^{-1}]	1	1.1	1.9	0.85	1.7
Accuracy, all [μg l^{-1}]		±0.4 ±24%	±1.4 ±90%	±0.4 ±22%	±1.2 ±85%
Accuracy, Case 1 [μg l^{-1}]			±0.6 ±32%		±0.5 ±30%

Values of measured chlorophyll are the mean concentrations of each sampling point in July 2001 (personal communication, S. Fietz) from 5 to 30 m depth. Only the cloud-free parts of SeaWiFS data (2001/07/16-26) could be chosen, and the most cloud-free acquisition was obtained on the 2001/07/19. Note that the accuracy of the complete calculated chl-*a* data set is reduced by the influences of terrigenous input.

in case 1 water areas, which are not influenced by terrigenous input. The calculated chlorophyll OC2 and OC4 concentrations are within an estimation error of ±32% for 2001 and ±27% for 2002 (when in 2001, only the cases of clear pelagic waters is considered). The best of the set of 11 fitting coefficients for case 1 waters listed in Iluz et al. (2003) was found in the coefficients of Gordon and Morel (1983) (Tables 4 and 6). Tables 5a and 5b show the accuracy and average deviation for the calculated chlorophyll concentrations of SeaWiFS acquisitions in the time frame of the CONTINENT cruises in 2001 and 2002. Fig. 2 shows the scattergram of calculated OC2 chlorophyll (case 1) against the ground truth pigment concentrations for 2001 and 2002.

Despite the high quality for the data sets in 2002, the comparison of ground truth data with calculated chlorophyll data shows that there is considerable chlorophyll overestimation for several data points in 2001 (Table 5a). These are the samples in terrigenously influenced areas of the lake, where there is considerable absorption in the blue wavelength range by yellow substances (e.g. around the Selenga Delta and Barguzin Bay). In the case of high organic fluvial terrigenous input, the absorption in the blue to green spectral wavelength range is caused by yellow substance and by phytoplankton. Because the standard chlorophyll algorithms do not have the capability to distinguish between yellow substance and phytoplankton absorption, they overestimate chlorophyll concentrations in these waters considerably. In contrast to clear pelagic waters, the chl-*a* output for fluvial influenced areas seems to be amplified by a factor of 3–5. Pozdnyakov et al. (2003) reported similar findings in a study on coastal waters of the White Sea. They estimated a threefold chlorophyll-model overestimation that is caused by the optical interactions of high organic terrestrial input.

Considering that there are regional and seasonal changes in pigment composition in Lake Baikal, as described above, we decided to rely on the robust global OC2 chlorophyll algorithm for processing the SeaWiFS acquisitions in the months of June, August and September 2001 and 2002. To exclude wrong processing in case 2 type waters, a 'mask of terrigenous input' is applied which is described in the following section. Due to case 2 conditions, i.e. widespread terrigenous influence during the snow melting season, acquisitions of the SeaWiFS time series in May were not evaluated for chlorophyll concentration.

Table 5b
Comparison between chl-*a* measured and chl-*a* calculated from SeaWiFS data in July 2002

2002	HPLC	OC4 07/02-13	OC4 07/20	OC2 07/02-13	OC2 07/20
n chl-*a*, all	22	18	17	18	17
n chl-*a*, case 1		18	17	18	17
Mean [μg l^{-1}]	1.6	1.6	1.35	1.45	1.3
Median [μg l^{-1}]	1.55	1.2	1.25	1.15	1.3
S.D. [μg l^{-1}]	0.8	0.9	0.5	0.8	0.4
Accuracy, all [μg l^{-1}]		±0.33 ±20%	±0.35 ±27%	±0.3 ±18%	±0.3 ±24%

Values of measured chlorophyll are the mean concentrations of each sampling point in July 2002 (personal communication, S. Fietz) from 5 to 30 m depth. Only the cloud-free parts of SeaWiFS data (2002/07/02-13) could be chosen, and the most cloud-free acquisition was obtained on the 2002/07/20. Note that the contributions of sampling points vary between the data sets of 2002/07/02-13 and 2002/07/20 due to different cloud coverage.

Table 6
Overview on accuracies of chl-*a* algorithms (see also Table 4) applied on SeaWiFS data in July 2002 (07/20)

2002/07/20	HPLC	OC4	OC2	This study, July 2001+2002
n chl-*a*, all	22	17	17	17
n chl-*a*, case 1		17	17	17
Mean [μg l^{-1}]	1.6	1.35	1.3	0.85
Median [μg l^{-1}]	1.55	1.25	1.3	0.8
S.D. [μg l^{-1}]	0.8	0.5	0.4	0.25
Accuracy, all [μg l^{-1}]		±0.35 ±27%	±0.3 ±24%	±0.38 ±27%

2002/07/20	HPLC	Iluz et al. (2003), years 1994–1996	Iluz et al. (2003), year 1996	Gordon and Morel (1983), case 1
n chl-*a*, all	22	17	17	17
n chl-*a*, case 1		17	17	17
Mean [μg l^{-1}]	1.6	0.6	1	0.85
Median [μg l^{-1}]	1.55	0.6	0.94	0.8
S.D. [μg l^{-1}]	0.8	0.1	0.4	0.25
Accuracy, all [μg l^{-1}]	±54%	±0.6 ±27%	±0.41 ±27%	±0.45

Chl-*a* algorithms are OC2 (A, Table 4) and OC4 (B, Table 4), empirical chl-*a* algorithm (D, Table 4) from ground truth data set of Lake Baikal in 2001 and 2002 (this study), chl-*a* algorithms from Iluz et al. (2003): coefficient of studies from 1994 to 1996 (F, Table 4), coefficient of 1996 separately (G, Table 4), and case 1, Gordon and Morel (1983) (H, Table 4).

According to ground truth and SeaWiFS spectra for 2001–2002, the green peak of the highly transparent waters of Lake Baikal is commonly located at SeaWiFS band 4 (510 nm). However, the absorbing and scattering optical activities in the presence of the terrigenous input shift the peak position towards SeaWiFS band 5 (555 nm). The waters in the observable cloud-free parts of the SeaWiFS acquisitions are not as turbid, so there does not occur a spectral shift in the peak position of the SeaWiFS spectra from SeaWiFS band 5 (555 nm) to band 6 (650 nm). This observed spectral behaviour of the peak shifting from 510 to 555 nm in the 2001–2002 SeaWiFS data sets of Lake Baikal can be simulated and reproduced using the bio-optical software 'Water Colour Simulator' (WASI) (Gege, 2004). This described spectral behaviour has been similarly shown from previous historical limnological studies. For example, Thomson and Jerome (1975) stated that clear waters of Lakes Ontario and Superior (USA) had a dominant wavelength of 490–530 nm, biologically more productive waters had a dominant wavelength of 550–560 nm, and waters with heavy sediment loadings had a dominant wavelength of >565 nm.

This spectral shift is regarded as an indicator for the terrigenous input and can be used by applying a 'mask of terrigenous input' on the atmospherically corrected SeaWiFS data defined by reflectance ratio values of $R_{RS}510/R_{RS}555$ below 0.9. This is in accordance to the SeaWiFS study done by Froidefond et al. (2002) in the Bay of Biscay, who observed chlorophyll overestimation (due to terrigenous input) in cases of $R_{RS}490/R_{RS}555$ below 1.

When calculating standard suspended matter products (Jørgensen, 2000; Binding et al., 2003), the high organic fluvial input in Barguzinski Bay and local fluvial input into the South Basin shows inverse grading with lowest calculated SPM concentrations towards the river inlets. Field spectrometer measurements and ground truth data show that, for several bio-optical provinces of Lake Baikal, the assumption

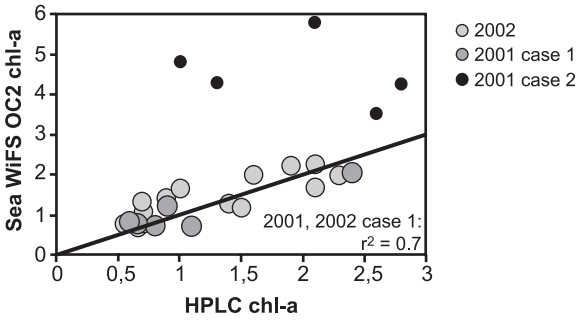

Fig. 2. The scattergram shows the relationship between concentrations of chl-*a* calculated from SeaWiFS OC2 and chl-*a* calculated determined from ground truth measurements during field expeditions in Lake Baikal during 2001 and 2002. Values of measured chlorophyll (HPLC) are the mean concentrations of each sampling point from 5 to 30 m depth. For the OC2 chl-*a* calculations, the most cloud-free acquisitions in 2001 (2001/07/19) and 2002 (2002/07/20) were chosen. Note the considerable chl-*a* overestimation caused by the influences of terrigenous input in case 2 waters. (Data available at: doi:10.1594/GFZ/ICDP/CON/2004).

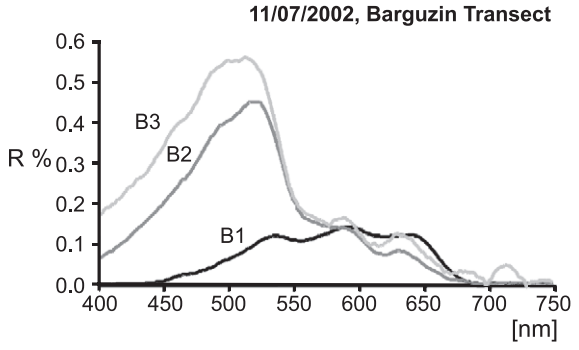

Fig. 3. Barguzin transect 2002/07/11, variation of volume reflectance data (GER 1500). B1: 0.9 km from Barguzin mouth: 4, 3.9, and 1.9 μg l^{-1} (DOC**, SPM, and chl-*a*); B2: 11.2 km from Barguzin mouth: 1.4, 1.3, and 1.8 μg l^{-1} (DOC**, SPM, and chl-*a*); B3: 19.2 km from Barguzin mouth: 0.5, 0.8, and 2 μg l^{-1} (DOC**, SPM, and chl-*a*). (Data available at:doi:10.1594/GFZ/ICDP/CON/2004.) ** Personal communication, Rosell-Melé, 2003.

that the suspended matter concentration correlates with the height of the reflectance peak is not appropriate (Fig. 3). This may be because absorption processes become dominant in highly organic waters and can reduce the water-leaving reflectance sufficiently to mask scattering by even relatively high quantities of suspended particles.

The approach chosen in this study quantifies the SPM concentration with the attenuation coefficient value instead of the water-leaving reflectance value. The limited set of in situ terrigenous particulate samples (n=6 in 2001) was linked to SeaWiFS K490 data by linear regression, leading to:

$$SPM = 9.4502 \times \left(0.016 + 0.15645 \times ([b4]/[b5])^{-1.5401}\right) - 0.6111 \text{ in} [\text{mg l}^{-1}] \quad (r^2 = 0.71) \qquad (4)$$

Here, due to the very limited ground truth data set of water samples, which were influenced by terrigenous input, this is a very preliminary calculation. Nevertheless, this approach demonstrates its potential to get an adequate representation of the high organic terrigenous input in the case of Lake Baikal.

Fig. 4 represents the result as concentrations of SPM (mg l^{-1}) of the 19/07/2001 acquisition. The

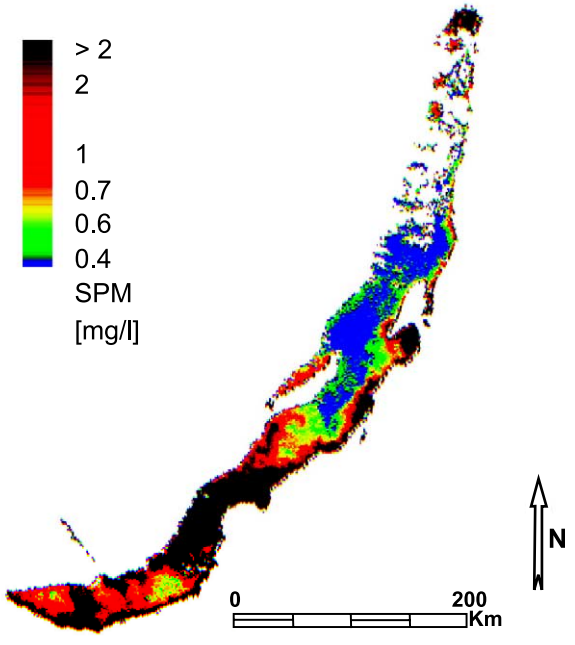

Fig. 4. SeaWiFS SPM map, 2001/07/19. SPM concentrations are in mg l^{-1}. This figure shows intense fluvial input by the Selenga River, the Barguzin River and local mountain rivers due to storm events that happened 2 weeks previously. (Data available at: doi:10.1594/GFZ/ICDP/CON/2004).

calculated SPM concentrations correctly highlight the Selenga River and other local river distributions. The data sets in July 2001 show considerable terrigenous input especially in the South Basin and represent exceptional hydrological conditions, due to catastrophic flooding events in early July in the Northern Mongolian and the Irkutsk region.

4.1.2. SeaWiFS time series

The limnological and geochemical field data enable the bio-optical classification of water types according to which constituents (phytoplankton pigments, suspended matter, yellow substance) mainly influence the water-leaving spectral signal. Important bio-optical provinces for Lake Baikal are the pelagic clear waters, the maximal oligotrophic gyres in the North Basin, the suspended matter-dominated Selenga river input, and the organic matter-dominated Barguzin river input.

The spatial overview of satellite data enables the interpretation of the CONTINENT sites in relation to discrete field data. In May, the North Basin is still under ice cover, while the Central and South Basins are influenced by substantial fluvial input from the Selenga and local mountain rivers. During this season, the Selenga River inflow is mainly distributed towards the South Basin along the Western coastlines and there is reduced terrigenous input into the Central Basin. Fig. 5 shows the typical situation of heavy terrigenous input in times of the ice break up and snow melt season during the month of May (2002). The terrigenous input firstly increased after the break-up of ice on the lake. Then, signals of the suspended and dissolved terrigenous material vanished quickly by the end of May/beginning of June, as the calculated SPM concentrations in the South Basin decline to levels below 1 mg l^{-1} again.

In late July and August 2001 and 2002, strong horizontal heterogeneity develops with eddy formation and phytoplankton development. There is also much less fluvial input coming into the lake from the rivers. This is

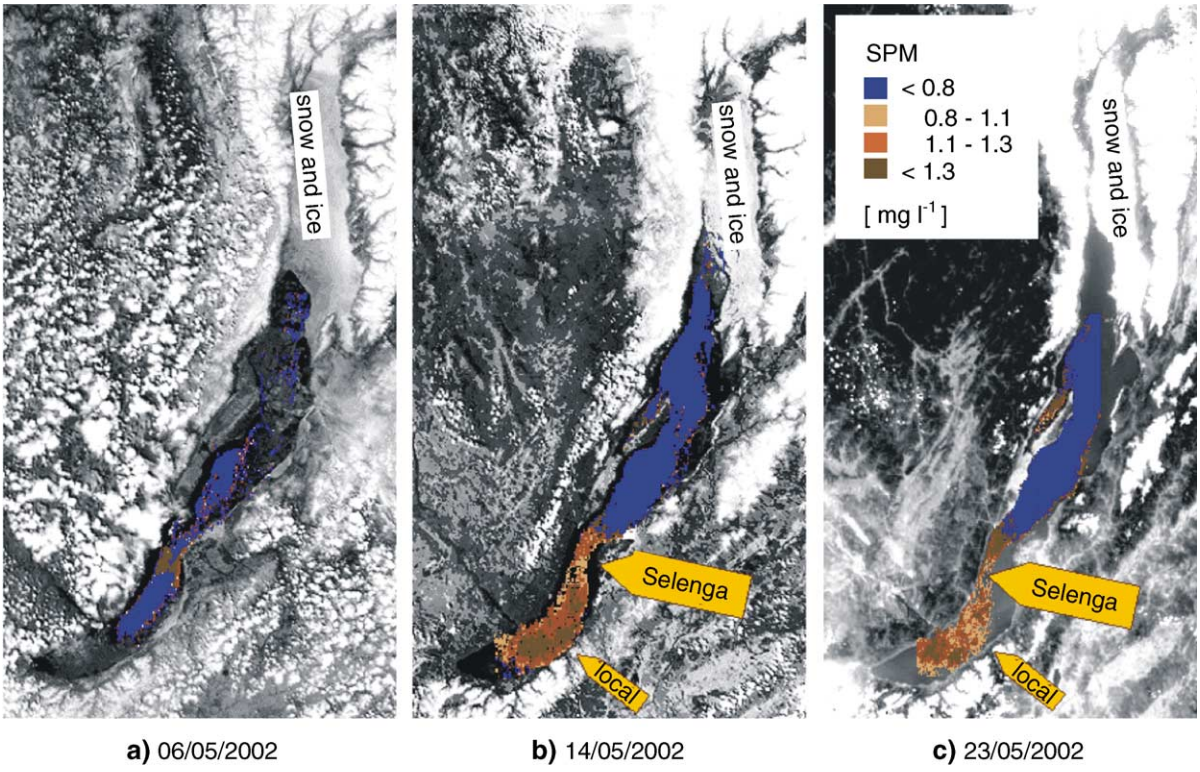

Fig. 5. SeaWiFS colour-coded SPM maps, May 2002. SPM concentrations are in mg l^{-1}. The time series shows the increase of the fluvial input during the snow melting season. Note the high input from 2002/05/14 to 2002/05/23 by the Selenga River and local mountain rivers into the Southern Basin. (Data available at: doi:10.1594/GFZ/ICDP/CON/2004).

associated with a change in the circulation patterns, where the relatively low fluvial inputs from the Selenga and Barguzin Rivers flow into the Central Basin.

According to the satellite data time series, the coring site 'Posolsky' is inter- and intra-annually highly influenced by the Selenga River input. Whereas, according to the distribution pattern on the calculated SeaWiFS SPM maps, the coring site 'Vydrino' is strongly influenced by the discharge from local mountain rivers, which is in accordance to the findings of Charlet et al. (2005-this issue). At Vydrino, pollen (personal communication, Heumann and Demske, 2004) and heavy mineral analyses (personal communication, Thamó-Bozsò, 2004) of core sediments further indicate that local influences are likely to have been present on the 'Vydrino' even during early Holocene. These findings are important as biological indicators from the shallow waters of the Selenga Delta and other regions in the South Basin are different, and will have implications for how to interpret sedimentary records in these two regions.

Within the central eddies of the North Basin, the trophic state is very low, representing very oligotrophic waters. In contrast, the satellite data highlight that the east coast of the North Basin (in the region of the coring site 'Continent') consistently has (inter- and intra-annually) more phytoplankton in patchy and heterogeneous patterns. Again, this demonstrates that coring locations are important when considering how proxy material is distributed around the lake, before settling into the sediment archive. Data from this core form the basis for the reconstruction of paleoclimatic conditions for the North Basin. Thus, as a result of the remote sensing investigation, the correlation between the core records (Granoszewski et al., 2005-this issue; Rioual and Mackay, 2005-this issue) and the findings from the sediment-traps in respect, e.g. to bio-markers and bioproductivity have to be done with great care.

In summer 2001, exceptional storm events occurred that led to catastrophic floods, manifested as high fluvial discharge signals from Selenga and local mountain rivers into Lake Baikal (see also Fig. 4). Because of these floods, the optical signal of yellow substance expressed itself in wider range around the lake, with a considerable absorption in the blue and green wavelength range. This optical signal can be distinguished by the 'mask of terrigenous input', and persisted for a minimum of 2 weeks in the SeaWiFS time series. This event shows how storm conditions may influence the terrigenous signals in the sediment cores.

5. Conclusions and outlook

For paleoclimate studies, the interpretation of selected climate proxies, such as diatoms, pigments, biomarkers, carbon, and clay material in marine and liminic sediment cores, may be validated with present-day data. The aim of this remote sensing study is to provide a spatial and temporal overview of limnological parameters such as the dynamics of phytoplankton and the allochthonous input. Global and empirical SeaWiFS algorithms have been applied to the atmospherically corrected satellite data for an estimation of chlorophyll and terrigenous suspended matter.

The calculated chlorophyll values are in good agreement not only with the CONTINENT ground truth data (±30%, meeting the NASA quality standard), but also with the long-term observation data values reported in literature (Kozhova and Izmesteva, 1998). For terrigenous influenced surface waters of Lake Baikal, the OC2 chlorophyll values are three- to fivefold overestimated. As a method for quantifying terrigenous suspended matter from the SeaWiFS satellite data, we initially found the best solution was to link our ground truth data (six selected samples during the flooding event in 2001) to the 'diffuse attenuation coefficient' calculated from the SeaWiFS data.

The results of this paper demonstrate that it is possible to map the fluvial input and phytoplankton pigments of Lake Baikal using high spectral resolution satellite data. The actuo-sediment flux into Lake Baikal varies regionally and seasonally. The SeaWiFS SPM maps provide spatial distribution information for overview, especially in times of maximal terrigenous input during the snow melting season, additional to the discrete cruise data that are less conclusive and restricted to the time window of the cruise.

The SeaWiFS chlorophyll time series will be combined with information on pigments (Fietz et al., 2005-this issue) and biomarkers (Russel and Rosell-Melé, 2005-this issue) to assist the interpretation of sediment trap data and develop realistic seasonal input parameters for the CONTINENT water column transfer model. The information on spatial variation will also

complement other investigations, such as the primary production of Lake Baikal of Straskrabova et al. (2005-this issue).

Acknowledgments

We would like to thank the SeaWiFS project and the HRPT station in Ulaanbaatar, Mongolia, for the processing and providing the satellite data used in this study. This research was conducted within the project CONTINENT (supported by the European Commission under contract EVK2-CT-2000-00057). Particular acknowledgement is made to A. Rosell-Mele from the Institute of Environmental Science and Technology (ICTA), Autonomic University of Barcelona, Spain, for assistance in the field, and for performing quantitative analyses of DOC. Thanks are given to A. Nicklisch from the Humboldt University, Berlin, Germany, to V. Straskrabova and J. Borovec from the Hydrobiological Institute (HUB), Academy of Sciences of the Czech Republic, for setting up of the monitoring projects, for consultation, and for providing important data sets. Thanks are due to A.W. Mackay, D.W. Morley, and P. Rioual from University College London (UCL), UK, for provision of data sets. Finally, many thanks are given to D. Jewson and to two anonymous referees, whose comments helped to considerably improve this paper.

Appendix A. Frequently used symbols

chl-*a*	chlorophyll *a* concentration in μg l^{-1}
δ	isotopic delta value
$\epsilon^{(i,j)}$	theoretical single-scattering aerosol reflectance ratio, bands *i*/*j*
$\epsilon^{(7,8)}$	imposed multiple-scattering aerosol reflectance ratio, bands 7:8,
K490	diffuse attenuation coefficient at 490 nm in m^{-1}
$L(\lambda)$	spectral radiance in W m^{-2} nm^{-1} sr^{-1}
n	number
r^2	*R*-square/coefficient of determination
$R(\lambda)$	spectral reflectance. Frequently used variants are as follows: $R_{toa}(\lambda)$, reflectance, top of atmosphere; $R_{RS}(\lambda)$, remote sensing reflectance (sr^{-1}); $R_{vol}(\lambda)$, water volume reflectance

Appendix B. Frequently used acronyms

ATSR	Along Track Scanning Radiometer
AVHRR	Advanced Very High Resolution Radiometer
CZSC	Coastal Zone SCanner
DOC	Dissolved Organic Carbon
DOM	Dissolved Organic Matter
ENVI	Environment for Visualizing Images, software
ERDAS	Earth Resources Data Analysis System Imagine, software
ESA	European Space Agency
GER	Geophysical and Environmental Research field spectrometer
GFZ	GeoResearchCenter Potsdam, Germany
HPLC	High Performance Liquid Chromatography
HRPT	High Resolution Picture Transmission
IGB	Leibniz Institute of Freshwater Ecology and Inland Fisheries, Berlin, Germany
ICTA	Institute of Environmental Science and Technology, Barcelona, Spain
L 1A	Level 1A data, unprocessed satellite data
L 1B	Level 1B data, calibrated radiances
L 2	Level 2 data, geophysical output parameters
MERIS	Medium Resolution Imaging Spectrometer
MODIS	MODderate resolution Imaging Spectrometer
NASA	National Aeronautics and Space Administration
NOVA60	Merck photometer
SeaDAS	SeaWiFS Data Analysis System
SeaWiFS	Sea-viewing Wide Field-of-view Sensor
SPM	Suspended Particulate Matter
TM	Thematic Mapper
ETM+	Enhanced Thematic Mapper

References

Balin, Y.S., Ershov, A.D., Penner, I.E., 2003. Shipborne lidar investigations of aerosol fields in the atmosphere over lake Baikal. Atmos. Ocean. Opt. 16 (7), 541–551.

Binding, C.E., Bowers, D.G., Mitchelson-Jacob, E.G., 2003. An algorithm for the retrieval of suspended sediment concentrations in the Irish Sea from SeaWiFS ocean colour satellite imagery. Int. J. Remote Sens. 24, 3791–3806.

Bolgrien, D.W., Granin, N.G., Levin, L.A, 1992. Satellite observations of Lake Baikal thermal structures. Proc. Mapping a Monitoring of Glob. Change. ASPRS/ACSM/RT Technical papers, 1, pp. 11–20.

Bolgrien, D.W., Granin, N.G., Levin, L., 1995. Surface temperature dynamics of Lake Baikal observed from AVHRR images. Photogramm. Eng. Remote Sens. 61 (2), 211–216.

Bukata, R.P., Harris, G.P., Bruton, J.E., 1974. The detection of suspended solids and chlorophyll *a* using digital multispectral ERTS-1 data. Proc. 2nd Canadian Symp., Remote Sensing, Guelph, Canada. University of Guelph, USA, pp. 551–564.

Burgess, Ph., 2003. Remote sensing water quality parameters in the lakes of Berlin and Brandenburg with high spatial resolution satellite sensors. Diploma thesis, Humbold University, Berlin, Germany.

Charlet, F., Fagel, N., De Batist, M., Hauregard, F., Minnebo, B., Meischner, D., SONIC Team, 2005. Sedimentary dynamics on isolated highs in Lake Baikal: evidence from detailed high-resolution geophsical data and sediment cores. Glob. Planet. Change 46, 125–144 (this issue).

Clifford, N.J., Richards, K.S., Brown, R.A., Lane, S.N., 1995. Laboratory and field assessment of an infrared turbidity probe and its response to particle size and variation in suspended sediment concentration. Hydrol. Sci. 40 (6), 771–791.

Dekker, A.G., 1993. Detection of optical water quality parameters for eutrophic waters by high resolution remote sensing. PhD thesis, Vrije Universiteit Amsterdam, Netherlands.

Doerffer, R., Fischer, J., 1994. Concentrations of chlorophyll, suspended matter, and gelbstoff in case II waters derived from satellite coastal zone color scanner data with inverse modeling methods. J. Geophys. Res. 99 (D), 7457–7466.

Doxaran, D., Froidefond, J.M., Castaing, P., 2002. A reflectance band ratio used to estimate suspended matter concentrations in sediment-dominated coastal waters. Int. J. Remote Sens. 23 (23), 5079–5085.

Evans, C.A., Helfert, M.R., Helms, D.R., 1992. Ice patterns and hydro-thermal plumes, Lake Baikal, Russia: insight from Space Shuttle hand-held photography. Proc. Intern. Geosc. Rem. Sens. (IEEE), Houston, USA.

Fietz, S., Nicklisch, A., 2004. An HPLC analysis of the summer phytoplankton assemblage in Lake Baikal. Freshw. Biol. 49, 332–345.

Fietz, S., Sturm, M., Nicklisch, A., 2005. Flux of lipophilic photosynthetic pigments to the surface sediments of Lake Baikal. Glob. Planet. Change 46, 29–44 (this issue).

Froidefond, J.M., Castaing, P., Prud'homme, R., 1999. Monitoring suspended particulate matter fluxes and patterns from the AVHRR/NOAA-11 satellite: application to the Bay of Biscay. Deep-Sea Res. II 46, 2029–2055.

Froidefond, J.M., Lavender, S., Laborde, P., Herbland, A., Lafon, V., 2002. SeaWiFS Data Interpretation in a coastal area in the bay of Biscay. Int. J. Remote Sens. 23 (5), 881–904.

Gege, P., 2004. The water color simulator WASI: an integrating software tool for analysis and simulation of optical in situ spectra. Comput. Geosci. 30, 523–532.

George, D.G., Malthus, T.J., 2001. Using a compact airborne spectrographic imager to monitor phytoplankton biomass in a series of lakes in north Wales. Sci. Total Environ. 268, 215–226.

Gippel, C.J., 1988. The effect of water colour, particle size and particle composition on stream water turbidity measurements. Departm.Geography and Oceanography, University College, Australian Defense Force Academy. Working Paper 1988/3.

Gitelson, A., Mayo, M., Yacobi, Y.Z., Parparov, A., Berman, T., 1994. Development and validation of the optical model for remote detection of chlorophyll in the Southeastern Mediterranean from CZCS data. Proc. 2nd Conf, Remote Sens. Mar. Coast. Environ., New Orleans. Environmental Research Institute of Michigan, USA, pp. 293–303.

Gitel'zon, I.I., Granin, N.G., Levin, L.A., Zavoruev, V.V., 1991. Mechanisms underlying the formation and maintenance of the spatial distribution nonuniformities of the phytoplankton in Lake Baikal. Hydrobiol. J. 318, 317–320.

Gordon, H.R., Morel, A.Y., 1983. Remote Assessment of ocean color for interpretation of satellite visible imagery. Lecture Notes in Coastal and Estuarine Studies. Springer, New York.

Gordon, H.R., Brown, O.B., Evans, R.H., Brown, J.W., Smith, R.C., Baker, K.S., Clark, D.K., 1988a. A semi-analytic radiance model of ocean color. J. Geophys. Res. 93 (D), 10909–10924.

Gordon, H.R., Brown, J.B., Evans, R.H., 1988b. Exact Rayleigh scattering calculations for use with the Nimbus-7 Coastal Zone Color Scanner. Appl. Opt. 7 (5), 862–871.

Granoszewski, W., Demske, D., Nita, M., Heumann, G., Andreev, A.A., 2005. Vegetation and climate variability during the Last Interglacial evidenced in the pollen record from Lake Baikal. Glob. Planet. Change 46, 187–198 (this issue).

Heege, T., 2000. Flugzeuggestützte Fernerkundung von Wasserinhaltsstoffen am Bodensee. PhD thesis, Free University of Berlin, Germany, DLR Research Report, No. 2000-40.

Heege, T., Fischer, J., 2004. Mapping of water constituents in Lake Constance using multispectral airborne scanner data and a physically based processing scheme. Can. J. Remote Sens. 30 (1), 77–86.

Heim, B., Magnussen, S., Oberhaensli, H., Kaufmann, H., 2003. Case 2 Lake Baikal: analyses of SeaWiFS data within the scope of the paleoclimate project CONTINENT. EARSeL eProceedings 3, 127–135.

Hoogenboom, H.J., Dekker, A.G., Althuis, I.J.H., 1998. Simulation of AVIRIS sensivity for detecting chlorophyll over coastal and inland waters. Remote Sens. Environ. 65, 333–340.

Iluz, D., Yacobi, Y.Z., Gitelson, A., 2003. Adaption of an algorithm for chlorophyll-*a* estimation by optical data in the oligortophic Gulf of Eilat. Int. J. Remote Sens. 24 (5), 1157–1163.

Jerlov, N.G., 1978. A transparency-meter for ocean water. Tellus 9, 229–233.

Jørgensen, P.V., 2000. Interpretation of remote sensing ocean color in Danish coastal waters. PhD thesis, Institute of Geography, Univ. Copenhagen.

Jørgensen, P.V., 2004. SeaWiFS data analysis and match-ups with in situ chlorophyll concentrations in Danish waters. Int. J. Remote Sens. 25 (7–8), 1397–1402.

Kahru, M., Mitchell, B.G., 1999. Empirical chlorophyll algorithm and preliminary SeaWiFS validation for the California current. Int. J. Remote Sens. 20, 3423–3429.

Kalle, K., 1949. Fluoreszenz und Gelbstoff im Bottnischen und Finnischem Meerbusen. Dt. Hydrogr. Z. 2, 117–124.

Kallio, K., Kutser, T., Hannonen, T., Koponen, S., Pulliainen, J., Vepsäläinen, J., Pyhälahti, T., 2001. Retrieval of water quality variables from airborne spectrometry of various lake types in different seasons. Sci. Total Environ. 268, 59–77.

Keller, P., 2001. Imaging spectroscopy of lake water quality parameters. Remote Sensing Series, vol. 36. Remote Sensing Laboratories, University of Zurich, Switzerland.

Kirk, J.T.O., 1976. Yellow substance (gelbstoff) and its contribution to the attenuation of the photosynthetically active radiation in some inland and coastal South-Eastern Australian waters. Aust. J. Mar. Freshw. Res. 27, 61–71.

Klemas, V., Otley, M., Philpot, W., Withe, C., Rogers, R., Shah, N., 1974. Correlation of coastal water turbidity and current circulation with ERTS-1 and skylab imagery. Proc. 9th Int. Symp., Remote Sens. Environ., Ann Arbor, USA. Environmental Research Institute of Michigan, USA, pp. 1289–1317.

Kloiber, S.M., Brezonik, P.L., Olmanson, L.G., Bauer, M.E., 2002. A procedure for regional lake water clarity assessment using Landsat and multispectral data. Remote Sens. Environ. 82, 38–47.

Knobelspiesse, K., Green, S., Vodacek, A., 2000. Atmospheric Compensation for SeaWiFS Images of Lake Superior Utilizing Spatial Information. Proc. 2000 Ocean Sciences Meeting, San Antonio, USA.

Koponen, S., Pulliainen, J., Kallio, K., Hallikainen, M., 2002. Lake water quality classification with airborne hyperspectral spectrometer and simulated MERIS data. Remote Sens. Environ. 79, 51–59.

Kozhova, O.M., Izmesteva, L.R., 1998. Lake Baikal: Evolution and Biodiversity. Backhuys, Leiden, 447 pp.

Krawczyk, H., Neumann, A., Walzel, Th., 1996. Application of a new remote sensing multispectral interpretation algorithm for water constituents in the Baltic sea. Proc. Ocean Optics XIII, Halifax, Canada.

Lawrence, S.P., Hogeboom, K., Core, H. le, 2002. A three-dimensional general circulation model of the surface layers of Lake Baikal. Hydrobiologia 487, 95–110.

Lillesand, T.M., Johnson, W.L., Duell, R.L., Lindstrom, O.M., Meisner, D.E., 1983. Use of Landsat data to predict the trophic state of Minnesota lakes. Photogramm. Eng. Remote Sens. 49, 219–229.

Malcolm, R.L., 1985. Geochemistry of stream fulvic and humic substances. In: Aiken, G.R. (Ed.), Humic Substances in Soil, Sediment and Water. New York, pp. 181–209.

Matthias-Maser, S., Obolkin, V., Khodzer, T., Jaenicke, R., 2000. Seasonal variation of primary biological aerosol particles in the remote continental region of Lake Baikal/Siberia. Atmos. Environ. 34, 3805–3811.

Mayo, M., Gitelson, A., Yacobi, Y.Z., Ben-Avraham, Z., 1995. Chlorophyll distribution in Lake Kinneret determined from LANDSAT Thematic Mapper data. Int. J. Remote Sens. 16 (1), 175–182.

McClain, C.R., Barnes, R.A., Eplee Jr., R.E., Franz, B.A., Hsu, N.C, Patt, F.S., Pietras, C.M., Robinson, W.D., Schieber, B.D., Schmidt, G.M., Wang, M., Bailey, S.W., Werdell, P.J., 2000. SeaWiFS Post Launch Calibration and Validation Analyses: Part 2. Hooker, S.B., Firestone, E.R. NASA Tech. Memo. 2000-206892, vol. 10. NASA Goddard Space Flight Center, 57 pp.

Mitchelson-Jacob, E.G., 1999. Utilisation of satellite ocean colour data for military applications: retrieval of suspended particulate matter concentrations from ocean colour imagery. Unit for Coastal and Estuarine Studies Report, U99-2.

Mogilev, N.Yu., Semovski, S.V., 1999. Studies of Lake Baikal snow cover dynamics using multispectral images AVHRR. Geograph. Nat. Res. 4, 90–93 (in Russian).

van Molderen, H., van Grieken, R., Khodzher, T., Obolkin, V., Potemkin, V., 1996. Composition of individual aerosol particles above Lake Baikal, Siberia. Atmos. Environ. 30 (9), 1453–1465.

Moore, G.F., Aiken, J., Lavender, S.J., 1999. The atmospheric correction of water colour and the quantitative retrieval of suspended particulate matter in case II waters: application to MERIS. Int. J. Remote Sens. 20, 1713–1733.

Morel, A.Y., Gordon, H.R., 1980. Report of the working group on water color. Boundary-Layer Meteorol. 18, 343–355.

Mueller, J.L., Austin, R.W., 1995. Ocean Optics Protocols for SeaWiFS Validation, Revision 1, NASA TM 104556 project, 25.

Munday, J.C., 1974. Water Quality for Lakes of Southern Ontario From ERTS-1. Proc. 2nd Canadian Symposium on Remote Sensing, Guelph, Canada. University of Guelph, USA, pp. 77–85.

Munday Jr., J.C., Alfoeldi, T.T., 1979. LANDSAT test of diffuse reflectance models for aquatic suspended solids measurements. Remote Sens. Environ. 8, 169–183.

Neumann, A., Krawczyk, H., Walzel, Th., 1995. A complex approach to quantitative interpretation of spectral high resolution imagery. Proc. 3rd Remote Sens. Marine and Coastal Environm., Seattle/Washington, USA, pp. II-641–II-652.

Novo, E.M.M., Handom, J.D., Curran, P.J., 1989. The effect of sediment type on the relationship between reflectance and suspended sediment concentration. Int. J. Remote Sens. 10, 1283–1289.

O'Reilly, J.E, Maritorena, S., Mitchell, B.G., Siegel, D.A., Carder, K.L., Garver, S.A., Kahru, M., McClain, C.R., 1998. Ocean colour chlorophyll algorithms for SeaWiFS. J. Geophys. Res. 103 (11), 24937–24953.

O'Reilly, J.E., et al., 2000. SeaWiFS Post Launch Calibration and Validation Analyses: Part 3. Hooker, S.B., Firestone, E.R. NASA Tech. Memo. 11, 2000-206892. NASA Goddard Space Flight Center.

Packman, J.J., Comings, K.J., Booth, D.B., 1999. Using turbidity to determine total suspended solids in urbanizing streams in the Puget Lowlands. Proc.-Can. Water Resour. Assoc., 158–165. (Vancouver).

Peters, S.W.M, Dekker, A.G., Pasterkamp, R., Woerd, H. van der, 1999. Demonstration Ocean Colour Satellites, Various aspects of TSM determinations using ocean colour satellite imagery. IVM/VU O-99/03.

Pozdnyakov, D., Petterson, L., Johanessen, O.M., Liaskovski, A., Filatov, N., Bobylev, L., 2003. SeaWiFS maps water quality parameters of the white sea. Int. J. Remote Sens. 24 (21), 4065–4071.

Ritchie, J.C., Cooper, C.M., Schiebe, F.R., 1990. The relationship of MSS and TM digital data with suspended sediments, chlor-

ophyll, and temperature in Moon Lake, Mississippi. Remote Sens. Environ. 33, 137–148.
Rioual, P., Mackay, A.W., 2005. A diatom record of centennial resolution for the Kazantsevo Interglacial stage in Lake Baikal (Siberia). Glob. Planet. Change 46, 199–219 (this issue).
Ruddick, K.G., Ovidio, F., Rijkeboer, M., 2000. Atmospheric correction of SeaWiFS imagery for turbid coastal and inland waters. Appl. Opt. 39 (6), 897–912.
Russel, M., Rosell-Melé, A., 2005. Preliminary study of fluxes of major lipid biomarker classes in the water column and sediments of Lake Baikal, Russia. Glob. Planet. Change 46, 45–56 (this issue).
Schiller, H., Doerffer, R., 1999. Neural network for emulation of an inverse model-operational derivation of Case II water properties from MERIS data. Int. J. Remote Sens. 20 (9), 1735–1746.
Semovski, S.V., 1999a. Water Ecosystems: from Satellite observations to Mathematic modelling. Russian Academic Press, Irkutsk. 199 pp. (Russian version with English abstracts).
Semovski, S.V., 1999b. The Baltic Sea and Lake Baikal underwater bio-optical fields simulation using ecodynamical model. Ecol. Model. 116 (2/3), 149–163.
Semovski, S.V., Shimaraev, M.N., Minko, N.P., Gnatovsky, R.Yu., 1998. Lake Baikal fronts and currents analysis studies using IR AVHRR imagery. Earth Stud. Space 5, 65–75 (in Russian, English edition is available).
Semovski, S.V., Shimaraev, M.N., Mogilev, N.Yu., Alpers, W., Schrum, C., 1999. Lake Baikal physical features studies using satellite remote sensing. Proc. Intern. Geosc. Rem. Sens. Sympos (IGARSS), Hamburg, Germany. Geoscience and Remote Sensing Society, USA, pp. 888–890.
Semovski, S.V., Mogilev, N.Yu., Sherstyankin, P.P., 2000. Lake Baikal ice: analysis of AVHRR imagery and simulation of under-ice phytoplankton bloom. J. Mar. Syst. 27, 117–130.
Semovski, S.V., Shimaraev, M.N., Minko, N.P., Gnatovsky, R.Yu., 2001. Use of satellite observations to study thermal fronts of Lake Baikal. Earth Obs. Remote Sens. 16 (5), 773–787.
Sherstyankin, P.P., 1975. Experimental Investigation of the Under-Ice Luminous Field of Lake Baikal. Nauka, Moscow, p. 91.
Shimaraev, M.N., Verbolov, V.I., Granin, N.G., Sherstayankin, P.P., 1994. Physical limnology of Lake Baikal: a review. In: Shimaraev, M.N., Okuda, S. (Eds.), BICER Publishers, Irkutsk and Okayama, 80 pp.
Smith, C.S., Baker, K.J.S., 1983. The analysis of ocean optical data. Proc. 7th SPIE, Ocean Optics, vol. 478, pp. 119–126.
Straskrabova, V., Izmest'yeva, L.R., Maksimova, E.A., Fietz, S., Nedoma, J., Borovec, J., Kobanova, G.I., Shchetinina, E.V., Pislegina, E.V., 2005. Primary production and microbial activity in the euphotic zone of Lake Baikal (Southern Basin) during late winter. Glob. Planet. Change 46, 57–73 (this issue).
Stumpf, R.P., Tyler, M.A., 1988. Satellite detection of bloom and pigment distributions in estuaries. Remote Sens. Environ. 24, 385–404.
Stumpf, R.P., Pennock, J.R., 1989. Calibration of a general optical equation for remote sensing of suspended sediments in a moderately turbid estuary. J. Geophys. Res., Oceans 94 (C10), 14363–14371.
Tassan, S., 1994. Local algorithms using SeaWiFS data for the retrieval of phytoplankton, pigments, suspended sediment, and yellow substance in coastal waters. Appl. Opt. 33, 2369–2378.
Thiemann, S., Kaufmann, H., 2000. Determination of chlorophyll content and trophic state of lakes using field spectrometer and IRS-1C satellite data in the Mecklenburg lake district, Germany. Remote Sens. Environ. 73, 227–235.
Thiemann, S., Kaufmann, H., 2002. Lake water quality monitoring using hyperspectral airborne data—a semiempirical multisensor and multitemporal approach for the Mecklenburg lake district, Germany. Remote Sens. Environ. 81, 228–237.
Thomson, K.P.B., Jerome, J., 1975. In situ colour measurements on the Great Lakes. Scientific Series, 51, Inland Waters Directorate, Environment Canada, Burlington, Ontario.
Vidot, J., Santer, R., 2003. Atmospheric correction for inland waters. Proc. 10th SPIE Remote Sens. Ocean and Sea Ice, p. 5233.
Williams, S.P., Szajna, E.F., Hovis, W.A., 1986. Nimbus 7 Coastal Zone Color Scanner (CZCS) Level 1 Data Product Users Guide. NASA TM 86203 project paper, p. 53.
Yacobi, Y.Z., Gitelson, A., Mayo, M., 1995. Remote Sensing of chlorophyll in Lake Kinneret using high-spectral resolution radiometer and LANDSAT TM: spectral features of reflectance and algorithm development. J. Plankton Res. 17 (11), 2155–2173.
Yacobi, Y.Z., Alberts, J.J., Takács, M., McElvaine, M., 2003. Absorption spectroscopy of colored dissolved organic carbon in Georgia (USA) rivers: the impact of molecular size distribution. Limnology 62 (1), 41–46.
Yoshioka, T., Ueda, S., Khodzher, T., Bashenkhaeva, N., Korovyakova, I., Sorokovikova, L., Gorbunova, L., 2002. Distribution of dissolved organic carbon in Lake Baikal and its watershed. Limnology 3, 159–168.
Young, A.T., 1981. On the Rayleigh-scattering optical depth of the atmosphere. J. Appl. Meteorol. 20, 328–330.

5.5 LIMNOLOGICAL DATA-SETS

5.5.1 Phytoplankton Investigations

The regional, vertical and seasonal variations in phytoplankton composition and pigment concentrations were assessed in 2001, 2002 and 2003 (Fietz 2005): Chl-*a* concentrations in pelagic waters ranged from 0.29 to 3.5 µg l^{-1}, with average concentrations for the central part of the North Basin of 0.4 to 0.7 µg l^{-1} Chl-*a*, for the Central Basin of around 0.8 µg l^{-1} Chl-*a,* for the South Basin of around 1.2 µg l^{-1} Chl-*a*, and for the areas influenced by the Selenga input to around 2 µg l^{-1} Chl-*a*. Table 1 of Heim et al. [2005] indicates the significantly lower mean Chl-*a* concentration for pelagic areas than the mean Chl-*a* concentration for the entire lake (including Selenga Delta and Barguzin Bay). The ratio of total carotenoids (photosynthetically active and photoprotective) to Chl-*a* differed between the regions, with highest ratios at the Academician Ridge between the Central and the North Basin and around the Selenga Delta, and lowest in the sub-basin Maloe More (Table 5.2).

Marker pigments (such as fucoxanthin, lutein, zeaxanthin or chl-b and chl-c, that are characteristic for distinct chemotaxonomic phytoplankton groups) allowed the contribution of the phytoplankton groups to the total Chl-*a* to be estimated by multiple linear regressions using the CHEMTAX matrix factorisation program [*Fietz and Nicklisch*, 2004]. The dominant groups in summers 2001, 2002, and 2003 incorporated Bacillariophyceae (diatoms) plus Chrysophyceae, Chlorophyta, cyanobacterial picoplankton, Cryptophyta, and Eustigmatophyceae [*Fietz and Nicklisch*, 2004; *Fietz*, 2005]. This phytoplankton composition varied within the Lake Baikal water body, mainly depending on stratification and latitude, the later probably connected to insolation [*Fietz and Nicklisch*, 2004; *Fietz*, 2005].

For an overview, Tables 4a,b in Annex A demonstrate the high spatial variability of phytoplankton composition in July 2001 and 2002. Diatoms and Chrysophyceae dominated the whole lake by biovolume. Their contribution to total Chl-*a* was highest in the Centre and North Basins, whereas the contribution of Chlorophyceae and Eustigmatophyceae to total Chl-*a* was highest in the South Basin. The cyanobacterial picoplankton formed the main part of the total Chl-*a* around the Selenga Delta (ca. 90 %), and a minor part in the North Basin (ca. 11 %). The autotrophic picoplankton was composed of cyanobacterial and eukaryotic picoplankton, whereby cyanobacterial picoplankton dominated in the Selenga Delta and eukaryotic picoplankton in the South [*Fietz and Nicklisch*, 2004; *Fietz*, 2005].

Table 5.2: Ratio of the sum of carotenoids against Chl-*a* (µg/µg) in the euphotic zone (CONTINENT field expeditions in 2001, 2002, and 2003).

Region	n	mean	σ
South Basin	41	0.58	0.14
Around Selenga Delta	49	0.64	0.17
Central Basin	44	0.57	0.13
North Basin	52	0.49	0.08
Barguzin bay	22	0.57	0.18
Academician ridge	6	0.69	0.07
Maloe More (only 2003)	6	0.39	0.13
All	220	0.57	0.15

Figure 2.1 shows Absorbance, A, measurements from phytoplankton cultures of Lake Baikal strains [pers., Fietz, 2004; *Fietz et al.*, 2005]. These strains had been grown under saturating nutrient and light conditions at 15° C in semi-continuous cultures [*Fietz et al.*, 2005], and therefore do not show the in-situ absorption behaviour. However, their A spectra are a suitable demonstration of the variability in spectral behaviour, depending upon the pigment composition of the phytoplankton groups. For example, Bacillariophyceae show a broad absorption shoulder due to carotenoids. Autotrophic cyanobacterial picoplankton strongly absorbs in longer wavelength ranges due to red phycobilins (phycoerythrin PE), and blue phycobilins (phycocyanin PC) respectively.

The results of the SRIB sampling at 2 km offshore from Bolshye Koti revealed seasonal variations in total Chl-*a* concentrations, biovolume and phytoplankton composition [*Fietz*, 2005]. Total Chl-*a*, nano- and microphytoplankton biovolume were high from the middle to the end of May 2002, and were dominated by Bacillariophyceae. Towards the beginning of July 2002, the contribution of Bacillariophyceae decreased at the Bolshye Koti site, and Chlorophyta became important. In August 2002, a second maximum of Chl-*a*, cell number and diversity occurred, and Chl-*a* pigment rich autotrophic picoplankton, with very low biovolume, contributed a large part to the Chl-*a*. In autumn 2002, the total Chl-*a* and biovolume declined. Then, in late winter 2003 under ice cover, the total Chl-*a*, biovolume, and diversity increased again. The temperature and hydrodynamical situation (stratification/mixing) were both driving forces for the seasonal fluctuations in phytoplankton composition.

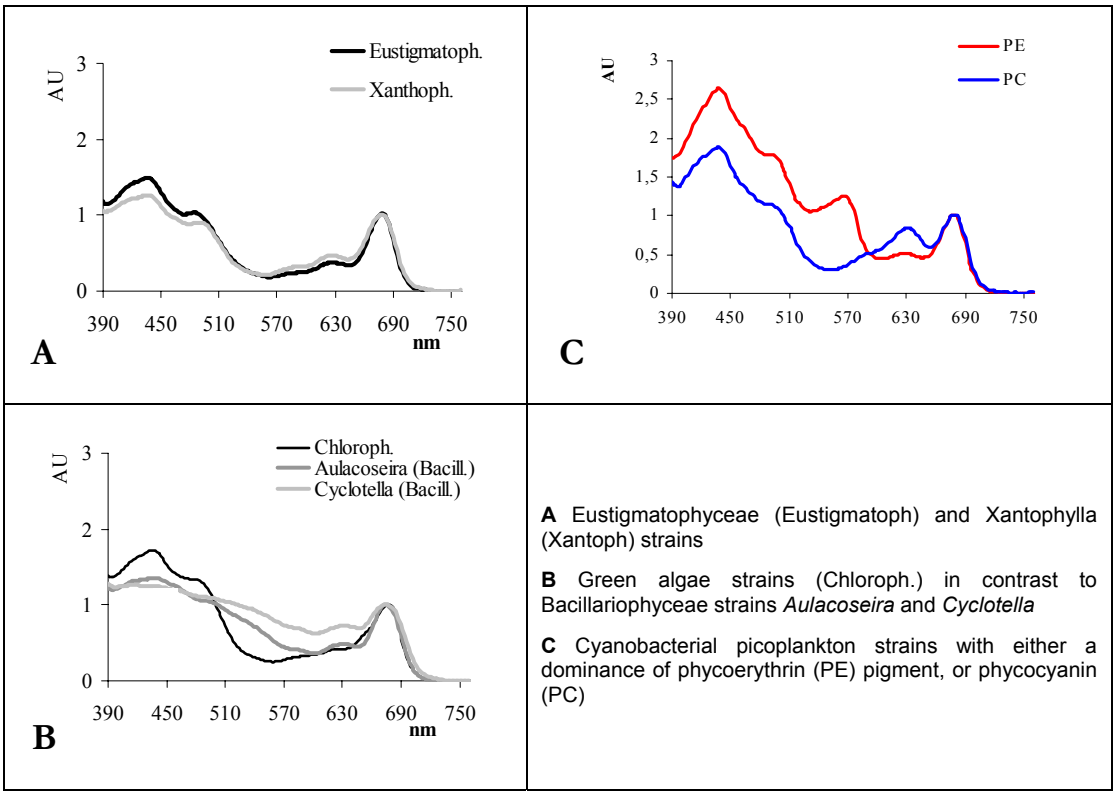

Figure 5.8: Spectra of Absorbance Units (AU)–normalized at 700 nm (A700/A)–of phytoplankton strains isolated from Lake Baikal [pers., Fietz, 2004, *Fietz et al.*, 2005].

During the CONTINENT CON02-8 and CON03-9 cruises (July 2002, July 2003) multispectral fluorescence (submersible FluoroProbe, bbe Moldaenke, Kiel, Germany) depth profiles were performed down to 100 m depth to determine Chl-*a* concentration and the contribution of the main chemotaxonomic phytoplankton groups [pers., Nicklisch, HU Berlin, Germany]. The depth profiles indicate that in July 2002 and July 2003, stratified conditions prevailed in the South and the Southern Central Basin, whereas unstratified conditions prevailed in the colder North Basin. Relative homogenous Chl-*a* depth distribution occurred most notably together with unstratified conditions in contrast to Chl-*a* maxima at several depths in case of stratified conditions. Additionally, Fietz [2005] describes fluorescence measurements made during the SRIB expedition in late summer 2002. These temperature and fluorescence profiles show that during the warming of the water during summer, the North Basin also developed stratified conditions and structured Chl-*a* depth profiles.

Straskrabova et al. [2005] investigated microbial biomasses and primary production in the euphotic zone in late winter 2003 and on two cruises in summer 2003, CON03-9 and a SRIB cruise. During the late summer SRIB cruise (August to September 2003) bacterial production and primary production were high from South to North (2.5 to 7 µg C $l^{-1}h^{-1}$). The dominant primary producer in both early and late summer 2003 was autotrophic picoplankton, which is characteristic for oligotrophic systems. Straskrabova et al. [2005] concluded that a major part of the primary production in summer might be directly used by protozoan grazers and by bacteria, and does not contribute to sedimenting material, in contrast to winter blooms where large-sized, non-grazable diatoms dominate.

5.5.2 Dissolved Organic Matter Investigations

In summer 2002, DOC measurements (0.2 µm filter pore-size) for the pelagic waters showed values lower than 0.5 mg l^{-1} for the Northern and Central basins in 2002, but up to 2 mg l^{-1} DOC in several regions of the South Basin [pers., Rosell-Melé, CEA, Spain]. In July 2003, DOC concentrations were on average 1.2 to 1.4 mg l^{-1} (0.45 µm filter pore-size) in the pelagic waters of the South and the Central basins [pers., Borovec, HUB, Budejovice, Czech Republic].

NOV laboratory Absorbance/Optical Density (OD) measurements in 2002 that were directly carried out on fresh samples on board the ship, were evaluated, as well as OD measurements at the HUB laboratory in 2003 [pers., Borovec, HUB, Budejovice, Czech Republic]. All OD measurements were converted towards absorption spectra [m^{-1}].

Figure 5.8 demonstrates the spectral NOV laboratory measurements in 2002 on fresh samples. Regrettably, the quality of these measurements was not adequate to evaluate the slope and exponent values (§2.1.3). Due to measurement series on samples of the German Lake Districts the failures could afterwards be related to different temperature settings of the fresh probe samples to the reference distilled water sample onboard the Russian research vessel. In fact, these erroneous spectral features due to different temperatures of the probe and the reference sample (see also §2.1.4) could be reproduced during spectroradiometrical laboratory investigations on fresh samples from Lake Wannsee (Berlin, Germany) and the Rheinsberg Lake district (Germany).

These samples show an exponential absorption behaviour (Figure 5.9) of S = 0.013 for the wavelength range 254 to 400 nm. However, as discussed in §2.1.3, S values strongly depend on the chosen wavelength range and should be calculated from 350 nm onwards, towards longer wavelengths. The particular S value for pelagic and fluvial influenced waters of Lake Baikal could not be retrieved. Therefore, to obtain an estimate for *cDOM* absorption in 2002, we extrapolated

the undisturbed absorption coefficients at 340 nm towards longer wavelengths using common S-values from the literature [§2.1.3], in this case, S = 0.014 [pers., Niklisch, Humbold University, Germany]. Table 5.3 shows the average calculated absorption values of fresh pelagic water samples (excluding the extrema of Selenga and the Barguzin influence and of the ultra-oligotrophic North Basin) in July 2002. Table 5.4 shows the average measured absorption values of aged pelagic water samples in July 2003. If comparing cDOM a_{340}, and a_{410} values of fresh samples in July 2002 with a_{350} and a_{400} values of cDOM samples in July 2003 (Tables 5.3 a,b), relatively high CON03-9 absorption coefficients a_{400} (Table 5.4) may also indicate measurement problems in the blue-to green wavelength range, as similarly shown in Figure 5.8 for the CON02-8 cDOM measurements.

cDOM absorption values a_{440} in the South Basin during July 2002 were approximately 0.2 m^{-1} (including Selenga influenced areas), the averaged values for pelagic waters were around 0.15 m^{-1} (Table 5.3a; Table 3b in Annex A) and below 0.1 m^{-1} for the Northern Central and the North Basin (Table 3b in Annex A). At the Barguzin transect (B1, B2, B3 on Figure 4.2), high cDOM absorption values (a_{440} from 0.7 to 3.8 m^{-1}) and DOC concentrations up to 4.8 mg l^{-1} (filter pore-size 0.2 µm) were recorded (see also in Heim et al. [2005]).

Around the CONTINENT and peeper sites in the eastern North Basin, cDOM and DOC values were highly variable in July 2002. The same is generally reported for Secchi depth measurements in early and late summer within this area. Table 3b, Annex A, gives an overview of DOC concentrations and cDOM absorption coefficients of surface water stations in July 2002.

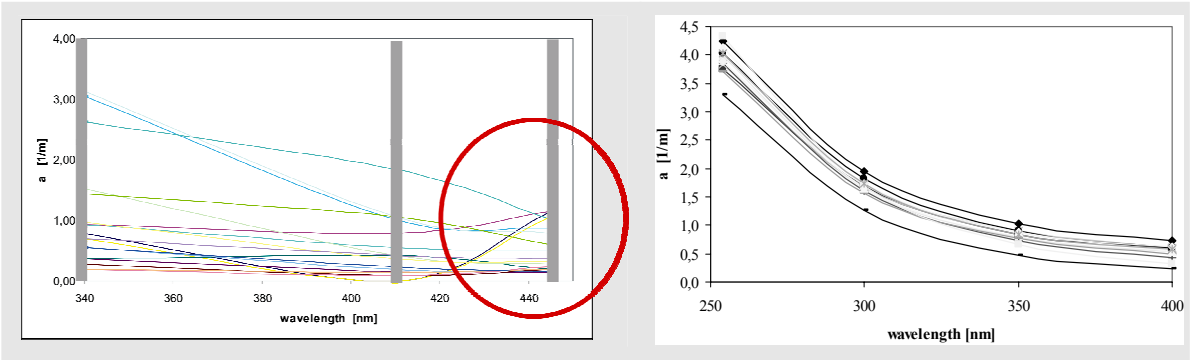

Figure 5.9: Left: Absorption spectra, *a*, on board the ship (CON02-8, 2002) show failures in the blue-to-green wavelength range instead of exponential absorption behaviour. Sources: pelagic and coastal waters. Right: *a* spectra (CON03-9, 2003) [pers., Baruvec, HUB, Czech Republic]. Sources: pelagic waters.

Table 5.3a,b. Left: averaged *a* values for Baikal pelagic waters (sample depth = 5 m, GF filter/ ~0.8 µm pore-size) in July 2002 (*a_{410} and a_{440} calculated by using S = 0.14 [pers., Niklisch, Humbold University, Germany]. Right: Averaged *a* values for South-Baikal pelagic waters (sample depth = 5 and 25 m, cellulose acetate filter/ 0.45 µm pore-size) in July 2003 [pers., Baruvec, HUB, Czech Republic]

CON02-8 (July 2002), fresh samples (n = 12)	
Wavelength [nm]	Absorption [m^{-1}]
340	0.65
410	0.24*
440	0.15*

CON03-9 (July 2003), aged samples (n = 14)	
Wavelength [nm]	Absorption [m^{-1}]
254	3.9
300	1.6
350	0.8
400	0.5

5.5.3 Suspended Particulate Matter Investigations

Results from the CON01-2 land expedition indicate that the Selenga River carried a mean SPM load of approx. 15 mg l^{-1} along its course in June and July 2001, while up to ca. 22 mg l^{-1} SPM river load reached the Selenga Delta area. These investigations took place shortly before the catastrophic flooding events during July 2001 in Southern Siberia and Mongolia.

Bulk mineralogy of river sediments along this South-North transect shows an increase of total feldspars toward the Selenga Delta, whereas total clays and flakes of micas and chlorites decrease [pers., Fagel, ULG Belgium]. Among clay minerals, vermiculite and mixed-layers first decrease and later increase along the Selenga South-North transect, while illite shows a reverse trend. Kaolinit only appears in the section between two tributaries of the Selenga River (Temnik River and Khilok River) and after the confluence with the Uda. The geochemical analysis shows even more homogeneity, implying no characteristic mineralogical sources and little anthropogenic influence during July 2001 [pers., Fagel, ULG, Belgium].

During the inspection of the Selenga Delta surface waters, for example along the river arms, intense brownish water colours were observed.

Figure 5.10: The field photo shows the intense brownish colour of a dead river arm in the Selenga Delta (June 2001).

SPM data collected during the 2001 ship cruise CON01-5 that followed the CON01-2 land expedition, exhibited the widest SPM concentration range in the pelagic waters of Lake Baikal (Table 1, Heim et al. [2005]). SPM concentrations in 2001 varied from 0.2 mg l^{-1} for the central region of the North Basin, to average concentrations from 0.4 to 1 mg l^{-1} for the Central and the South Basins and up to 5 mg l^{-1} around the shallow waters of the Selenga Delta (Table 3a in Annex A). This occurred one week after a catastrophic flooding in the Southern Lake Baikal area in July 2001, while during summer 2002 and 2003, the hydrological conditions were unexceptional (Table 3b in Annex A).

The CONTINENT SPM samples are clay-rich agglomerates with illit and smectit dominance. Little iron appears adsorbed onto the clay minerals in the form of an organic-rich coating, the dominating colour-giving component being the humic substances.

5.5.4 Ground-Truth Investigations at Mecklenburg and Brandenburg Lake Districts (Germany)

Field investigations covered predominantly eutrophic to hypertrophic lakes. Mannheim et al. [2004b] demonstrated the high potential of the hyperspectral CHRIS-PROBA satellite data to monitor the trophic parameters Chl-*a* and Secchi depth in the Rheinsberg Lake district (Germany) and in the Havel lakes of Berlin (Germany). These eutrophic to hypertrophic inland waters show concentrations and signals over one order of magnitude higher than the ultra-transparent oligotrophic Lake Baikal water (Table 5.4).

In all cases, the spectral reflectance maxima are situated in the green-wavelength range (around 550 nm). Even one to more reflectance maxima in the near-infrared wavelength range are rising. In case of hypertrophic waters, the first near-infrared maximum rises even to reflectance heights comparable to the green reflectance maximum. These spectral water-leaving signals in the red-to-near-infrared wathlength ranges are induced by scattering processes on highly abundant phytoplankton. Generally, Chl-*a* algorithms for trophic evaluation of eutrophic to hypertrophic inland water bodies are based on these stable and significant spectral features in the red to near-infrared wavelengths. Mannheim et al. [2004b] improved the accuracy of Chl-*a* algorithms by optimizing spectral algorithms specifically onto the different trophic states (oligotrophic to mesotrophic, mesotrophic to eutrophic, and polytrophic to hypertrophic).

The spectroradiometrical Lambda measurements show the spectral specifications of phytoplankton and cDOM of eutrophic to hypertrophic inland waters (Table 5.5, Table 5.6). Table 5.7 refers to samples from Lake 'Schwarzer See', Rheinsberg Lake District (Germany), showing different slope S dependent on wavelength ranges.

Table 5.4: Value span of Chl-*a* concentration and Secchi depth investigations in the Rheinsberg Lake District from 2002 to 2004 (including spring, summer and autumn seasons).

transparency indicators	Min	Max
Chl-a DIN 38412-L16 [µg l^{-1}]	1 (Lake Wummsee, oligotrophic)	120 (Lake Braminsee)
Secchi depth [m]	0.3 (Lake Braminsee, hypertrophic)	7.5 (Lake Wummsee)

Table 5.5: Specific absorption coefficients of phytoplankton, $a^*_{phyto}(440)$.

Authors	$a^*_{phyto}(440)$ [m^2 mg^{-1}]	Water types
Mannheim, Heim, Tirsch [unpublished data]		
Rheinsberg Lake district (without Lake Bramin), summer season	0.034 ± 0.006	Mesotrophic to eutrophic freshwater stations, n = 7
Havel lakes (near Berlin) and Lake Bramin (Rheinsberg Lake district), summer season	0.022 ± 0.006	Poly- to hypertrophic freshwater stations, n = 8

Table 5.6: Averaged Slope S values of cDOM from various sources.

Authors	S	Wavelength range	Source
Mannheim, Heim, Tirsch, [unpublished data]	0.016 ± 0.0023	380 – 500	(Spring, summer, and autumn seasons) Mesotrophic to polytrophic lakes, Rheinsberg Lake district (G), n = 55
2002, 2003, 2004	0.0155 ± 0.0027	380 – 500	Poly- to hypertrophic Havel lakes (G), n = 20

Table 5.7: Slope S value of cDOM, defined for different wavelength ranges.

Authors	S	Wavelength range	Source
Mannheim, Heim, Tirsch [unpublished data]	0.0165 0.0178 0.0214	380 – 500 350 – 400 250 – 270	Lake Schwarzer See (early autumn 2003)

5.5.5 GIS Catchment Analyses of Source Rocks

The new generated GIS layer "Lake Baikal catchment with lithological attribution" is shown in Figure 5.11. Lake Baikal stretches over three UTM zones (zone 47, 48, 49), whereby zone 48 is the central UTM zone. Swierz (2004) evaluated the error in area calculation for Lake Baikal for the case of reprojecting zone 47 and 49 onto zone 48 to be approximately 0.3 %.

The results of the spatial GIS analysis describe the area and relative percentage of the main source rocks within the different catchment areas (Table 9 in Annex B). From this analysis, the catchment areas of the rivers flowing into Lake Baikal have as the main source rocks granitoids. Granitoid rocks dominate the catchment areas of the Selenga, Barguzin, and Upper-Angara rivers, and short small rivers at the northern and western shore of Lake Baikal. GIS analyses of the delineated total lake catchment, as well as the separate main catchment areas (Selenga, Barguzin, Upper Angara), result for all cases in 50 to 60 % coverage by granitoids.

The lithological provinces including basalts and different volcano-clastica are the second most important source rocks of the catchment of Selenga River, taking into account the size of their outcrop area (ca. 70500 km^2, 16 %, Table 9, Annex B).

A minor source area contains metamorphic rocks with mainly granulite and amphibolite facies (gneiss, amphibolite, marble), quartzite, green and black schists, meta-sandstone. Metamorphic Precambrian rocks cover 7 % of the Selenga catchment, but reach 17 and 24 % in the Barguzin and Upper Angara catchment areas, respectively. On the other hand, these metamorphic rocks are the most important source along the south coast and also occur in the northwest of Lake Baikal.

Basic intrusive rocks (mainly gabbroids) occur subordinate on the surface (1 %) near the rivers of the NE bank of the lake (Upper-Angara, Barguzin, and others) and in the NE of the Selenga catchment (ca. 9000 km^2, i.e., 2 % of the area).

Finally, Quaternary alluvial sediments that represent the reworking of the surrounding source lithologies cover a certain proportion in all catchment areas:

11 % in the Selenga, 19 % in the Barguzin and up to 31 % in the Upper Angara catchment.

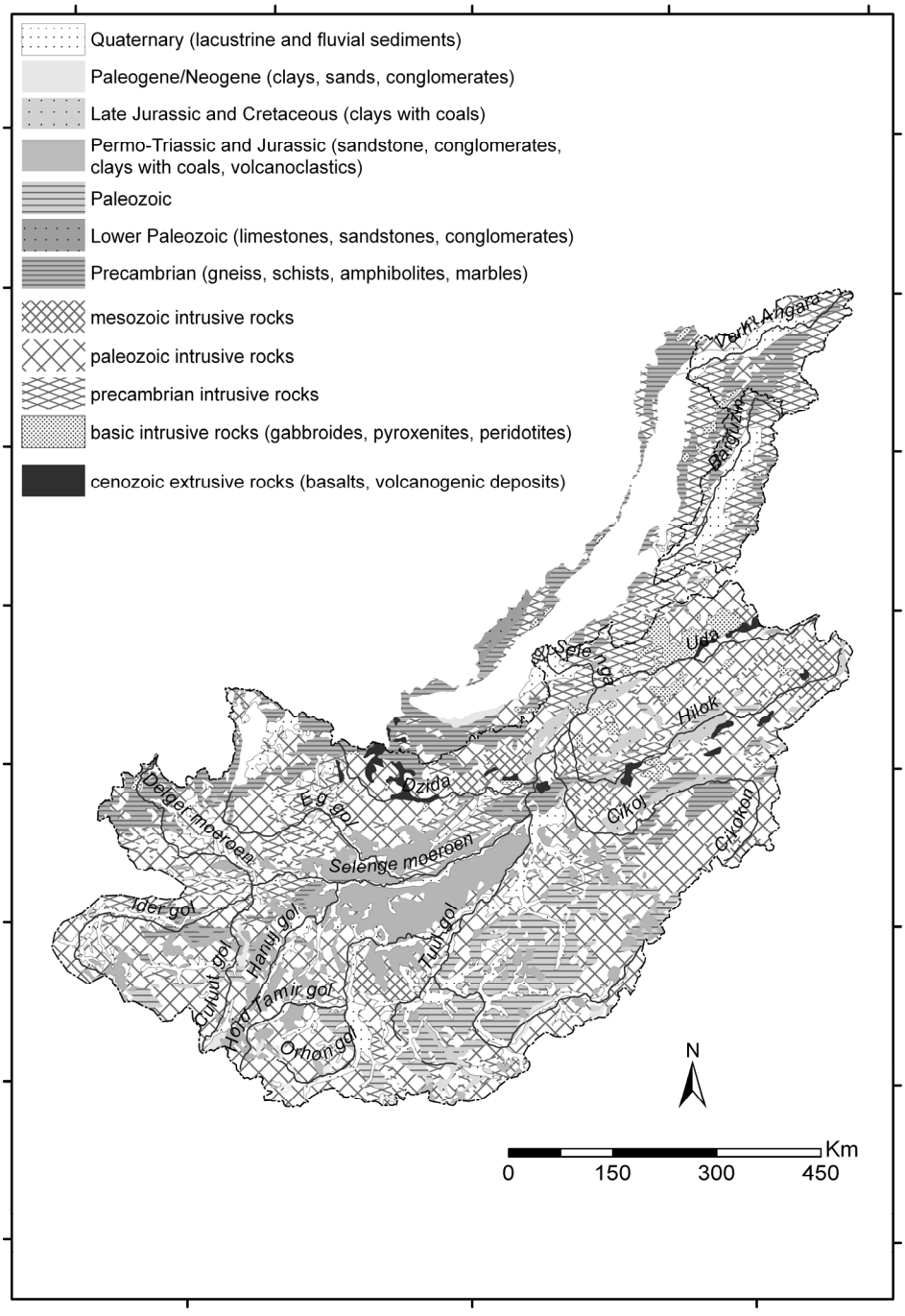

Figure 5.11: Geological GIS layer “Lake Baikal catchment with lithological attribution”.

6 DISCUSSION

6.1 VALIDITY OF ATMOSPHERIC CORRECTIONS

For the case of highly-transparent water-body targets, more than 99 % of the radiometric signal that is scanned by satellite sensors originates from the atmospheric contribution and specular reflection of sky radiance at the air-water interface (§2.2, §4.2). The extraction of oceanological and limnological parameters from these transparent waters is therefore predominantly dependant on the atmospheric correction process.

When considering a clear atmosphere, the aerosol contribution is very low and there are problems in deducing the spectral-atmospheric behaviour from measurements in the near-infrared wavelength range only. This may be one reason why the atmospheric correction in the SeaDAS 'band7/band 8' model performed poorly and produced very noisy output data.

The SeaDAS atmospheric correction of the High Resolution Picture Transmission (HRPT) SeaWiFS data of Lake Baikal performed best with the assumption of spectral-white aerosol behaviour. This approach is considered preliminary, however, it robustly performed for the complete SeaWiFS data-sets in 2001 and 2002, providing an adequate base for Ocean Colour investigations and chlorophyll, Chl-*a*, and Suspended Particulate Matter, SPM, calculations. This choice of spectral-white aerosol behaviour prevents an atmospheric over-correction of the aerosol contribution in the blue wavelength range that may lead to negative Remote Sensing Reflectances, R_{RS}, as it is described in a variety of studies [e.g., *Sturm et al.*, 2002].

However, how indicative is this parameter choice for the atmospheric conditions at Lake Baikal? A general overview on atmospheric conditions in rural Siberia is given in an interim report of the International Institute for Applied Systems Analysis (IIASA) [*Petelina*, 1998]. Petelina [1998], citing Koutzenogii [1996], discusses how aerosol-size distributions were more similar for the rural stations Novosibirsk and the Baikal Lake region (stations: Lystvyanka and Tanhoi), than, for example, the semi-arid Almaty region (South Kazakhstan) (Figure 6.1). Petelina examined SATOR aerosol investigations from the years 1992-1995 that were conducted at scientific stations of the Siberian Branch of Russian Academy of Sciences. The average values of spectral dependencies in Siberia were found to be different, especially in the short-wavelength range (0.45 to 0.65 μm) relative to the continental aerosol models of the World Meteorological Organization (*WMO*) [*World Climatic Program*, 1986], where *WMO-continental 1* corresponds to background rural conditions and *WMO-continental 2* to dust assemblages (desert-like) (e.g, Figure 6.1). Petelina [1998] explained the spectral behaviour of Aerosol Optical Depths, AODs, from the Siberiam AERONET stations by the presence of larger-sized aerosol particles. This assumption seemed to be underlined by airborne aerosol measurements at different heights over Western Siberia, which confirmed the relatively high abundance of large-sized aerosols in the lower troposphere [*Panchenko et al.,* 1996; cited in *Petelina*, 1998).

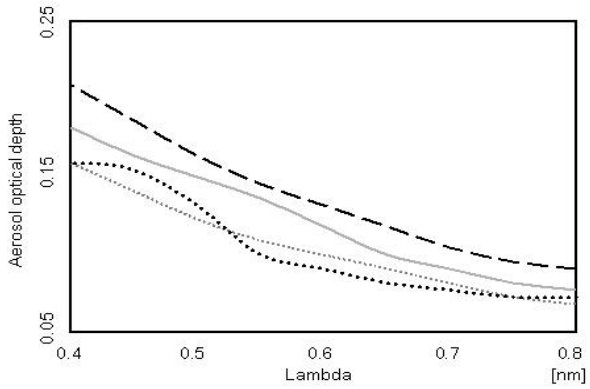

Figure 6.1: AOD spectra for the AERONET stations Tomsk (grey line) and Almaty (black points), and the continental aerosol models *WMO-1* (grey points) and *WMO-2* (dashed line) [*Petelina*, 1998].

My own investigations of Siberian AErosol RObotic NETwork (AERONET) stations found Ångström coefficients, α, in summer months showing a high variability (α = 0.5 to 2.5), and an averaged intra-annual value α = 1.2, that does not indicate a predominant absence of large aerosols. To what extent does this information account for the atmospheric conditions above Lake Baikal? In contrast to the Siberian AERONET stations (rural areas along the Trans-Siberian Railway), while where Lake Baikal is situated, there is only taiga, with the Baikal basin situated within the boreal biome with a vast extent of dense forests and relatively low atmospheric anthropogenic influence.

Additional information from other observations of aerosol composition in boreal areas was examined. For example, the Canadian AEROCAN (AERosol CANada) sunphotometer network provides information about AOD, α, and aerosol particle size distribution. However, the boreal stations seemed to be strongly influenced by forest fires and showed highly variable and on average rather large α = 1 to 2.5, as also described by Bokoye et al. [2001], who examined AERONET/ AEROCAN sites between 40° N and 60° N latitudes between 1994 to 1999.

The atmosphere over Lake Baikal itself is reported to be very transparent, with low aerosol concentrations over the Central and North Basins [*van Molderen et al.*, 1996]. Matthias-Maser et al. [2000] described the dominance in volume fraction of conifer spores and pollens in June and July 1996 (Lystvyjanka, Lake Baikal). Even calculated for the annual averaged aerosol assemblage, the volume fraction of large biogenic aerosols (> 2 µm) still covered ca. 30 %.

Balin et al. [2003] proposed that atmospheric processes force upwelling above the centre of the lake basins, and this in turn is accompanied by wide areas of high humidity (90 %), humidifying of aerosols, and by advective fogs. Here again, the atmospheric conditions do not reflect standard continental *WMO* atmospheric conditions that generally have a low humidity and relatively high amounts of small sized aerosols.

Despite the aerosol-problem during the atmospheric correction process, there are also problems by cloud-contaminated and by the land adjacency effect contaminated pixels. In addition, at Lake Baikal during the summer, along-shore cloud belts arise along the coast. Also in the vicinity of cloud pixels, water pixels may be affected by clouds shadows and by stray light. SeaDAS automatically masks cloud pixels (§4.2.1). Also pixels were not considered that could obviously be traced back to atmospheric features, such as airplane trails and fog or cloud features, and the coastline pixels. Pixels from shallow areas (<20 m water depth, source: *http://allserv.rug.ac.be/ ~jphenrie*) around the Selenga Delta were also excluded from the SeaWiFS analyses, because the bottom reflection from the shallow delta bottom added to the remote-sensing signal (§5.2).

In June/July, the surface waters of Lake Baikal, especially in the North Basin, are frequently covered by a surface film of pollens and dead insects (Figure 6.2). Conditions quickly change during the course of a few days due to intense zooplankton grazing and weather conditions. However, how this is expressed in the remote-sensing signal is unknown, since no related investigations at other water bodies can be found.

Figure 6.2: Field photo of the lake water surface from on board the 'Vereshchagin', North Basin, July 2002. Please note the striking surface film of pollens and dead insects. To the right (Sergeyev, 1989), flies cover a shingle shore at Lake Baikal in early summer.

Further problematic is that Lake Baikal stretches over 4 degrees of geographical latitudes (from 51.5° N to 55.5° N), implying high regional and seasonal variations of the zenith sun elevation angle. For example, at 51.5° N, the maximal sun zenith angle varies in summer from 60°, decreasing towards 40° in September, down to 30° in October. This also implies high latitudinal variations of the amount of directly reflected sky-light from the air-water interface (§2.2, §4.2), where it is expressed in the Lake Albedo value. Long-term Albedo measurements at Lake Baikal showed for example large latitudinal variations of the order of 5 % from the South to the North Basin every year during high summer (August) [pers., Vladimir, LIN, Russia]. These long-term Albedo field investigations also showed averaged Albedo values of 5 % for the South Basin in June that increased to 12 % in October for the South Basin, only as a result of decreasing sun zenith. The problem of non-correcting the direct reflection at the air-water interface especially holds for the land-adapted atmospheric correction of the visible AVHRR bands in Sherstyankin (1999b), where the AVHRR Top-of-Atmosphere Reflectances, R_{TOA}, were corrected towards Albedo data, and not towards Remote Sensing Reflectances, R_{RS}. Because Albedo values predominantly show the seasonal and longitudinal variations of the directly backscattered sky component, the bio-optical bulk water properties could not be extracted, and no higher level products could be generated within the described AVHRR study.

Finally, I address the possibility of evaluating the atmospheric correction by comparing field-spectrometer measurements to the atmospherically-corrected satellite reflectances. Regrettably, due to summer monsoonal weather conditions and frequent fog cover (see also §3.3), only a few in-situ reflectance measurements happened under clear-sky conditions. However, even if SeaWiFS spectra and field-spectrometer measurements cannot be compared exactly for the same day, and place, the comparison of spectral shapes of bio-optical provinces – even on different dates - still describes the success of the atmospheric correction. For example, Figure 6.3 visualizes the coincidence in spectral shape and characteristics of in-situ R_{RS} and SeaWiFS R_{RS} spectra.

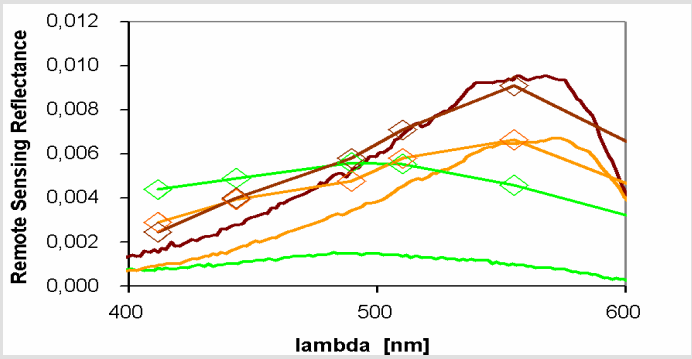

Comparison of SeaWiFS R_{RS}(bands1,2,3,4,5 as diamonds), and in-situ R_{RS} from contrastable water regions

Case 2, Selenga influence
SeaWiFS 01/07/19
GER1500 01/07/21 8:35 local time at CON01-21, no clouds, diffuse sky

Case 2, Selenga influence
SeaWiFS 01/07/19
GER1500 01/07/21 10:10 local time at CON01-22, no clouds, diffuse sky, waves

Central Basin
SeaWiFS 01/07/19
GER1500 01/07/15 16:45 local time at CON01-1, darkening sky, high waves

Figure 6.3: Overview of the atmospherically-corrected SeaWiFS R_{RS} spectra and GER1500 R_{RS} spectra of Case 1 and Case 2 waters in Lake Baikal.

6.2 VALIDITY OF FIELD-SPECTROMETER MEASUREMENTS

There were distinctive technical and field drawbacks for the field-spectrometer measurements on the Lake Baikal CONTINENT cruises. For example, a considerable proportion of the measurements had to be undertaken during foggy, or very cloudy and rainy weather conditions, which especially affect the corrections for above-water measurements. A problem encountered with transparent oligotrophic water bodies is that there cannot be any analyses of non-corrected above-water measurements of the upwelling radiance, L_{up}, only, because the data is distorted by the noise of the back-reflection at the air-water interface, especially in the blue-wavelength range. This is even more significant for the case of Lake Baikal with its extremely high transparency. Therefore, the spectral information in our study had to be taken from the in-water field-spectrometer measurements.

Regrettably, for the case of in-water measurements, the coupled GER1500 spectrometer measurements were affected by serious technical problems (see also §4.2.3), the most problematic being that the configuration did not allow accurate retrieval of the attenuation coefficient that is, however, needed to extrapolate the under-water measurements in different depths towards the subsurface. It would have been more useful to undertake continuous depth profiling throughout the photic zone using commercially available submersible field-spectrometers. Therefore, the coupled GER1500 measurement set-up is not considered to be accurate in terms of absolute reflectance measurements. Although, these in-situ spectra can be used for investigations of spectral reflectance maxima positions and spectral reflectance shapes.

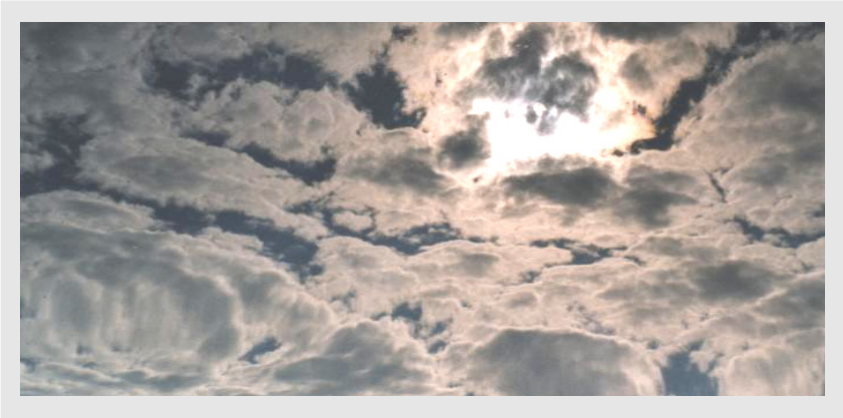

Figure 6.4: Field photo of the lake water surface itself, showing the sky reflection at unfavourable measurement conditions.

The field-spectrometer measurement experiments from 2001 and 2002 in shallow lakes in Germany (§4.2.5) indicated that in-water measurements, using the dual GER1500 set-up, were also not practical for spectro-radiometrical investigations of turbid lake waters. Generally, measurements in turbid waters with low Secchi depths acquire small and exact measurement steps, as described in Boine et al. [1999]. A similar set-up as in Boine et al. [1999] could not be established due to the massive metallic weight element that covers the fibre optic cable in order to perform stable measurements in turbulent and deep waters. Instead, the dual GER1500 set-up is recommended to be used for in-water reflectance measurements of bottom material (sand, silt, submerse macrophytes, etc.) in shallow waters.

Above-water measurements are favoured for eutrophic to hypertrophic surface waters. With turbid water bodies, the intensity of the water-leaving signal surmounts the directly back-reflected signal at the air-water interface. In addition, the scientific focus of the spectral analyses for these waters lies on the red-to-near-infrared wavelength ranges [*Thiemann and Kaufmann*, 2000; *Mannheim et al.*, 2004a; *Mannheim et al.*, 2004b], by this eluding the problematic blue-to-green spectral wavelength range.

In-situ measurements of the turbid Selenga River waters showed reflectance values that were one-to-two orders of magnitude higher compared to reflectance measurements of Lake Baikal water. The Selenga River spectra all show the second absorption band of Chl-*a* that is active around 675 nm, and in addition to the green reflectance maxima, additional maxima in the near-infrared at 690 nm and 820 nm (Figure 6.5). The near infra-red reflectance maximum beyond the second Chl-*a* absorption band is shaped by the fluorescence (for example, Fell and Fischer, [1999]) and back-scattering processes (for example, Thiemann and Kaufmann, [1999]) and the sharply increasing absorption of water beyond 710 nm. Water samples collected during the Selenga River expedition were not analyzed for pigments, due to limitations in the conservation of phytoplankton filters. The labels on Figure 6.5 are therefore based on theoretical knowledge of bio-optical processes (§2.1.1, 2.1.2, 2.1.3).

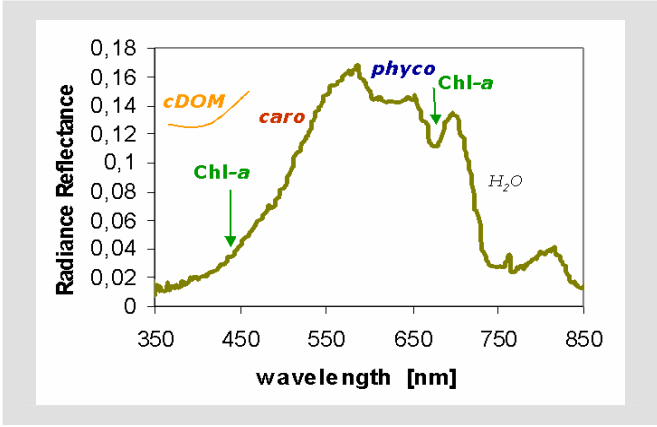

Figure 6.5: Surface reflectance spectra of Selenga River waters. SPM concentration was 22.7 mg l^{-1}. Absorbing processes by Chl-*a*, carotenoids (caro), phycobilins (phyco), cDOM, and H_2O are indicated.

As outlined in §5.3.2, a stable correlation between the green reflectance maximum (555 nm), equivalent to SeaWiFS band 5, and the SPM concentration was not given due to varying optical properties of the SPM in the Selenga river (phytoplankton, dissolved organic matter, organic particulates, organo-clay complexes and organic coatings on minerogenic SPM). Due to the high amounts of absorbing water constituents in the Selenga River, the minimum SPM value that can be calculated by using equation 5.1 equals 6 mg l^{-1}. This demonstrates that the Selenga SPM algorithm is not a transferable SPM algorithm for the much lower SPM concentration range encountered in Lake Baikal.

6.3 THE APPARENT WATER COLOURS OF LAKE BAIKAL

Due to the high transparency of Lake Baikal, the relevant information describing the optically-visible water constituents steams from a considerable depth of the photic water layer. Therefore, the question arose as to what sampling depths may be the most representative. The two-flow model of Gordon and McCluney [1975] describes the penetration depth (Z_{90}), where 90 % of the remote-sensing signal originates, by:

$$Z_{90}(\lambda) = \frac{2.3}{2 \times K(\lambda)} \quad [\mathrm{m}] \qquad (6.1)$$

where K(λ) is the diffuse-attenuation coefficient. For transparent pelagic waters with attenuation depths of K = 0.06 to 0.1 m^{-1}, this results in $Z_{90}(\lambda)$ values of 12 to 20 m. This is supported by the investigations of Straskrabova (pers.), who concluded that primary production is light-inhibited down to a depth over 20 meters in Lake Baikal in summer.

CONTINENT field data showed structured fluorescence Chl-*a* profiles, with Chl-*a* maxima occurring from 10 to 40 m depth. The Chl-*a* concentrations from the discrete 10 m to 20 m water samples generally showed similar concentrations compared to the 5 m water. Therefore, the averaged Chl-*a* concentration over the first 30 metres of all sample depths that were available has been taken as the remote-sensing reference.

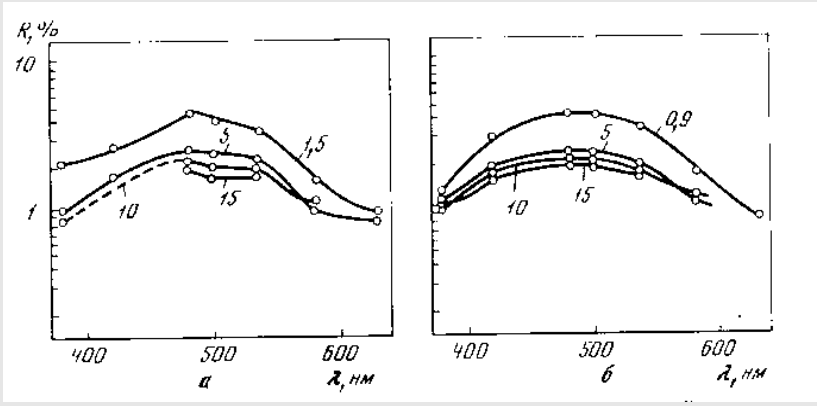

Hemispherical in-water reflectances [*Sherstyankin*, 1975]

a.1970/03/21 South Basin, under ice (0.8 m) with 2.5 cm snow coverage.

b.1970/03/28 South Basin, under ice (0.8 m) without snow coverage.

Numbers indicate depths of in-water measurements

Figure 6.6: An example from long-term studies in Lake Baikal of hemi-spherical reflectances under transparent ice [*Sherstyankin*, 1975].

The maximum position of R_{RS} spectra evolved to be a suitable spectral indicator for identifying Case 1 in contrast to fluvial-influenced waters. A reflectance maximum position around 490 to 510 nm for the case of highly transparent waters is also confirmed by several bio-optical investigations in transparent marine and freshwater bodies. In contrast, the European most transparent water bodies (pelagic areas in the North Sea, less in the Baltic Sea, and oligotrophic fresh water bodies) show significantly lower Secchi depths (8 to 15 m) due to enhanced input by intensively used rural and urban environments, and therefore, their reflectance shapes have reflectance maximum positions only around 550 nm, and at longer wavelengths.

For Lake Baikal, Sherstyankin's long-term measurements confirm spectral reflectance maximum positions between 490 to 500 nm in Case 1 waters in Lake Baikal (Figure 6.6) [1975]. The switching of the reflectance maximum position towards wavelengths at around 550 nm in Case 2 waters (§5.2) has also been yet described by Thomson and Jerome [1975], for the case studies of the Lakes Ontario and Superior (USA). They state that the most transparent waters had a dominant wavelength of 490 to 530 nm, whereas biologically more productive onshore waters had a dominant wavelength of 550 to 560 nm, while waters with heavy sediment loadings had a dominant wavelength of >565 nm.

CONTINENT field data confirmed the optical complexity of the Lake Baikal water body. Spectrometric investigations and varying Chl-*a* /carotenoid ratio values (Tables 3 and 4 in Annex B) indicate a complex optical background even for the pelagic Case 1 waters of Lake Baikal. DOC and cDOM CONTINENT field data also shows that there is considerable regional spatial variability in the concentrations of organic material (Tables 3a,b in Annex B), further impacting on the lake's optical properties. Therefore, despite the high transparency of Lake Baikal, there is a strong spatial variability in apparent water colour that can be evaluated using the spectral information derived from the atmospherically-corrected SeaWiFS data-sets. Figure 6.7 gives an overview of the spatial inhomogenity in apparent water colour.

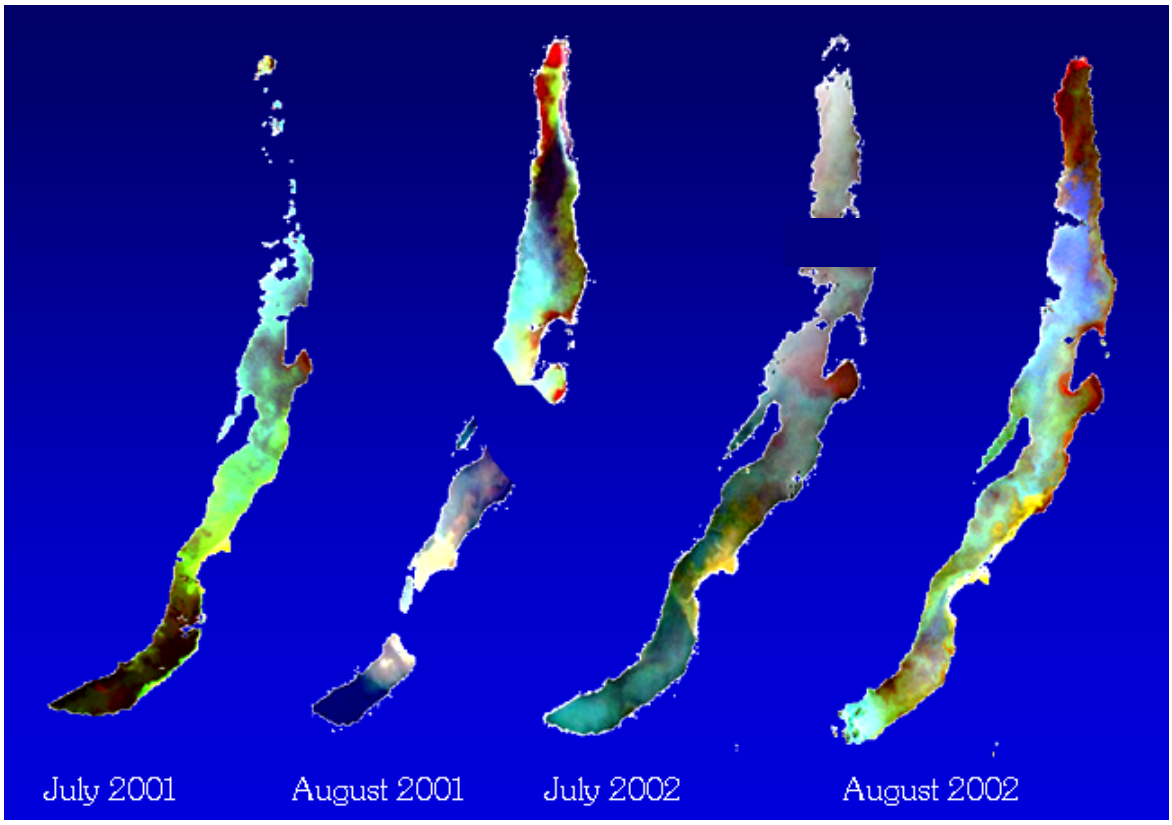

Figure 6.7: Red Green Blue composite (RGB 642) of SeaWiFS R_{RS} demonstrates horizontal heterogenity in apparent water colour.

6.4 APPLICABILITY OF SEAWIFS PRODUCTS IN CASE OF LAKE BAIKAL

6.4.1 SeaWiFS Chlorophyll Products

Factors influencing the quality of Chl-*a* algorithms in Case 1 waters are the variations in phytoplankton composition and physiological state, which in turn implement changes in the carotenoid/Chl-*a* ratio, the pigment composition and the phytoplankton morphology. The spectral influences of these factors, and a varying specific phytoplankton absorption capacity depending on temperature-nutrient provinces (§2.1.1), generally lower the accuracy of Chl-*a* algorithms.

The usable ground-truth data-set in this study at Lake Baikal is restricted to only a few concomitant spectral and Chl-*a* data, owing to weather restrictions during summer in central Asia. In addition, our sample distribution does not refer to a regular grid and therefore represents the bio-optical provinces of Lake Baikal differently in frequency of samples. It also must be considered that there is a distinct seasonal succession in phytoplankton composition in Lake Baikal (§5.5.1), and the field data represents the early summer phytoplankton assemblages specifically. Considering these various factors, it is not surprising that the empirical Chl-*a* algorithms for Lake Baikal, which were constructed from n = 26 Chl-*a* data Case 1 sets, including n = 5 in July in 2001 and n = 22 in July in 2002, performed well for 2002, although not for 2001 (§5.3.1). For example, similarly, the empirical coefficients in the SeaWiFS satellite data investigations of Iluz et al. (2003) of the oligotrophic Gulf of Eilat (Red Sea) showed different values each year during three successive years.

In contrast, the global OC2 and OC4 Chl-*a* algorithms were derived from a large, seasonally and geographically variable ground-truth data-set. The OC4 performs as a switching-ratio algorithm, adapted for a wider range of trophic states, whereas the OC2 is fixed to the $R_{RS}490/R_{RS}555$ ratio. According to the SeaWiFS experiment (*http://oceancolor.gsfc.nasa.gov/REPROCESSING*), the $R_{RS}490/R_{RS}555$ ratio of the OC2 Chl-*a* algorithm is especially well adapted to a trophic phytoplankton composition within the range of 0.7 to 2 µg/l Chl-*a* (Figure 6.8), favourably representing the oligotrophic state of Lake Baikal. In fact, the OC2 and OC4 Chl-*a* algorithms proved to robustly perform for all SeaWiFS data-sets in 2001 and 2002. Calculations of atmospherically-corrected SeaWiFS data-sets in 2001 and 2002 using OC2 gave results within 30 %, even meeting the NASA accuracy standard [*O'Reilly et al.*, 2000] for marine case 1 waters.

As a consequence of the Chl-*a* algorithm testing (§5.3.1), the OC2 is applied to the complete SeaWiFS data-set (2001 to 2002) to generate the Chl-*a* time series.

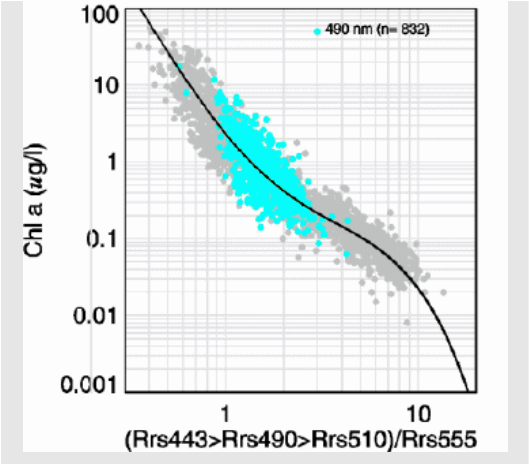

Figure 6.8: Scatterplot of R_{RS} ratio values against Chl-*a* values, both derived from the SeaBAM data-set (§1.2, *http://oceancolor.gsfc.nasa.gov/ REPROCESSING)*. $R_{RS}490/R_{RS}555$ ratio values are highlighted, because they favourably represent the oligotrophic state of Lake Baikal.

6.4.2 Influences of Terrigenous Input

Despite the adequate quality of all data-sets from July 2002, the comparison of ground-truth data with calculated Chl-*a* data showed that there is considerable Chl-*a* overestimation for several data points in July 2001 (for example, Figure 2 in Heim et al. [2005]). This overestimation is evident for the case of using all available Chl-*a* algorithms. These are the samples from the terrigenously influenced areas of the lake, where there is considerable absorption in the blue-wavelength range by cDOM (e.g., around the Selenga Delta). For high-organic fluvial-terrigenous input, the absorption in the blue to green spectral wavelength range is caused by cDOM and phytoplankton. Because standard Chl-*a* algorithms assign spectral characteristics only to Chl-*a* concentration, they overestimate Chl-*a* concentrations considerably in the presence of absorbing allochthonous organic matter. In contrast to clear pelagic waters, the Chl-*a* output within fluvial influenced areas after high discharge events due to strom events seems to be amplified by a factor up to 3 in Lake Baikal (e.g, Figure 6.9).

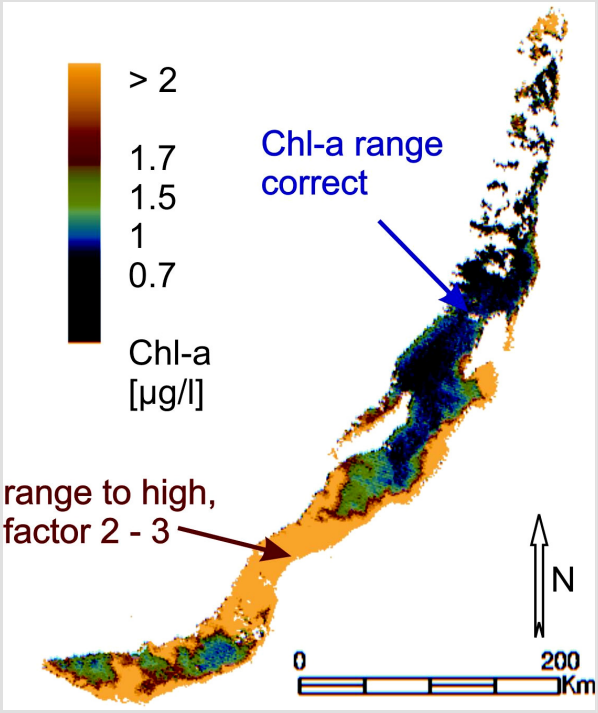

"The ITAR-TASS reported that torrential rains that resulted from a tropical cyclone that hit the Baikal area caused flooding…. Precipitation exceeded a monthly figure in several days, flooding a number of populated localities, roads and farms. …Almost 300000 residents of the Irkutsk region have reportedly suffered from the flooding that occurred from July 7th-9th 2001…." [*NOAA*, 2001]

Field photo while crossing a flooded road bridge on the 01/07/09: the Trans-Siberian Railway bridge spans above a flooded river valley, directly beyond is Lake Baikal.

Figure 6.9: OC2 Chl-*a* map of Lake Baikal, 2001/07/19, representing an exceptional hydrological situation with considerable terrigenous influences due to flooding events 10 days before.

Pozdnyakov et al. [2003] reported similar findings in a study of the coastal waters of the White Sea (Russia). They estimated a three- to five-fold Chl-*a* model overestimation that is caused by the optical interactions of high organic terrestrial input. Similarly, based on SeaWiFS investigations of San Francisco Bay (California, USA) during exceptional heavy rainfall events in 1998, Kuever and Chavez [2004] reported SeaWiFS OC2 Chl-*a* concentrations that were five-fold overestimated, probably due to terrigenous input.

Therefore, to reduce the possibility of misinterpretations in interpreting Chl-*a* maps of the SeaWiFS time series, all Case 2 waters, influenced by absorption and scattering process of allochthonous material, had to be identified. The reflectrance maxima position of R_{RS} spectra has in turn been used for discriminating fluvial-influenced waters in contrast to offshore Case 1 waters. The criteria 'reflectance ratio values of $R_{RS}510/R_{RS}555$ below 0.9' has been defined to build up a 'mask of terrigenous input' on the atmospherically-corrected SeaWiFS data. In case of this criteria, this mask of terrigenous input ($R_{RS}510/R_{RS}555 < 0.9$) was applied onto SeaWiFS Chl-*a* maps (2001 to 2002) to exclude Chl-*a* overestimation.

Similarly, Figueras et al. [2004] also reported a shift in the reflectrance maxima position of R_{RS} spectra for the case of terrigenous input by the river Nil in the Eastern Mediterranean Sea. In their SeaWiFS study, terrigenous input is masked to exclude erroneous high Chl-*a* concentrations by assuming a threshold value at 510 nm for R_{RS} values above 0.0055 sr^{-1}. However, at Lake Baikal, low $R_{RS}510$ values below 0.0055 sr^{-1} may be related however to terrigenous input signals due to the absorbing activities of high concentrations of organic matter (for example Figure 3 in Heim et al. [2005]). Therefore, the approach of Figueras et al. [2004] was not applicable for Lake Baikal. In another SeaWiFS study about the Bay of Biscay, Froidefond et al. [2002] referred to the reflectance maxima shift and defined the criteria '$R_{RS}490/R_{RS}555$ below 1' to exclude Chl-*a* overestimation due to terrigenous input.

The terrigenous input, naturally, has considerable influences on the Secchi depths. The empirical algorithm of Kratzer [2003] was used to extract Secchi depth values from the SeaWiFS data. Figure 6.10 shows as an example a Secchi depth profile along Lake Baikal from North to South, in July 2001. The optical influence of the Selenga River and local mountain rivers (in the South Basin) is obvious.

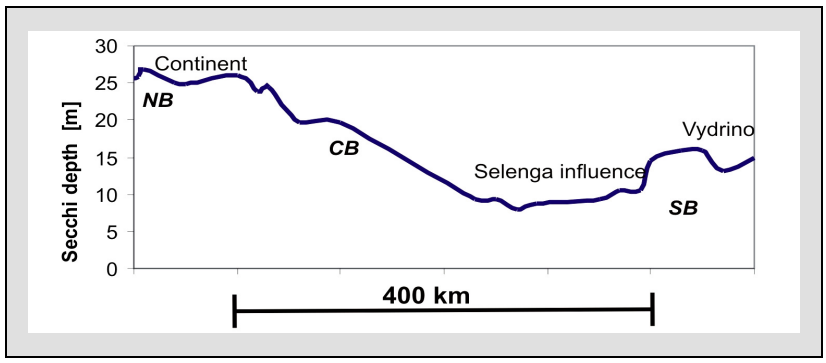

Figure 6.10: North-South transect of Secchi depths, calculated from SeaWiFS data (2001/07/19) by using: Secchi depth^{-1} = 0.55 SeaWiFS K490 - 0.04 [Kratzer 2003].
NB = North Basin; CB = Central Basin; SB = South Basin.

6.4.3 SeaWiFS Terrigenous Input Products

Generally, within bio-optical studies, there still exists a large uncertainty in the optical properties of the in-situ state of SPM (due in part to a lack of detailed field observations to derive accurate parameterizations of processes such as flocculation, re-suspension, etc.). Results of investigations include findings that optical variability (e.g. in attenuation, scattering, and reflection) depends not only on the SPM concentration, but also significantly on the shape, size and composition of the suspended particles [*Clifford et al.*, 1995; *Gippel*, 1988] as with the cDOM content [*Malcolm*, 1985]. On one hand, the fluvial influenced areas in Lake Baikal could be identified by $R_{RS}510/R_{RS}555 < 0.9$, and subsequently processed by applying the SPM algorithm linked to the SeaWiFS attenuation coefficient (equation 5.3, §5.3.2) onto the SeaWiFS time series. On the other hand, because of the limited ground-truth data-set of water samples that were influenced by terrigenous input, this still is a preliminary approach. For example, the validity of this SPM algorithm during the snow-melting season in May and April is unknown. Terrigenous input events during the melt season may be higher reflective, due to high proportions of anorganic silt and fine sand.

6.5 THE REMOTE-SENSING AND GIS PRODUCTS IN 'CONTINENT'

The Ocean Colour for the time span from early summer 2001 to winter 2002/2003 were processed. The geocoded Ocean Colour products can be integrated into the CONTINENT GIS and be combined with additional parameterized layers, for example with the bathymetric map.

There have been some constraints on bio-optical remote-sensing studies at Lake Baikal: Due to widespread terrigenous influence during the snow-melting season, acquisitions of the SeaWiFS time series in May 2002 could not be evaluated for Chl-*a* concentration. Summer monsoonal cloud coverage limited the number of usable acquisitions, especially between June and July. Remote-sensing investigations between late September and October are also limited due to low insolation

and low sun zenith that cause considerable direct back-reflection of skylight at the air-water interface (≥10 % reflectance). In addition, the water-leaving reflectances during this season of the year will be remarkably reduced due to low sun insolation. This is also expressed in the grey apparent water colours during the autumn months [*Sergeyev*, 1989]. Therefore, there exists on one side a pool of geocoded cloudfree water pixels in 2001 and 2002, on the other side there are actually only very few cloudfree acquisitions gieving information about the whole lake. Despite this constraints, the generated Ocean Colour products provided valuable information about the spatial and seasonal variability of autochthonous and allochthonous material for the open-water seasons in 2001 and 2002.

6.5.1 Chlorophyll: Spatial Information

In early June 2001, Chl-*a* distribution in the South and Central Basin appeared relatively homogenous from calculated Chl-*a* maps. In August 2001 and late July and August 2002, horizontal heterogeneity developed with eddy formation. Chl-*a* maps show Chl-*a* concentrations during summers 2001 and 2002 increasing southwards towards the Southern coast.

In contrast to the northern coastline of the South Basin, where the biological station Bolshye Koti and the offshore SRIB sampling site are situated, which was characterized in June and July 2001 and 2002 by irregular structures of relatively low Chl-*a* concentrations (Figure 6.11, left). The SRIB field data confirmed cold-water events during this season in 2001, 2002, and 2003 [*Straskrabova et al.,* 2005]. In addition, benthic phytoplankton species in SRIB surface-water samples at Bolshye Koti also indicated mixing events between water layers due to storm events [pers., Fietz, IGB, Germany]. It seems that during this time of the year, cold-water events are common along this coast due to a strong mountain winds blowing from the land (see also Figure 3.2, §3.3).

As a consequence, spatial remote-sensing data indicates that a correlation between the autochthonous production at the SRIB sampling site near Bolshye Koti (North coast of South Basin) with the findings from sediment-traps (centre of South Basin), and with the coring site 'Vydrina' (southern coast of South Basin) cannot be directly made. Such correlations may therefore only be done with great care, and with the support of additional limnological data and Ocean Colour data.

Within the central eddies of the North Basin, Chl-*a* concentrations are the lowest (Figure 6.11, right). In contrast, the Ocean Colour data highlights that the east coast of the North Basin (where the coring site '*Continent'* is located) consistently had more phytoplankton in patchy and heterogeneous patterns in 2001 and 2002. Data from the core 'Continent' forms the basis for the reconstruction of paleoclimatic conditions for the North Basin. Therefore, spatial remote-sensing information indicates that the CONTINENT core records and the findings from the sediment-traps in the North Basin with respect e.g. bio-markers [e.g., *Russel and Rosell-Melé*, 2005] and phytoplankton productivity [e.g., *Straskrabova et al.*, 2005], must be carefully considered for correlation.

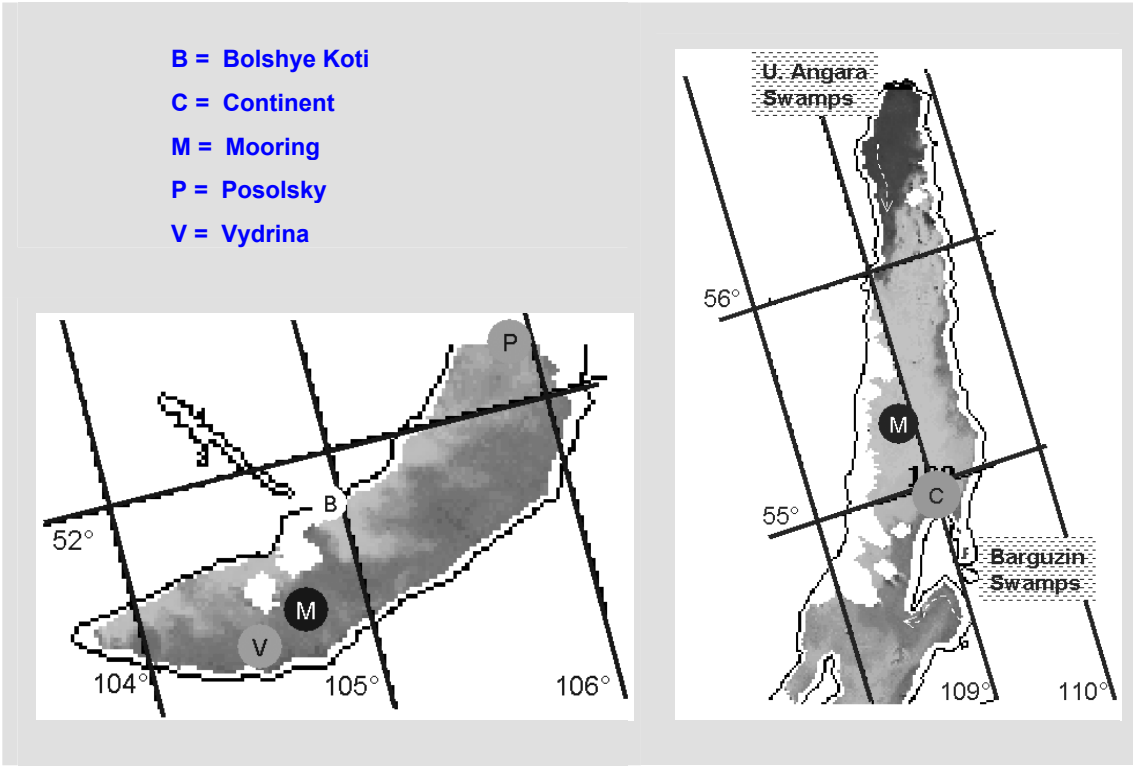

Figure 6.11: SeaWiFS Chl-*a* map of 2002/07/20. Left: The map indicates the hydrodynamic features showing relatively low Chl-*a* concentrations (below 1 µg l^{-1}) along the northern coast of the South Basin. Right: The Northern mooring is situated within an ultra-oligotrophic environment, while higher phytoplankton abundance prevails at the coring site 'Continent'.

6.5.2 Chlorophyll: Seasonal Information

Chl-*a* acts as an indicator for autochthonous processes, such as phytoplankton productivity [*Kiefer and Mitchell*, 1983; *Gervas and Behrend,* 2003]. Therefore, the OC2 Chl-*a* data may provide the information about the phytoplankton dynamics from early to late summer in 2001 and in 2002.

Averaged Chl-*a* values were calculated from selected Regions of Interest (ROIS) that were generated for the NW North Basin where the CONTINENT mooring is located (within an ultra-oligotrophic gyre), the coastal waters in the NE of the North Basin ('Continent'), the region between the Central and the North Basin ('Academician Ridge'), the Central Basin (without Selenga influence), SW of Selenga Delta ('Posolsky'), and the centre of the South Basin (also without Selenga and coastal influences) where the second mooring is located. The quantitative Ocean Colour information reveals the dynamical behaviour of autochthonous processes in Lake Baikal (Figure 6.12). A slight decrease in Chl-*a* at the end of June/ beginning of July in 2001 and 2002 is visible, although it is not significant. Then, during the course of the summers in 2001 and 2002, Chl-*a* concentrations significantly increased in all basins. These relatively high Chl-*a* concentrations (2-3 µg l^{-1}) at the end of the month of August were also found during SRIB investigations in late August and early September 2003. Note the restricted seasonal specific information of a two-week field cruise (CON01-4, CON02-8).

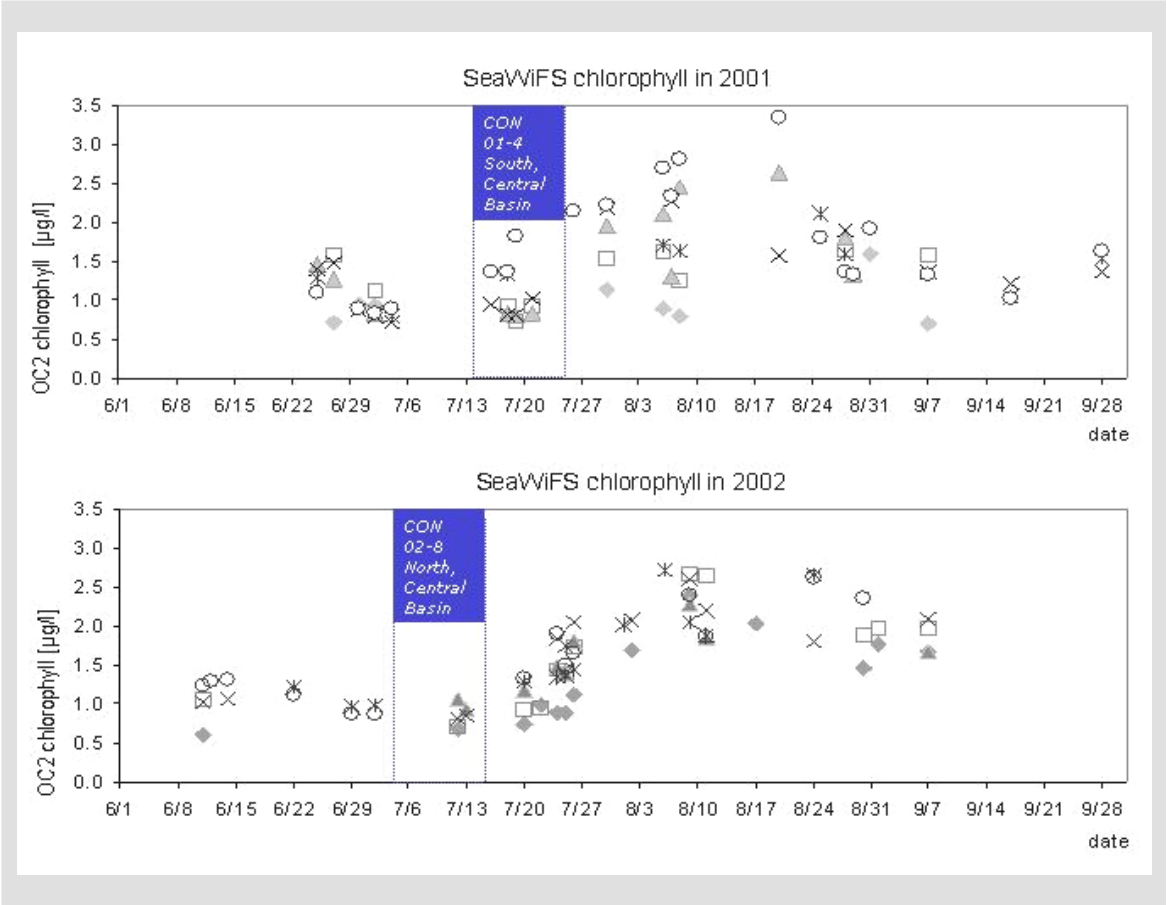

Figure 6.12: OC2 Chl-*a* seasonal succession in 2001 and 2002. The time windows of the field data (CON01-4, CON02-8) are highlighted (in blue). Diamonds: Northern mooring (oligotrophic central North Basin); squares: 'Continent' site (Eastern North Basin); triangles: 'Academician Ridge' (between Central and North Basin); crosses: Central Basin (without Selenga influence); stars: 'Posolsky'; circles: South Basin (without Selenga influence).

Interesting is the obvious rising of autochthonous productivity during the course of summer in all basins of Lake Baikal. This seasonal cycle is in accordance with known events in oligotrophic lakes, showing a broad peak to early summer that may be structured by cold water events, followed by an increase in phytoplankton productivity during the course of summer [pers., V. Straskrabova, HUB, Czech Republic).

6.5.3 Suspended Particulate Matter: Spatial Information

In the beginning of July 2001, exceptional storm events that led to catastrophic flooding were manifested as high fluvial discharge signals from the Selenga and local mountain rivers, predominantly into the southern part of Lake Baikal (for example, Figures 5.7 and 6.9). The optical signal of the terrigenous material still persisted three weeks after the high-energy discharges due to the tropical cyclone event in South Siberia and North Mongolia (2001/07/07-09). This exceptional event showed how storm conditions may have an unexpectedly large spatial extent, and will influence the terrigenous signals recorded in the sediment cores. The extension of fluvial optical influence over 100 km offshore (for example, Figure 5.6) and the duration of this signal for a period of several weeks, was similarly described in recently published remote-sensing investigations.

Kudela and Chavez [2004] stated in a SeaWiFS study in San Francisco bay (USA) in 1998 that the optical influence of terrigenous input extended considerably further than the 30 km originally estimated for sediment transport. They describe the terrigenous input after unexceptionally heavy rainfall to extend as a low salinity, high cDOM field on to 300 km offshore. This means that it is not appropriate to conclude from only discrete and seasonally restricted field data-sets what the terrigenous influences are at the CONTINENT coring sites. For example, in 2001, while our survey cruise was one week after the flooding events, the terrigenous input could not be deduced from our limnological field data, because we focused on phytoplankton analyses, and did not undertake at this time DOC and cDOM investigations. The extent of terrignous input was finally detected and deduced from the maps of Ocean Colour products.

According to the calculated SPM maps, the coring site 'Posolsky' is highly influenced by the Selenga River input inter- and intra-annually. According to the distribution pattern on the SPM maps, the coring site 'Vydrina' is strongly influenced by discharge from local mountain rivers. This is in accordance to the findings of Charlet et al. [2005], who inferred transport directions at 'Vydrina' from sedimentary bottom features using Sonar data. In addition, pollen [*Demske et al.*, 2005] and heavy-mineral analyses [*Fagel et al., in press*] of core sediments indicate that local influences were likely to have been present at 'Vydrina' even during the early Holocene. Hence, findings from the 'Vydrina' site are considered to include a strong local signal, and correlations to the CONTINENT mooring, located in the central South Basin, must be considered and done with great care. SeaWiFS data indicates that Selenga terrigenous input is probably not important for 'Vydrina', while terrigenous input from local mountain rivers prevails.

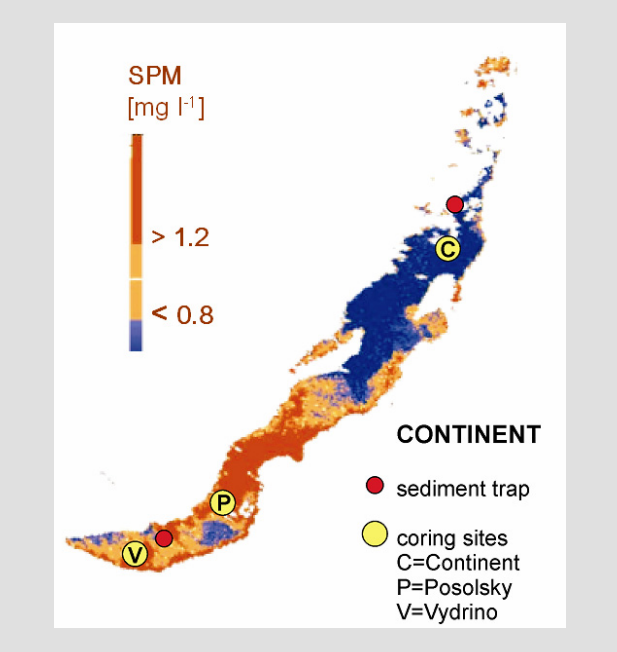

Figure 6.13: SeaWiFS terrigenous input map of the parameter 'SPM', 2001/07/19, representing the exceptional hydrological situation due to flooding events 10 days before (see also Figure 6.9). The map highlights that terrigenous input from local mountain river prevailed for the CONTINENT coring sites 'Vydrina(/Vydrino)' and 'Posolsky' .

6.5.4 Suspended Particulate Matter: Seasonal Information

In April 2002, the North Basin was still under continuous ice cover, while in the Central and South Basins the ice cover was gradually decreasing. In turn, in May 2002, during the snow-melting season, the then ice-free South Basin and the southern part of the Central Basin were influenced by substantial fluvial input from the Selenga and local mountain rivers. During this season, the Selenga River inflow is mainly distributed towards the South Basin along the western coastlines, and there is reduced terrigenous input into the Central Basin. Figure 5 in Heim et al. [2005] (calculated SPM maps overlayed on non-atmospherically-corrected SeaWiFS quasi-true colour data) describes the typical situation of high-energy terrigenous input events during times of ice break-up and the snow-melt season in the month of May 2002.

The fluvial input in late July and August 2001 and 2002 diminishes on the calculated SPM maps. However, the input of humic substances into the lake still seems to be considerable high even in summer. Yoshioka et al. [2000] report it to be as high as 200 to 500 µMC DOC (equals 2.4 to 6 mg l^{-1} DOC) measured several kilometres downstream from the Selenga and the Barguzin rivers. Yoshioka et al. [2000] confirmed that the main origin of DOC in Lake Baikal, even in pelagic waters, seems to be terrestrial because the δ^{13} C values of DOM in Lake Baikal (-26 to -25 ‰) and in the tributaries (-27 to -26 ‰) are comparable. The high volumes of dissolved and particulate organic matter in the Lake Baikal catchment area seems to us to be due to the high humidity, large coverage of boreal forest, permafrost soil and tectonic sub-basins that facilitate the development of swamps and bogs.

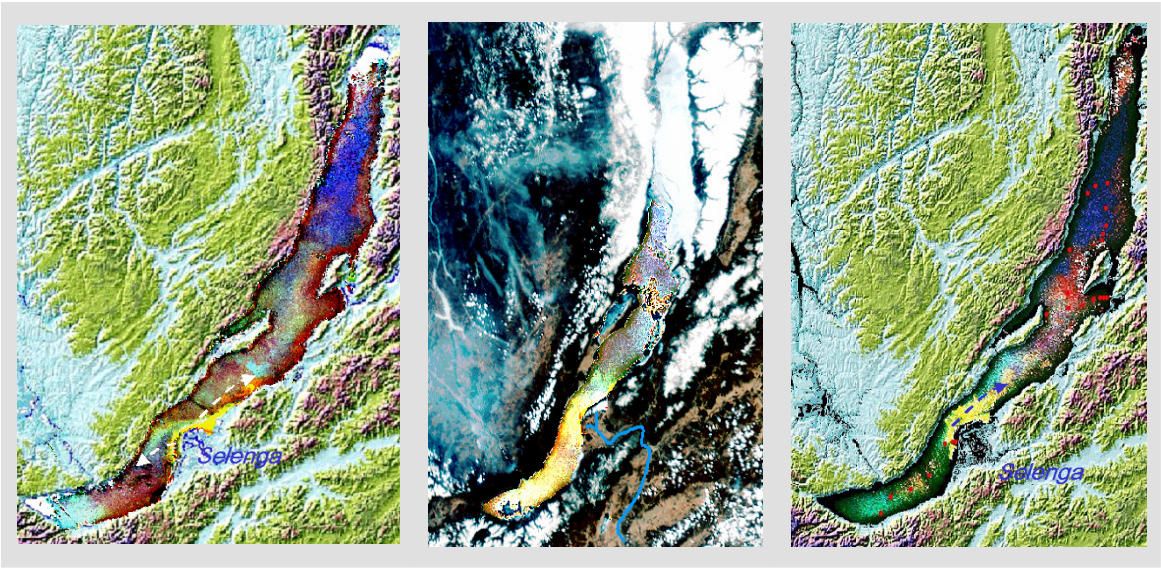

Figure 6.14: Red Green Blue composits (RGB 642) of SeaWiFS R_{RS} showing the appareren water - leaving colour after successful atmospheric correction. A colour-shaded DEM shows the high mountain ranges around Lake Baikal, and the break-through of theSelenga River and its enourmous delta region. Left: 2001/08/06, the terrigenous input is forced by the lake hydraulics towards SW into the South Basin and along the E coast of the Central Basin. Right: 2002/26/07, again in summer, the terrigenous input flows along the E coast of the Central Basin. Center: 2002/05/13, high-energy discharge into the South Basin during the snow-melting season. Here, the RGB 642 R_{RS} is mosaiked (path-coded, not geo-coded) into the RGB 642 R_{TOA} to show that in late spring the North Basin is still covered by ice.

During summer, there seems to be a confined optical signal showing a jet of terrigenous influence leaving the Selenga Delta in a south-west direction, and a second one being predominantly confined as a northwards flow. Both hydraulic features are in accordance with the surface current circulation pattern as proposed by Kozhov [1963]. This observed seasonal Selenga River plume dynamics culminating in a northwards flow in summer, are also confirmed by Hohman et al. [1996], who described the hydrodynamical behaviour of the Selenga River plume in late summer 1993, that owing to the thermal bar development in early summer (§3.4), the Selenga waters are forced to flow northwards along the Eastern coast of the Central Basin.

6.5.5 Suspended Particulate Matter: Quantitative Information

An interesting aspect would have been to quantify the SPM discharge from the Ocean Colour data. However, a problem for estimating the SPM of high-energy discharge due to heavy rainfall is the time gap between the short-term peak of discharge and the time of observation. For example, in the case of the flooding in July 2001 at Lake Baikal, cloudfree SeaWiFS acquisitions were from dates several days after the peak discharges, where settling and dilution of the main part of terrigenous matter had yet occurred.

In addition, for the case of high-energy discharges, the hydraulics of the transport are complex and may occur in different water depths according to particle sizes. For example, Mertes and Warrik [2001] carefully calculated order-of magnitude estimates of total SPM output from SeaWiFS SPM maps (± 10 mg l^{-1} SPM error) of the Californian Coast, taking into account river plume dynamics and the layer thickness of suspension as exactly as possible. They compared the estimated river mass output to previously estimated sediment-discharge data, concluding that the mass output estimated from remote-sensing data of surface plumes accounted for only 1 % to 2 % of the total river discharge.

Investigations of the hydrophysical dynamics of the Selenga River plume are described in Hohman et al. [1996] using seasonal CTD (Conductivity-Temperature-Density) and mooring station data along the sub-aquatic Kukui Canyon (leaving the Selenga Delta in the NE direction) in 1993. Hohman et al. [1996] inferred from these measurements that the main fluvial mass transport occurs in spring as a plunging negative boat river plume. In early summer, the main Selenga River plume spreads at an intermediate water depth. During the course of the summer only, the Selenga River discharge occurs as a positively buoyant plume [*Hohman et al.*, 1996]. Hence, due to the complexity of the river plume hydraulics, no SPM mass discharge calculations of the Selenga River plume were undertaken.

6.5.6 GIS for Geological Catchment Analyses

Within this context, our approach shall show the benefit of using GIS analyses to support provenance analysis. The SPM field samples show a wide-spread occurrence of clay-rich agglomerates dominated by illit and smectit [pers., Fagel, UCL, Belgium]. This agrees with the fact that weathering of mainly granitoid source rocks under moderate and colder climatic conditions generally produces weathering crusts and soils with a clay assemblage of illite and smectite [*Scheffer and Schachtschnabel*, 1992], and that the GIS analyses of the lithology of the catchment areas of Lake Baikal confirms a 50 to 60 % coverage by granitoids in all catchment areas. The exception is the metamorphic rock assemblage, building up the Southern coastline of Lake Baikal, where the coring location 'Vydrina' is located. The results of mineral cluster analysis in Fagel et al.

[in press] specifies that the sediment samples of the 'Vydrina' core are characterized by totally different detrital heavy mineralogical composition than samples of the 'Posolsky' and 'Continent' cores. Hence, the laboratory and the GIS analyses indicate different source rocks for 'Vydrina' in contrast to 'Posolsky' and 'Continent'.

On the other hand, the studied sediment samples of the 'Posolsky' and 'Continent' cores have very similar detrital heavy mineralogical composition, while they are approximately 300 km apart in different lake sub-basins. The light and heavy mineralogical composition of the studied samples from both cores indicate that the source rocks of the sediments were mainly granitoids. The, on first sight, astonishing fact that the sedimentary record for source rocks of the 'Continent' core from the North Basin mimics the mineralogical signature of the 'Posolsky' core, and of the SPM in the Selenga River, is explained to be due to this homogeneous geological coverage by granitoids in the eastern catchment areas of the Central and the North Basin. The GIS analysis convincingly performed as a supportive tool for provenance analyses, providing an accurate area quantification of the source rocks.

6.5.7 Lake Ice Cover

Although the SeaWiFS data cannot be used for bio-optical analyses during autumn, winter and early spring, it provides information about the lake ice, different ice types, and the degradation of the ice cover. Especially the winter months in the Baikal area are characterized by very low cloud coverage due to the Central Asian high-pressure system. The SeaWiFS R_{TOA} data for December 2001 and January 2002 demonstrates the freezing of the lake and the establishing of a continuous ice cover. SeaWiFS data for February 2002 shows the distribution of transparent and non-transparent ice types and snow cover. These optimal cloudfree conditions for optical remote sensing applications change in spring while the Siberian anticyclone is decreasing. In April and June, SeaWiFS data reveals the processes of ice break up (Figure 6.12). This information is of high potential for multi-disciplinary limnological studies about the hydrodynamics during ice break up, and regions of transparent ice with preferred phytoplankton development.

Here, microwave satellite data may increase the capacity of monitoring ice cover and different ice types on Lake Baikal through a wide range of cloud cover conditions. So far, active non-imaging microwave altimeters and passive radiometers with low spatial resolution were used to monitor freeze-up date evolution and fast-ice duration on Lake Baikal [*Kouraev et al.*, submitted]. Currently, multi-polarization Synthetic Apertur Radar (SAR) algorithms for fresh-water ice are being developed at the Great Lakes (USA) [*Nghiem et al.*, 2002]. These airborne-based SAR algorithms may be applied to Envisat (ESA) data to map fresh-water ice cover on great lakes in high-spatial resolution [*Leshkevich and Nghiem*, 2005].

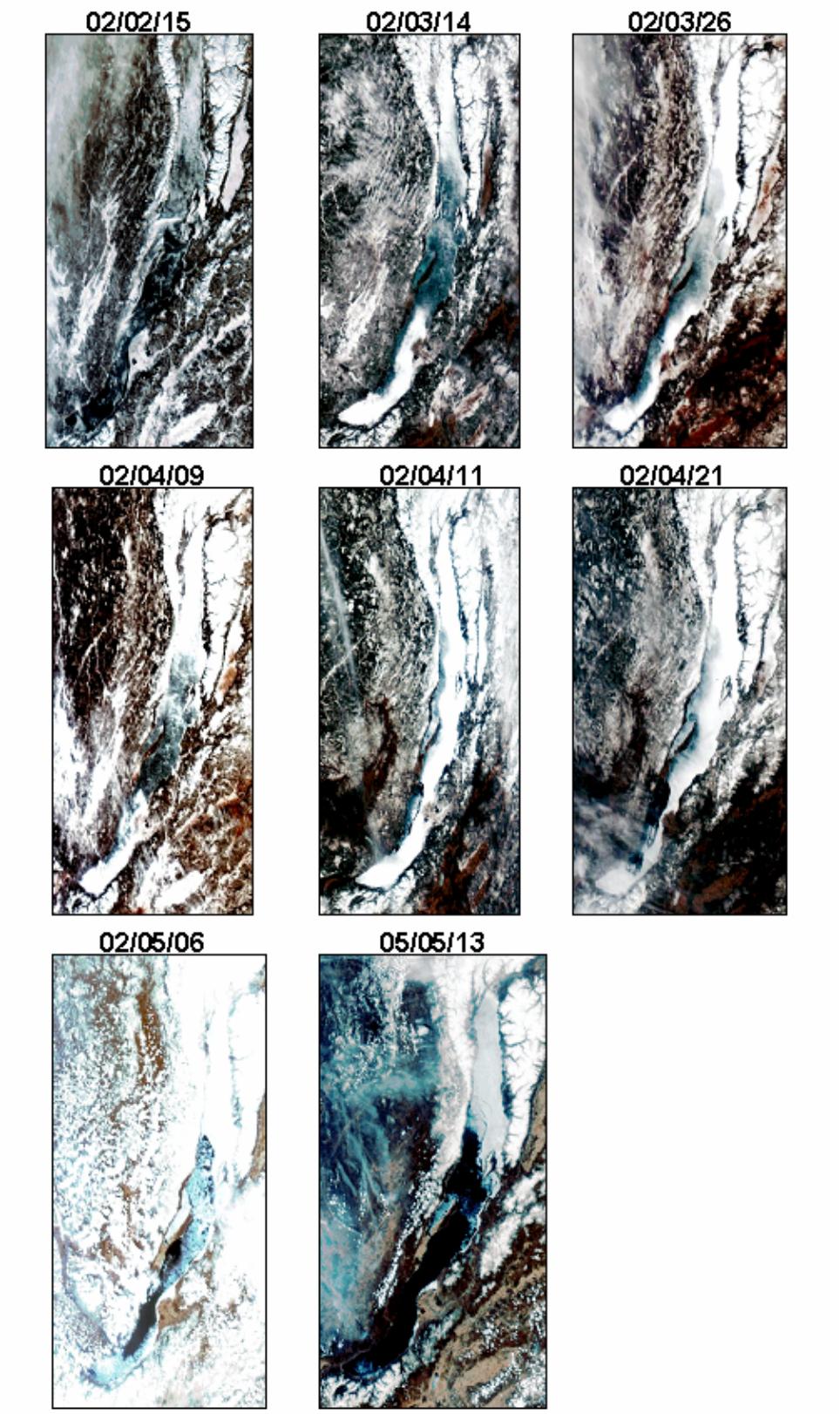

Figure 6.15: Red Green Blue composites (RGB 642) of SeaWiFS R_{TOA} for late winter and spring 2002. The satellite data shows the dynamics of ice and snow cover on Lake Baikal.

7 CONCLUSIONS AND OUTLOOK

In this thesis, it has been shown that optical remote-sensing is a suitable technique for monitoring the Lake Baikal. This bio-optical satellite study, the first for Lake Baikal, was based on the interpretation of limnological ground-truth data-sets from both my own data-sets (SPM, cDOM, spectro-radiometrical field data) and data-sets provided by the CONTINENT project (Chl-*a*). The limnological field data-sets and the field-spectrometer measurements provided information about the different bio-optical provinces and how to estimate the quality of the calculated remote-sensing products, Chl-*a* and SPM.

Within this study, the SeaDAS atmospheric correction was adapted to best suit the case of Lake Baikal and its continental boreal environment. Adequately atmospherically corrected SeaWiFS data only can provide the basis for the sensitive Ocean Colour analyses of the highly transparent water body.

Due to the considerable heterogeneity in the phytoplankton composition of Lake Baikal - in addition to distinct seasonal variations - the Chl-*a* algorithm should be derived from a large, and multi-temporal ground-truth data basis. The SeaWiFS OC2 Chl-*a* algorithm, optimized for the trophic range of 0.7 to 2 µg l^{-1} Chl-*a*, performed best for the SeaWiFS data-sets from 2001 and 2002. The accuracy of the Chl-*a* determination for Case 1 waters was even in accordance with the NASA quality standard for Case 1 waters (< ± 35 %). Case 2 waters, which were influenced by additional optical processes due to terrigenous input, and therefore showed Chl-*a* overestimation, were masked by using a spectral-ratio threshold defined as '$R_{RS}510/R_{RS}555 < 0.9$'.

The spatial information from the Chl-*a* maps was used to assist with analyzing the relationships between the various discrete data about the autochthonic material obtained during the CONTINENT field work. The remote-sensing parameter Chl-*a* acts as an indicator of phytoplankton productivity, which in turn is indicative of autochthonic biogenic climate proxies. The SeaWiFS time series for summer 2001 and summer 2002 provided additional seasonal information about the times of a rising of phytoplankton productivity in all basins of Lake Baikal.

The empirical SPM algorithm determined from this study was calculated by using the attenuation coefficient algorithm to account for the organic SPM fluvial-input type encountered at Lake Baikal. These calculated SPM maps showed realistic SPM distribution with the highest concentrations near the river outlets, in contrast to standard SPM calculations that usually correlate the reflectance height with SPM. The extent of the terrigenous SPM distribution on seasonal SPM maps offers information about the allochthonous influences on the different CONTINENT sites.

The Chl-*a* and SPM maps demonstrated the potential of remote-sensing data to detect meso- and large-scale features, and to provide information about seasonal dynamics. Hence, considering the enormous size of Lake Baikal, the spatial information of the Ocean Colour data was useful for the interpretation of field cruise and field sediment trap data. This study also shows that Lake Baikal with its optical complexity and spatial variations of Case 1 and Case 2 waters is a highly interesting case study for Ocean Colour analyses. One of Lake Baikal's optical peculiarities is that its Case 2 waters still show a higher transparency, and therefore different spectral features (e.g., the maximum position of reflectance spectra), than, for example, clear waters of European semi-enclosed seas or inland waters.

An interesting future task within a bio-optical study of Lake Baikal may be to investigate the phytoplankton composition correlated to the averaged spectral light field of the photic zone. If the terrigenous input into the Southern and Central Basin induces a reduction of the available light for the photosynthesis in the blue wavelength range, the amount of available blue light will successively be reduced within deeper water layers of these regions, in contrast to the highly transparent waters of the northern end of the Central Basin and the North Basin. The question arises if the differences in the averaged spectral light field of the photic zone may have an effect upon the phytoplankton composition. For example, spectroradiometrical investigations in Lake Michigan (USA) [*Bergmann et al.*, 2004] confirmed that within a spectral underwater light field, where the blue light was reduced, phytoplankton groups were favoured which had pigment groups also using photosynthetically available light in the green wavelength range, such as the phycobilin containing Cryptophta and cyanobacteria picoplankton. This will be even more significant for phytoplankton maxima in depths of 10 to 30 meters and below due to the exponential behaviour of the diffuse absorption coefficient, K.

This leads to an interesting speculation, how flushes of terrigenous input during colder climates (perhaps containing organic matter due to swampy tundra areas) may have influenced the available spectral light field in the photic layer of the ancient Lake Baikal water body. How possible is it that the reduction of blue light available for photosynthesis was unfavourable for the diatoms, which preferably absorb in the blue-to-green wavelength range of 400 to 500 nm, in addition to other unfavourable environmental conditions during colder climates?

It is emphasized, that for future bio-optical investigations of Lake Baikal, the following aspects need to be clarified, and the following technical equipment is advisable:

- Sun photometer measurements of Angström coefficients
- Profiling spectral-radiometer measurements that continuously record the spectral underwater light field at depth, reaching the depths of phytoplankton maxima (10 to 30 meters) and deeper.
- Continuously profiling absorption/attenuation meter and backscatter-sensor measurements
- Continuous cDOM absorption mapping system using spectrometric and fluorometric sensors that measure water continuously pumped, before filtering and filtered.
- On board laboratory spectroradiometer measurements for in-situ $a^*_{phyto}(\lambda)$ and $a^*_{detritus}(\lambda)$ measurements.

Such field investigations will provide more specific information about the optical properties of Lake Baikal. Yet, there exist extensive Russian optical-field investigations in Lake Baikal [*Sherstankin*, 1975; *Shimarav et al.*, 1994; *Bunev et al.,* 2000]. The investigations are focused especially on the deep water layers, and on the season during winter and spring under ice cover. Semowski [1999b] used the vertical profiles of optical coefficients in the South Basin of Lake Baikal (measured by Sherstyankin [1975]) for bio-optical modelling. He concluded that compared to pelagic marine waters he had to account for high absorption in the blue wavelength range due to cDOM. Semowski [2000] also proposes that the optical field will be dependant upon the phytoplankton composition due to the very different scattering functions of picoplankton, and the exceptionally large-sized Baikal diatoms on the other hand.

Our field investigations at Lake Baikal confirmed this high spatial and seasonal variability in the composition of the optically relevant water constituents. We encountered a variability of optical variables also during our investigations of the much more turbid German lakes (Rheinsberg and

Brandenburg Lake districts, Havel river lakes), where the optical coefficients seem to be partly dependant on the trophic state of the investigated water bodies.

Following questions may be clarified by future specific investigations on the inherent optical properties of Lake Baikal: which bio-optical parameters can be taken from other investigations at comparable water bodies, and for which ones there is a need to measure them in Lake Baikal? For example, there is this distinctive regional differentiation and the distinct seasonal succession of optically extremely differing phytoplankton groups, such as the large-sized Baikal diatoms with brownish appearance (coloured by carotenoids), or the reddish- to cyan-coloured cyanobacterial picoplankton (coloured by phycobilins).

Which $a^*_{phyto}(\lambda) = A_{phyto}(\lambda)\,[\text{Chl-a}]^{B_{phyto}(\lambda)}$ will be appropriate? And which analytical solution will be appropriate for the bio-otpical representation of a high organic terrigenous input?

The optical complexity of inland and coastal waters drives a need for a high-spectral sensor resolution. On the other hand, the mapping of nearshore, estuarine or inland water features also require high-spatial resolution. To cover the needs of high spatial and high spectral and radiometric performance, the design of new satellite missions is driven towards small, mobile hyperspectral satellite sensors [Thiemann, 2000]. These sensors will allow a regular surveying of inland and coastal lake water quality, as is claimed in the European Water Framework Directive [*WFD*, 2000]. The launches of the satellite ARIES (Australian Resource Information and Environment Satellite) and COIS (Coastal Ocean Imaging Spectrometer), both hyperspectral sensors, have been delayed at this time. Hyperspectral research sensors that are now in orbit are HYPERION and CHRIS-PROBA. Both sensors are currently on extended missions, however they are not operational. In the near future, hyperspectral operational satellite data that is very suitable for lake-water quality monitoring may be provided by the operational EnMAP (Environmental Mapping and Analysis Program) mission (GFZ, DLR, Kayser-Threde). EnMAP is designed to provide a spatial resolution of 25 m, and a spectral resolution of 200 programmable bands in 'water' and 'land' mode.

For the case of an optical study of Lake Baikal, EnMAP data may provide detailed information about the Selenga and local river input, and ecological information for selected coastal regions of Lake Baikal, supporting the large-scale information of Ocean Colour data from the pelagic waters. Valuable remote-sensing applications for water-quality surveillance at Lake Baikal could also include, for example, LIDAR and hyperspectral airborne campaigns near the inlet of the pulp and paper plants in the South Basin to determine the pathways and concentrations of anthropogenic organic compounds in the lake surface water.

For further studies at Lake Baikal, combining the hydro-physical information of Sea Surface Temperature (SST) from thermal satellite data with the Ocean Colour information will support the remote-sensing analyses from optical data. The highly performing Ocean Colour data of MERIS (ENVISAT) has become available since recently, and will provide adequate data to resolve the optical complexity of Lake Baikal.

There has been much debate over the utility of remote-sensing in aquatic sciences, especially for the dynamic coastal environments. Remote-sensing data provides spatially-highly resolved information about parameters over ecologically relevant scales, and - another important fact - about short-term episodic events. Like this, remote sensing data can potentially support the investigative, the operational and the surveillance monitoring of water quality services as it is claimed for in national and international environmental directives (e.g., *WFD*, 2000).

Despite there is userfriendly remote sensing software available, such as it is the case for processing Ocean Colour sensor data (e.g., the high-quality, freely available NASA software SeaDAS), problems have however arisen for the case of coastal and inland water bodies that are bio-optically more complex, and are in addition overlaid by a spectrally unknown and complex atmosphere. Ocean Colour studies and similar advanced remote-sensing and GIS raster applications require large disk space and storing capacities, advanced platforms and skilled users. Therefore, the possibility of accessing higher-level satellite data products will be an obvious benefit to research projects and water quality services from different disciplinary backgrounds that nonetheless intend to use Ocean Colour information. MODIS and MERIS for example deliver Chl-*a* and SPM products, and servers such as SISCAL and COASTWATCH regularly provide, or will provide in the future, water quality parameters (SST, Chl-a, SPM, Secchi depth, et al.).

The challenging tasks in future will be to define the accuracy and validity of the higher-level products for regional studies. The challenge will be to determine, for which scientific questions this remote-sensing data is of value, and to develop applications and the integration of water remote-sensing products for the benefit of the broader scientific community.

REFERENCES

1979, Atlas of World Water Balance, Gidrometeorizdat: Leningrad, UNESCO.

1993, Baikal Atlas, in Galazy, G.I., ed.: Moscov, Federal Agency for Geodesy and Cartography.

Austin, R.W., 1974, The remote sensing of spectral radiance from below the ocean surface, in Jerlov, N.G., and Steemann-Neilsen, eds., Optical aspects of oceanography: London, England, Academic Press, p. 317-344.

Austin, R.W., and Halikas, G., 1976, The Index of Refraction of Seawater: La Jolla, CA, Visibility Laboratory, Scripps Institute of Oceanography, p. 64.

Babin, M., 2000, Coastal surveillance through observation of ocean colour (COASTLOOC): Villefranche-sur-mer, France, Laboratoire de Physique et Chimie Marines.

Babin, M., Morel, A., Fournier-Sicre, Fell, F., and Stramski, D., 2003, Light scattering properties of marine particles in coastal and open ocean waters as related to the particle mass concentration: Limnol. Oceanogr., v. 48, p. 843-859.

Baikal Drilling Project-96, M., 1997, Continuous paleoclimate record recovered for last 5 million years: EOS Trans., v. 78, p. 597-604.

Balin, Y.S., Ershov, A.D., and Penner, I.E., 2003, Shipborne lidar investigations of aerosol fields in the atmosphere over Lake Baikal: Atmos. Ocean. Opt., v. 16, p. 541-551.

Bangs, M., Battarbee, R.W., Flower, R.J., Jewson, D., Lees, J.A., Sturm, M., Vologina, E.G., and Mackay, A.W., 2000, Climate change in Lake Baikal: diatom evidence in an area of continuous sedimentation: Int. Journ. Earth Sciences, v. 89, p. 251-259.

Barnes, R.A., and Zalewski, E.F., 2003, Reflectance-based calibration of SeaWiFS. I. Calibration coefficients: Appl. Opt., v. 42, p. 1629-1647.

Barnes, W.L., Pagano, T.S., and Salomonson, V.V., 1998, Prelaunch characteristics of

the Moderate Resolution Imaging Spectroradiometer (MODIS) on EOS-AM1: IEEE Trans. Geosci. Remote Sens., v. 36, p. 1088-1100.

Bergmann, T., Fahnenstiel, G., Lohrenz, S., Millie, D., and Schofield, O., 2004, Impacts of recurrent resuspension event and variable phytoplankton community on remote sensing reflectance: J. Geophys. Res., v. 109.

Bézy, J.-L., Delwart, S., and Rast, M., 2000, A new generation of Ocean Colour Sensor onboard Envisat: ESA Bulletin, v. 103, p. 48-56.

Bidigare, R.R., Marra, J., Dickey, T.D., Iturriaga, R., Baker, K.S., Smith, C.S., and Pak, H., 1990, Evidence for phytoplankton succession and chromatic adaptation in the Sargasso Sea during spring 1985: Marine Ecology Progress Series, v. 60, p. 113-122.

Bidigare, R.R., Ondrusek, M.E., Morrow, J.H., and Kiefer, D.A., 1990, In vivo absorption properties of algal pigments, Ocean Optics X, Proc. SPIE Int. Soc. Opt. Eng., Volume 1302, p. 290-302.

Binding, C.E., Bowers, D.G., and Mitchelson-Jacob, E.G., 2003, An algorithm for the retrieval of suspended sediment concentrations in the Irish Sea from SeaWiFS ocean colour satellite imagery: Int. J. Remote Sens., v. 24, p. 3791-3806.

Boine, J., Olbert, C., Gläser, C., and Fischer, J., 1999, Preliminary spectral investigations of lignite open cast residual lakes in Central Germany, in Gläser, C., Will, H., and Engler, T., eds., 3th German-Dutch Symposium on Environm. Assesment and Monitoring/DGPF-working group "Interpretation von Fernerkundungsdaten": Halle, p. cDROM.

Bokoye, A.I., Royer, A., O'Neill, N.T., Fedosejevs, G., Teillet, P.M., McArthur, L.J.B., and Cliche, P., 2001, Characterization of atmospheric aerosols across Canada from a ground based sunphotometer network: AEROCAN: Atmosphere-Ocean, v. 39, p. 429-456.

Bolgrien, D.W., Granin, N.G., and Levin, L.A., 1992, Satellite observations of Lake Baikal thermal structures, Mapping a monitoring of glob. change, Volume 1: ASPRS/ACSM/RT Technical Papers, p. 11-20.

—, 1995, Surface temperature dynamics of Lake Baikal observed from AVHRR images: Photogramm. Eng. Remote Sens., v. 61, p. 211-216.

Bricaud, A., Morel, A., Babin, M., and Claustre, H., 1995, Variability in the chlorophyll-specific absorption coefficients of natural phytoplankton: Analyses and parameterization.: J.Geophys.Res., v. 100, p. 13321-1332.

Bricaud, A., Morel, A., and Prieur, L., 1981, Absorption by dissolved organic matter (yellow substance) in the UV and visible domains: Limnol. Oceanogr., v. 26, p. 43-53.

—, 1983, Optical efficiency factors of some phytoplanters: Limnol. Oceanogr., v. 28, p. 816-832.

Bricaud, A., and Stramski, D., 1990, Spectral absorption coefficients of living phytoplankton and nonalgal biogenous matter: A comparison between Peru upwelling area and the Sargasso Sea: Limnol. Oceanogr., v. 35, p. 562-582.

Budnev, N.M., Mirgazov, R.R., and Tarashchancky, B.A., 2000, Possibilities and advantages of using in hydrobiology of in situ monitoring of optical water parameters, in Semovski, S.V., ed., 5th Physical Processes in Natural Waters: Irkutsk, Russia, p. 59-62.

Buiteveld, H., Hakvoort, J.H.M., and Donze, M., 1994, The optical properties of pure water, SPIE Ocean Optics XII, Volume 2258: Bellingham, Wash., p. 174-183.

Bukata, R.P., Harris, G.P., and Bruton, J.E., 1974, The detection of suspended solids and chlorophyll a using digital multispectral ERTS-1 data, 2nd Canadian Symp. Remote Sensing: Guelph, Canada, University of Guelph, p. 551-564.

Bukata, R.P., Jerome, J., and Bruton, J.E., 1988, Relationships among Secchi disk depth, beam attenuation coefficient, and irradiance attenuation coefficient for Great Lakes waters: Journ. of Great Lakes Research, v. 14, p. 347–355.

Bukata, R.P., Jerome, J., Bruton, J.E., Jain, S.C., and Zwick, H.H., 1981, Optical water quality model of Lake Ontario: determination of the optical cross sections fo organic and inorganic particulates in Lake Ontario: Appl. Opt., v. 20, p. 1686-1703.

Bukata, R.P., Jerome, J., Kondratyev, K.Y., and Pozdnyakov, D.V., 1991, Estimation of organic and inorganic matter in inland waters: Optical cross sections of Lakes Ontario and Ladoga: J. of Great Lakes Res., v. 17, p. 461-469.

—, 1991, Optical properties and remote sensing of inland and coastal waters: J. of Great Lakes Res., v. 17, p. 461-469.

Burgess, P., 2003, Remote sensing water quality parameters in the lakes of Berlin and Brandenburg with high spatial resolution satellite sensors: Berlin, Germany, Humbold University.

Buryat Republic, 2000, Environmental report for the year 1999, (cited in Greenpeace 2003).

Carder, K.L., Gregg, W.W., Costello, D.K., Haddad, K., and Prospero, J.M., 1991, Determination of Saharan dust radiance and chlorophyll from CZCS imagery.: Journ. Geoph. Res., v. 96, p. 5369-5378.

Charlet, F., Fagel, N., De Batist, M., Hauregard, F., Minnebo, B., Meischner, D., and Team, S., 2005, Sedimentary dynamics on isolated highs in Lake Baikal: evidence from detailed high-resolution geophysical data and sediment cores: Global and Planetary Change, v. 46, p. 125-144.

Chen, C., Wang, L., Ji, R., Budd, J.W., Schwab, D.J., D., B., Fahnenstiel, G., Vanderploeg, H., Eadie, B., and Cotner, J., 2004, Impacts of suspended sediment on the ecosystem in Lake Michigan: a comparison between the 1998 and the 1999 plume events.: Journ. Geoph. Res., v. 109.

Clark, D.K., 1981, Phytoplankton algorithms for the Nimbus-7 CZCS, in Gower, J.F.R., ed., Oceanography from Space, Plenum Press, p. 227-238.

Clifford, N.J., Richards, K.S., Brown, R.A., and Lane, S.N., 1995, Laboratory and field assessment of an infrared turbidity probe and its response to particle size and variation in suspended sediment concentration: Hydrol. Sci., v. 40, p. 771-791.

Cobbold, P.R., and Davy, P., 1988, Indentation tectonics in nature and experiment. 2. Central Asia: Bulletin of the Geological Institutions of Uppsala, New Series, v. 14, p. 143-162.

Colman, S.M., Peck, J.A., Karabanov, E.B., Carter, S.J., Bradbury, J.P., King, J.W., and Williams, D.F., 1995, Continental climate response to orbital forcing from biogenic silica records in Lake Baikal: Nature, v. 378, p. 769-771.

Cox, C., and Munk, W., 1954, Measurements of the roughness of the sea surface from photographs of the sun's glitter: J.Opt.Soc.Am., v. 44, p. 838-850.

—, 1954, Statistics of the sea surface derived from sun glitter: J. Marine Res., v. 13, p. 198-227.

—, 1956, Slopes of the sea surface deduced from photgraphs of sun glitter: Bull. Scripps. Inst. Oceanograr. Univ. Calif., v. 6, p. 401-488.

Dekker, A.G., 1993, Detection of optical water parameters for eutrophic waters by high resolution remote sensing: Amsterdam, Netherlands, Vrije Universiteit Amsterdam.

Demske, D., Heumann, G., Granozewski, W., Nita, M., Mamakowa, K., Tarasov, P.E., and Oberhaensli, H., 2005, Late glacial and Holocene vegetation and regional climate variability evidenced in high-resolution pollen records from Lake Baikal: Global and Planetary Change, v. 46, p. 255-279.

Demske, D., Mohr, B., and Oberhaensli, H., 2000, Paleoclimatic changes from 3.6 to 2.2 Ma BP derived from palynological studies on Lake Baikal sediments, in Minoura, K., ed., Lake Baikal: a Mirror in Time and Space for Understanding Global Change Processes: Amsterdam, Elsevier, p. 85-89.

Deschamps, P.Y., Herman, M., and Tanre, D., 1993, Modeling of the atmospheric effects and its application to the remote sensing of ocean color: Appl. Opt., v. 22, p. 3751-3758.

Dodson, J., and Lui, T., 1995, PEPII: the Austral-Asian Transect., Plaleoclimates of the Northern and Southern Hemispheres., Volume 95: Pages Rep. Ser., p. 43-64.

Doerffer, R., and Fischer, J., 1994, Concentrations of chlorophyll, suspended matter, and gelbstoff in case II waters derived from satellite coastal zone color scanner data with inverse modeling methods: J. Geophys. Res., v. 99, p. 7457-7466.

—, 1994, Concentrations of chlorophyll, suspended matter, and gelbstoff in case II waters derived from satellite CZCS data with inverse modeling methods: J. Geophys. Res., v. 99, p. 7457-7466.

Doerffer, R., Sorensen, K., and Aiken, J., 1999, MERIS: Potential for Coastal Zone Applications. International Journal of Remote Sensing: Int. J. Remote Sens., v. 20, p. 1809-1818.

Doxaran, D., Froidefond, J.M., and Castaign, P., 2002, A reflectance band ratio used to estimate suspended matter concentrations in sediment-dominated coastal waters: Int. J. Remote Sens., v. 23, p. 5079-5085.

Effler, S.W., and Auer, M.T., 1987, Optical heterogeneity in Green Bay: Water Resources Bulletin of the Geological Institutions of Uppsala, v. 23, p. 937-941.

Eisma, D., 1986, Flocculation and deflocculation of suspended matter in estuaries: Neth. J. Sea Res., v. 20, p. 183-199.

Eisma, D., Boon, J.J., Groenewegen, R., Ittekkot, V., Kalf, J., and Mook, W.G., 1983, Observations on macro-aggregates, particle size and organic composition of suspended matter in the Ems estuary, in Degens, E.T., Kempe, S., and Soliman, H., eds., Transport of Carbon and Minerals in Major World Rivers: Mitt. Geol.-Paläont. Inst. Univ. Hamburg, p. 295-314.

Environmental Year Report Buryatia, 2001, Quality of the environment and situation of the natural resources: Ulan-Ude, Ministry of Natural Resources of the Buryat Republic (cited in Greenpeace, 2003).

ESA Scientific Campaign Unit, 1999, Explotation of CHRIS data from the PROBA mission for Science and Applications. Experimenters Handbook: Estec, p. 17.

Evans, C.A., Helfert, M.R., and Helms, D.R., 1992, Ice patterns and hydro-thermal plumes, Lake Baikal, Russia: insight from Space Shuttle hand-held photography, Intern. Geosc. Rem. Sens. (IEEE): Houston, USA.

Everett, D.H., 1999, Basic principles of colloid science: London, The Royal Society of Chemistry.

Fagel, N., Thamó-Bozsò, E., and Heim, B., in press, Mineralogical signatures of Lake Baikal sediments: Sources of sediment supplies through Late Quaternary: Sedimentary Geology.

Fargion, G.S., and Mueller, J.L., 2000, Ocean Optics protocols for satellite ocean colour sensor validation, NASA Techn. Mem.: Greenbelt, Md., NASA Goddard Space Flight Cent., p. 98.

Fell, F., 1997, Validierung eines Modells zur Simulation des Strahlungstransportes in Atmosphäre und Ozean: Berlin, Germany, Freie Universitaet Berlin.

Fell, F., and Fischer, J., 2001, Numerical simulation of the light field in the atmosphere-ocean system using the matric-operator: JQSRT, v. 69, p. 351-388.

Fialkov, V.A., 1983, Currents of the Coastal Zone of Lake Baikal: Novosibirsk, 192 p.

Fietz, S., and Nicklisch, A., 2004, An HPLC analysis of the summer phytoplankton assemblage in Lake Baikal: Freshw. Biol., v. 49, p. 332-345.

Fietz, S., Sturm, M., and Nicklisch, A., 2005, Flux of lipophilic photosynthetic pigments to the surface sediments of Lake Baikal: Global and Planetary Change, p. (in print).

Figueras, D., Karnieli, A., Brenner, A., and Kaufman, Y.J., 2004, Masking turbid water in the southeastern Mediterranean Sea utilizing the SeaWiFS 510 nm spectral band: Int. J. Remote Sens., v. 25, p. 4051-4059.

Firestone, E.R., and Hooker, S.B., 1998, SeaWiFS Prelaunch, Final Cumulative Index, in Firestone, E.R., and Hooker, S.B., eds., NASA Technical Report Series, NASA Goddard Space Flight Center, p. 4-8.

Fischer, J., 1983, Fernerkundung vom Schwebstoff im Ozean: Hamburg, Deutschland, Universitaet Hamburg.

Fischer, J., and Doerffer, R., 1987, An inverse technique for remote detection of suspended matter, phytoplankton and yellow substance from CZCS measurements: Adv. Space Res., v. 7, p. 21-26.

Fischer, J., and Fell, F., 1999, The potential of chlorophyll fluorescence for the space-borne retrieval of phytoplankton in European coastal and open ocean waters, IGARSS: Hamburg, Germany.

Fischer, J., and Grassl, H., 1984, Radiative transfer in an atmosphere-ocean system: an azimuthally dependent matrix-operator approach: Appl. Opt., v. 23, p. 1032-1039.

Flower, R.J., Battarbee, R.W., Lees, J.A., Levina, O.V., Jewson, D., Mackay, A.W., Ryves, D., Sturm, M., and Vologina, E.G., 1998, ANERC-GEOPASS project on diatom deposition and sediment accumulation in Lake Baikal, Siberia: FreshwaterForum, v. 11, p. 16-29.

Froidefond, J.M., Castaign, P., and Prud'homme, R., 1999, Monitoring suspended particulate matter fluxes and patterns from the AVHRR/NOAA-11 satellite: application to the Bay of Biscay: Deep-Sea Res., v. 2, p. 2029-2055.

Froidefond, J.M., Lavender, S., Laborde, P., Herbland, A., and Lafon, V., 2002, SeaWiFS data interpretation in a coastal area in the bay of Biscay: Int. J. Remote Sens., v. 23, p. 881-904.

Frouin, R.M., Schwindling, M., and Deschamps, P.Y., 1996, Spectral reflectance of sea foam in the visibe and near infrared: In situ measuements and remote sensing implications: J.Geophys.Res., v. 101, p. 361-371.

Gege, P., 2004, The water color simulator WASI: an integrating software tool for analysis and simulation of optical in situ spectra: Comput. Geosci., v. 30, p. 523-532.

Genkai-Kato, M., Sekino, T., Yoshida, T., Miyasaka, H., Khoszher, T., Belykh, O., Melnik, N., Kawabata, Z., Higashi, M., and Nakanishi, M., 2002, Nutritional diagnosis of phytoplankton in Lake Baikal: Ecological Research, v. 17, p. 135-142.

George, D.M., and Malthus, T.J., 2001, Using a compact airborne spectrographic imager to monitor phytoplankton biomass in a series of lakes in North Wales: Sci. Total Environ., v. 268, p. 215-226.

Gervais, F., and Behrendt, H., 2003, Primary productivity in a polymictic lake - temporal dynamics, controlling factors and trophic state: International Review of Hydrobiology, v. 88, p. 16-33.

Gippel, C.J., 1988, The effect of water colour, particle size and particle composition on stream water turbidity measurements, Departm. Geography and Oceanography, University College, Australian Defense Force Academy.

Gitel'zon, I.I., Granin, N.G., Levin, L.A., and Zavoruev, V.V., 1991, Mechanisms underlying the formation and maintenance of the spatial distribution nonuniformities of the phytoplankton in Lake Baikal: Hydrobiol. J., v. 318, p. 317-320.

Gitelson, A., Mayo, M., Yacobi, Y.Z., Parparov, A., and Berman, T., 1994, Development and validation of the optical model for remote detection of chlorophyll in the Southeastern Mediterranean from CZCS data, 2nd Remote Sens. Mar. Coast. Environ., Volume 293-303: New Orleans, USA, Environmental REsearch Institute of Michigan, USA.

Gohin, F., Druon, J.N., and Lampert, L., 2002, A five channel chlorophyll concentration algorithm applied to SeaWiFS data processed by SeaDAS in coastal waters: Int. J. Remote Sens., v. 23, p. 1639-1661.

Goldman, C.R., 1993, The conservation of two large lakes: Tahoe and Baikal: Verh. Internat. Verein. Limnol., v. 25, p. 388-391.

Goldman, C.R., Elser, J.J., Richards, R.S., Priscu, J.C., and Levin, L.A., 1996, Thermal stratification, nutrient dynamics, and phytoplankton productivity during the onset of spring phytoplankton growth in Lake Baikal, Russia: Hydrobiologia, v. 331, p. 9-24.

Gordon, H.R., 1985, Ship perturbation of irradiance measurements at sea part 1: Monte Carlo simulations: Appl. Opt., v. 24, p. 4172-4182.

—, 1997, Atmospheric Correction of Ocean Color Imagery in the Earth Observing System Era: Journ. Geoph. Res., v. 102, p. 17081-17106.

Gordon, H.R., and Brown, O.B., 1973, Irradiance Reflectivity of a Flat Ocean as a Function of Its Optical Properties: Appl. Opt., v. 12, p. 1549-1551.

Gordon, H.R., Brown, O.B., and Evans, R.H., 1988, Exact Rayleigh scattering calculations for use woth the Nimbus-7 Coastal Zone Color Scanner: Applied Optics, v. 7, p. 862-871.

Gordon, H.R., Brown, O.B., Evans, R.H., Brown, J.W., Smith, R.C., Baker, K.S., and Clark, D.K., 1988, A semi-analytical radiance model of ocean color: J. Geophys. Res., v. 93, p. 10909-10924.

Gordon, H.R., and Ding, K., 1992, Self-shading of in-water optical instruments: Limnol. Oceanogr., v. 37, p. 491-500.

Gordon, H.R., and McCluney, W.R., 1975, Estimation of the depth of sunlight penetration in the sea for remote sensing: Appl. Opt., v. 14, p. 413-416.

Gordon, H.R., and Morel, A.Y., 1983, Remote Assessment of ocean color for interpretation of satellite visible imagery, Lecture Notes in Coastal and Estuarine Studies: New York, Springer.

Gordon, H.R., and Wang, M., 1992, Surface-roughness considerations for atmospheric correction of ocean color sensors. I: The Rayleigh-scattering component: Appl. Opt., v. 31, p. 4247-4260.

—, 1994, Influence of oceanic whitecaps on atmospheric correction of ocean-color sensor: Appl. Opt., v. 33, p. 7754-7763.

—, 1994, Retrieval of water-leaving radiance and aerosol optical thickness over the oceans with SeaWiFS: a preliminary algorithm: Appl. Opt., v. 33, p. 443-452.

Grachev, M.A., Vorobyova, S.S., Likhoshway, Y.V., Goldberg, E.L., Ziborova, G.A., Levina, O.V., and Khlystov, O.M., 1998, A high-resolution diatom record of the paleoclimates of East Siberia for the last 2.5 My from Lake Baikal: Quat. Sci. Rev., v. 17.

Granina, L.Z., Karabanov, E.B., Shimaraeva, M.K., Williams, D.F., and Kuptsov, V.M., 1992, Biogenic silica of Baikal bottom sediments used for palaeo reconstruction: Int. Proj. Palaeolimnol. Late Cenozoic Clim. Newsl., v. 6, p. 53-59.

Granozewski, W., Demske, D., Nita, M., Heumann, G., and Andreev, A.A., 2005, Vegetation and climate variability during the Last Interglacial evidenced in the pollen record from Lake Baikal.: Global and Planetary Change, v. 46, p. 187-198.

Great Lakes Water Quality Board, 1989, Report on Great Lakes Water Quality, International Joint Commission (IJC).

Greenpeace, 2003, The environmental situation of Lake Baikal, Greenpeace Executive Summary, p. 118.

Gregg, W.W., and Conkright, M.E., 2001, Decadal changes in global ocean chlorophyll: Geophys. Research Letters, v. 29, p. 14-15.

Gregg, W.W., and Woodward, R.H., 1998, Improvements in high frequency ocean color observations: Combining data from SeaWiFS and MODIS: IEEE Trans. Geosci. Remote Sens., v. 36, p. 1350-1353.

Haltrin, V.I., and Kattawar, G., 1991, Light fields with Raman scattering and fluorescence in sea water, Tech. Report, Texas A&M Univ., Dept. of Physics, p. 74.

Harris, G.P., Feldman, G.C., and F.B., G., 1993, Global Oceanic Production and Climate Change, in Barale, V., and Schlittenhardt, P.M., eds., Ocean Colour: Theory and Applications in a Decade of CZCS Experience, Kluwer Academic Publishers, p. 237-270.

Hedges, J.I., 1977, The association of organic molecules with clay minerals in aqueous solutions.: Geochim. Cosmochim. Acta 41, p. 1119-1123.

Heege, T., 2000, Flugzeuggestützte Fernerkundung von Wasserinhaltsstoffen am Bodensee [DLR Research Report thesis]: Berlin, Germany, Free University of Berlin.

Heege, T., and Fischer, J., 2004, Mapping of water constituents in Lake Constance using multispectral airborne scanner data and a physically based processing scheme: Can. J. Remote Sens., v. 30, p. 77-86.

Heim, B., Braune, S., Schneider, S., Klump, J., Swiercz, S., and Dachnowsky, G.T., 2003, Der Einsatz von GIS bei der Untersuchung von Sedimenteintrag in den Baikalsee und die Online-Darstellung der Ergebnisse, in Strobl, J., Blaschke, T., and Griesebner, G., eds., Angewandte Geographische Informationsverarbeitung XV: Salzburg, Wichmann, p. 135-140.

Heim, B., Magnussen, S., Oberhaensli, H., and Kaufmann, H., 2004, Case 2 Lake Baikal: analyses of SeaWiFS data within the scope of the paleoclimate project CONTINENT: EARSEL eProceedings, v. 3, p. 127-135.

Heim, B., Oberhaensli, H., Fietz, S., and Kaufmann, H., 2005, Variation in Lake Baikal's phytoplankton distribution and fluvial input assessed by SeaWiFS satellite data: Global and Planetary Change, v. 46, p. 9-27.

Heim, B., Oberhaensli, H., and Kaufmann, H., 2002, A study on Lake Baikal (Siberia, Russia) with seaWiFS satellite data, shipborne optical measurements and field data of pigments and suspended matter, 7th Intern. Conference on Remote Sensing for Marine and Coastal Environments: Miami, USA, p. CDROM.

—, 2003, Recent remote sensing SeaWiFS data reveal the dynamics of water constituents in Lake Baikal (Siberia) within the scope of the international paleoclimate project CONTINENT, in Mischke, S., Wuennemann, B., and Riedel, F., eds., Intern. Symp. Environmental Change in Central Asia: climate, geodynamics, evolution, human impact, Volume 2: Berlin, Berliner Paläobiologische Abhandlungen, p. 41-43.

Hoepffner, N., and Sathyendranath, S., 1991, Effect of pigment composition on absorption properties of phytoplankton: Mar. Ecol. Prog. Ser., v. 73, p. 11-23.

Hohmann, R., Kipfer, R., Peeters, F., Piepke, G., Imboden, D.M., and Shimaraev, M.N., 1997, Deep-water renewal in Lake Baikal: Limnol. Oceanogr., v. 42, p. 841-855.

Holden, C., 2001, The perfect dust storm: Science, v. 294, p. 2469.

Hoogenboom, H.J., Dekker, A.G., and Althuis, I.J.H., 1998, Simulation of AVIRIS sensivity for detecting chlorophyll over coastal and inland waters: Remote Sens. Environm., v. 65, p. 333-340.

Hutchinson, D.R., Golmshtok, A.J., Zonenshain, L.P., Morre, T.C., Scholz, C.A., and Klitgord, K.D., 1992, Depositional and tectonic framework of the rift basins of Lake Baikal from multichannel seismic data: Geology, v. 20, p. 589-600.

Iluz, D., Yacobi, Y.Z., and Gitelzon, A., 2003, Adaption of an algorithm for chlorophyll-a estimation by optical data in the oligotrophic Gulf of Eilat: Int. J. Remote Sens., v. 24, p. 1157-1163.

Imberger, J., 1998, Physical Processes in Lakes and Oceans, 661 p.

Jansin, A.L., Zajcev, I.S., Kovalenko, V.I., Juvsandanzan, B., Lusickiy, I.V., and Jarmolyuk, V.V., 1989., Map of geological formations of Mongolia 1: 2 000 000, Geological Ministry of CCCP (in Russian).

Jerlov, N.G., 1978, A transparency-meter for ocean water: Tellus, v. 9, p. 229-233.

Jørgensen, P.V., 2000, Interpretation of remote sensing ocean color om Danish coastal waters: Copenhagen, Danmark, Univ. Copenhagen.

—, 2004, SeaWiFS data analysis and match-ups with in situ chlorophyll concentrations in Danish waters: Int. J. Remote Sens., v. 25, p. 1397-1402.

Kabanov, M.V., and Sakerin, S.M., 1996, Variations of the atmospheric aerosol optical depth in the Tomsk region for several seasons during the period 1992-1995: Optics of the Atmosphere and Ocean, v. 9, p. 727-736.

Kahru, M., and Mitchell, B.G., 1999, Empirical chlorophyll algorithm and preliminary SeaWiFS validation for the California current: Int. J. Remote Sens., v. 20, p. 3423-3429.

Kalinin, V.A., and Moiseeva, E.G., 1981, Petrological map of of geological formations of CCCP 1:10 000 000, Geological Ministry of CCCP (in Russian).

Kalle, K., 1937, Meereskundliche chemische Untersuchungen mit Hilfe des Zeisschen Pulfrich Photometers: Ann. Hydrogr. Berlin, v. 65, p. 276-282.

—, 1949, Fluoreszenz und Gelbstoff im Bottnischen und Finnischem Meerbusen: Dt. Hydrogr. Z., v. 2, p. 117-124.

Kallio, K., Kutser, T., Hannonen, T., Koponen, S., Pulliainen, J., Vepsäläinen, J., and Pyhälahti, T., 2001, Retrival of water quality variables from airborne spectrometry of various lake types in different seasons: Sci. Total Environ., v. 268, p. 59-77.

Kamp, U., Olbert, C., Schaale, M., and Fischer, J., 1997, Umweltmonitoring durch flugzeuggestützte Fernerkundung und neuronale Netze: Geodynamik, v. 18, p. 41-60.

Karabanov, E.B., Propenko, A.A., Williams, D.F., and Khursevich, G.K., 2000, A new record of Holocene climate change from the bottom sediments of Lake Baikal: Palaeogeogr. Palaeoclimatol. Palaeoecol., v. 156, p. 211-224.

Keller, P., 2001, Imaging spectroscopy of lake water quality parameters: Remote Sensing Series, v. 36.

Kieber, R.J., Zhou, X., and Mopper, K., 1990, Formation of carbonyl compounds from UV-induced photodegradation of humic substances in natural waters: Fate of riverine carbon in the sea: Limnol. Oceanogr., v. 35, p. 1503-1515.

Kiefer, D.A., and Mitchell, B.G., 1983, A simple, steady state description of phytoplankton growth based on absorption cross section and quantum efficiency: Limnol. Oceanogr., v. 28, p. 770–776.

Kirk, J.T.O., 1976, Yellow substance (gelbstoff) and its contribution to the attenuation of the photosynthetically active radiation in some inland and coastal South-Eastern Australian waters: Aust. J. Mar. Freshw. Res., v. 27, p. 61-71.

—, 1981, Monte Carlo study of the nature of the underwater light field in, and the relationships between, optical properties of turbid yellow waters: Australian journal of marine and freshwater research, v. 32, p. 517-532.

—, 1983, Light and photosynthesis in aquatic ecosystems: Cambridge, Cambridge University Press, 210 p.

Klemas, V., Otley, M., Philpot, W., White, C., Rogers, R., and Shah, N., 1974, Correlation of coastal water turbidity and current circulation with ERTS-1 and skylab imagery, 9th Int. Symp.

Remote Sens. Environ.: Ann Arbor, USA, Environmental Research Institute of Michigan, USA, p. 1289-1317.

Kloiber, S.M., Brezonik, P.L., Olmanson, L.G., and Bauer, M.E., 2002, A procedure for regional lake water clarity assessment using Landsat and multispectral data: Remote Sens. Environm., v. 82, p. 38-47.

Klump, J., and Schneider, S., 2004, Anwendung von GIS für den Vergleich der regionalen Vegetation mit der Verteilung von Pollen im Baikalsee, in Strobl, J., Blaschke, T., and Griesebner, G., eds., Angewandte Geographische Informationsverarbeitung XVI: Salzburg, Wichmann, p. 354-358.

Knobelspiesse, K., Green, S., and Vodacek, A., 2000, Atmospheric compensation for SeaWiFS images of Lake Superior utilizing spatial information, 2000 Ocean Science Meeting: San Antonio, USA.

Kohl, J.-G., and Nicklisch, A., 1988, Ökophysiologie der Algen: Wachstum und Ressourcennutzung: Berlin, Germany, Akademie-Verlag Berlin, 251 p.

Koponen, S., Pulliainen, J., Kallio, K., and Hallikainen, M., 2002, Lake water quality classification with airborne hyperspectral spectrometer and simulated MERIS data: Remote Sens. Environm., v. 79, p. 51-59.

Kouraev, A.V., Semovski, S.V. , Shimaraev, M.N., Mognard, N.M., Legresy, B., Remy, F., submitted, Observations of lake Baikal ice from satellite altimetry and radiometry. Remote Sens. Environm.

Koutzenogii, K.P., 1996, Monitoring of atmospheric aerosols in Siberia: Optics of the Atmosphere and Ocean, v. 9, p. 704-711.

Kozhov, M., 1963, Lake Baikal and its life: The Hague, Dr. W. Junk Publishers, 344 p.

Kozhova, O.M., and Izmesteva, L.R., 1998, Lake Baikal: Evolution and Biodiversity: Leiden, Backhuys, 447 p.

Kratzer, S., Hakansson, B., and Sahlin, C., 2003, Assessing Secchi and photic zone depth in the Baltic Sea from satellite data: AMBIO, v. 32, p. 577-585.

Krawczyk, H., Neumann, A., and Walzel, T., 1996, Application of a new remote sensing multispectral interpretation algorithm for water constituents in the Baltic Sea, Ocean Optics XIII: Halifax, Canada.

Kudela, R.M., and Chavez, F.P., 2004, The impact of coastal runoff on ocean color during an El Niño year in central California: Deep-Sea Research II.

Lawrence, S.P., Hogeboom, K., and le Core, H., 2002, A three-dimensional general circulation model of the surface layers of Lake Baikal: Hydrobiologia, v. 487, p. 95-110.

Leshkevich, G. A., Nghiem, S. V., 2005, Satellite SAR remote sensing of freshwater ice cover, 48th International Association for Great Lakes Research: Ann Arbor, USA.

Lillesand, T.M., Johnson, W.L., Duell, R.L., Lindstrom, O.M., and Meisner, D.E., 1983, Use of Landsat data to predict the trophic state of Minnesota lakes: Photogramm. Eng. Remote Sens., v. 49, p. 219-229.

Logachev, N.A., 1993, History and geodynamics of the Lake Baikal Rift in the context of the Eastern Siberia Rift System: a review: Tectonophysics, v. 14, p. 225-234.

Lydolph, P.-E., 1977, Climates of the Soviet Union. World Survey of Climatology: Amsterdam, Oxford, New York.

Mac, V.D., Ufimtsev, G.T., and Mandelbaum, M.M., 2001, Architecture and geological history of Cenozoic Baikal rift.: Novosibirsk (in Russian).

Mackay, A.W., Flower, R.J., Kuzmina, A.E., Granina, L.Z., Rose, N.L., Appleby, P.G., Boyle, J.F., and Battarbee, R.W., 1998, Diatom succession trends in recent sediments from Laake Baikal and relationship to atmospheric pollution and to climate change: Philos. Trans. R. Soc. London, v. 353, p. 1011-1055.

Makarewicz, J.C., and Bertram, P., 1993, Evidence for the the Lake Erie ecosystem: Bio Science, v. 41, p. 216-223.

Malcolm, R.L., 1985, Geochemistry of stream fulvic and humic substances, in Aiken, G.R., ed., Humic Substances in Soil, Sediment and Water: New York, p. 181-209.

Mannheim, S., Segl, K., Heim, B., and Kaufmann, H., 2004, Monitoriing of the trophic parameter Chl-a using hyperspectral CHRIS-PROBA data., SPIE, p. 196-203.

—, 2004, Monitoring of lake water quality using hyperspectral CHRIS-PROBA data, 2nd ESA CHRIS/PROBA Workshop: Frascati, Italy.

Matthias-Maser, S., and Obolkin, V., 2000, Seasonal variation of primary biological aerosol particles in the remote continental region of Lake Baikal/ Siberia: Atmos. Environ., v. 34, p. 3805-3811.

Mayo, M., Gitelson, A., Yacobi, Y.Z., and Ben-Avraham, Z., 1995, Chlorophyll distribution in Lake Kinneret determined from LANDSAT Thematic Mapper data: Int. J. Remote Sens., v. 16, p. 175-182.

McCave, I.N., 1984, Size spectra and aggregation of suspended particles in the deep ocean: Deep-Sea Res., v. 31, p. 329-352.

McClain, C.R., Barnes, R.A., Eplee Jr., R.E., Franz, B.A., Hsu, N.C., Patt, F.S., Pietras, C.M., Robinson, W.D., Schieber, B.D., Schmidt, G.M., Wang, M., Bailey, S.W., and Werdell, P.J., 2000, SeaWiFS Post Launch Calibration and Validation Analyses: Part 2, in Hooker, S.B., and Firestone, E.R., eds., NASA Techn. Memo, NASA Goddard Space Flight Center, p. 57.

Mertes, L.A.K., and Warrick, J.A., 2001, Measuring flood output from 110 coastal watersheds in California with field measurements and SeaWiFS: Geology, v. 29, p. 659-662.

Mitchelson-Jacob, E.G., 1999, Utilization of satellite ocean colour data for military applications: retrieval of suspended particulate matter concentrations from ocean colour imagery, Unit for Coastal and Estuarine Studies.

Mobley, C.D., 1999, Estimation of the remote-sensing reflectance from above-surface measurements: Appl. Opt., v. 38, p. 7442–7455.

Mobley, C.D., and Sunfman, L.K., 2001, Hydrolight 4.2 Users' Guide: Redmond, WA, Sequoia Scientific, p. 87.

Mogilev, N.Y., and Semovski, S.V., 1999, Studies of Lake Baikal snow cover dynamics using multispectral images AVHRR: Geograph. Nat. Res., v. 4, p. 90-93.

Moore, G.F., Aiken, J., and Lavender, S., 1999, The atmospheric correction of water colour and the quantitative retrieval of suspended particulate matter in case II waters: application to MERIS: Int. J. Remote Sens., v. 20, p. 1713-1733.

Moore, K.D., Voss, K.J., and Gordon, H.R., 2000, Spectral reflectance of whitecaps: Their contribution to water-leaving radiance: J.Geophys.Res., v. 105, p. 6493-6499.

Morel, A., 1974, Optical properties of pure water and pure seawater: London, Academic Press, 1-24 p.

—, 1987, Chlorophyll-specific scattering coefficient of phytoplankton. A simplified theoretical approach: Deep-Sea Res., v. 34, p. 1093-1105.

—, 1988, Optical Modeling of the upper ocean in relation to its biogenous matter content (case 1 waters): J. Geophys. Res., v. 93, p. 10749-10768.

Morel, A., and Ahn, Y.H., 1990, Optical efficiency factors of free living marine bacteria: influence of bacterioplankton upon the optical properties and particulate organic carbon in oceanic waters: J. of Marine Res., v. 48, p. 145-175.

Morel, A., Ahn, Y.H., Partensky, F., Vaulot, D., and Claustre, H., 1993, Prochlorococcus and Synechococcus: a comparative study of their optical properties in relation to their size and pigmentation: Journal of Marine Research, v. 51, p. 617-649.

Morel, A., and B., G., 1993, Diffuse reflectance of oceanic waters. II. Bidirectional aspects: Appl. Opt., v. 32, p. 6864-6879.

Morel, A., and Bricaud, A., 1981, Theoretical results concerning light absorption in a discrete medium, and application to specific absorption of phytoplankton: Deep-Sea Research, v. 28, p. 1375-1393.

Morel, A., and Maritorena, S., 2001, Bio-optical properties of oceanic waters: a reappraisal: J.Geophys.Res., v. 106, p. 7163-7180.

Morel, A., and Mueller, J.L., 2002, Normalized water-leaving radiance and remote sensing reflectance: Bidirectional reflectance and other factors, in Mueller, J.L., and Fargion, G.S., eds., Ocean optics protocols for satellite ocean color sensor validation, p. 183-210.

Morel, A., and Prieur, L., 1977, Analysis of Variations in Ocean Color: Limnol. Oceanogr., v. 22, p. 709-722.

Morel, A.Y., 1980, In-water and remote measurements of ocean colour: Boundary-Layer Meteorol., v. 18, p. 177-201.

Morel, A.Y., and Gordon, H.R., 1980, Report of the working group on water colour: Boundary-Layer Meteorol., v. 18, p. 343-355.

Mueller, J.L., and Austin, R.W., 1995, Ocean Optics Protocols for SeaWiFS Validation, Revision 1, NASA TM, NASA, p. 25.

Müller, J.L., and Austin, R.W., 1992, Ocean Optic Protocols for Satellite Ocean Colour Sensor Validation, in NASA, ed., Sensor Intercomparison and Merger for Biological and Interdisciplinary Ocean Studies (SIMBIOS) Project Technical Memoranda, p. 45.

Müller, J.L., and Fargion, G.S., 2002, Ocean Optic Protocols for Satellite Ocean Colour Sensor Validation, in NASA, ed., Sensor Intercomparison and Merger for Biological and Interdisciplinary Ocean Studies (SIMBIOS) Project Technical Memoranda, p. 308.

Munday, J.C., 1974, Water quality for lakes of Southern Ontario from ERTS-1, 2nd Canadian Symposium in Remote Sensing: Guelph, Canada, University of Guelph, p. 77-85.

Munday, J.C., and Alfoeldi, T.T., 1979, LANDSAT test of diffuse reflectance models for aquatic suspended solids measurements: Remote Sens. Environm., v. 8, p. 169-183.

National Air Quality and Emissions Trends Report, 2003, Impact of April 2001 Asian Dust Event on Particulate Matter Concentrations in the United States, 2003 Special Studies, U.S. Environmental Protection Agency, Office of Air Quality Planning and Standards, p. 1-12.

Neumann, A., Krawczyk, H., and Walzel, T., 1995, A complex approach to quantitative interpretation of spectral high resolution imagery, 3rd Remote Sens. Marine and Coastal Environm., Volume II: Seattle, USA, p. 641-652.

Nghiem, S. V., Leshkevich, G. A., 2003, Great Lakes Winter Experiment 2002 (GLAWEX 2002). Synthetic aperture radar applications to ice-covered lakes and rivers. JPL D-26226, NASA.

Novo, E.M.M., Handom, J.D., and Curran, P.J., 1989, The effect of sediment type on the relationship between reflectance and suspended matter concentration: Int. J. Remote Sens., v. 10, p. 1283-1289.

O'Reilly, J.E., and al, e., 2000, SeaWiFS Post Launch Calibration and Validation Analyses: Part 3, NASA Techn. Memo., NASA Goddard Space Flight Center.

O'Reilly, J.E., Maritorena, S., Mitchell, B.G., Siegel, D.A., Carder, K.L., Garver, S.A., Kahru, M., and McClain, C.R., 1998, Ocean colour chlorophyll algorithms for SeaWiFS: J. Geophys. Res., v. 103, p. 24937-24953.

Ocean Optics, 2000, Ocean Optic Protocols for Satellite Ocean Colour Sensor Validation, in NASA, ed., Sensor Intercomparison and Merger for Biological and Interdisciplinary Ocean Studies (SIMBIOS) Project Technical Memoranda.

—, 2001, Ocean Optic Protocols for Satellite Ocean Colour Sensor Validation, in NASA, ed., Sensor Intercomparison and Merger for Biological and Interdisciplinary Ocean Studies (SIMBIOS) Project Technical Memoranda.

Olbert, C., 1999, Bestimmung räumlicher Verteilungsmuster von Wasserinhaltsstoffen in ausgewählten Berliner und Brandenburger Gewässern mit Methoden der Fernerkundung: Berlin, Germany, Freie Universitaet Berlin.

Packman, J.J., Comings, K.J., and Booth, D.B., 1999, Using turbidity to determine total suspended solids in urbanizing streams in the Puget Lowlands, Can. Water. Resour. Assoc.: Vancouver, Canada, p. 158-165.

Panchenko, M.V., Terpugova, S.A., and Tumakov, A.G., 1996, Seasonal factors of the variability of submicron aerosol characteristics: Atmos. Res., v. 41, p. 203-215.

Petelina, S.V., 1998, Optical model of atmospheric aerosols in Russian Siberia for correction of satellite data, IIASA Interim Report, International Institute for Applied Systen Analysis, p. 37.

Peters, S.W.M., Dekker, A.G., Pasterkamp, R., and Woerd, H.v.d., 1999, Demonstration of Ocean Colour satellites, various aspects of TSM determinations using ocean colour satellite imagery.

Petzold, T.J., 1972, Volumen scattering functions for selected ocean waters, Light in the sea: La Jolla, Scripps Inst. Oceanogr., p. 72-97.

Pope, R., and Fry, S.E., 1997, Absorption spectrum (380-700) of pure water: II. Integrating cavity measurements: Appl. Opt., v. 36, p. 8710-8722.

Popovskaya, G.I., 2000, Ecological monitoring of phytoplankton in Lake Baikal: Aquat. Ecosyst. Health Manag., v. 3, p. 215-225.

Pozdnyakov, D., Petterson, L., Johanessen, O.M., Liaskovski, A., Filatov, N., and Bobylev, L., 2003, SeaWiFS maps water quality parameters of the White Sea: Int. J. Remote Sens., v. 24, p. 4065-4071.

Preisendorfer, R.W., 1961, Application of radiative transfer theory to light measurements in the sea: Monogr. Int. Union Geod. Geophys., v. 10, p. 11-30.

Prieur, L., and Sathyendranath, S., 1981, An optical classification of coastal and oceanic waters based on the specific apbsorption curves of phytoplankton pigments, dissolvd organic matter, and other particulate materials: Limnol. Oceanogr., v. 26, p. 671-689.

Propenko, A.A., Williams, D.F., Karabanov, E.B., and Khursevich, G.K., 1999, Response of Lake Baikal ecosystem to climate forcing and pCO2 change over the last glacial/interglacial transition: Earth Planet. Sci. Lett., v. 172, p. 239-253.

Rast, M., and Bezy, J.L., 1999, The MERIS instrument: Int. J. Remote Sens., v. 20, p. 1681-702.

Rengasamy, P., 1987, Soil Structure and Aggregate Stability.

Rioual, P., and Mackay, A.W., 2005, A diatom record of centennial resolution for the Kazanetsevo Interglacial stage in Lake Baikal (Siberia): Global and Planetary Change, p. (in print).

Ritchie, J.C., Cooper, C.M., and Schiebe, F.R., 1990, The relationship of MSS and TM digital data with suspended sediments, chlorophyll, and tempreature in Moon Lake, Mississippi: Remote Sens. Environm., v. 33, p. 137-148.

Roesler, C.S., Perry, M.J., and Carder, K.L., 1989, Modeling in situ phytoplankton absorption from total absorption spectra in productive inland marine waters: Limnol. Oceanogr., v. 34, p. 1510-1523.

Ruddick, K.G., Ovidio, F., and Rijkebore, M., 2000, Atmospheric correction of SeaWiFS imagery for turbid coastal and inland waters: Applied Iotics, v. 39, p. 897-912.

Russel, M., and Rosell-Melé, A., 2005, Preliminary study of fluxes of major lipid biomarker classes in the water column and sediments of Lake Baikal, Russia: Global and Planetary Change, v. 46, p. 45-56.

Russian Governmental Comission, 1999, Annual report of the governmental commission on Baikal Lake 1998, Lake preservation and efficient natural resources mangement in the Baikal region: Moscow (cited in Greenpeace, 2003).

Sathyendranath, S., Lazzara, L., and Prieur, L., 1987, Variations in the spectral values of specific absorption of phytoplankton: Limnol. Oceanogr., v. 32, p. 403-415.

Sauberer, F., 1962, Empfehlungen für die Durchführung von Strahlungsmessungen an und in Gewässern, 77 p.

Scheffer, F., and Schachtschnabel, P., 1992, Lehrbuch der Bodenkunde: Stuttgart, Enke.

Schiller, H., and Doerffer, R., 1999, Neutral network of emulation of an inverse model-operational derivation of Case II water properties from MERIS data: Int. J. Remote Sens., v. 20, p. 1735-1746.

Scholz, C.A., Klitgord, K.D., Hutchinson, D.R., Ten Brink, U.S.T., Zonenshain, L.P., Golmshtok, A.J., and Moore, T.C., 1993, Results of 1992 seismic reflection experiment in Lake Baikal: Am. Geophys. Union, v. 74, p. 465-470.

Schroeder, T., and Fischer, J., 2003, Atmospherric correction of MERIS imagery above case-2 waters, ESA/ESRIN MERIS User Workshop: Frascati, Italy.

Schroeder, T., Schaale, M., Fell, F., and Fischer, J., 2002, Atmospherric correction algorithm for satellite data over case-1 waters, 7th Intern. Conference on Remote Sensing for Marine and Coastal Environments: Florida, USA.

Schwarz, J.N., Kowalczuk, P., Kaczmarek, S., Cota, G.F., Mitchell, B.G., Kahru, M., Chavez, F.P., Cunningham, A., McKee, D., Gege, P., Kishino, M., Phinney, D., and Raine, R., 2002, Two models for absorption by coloured dissolved organic matter (CDOM): Oceanologia, v. 44, p. 209-241.

SCOR-UNESCO, 1964, Determination of photosynthetic pigments, Report of Working Group 17: Paris, UNESCO.

Segl, K., 1998, Klassifizierung mit neuronalen Netzen, in Baehr, H.-P., and Vögtle, T., eds., Digitale Bildverarbeitung: Anwendung in Photogrammetrie, Kartographie und Fernerkundung: Karlsruhe, Wichmann, p. 186-219.

Seinfeld, J.H., Carmichael, G.R., Arimoto, R., Conant, W.C., Brechtel, F.J., Bates, T.S., Cahill, T.A., Clarke, S.J., Doherty, P.J., Flatau, J., Huebert, B.J., Kim, J., Markowicz, K.M., Quinn, P.K., Russel, L.M., Russel, P.B., Shimizu, A., Shinozuka, Y., Song, C.H., Tang, Y.H., Uno, I., Vogelmann, A.M., Weber, R.J., Woo, J.H., and Zhang, X.Y., 2004, ACE-ASIA: Regional Climatic and Atmospheric Chemical Effects of Asian Dust and Pollution: Bulletin of the American Meteorological Society, v. 85, p. 367-380.

Selenga Conference Reports, 2002, Selenga - river without borders: Ulan-Ude (cited in Greenpeace, 2003).

Semovski, S.V., 1999, The Baltic Sea and Lake Baikal underwater bio-optical fields simulation using ecodynamical model: Ecol. Model., v. 116, p. 149-163.

—, 1999, Water Ecosystems: from satellite observations to mathematic modelling: Irkutsk, Russian Academic Press, 199 p.

Semovski, S.V., Mogilev, N.Y., and Sherstyankin, P.P., 2000, Lake Baikal ice: analysis of AVHRR imagery and simulation of under-ice phytoplankton bloom: J Mar. Syst., v. 27, p. 117-130.

Semovski, S.V., Popovskaya, G.I., Belyk, O., and Sherstyankin, P.P., 2000, Impact of taxonomic composition of phytoplankton on the formation of hydrooptical fields, in Semovski, S.V., ed., 5th Physical Processes in Natural Waters: Irkutsk, Russia, p. 72-75.

Semovski, S.V., Shimaraev, M.N., Minko, N.P., and Gnatovsky, R.Y., 1998, Lake Baikal fronts and currents analyses studies using IR AVHRR imagery: Earth. Stud. Space 5, v. 5, p. 65-75.

—, 2001, Use of satellite observations to study thermal fronts of Lake Baikal: Earth Obs. Remote Sens., v. 16, p. 773-787.

Semovski, S.V., Shimaraev, M.N., Mogilev, N.Y., Alpers, W., and Schrum, C., 1999, Lake Baikal physical features studies using satellite remote sensing, in Geoscience and Remote Sensing Society, U., ed., Intern. Geosc. Rem. Sens, Sympos. (IGARSS): Hamburg, Germany, p. 888-890.

Senesi, N., and Miaono, T.M., 1994, Humic substances in the global environment, Elsevier.

Sergeyev, M., 1989, The Wonders and Problems of Lake Baikal: Moscow, Novost Press Agency Publishing House, 76 p.

Sherstyankin, P.P., 1975, Experimental investigation of the under-ice luminous field of Lake Baikal: Moscow, Nauka, 91 p.

Shettle, E.P., and Fenn, R.W., 1979, Models for the aerosols of the lower atmosphere and the effects of humidity variations on their optical properties, AFGL-TR-79-0214, AFGL.

Shimaraev, M.N., Verbolov, V.I., Granin, N.G., and Sherstyankin, P.P., 1994, Physical limnology of Lake Baikal: a review: Irkutsk and Okayama, BICER Publishers, 80 p.

SISCAL, 2004, SISCAL Algorithm Theoretical Basis Document, p. 120.

Smith, C.S., and Baker, K.J.S., 1983, The analysis of ocean optical data, 7th SPIE, Ocean Optics, Volume 478, p. 119-126.

Smith, R.C., Tyler, J.C., and Goldman, C.R., 1973, Optical properties and color of Lake Tahoe and Crater Lake: Limnol. Oceanogr., v. 18, p. 189-199.

Sogandares, F.M., and Fry, E.S., 1997, Absorption spectrum (340-640 nm) of pure water. I Photothermal measurements: Appl. Opt., v. 36, p. 8699-8709.

Solotchina, E.P., Propenko, A.A., Vasilevsky, A.N., Gavshin, V.M., Kuzmin, M.I., and Williams, D.F., 2002, Simulation of XRD patterns as an optimal technique for studying glacial and interglacial clay mineral associations in bottom sediments of Lake Baikal: Clay Miner. 37, p. 105-119.

Stramski, D., and Kiefer, D.A., 1991, Light scattering by microorganisms in the open ocean: Progress in Oceanography, v. 28, p. 343-383.

Straskrabova, V., Callieri, C., Carrillo, P., Cruz-Pizarro, L., Fott, J., Hartman, P., Macek, M., Medina-Sánchez, J.P., Nedoma, J., and Simek, K., 1999, Investigations on pelagic food webs in mountain lakes – aims and methods: J. Limnol., v. 58, p. 77-87.

Straskrabova, V., Izmest'yeva, L.R., Maksimova, E.A., Fietz, S., Nedoma, J., Borovec, J., Kobanova, G.I., Shchetinia, E.V., and Pislegina, E.V., 2005, Primary production and microbial

activity in the euphotic zone of Lake Baikal (Southern Basin) during late winter: Global and Planetary Change, v. 46, p. 57-73.

Strickland, J.D.H., and Parsons, T.R., 1972, A practical handbook of sea water analysis.

Stumpf, R.P., and Pennock, J.R., 1989, Calibration of a general optical equation for remote sensing of suspended sediments in a moderately turbid estuary.: J. Geophys. Res., v. 94, p. 14363-14371.

Stumpf, R.P., and Tyler, M.A., 1988, Satellite detection of bloom and pigment distribution in estuaries: Remote Sens. Environ.24, v. 24, p. 385-404.

Sturm, B., and Zibordi, G., 2002, Atmospheric correction of SeaWiFS data by an approximate model and vicarious calibration: Int. J. Remote Sens., v. 23, p. 489-501.

Suzuki, R., Takahashi, M., Furuya, K., and Ishimaru, T., 1993, Simplified technique for the rapid determination of phytoplankton pigments by reverse-phase high-performance liquid chromatography: Journal of Oceanography, v. 49, p. 571-580.

Swiercz, S., 2004, Charakterisierung des Baikalsee Einzugsgebietes (Sibirien) unter Anwendung von GIS-Analysen, Freie Universitaet Berlin, Germany.

Swiercz, S., Heim, B., Pekdeger, A., and Oberhaensli, H., 2003, GIS supported characterization of the Lake Baikal catchment area, in Mischke, S., Wuennemann, B., and Riedel, F., eds., Intern. Symp. Environmental Change in Central Asia: climate, geodynamics, evolution, human impact, Volume 2: Berlin, Berliner Paläobiologische Abhandlungen, p. 116-118.

Tarasova, E.A., and Mamontov, A.A., 1998, Pollution and eutrophication in Lake Baikal: Journal of Lake Science, v. 10, p. 165-178.

Tassan, S., 1994, Local algorithms using SeaWiFS data for the retrieval of phytoplankton, pigments, suspended sediment, and yellow substance in coastal waters: Appl. Opt., v. 33, p. 2369-2378.

Tassan, S., and Ferrari, G.M., 1995, An alternative approach to absorption measurements of aquatic particles retained on filters.: Limnol. Oceanogr., v. 40, p. 1358-1368.

Tassan, S., and Sturm, B., 1986, An algorithm for the retrieval of sediment content in turbid coastal waters from CZCS data: Int. J. Remote Sens., v. 7, p. 643-655.

Tessier, D., and Chenu., C., 1997, Importance of clay fabrics in soils, an approach by electron microscopy: Geologica Carpathica - Series Clays, v. 6, p. 35-45.

Theng, B.K.G., 1987, Clay-humic interactions and soil aggregate stability, in Rengasamy, P., ed., Soil Structure and Aggregate Stability, p. 32-73.

Thiemann, S., 1999, The origin of the reflectance peak near 700 nm in chlorophyll-a laden waters - an experiment, IGGARSS: Hamburg, Germany.

—, 2000, Erfassung von Wasserinhaltsstoffen und Ableitung der Trophiestufen nordbrandenburgischer Seen mit Hilfe von Fernerkundung: Germany, Ludwig-Maximilians-Universität München, GFZ Potsdam.

Thiemann, S., and Kaufmann, H., 2000, Determination of chlorophyll content and trophic state using field spectrometer and IRS-1C satellite data in the Mecklenburg Lake District, Germany: Remote Sens. Environ., v. 73, p. 227-235.

—, 2002, Lake water quality monitoring using hyperspectral airborne data - a semiempirical multisensor and multitemporal approach for the Mecklenburg lake district, Germany.: Remote Sens. Environ., v. 81, p. 228-237.

Thomson, K.P.B., and Jerome, J., 1975, In situ colour measurements on the Great Lakes, Scientific Series, Volume 51: Burlington, Ontario, Inland Waters Directorate, Environment Canada.

Toole, D.A., Siegel, D.A., Menzies, D.W., Neumann, M.J., and Smith, R.C., 2000, Remote-sensing reflectance determinations in the coastal ocean environment: impact of instrumental characteristics and environmental variability: Appl. Opt., v. 39, p. 456-469.

Tyler, J.E., 1960, Radiance distribution as a function of depth in an underwater environment.: Bull. Scripps Inst. Oceanogr., v. 7, p. 363-341.

UNESCO, 1996, Convention Concerning the Protection of the World Cultural and Natural Heritage. Report from 20th Session: Merida, Mexico.

—, 2000, Information on the environmental situation of the World heritage site "Lake Baikal" on behalf of UNESCO, Annual Reports: Moscow.

—, 2004, Properties inscribed on the World Heritage List, World Heritage Centre (WHC), p. 21.

UnitedNationsEnvironmentProgramme(UNEP), InternationalLabourOrganization(ILO), and HealthOrganization(WHO), W., 2003, Polychlorinated biphenyls: Human health aspects, Concise International Chemical Assessment Document 55: Geneva.

van Molderen, H., van Grieken, R., Khodzher, T., Obolkin, V., and Potemkin, V., 1996, Composition of individual aerosol particles above Lake Baikal, Siberia: Atmos. Environ., v. 30, p. 1453-1465.

Verbolov, V.I., Sokolnikov, V.N., and Shimaraev, M.N., 1965, Hydrometeorological Conditions and Heat Bailance of Lake Baikal, Nauka, 376 p.

Vidot, J., and Santer, R., 2003, Atmospheric correction for inland waters, 10th SPIE Remote Sens. Ocean and Sea Ice, p. 5233.

Wang, M., 1999, Atmospheric correction of ocean color sensors: Computing atmospheric diffuse transmittance: Appl. Opt., v. 38, p. 451-455.

Wang, M., and Gordon, H.R., 1994, Radiance reflected from the ocean-atmosphere system: Synthesis from individual components of the aerosol size distribution: Appl. Opt., v. 33, p. 7088-7095.

Warrington, D.S., Budd, J.W., Stumpf, R.P., and Vransibrahmanakul, V., 1999, Remote Sensing of Great Lakes Water Quality using SeaWiFS imagery, ASLO Aquatic Sciences Meeting: Santa Fe, NM, p. 187.

Wells, J.T., and Kim, S.-Y., 1989, Variability of large aggregates and their effect on the attenuation of light: field observations.

Williams, D.F., Peck, J., Karabanov, E.B., Propenko, A.A., Kravchinsky, V., and Kuzmin, M.I., 1997, Lake Baikal record of continental climate response to orbital insulation during the past 5 million years: Science, v. 278, p. 1114-1117.

Williams, S.P., Szajna, E.F., and Hovis, W.A., 1986, Nimbus 7 Coastal Zone Color Scanner (CZCS) Level 1 Data Product Users Guide, NASA Techn. Mem., NASA, p. 53.

Woitke, P., Martin, C.-D., Nicklisch, A., and Kohl, J.-G., 1994, HPLC determination of lipophilic photosynthetic pigments in algal cultures and lake water samples using a non-endcapped C18-RP-column: Fresenius J Anal Chem, v. 348, p. 762-768.

Wong, H.K., Anton, K., von Haugewitz, W., Kempe, S., and Michaelis, W., 1991, Geologische Entwicklung und das rezente Sedimentationsregime im Baikalsee, Final Report BMFT: Hamburg, p. 192.

World Meteorological Organization, 1986, A preliminary cloudless standard atmosphere for radiation calculations, World Climatic Program: Boulder, Colorado, USA, p. 112.

Wózniak, B., Dera, J., Ficek, D., Majchrowski, R., Kaczmarek, S., Ostrowska, M., and Koblentz-Mishke, O.I., 1998, Modelling the influence of photo- and chromatic- acclimation on the

absorption properties of marine phytoplankton, SPIE, Ocean Optics: Kailua-Kona, Hawaii, USA.

Wózniak, B., Dera, J., and Koblentz-Mishke, O.I., 1992, Bio-optical relationships for estimating primary production in the ocean: Oceanologia, v. 33, p. 5-38.

Yacobi, Y.Z., Alberts, J.J., Takács, M., and McElvaine, M., 2003, Absorption spectroscopy of coloured dissolved organic carbon in Georgia (USA) rivers: the impact of molecular size distribution.: Limnology, v. 62, p. 41-46.

Yentsch, C.S., 1993, CZCS: Its role in the study of the growth of oceanic phytoplankton, in Barale, V., and Schlittenhardt, P.M., eds., Ocean Colour: Theory and Applications in a Decade of CZCS Experience, Kluwer Academic Publishers, p. 17-23.

Yoder, J.A., McClain, C.R., Feldman, G.C., and Esaias, W.E., 1993, Annual cycles of phytoplankton chlorophyll concentrations in the Global Ocean: A satellite view.: Global Biogeochemical Cycles, v. 7, p. 181-193.

Yoshioka, T., Ueda, S., Khodzher, T., Bashenkhaeva, N., Korovyakova, I., and Sorokovikova, L.G., L, 2002, Distribution of dissolved organic carbon in Lake Baikal and its watershed: Limnology, v. 3, p. 159-168.

Young, A.T., 1981, On the Rayleigh-scattering optical depth of the atmosphere: J. Appl. Meteorol., v. 20, p. 328-330.

Zaneveld, J.R.V., 1982, Remotely sensed reflectance and its dependence on vertical structure: A theoretical derivation: Appl. Opt., v. 21, p. 4146-4150.

Zaneveld, J.R.V., Boss, E., and Barnard, A.H., 2001, The influence of surface waves on measured and modeled irradiance profiles: Appl. Opt., v. 40, p. 1442- 1449.

Zhang, T., Fell, F., Liu, Z.S., Preusker, R., Fischer, J., and He, M.X., 2003, Evaluating the performance of artificial neural network techniques for pigment retrieval from ocean colour in Case I waters: J. Geophys. Res., v. 108, p. 3286.

Zimmermann, G., and Neumann, A., 1997, MOS, a spaceborne imaging spectrometer for ocean remote sensing. Backscatter: Backscatter, v. 5, p. 9-13.

Zonenshain, L.P., and Savostin, L.A., 1981, Geodynamics of the Baikal Rift Zone (BRZ) and plate tectonis of Asia: Tectonophysics, v. 76, p. 1-45.

Zuev, V.V., Burlakov, V.D., and El'nikov, A.V., 1998, Ten years (1986-1995) of lidar observations of temporal and vertical structure of stratospheric aerosols over Siberia: J. Aerosol Sci., v. 29, p. 1179-1187.

ANNEX A

Table 1: Selected participating institutes, subcontractors and NAS-partners within the EU paleoclimate project CONTINENT.

Institute	Country	Code	Activities
GeoForschungsZentrum Potsdam	G	GFZ	Project management, site survey, remote sensing, retrieval of sediment cores, carbon analyses, grain size analyses, paleomagnetics, data management.
Institut für Gewässerökologie und Fischereibiologie, Berlin	G	IGB	Quantitative analysis of lipophilic photosynthetic pigments from green algae, diatoms, Cryptophycae and cyanobacteria; culture experiments on algae; sediment traps.
Humboldt-Universität zu Berlin, Institut für Biologie/AG Ökophysiologie	G	HU	Quantitative analysis of lipophilic photosynthetic pigments from green algae, diatoms, Cryptophycae and cyanobacteria; culture experiments on algae; sediment traps.
Hydrobiological Institute, Academy of Sciences of the Czech Republic, Budejovice	Czech Republic	HUB	Primary production, phytoplankton, DOC
(Subcontractor) Irkutsk State University, Scientific Research Institute of Biology, Irkutsk	RU	SRIB	Long-time monitoring (phytoplankton, Chl-*a*) at Bolshye Koti (Lake Baikal South Basin)
(Subcontractor) SB Russian Academy of Sciences, Limnological Institute, Irkutsk	RU	LIN	Operation of research vessels (RV Vereshagin and RV Titov) and local infrastructure,
(Subcontractor) Institute of Earth Crust, Irkutsk	RU		Organisation of Selenga fieldtrip
Swiss Federal Institute for Environmental Science and Technology	CH	EAWAG	Sediment traps, acoustic current meters and thermistors on moorings, retrieval of sediment trap material and data, remote sensing data, gravity coring, lithological sedimentological characterisation, 210Pb dating.
Autonomous University of Barcelona, Centre of Environmental Studies	E	CEA	Quantification of biomarker lipids, carbon isotopic analyses.
Université de Liège, U.R. Argiles et Paléoclimats	Be	ULG	Field geological sampling, mineralogical analyses, geochemical analyses, analysis of thinsections.
University College London, Department of Geography, Environmental Change Research Centre	UK	UCL	Plankton monitoring and analysis, oxygen isotope analysis of biogenic silica, diatom and chrysophite analysis on sediment cores, development of transfer functions for climate reconstruction.
University of Gent, Department of Geology and Soil Science, Renard Centre of Marine Geology	Be	RUG	Geophysical site survey (seismics, sub-bottom profiling and sidescan sonar) for selecting the most suitable coring sites in each of the three CONTINENT study areas.
Magyar Állami Földtani Intézet - The Geological Institute of Hungary, Budapest	U	MAFI	Heavy mineral analyses
Freie Universität Berlin, Institut für Paläontologie	G	FUB	Analysis of pollen assemblages; preparation of pollen samles for AMS 14C dating
PAS, Szafer Institute of Botany	P	PAN	Analysis of pollen assemblages

Table 2 a,b: Locations and conditions of spectro-radiometrical GER1500 field measurements in July 2001 and 2002 at Lake Baikal (CON01-4, CON02-8)

N° *2001*	Location	Date	Local time	Latitude N	Longitude E	Sky around sun	Weather and sea state
1	Central Basin	**15.07.01**	16:35	**52,6667**	**107,0000**	clear, darkening	increasing wind, waves
2	Central Basin	**16.07.01**	14:30	**52,9561**	**107,5926**	irregular cloudy	wind, waves
3	Acad. Ridge	**16.07.01**	20:05	**53,2565**	**108,1909**	diffuse overcast	little wind, calm sea
4	Continent	**17.07.01**	19:40	**53,9581**	**108,9133**	clouds, darkening	increasing wind, waves
5	North basin	**18.07.01**	09:50	**53,7878**	**108,4755**	clear, then cloud	sunny, windy, waves
6	Selenga I	**21.07.01**	08:35	**52,4614**	**106,7233**	no clouds, but diffuse	little wind, calm sea
7	Selenga II	**21.07.01**	10:10	**52,4112**	**106,4977**	no clouds, but diffuse	increasing wind, waves
8	Selenga III	**21.07.01**	11:30	**52,3751**	**106,2707**	diffuse, cloudy	increasing wind, waves
9	Selenga IV	**21.07.01**	13:45	**52,1472**	**106,0950**	irregular cloudy	increasing wind, waves
10	Posolsky	**21.07.01**	15:25	**52,0770**	**105,8557**	overcast, darkening	increasing wind, waves
11	South basin	**22.07.01**	17:20	**51,7074**	**105,0203**	diffuse, cloudy	little wind, small waves
12	South basin	**24.07.01**	15:10	**51,9233**	**105,4893**	clear, cloud at end	sunny, windy, waves

N° *2002*	Location	Date	Local time	Latitude N	Longitude E	Sky around sun	Weather and sea state
1	MOORING S	**05.07.02**	13:52	**51 42,408**	**105 01,132**	cirrus, edges in middle	calm weather short after strom front
2	MOORING N	**08.07.02**	11:15	**54 28,008**	**109 04,322**	overcast, rainy	calm, cold, misty, rainy
3	SE of N-basin	**09.07.02**	10:58	**54 14,074**	**109 01,969**	overcast	calm, cold, misty
4	SE of N-basin	**09.07.02**	13:15	**54 00,474**	**108 56,709**	overcast	calm, cold, misty
5	MOORING N	**10.07.02**	13:30	**54 26,680**	**108 59,945**	clear, then cloud	warm(20°C),sunny,calm
6	Barguzin I	**11.07.02**	15:25	**53 25,836**	**108 58,191**	clear	sunny, windy
7	Barguzin II	**11.07.02**	16:45	**53 26,079**	**108 54,621**	clear, cloud in middle	sunny, very windy
8	Barguzin III	**11.07.02**	18:00	**53 26,363**	**108 50,270**	clouds, darkening	increasing wind, waves
9	Barguzin IV	**11.07.02**	19:00	**53 25,541**	**108 45,884**	clouds, darkening	strong wind, ca. 6-7 Bft.
10	Barguzin VII	**12.07.02**	08:55	**53 18,711**	**107 51,339**	clear	sunny, little wind, calm sea
11	Barguzinskij	**12.07.02**	12:45	**53 26,074**	**108 43,238**	clear	sunny, little wind, calm sea
12	Barguzin VIII	**12.07.02**	13:30	**53 26,066**	**108 43,475**	clear, cloud in middle	sunny, warm, no wind, calm sea
13	Acad. Ridge	**12.07.02**	15:30	**53 30,045**	**108 14,902**	clear	sunny, warm, no wind, calm sea
14	North basin	**12.07.02**	19:05	**53 53,007**	**108 18,774**	clear, darkening	sunny, warm, no wind, calm sea
15	PEEPER I	**13.07.02**	12:55	**53 57,367**	**108 55,054**	overcast, drizzling	calm sea, covered sky, ligth rain
16	PEEPER II	**13.07.02**	15:10	**54 05,081**	**109 00,370**	overcast, rainy	calm sea, covered sky, ligth rain
17	Selenga N	**14.07.02**	11:10	**52 40,135**	**106 59,983**	overcast, drizzling	calm sea, overcast, drizzling
18	Posolsky	**14.07.02**	19:00	**52 04,639**	**105 51,540**	irregular overcast	wavy, cloudy
19	Selenga I	**15.07.02**	07:30	**52 11,804**	**106 10,084**	dark overcast, rainy	calm sea, rain
20	Selenga II	**15.07.02**	08:15	**52 11,139**	**106 07,011**	overcast, rainy, brightening	calm sea, rain
21	Selenga V	**15.07.02**	10:10	**52 11,028**	**105 59,041**	overcast, brightening	calm sea, overcast
22	South basin	**15.07.02**	12:40	**51 53,974**	**105 41,915**	clear, cloud at end	small waves, no wind
23	South basin	**15.07.02**	14:40	**51 46,458**	**105 22,583**	clear, then cloud	small waves, no wind

Table 3 a,b: Ground truth data sets (pigments, SPM, cDOM, DOC) in July 2001 and 2002 at Lake Baikal (CON01-4, CON02-8)

Continent Code	Optical measurement N°	Location	Latitude N	Longitude E	SPM [mg/l]	Chl-a [µg/l]	Sum Caro [mg/l]
1	1	Central Basin	**52,6667**	**107,0000**	0,5	0,90	0,45
2	2	Central Basin	**52,9561**	**107,5926**		0,60	0,27
3	3	Acad. Ridge	**53,2565**	**108,1909**		0,80	0,48
5	4	Continent	**53,9581**	**108,9133**		1,10	0,60
7	5	North basin	**53,7878**	**108,4755**	0,2	0,66	0,40
21	6	Selenga I	**52,4614**	**106,7233**	2,4	2,80	1,40
22	7	Selenga II	**52,4112**	**106,4977**	3,8	2,10	1,00
23	8	Selenga III	**52,3751**	**106,2707**	2,6	1,00	0,65
24	9	Selenga IV	**52,1472**	**106,0950**	5,1	1,30	0,78
25	10	Posolsky	**52,0770**	**105,8557**		2,60	2,40
26	11	South basin	**51,7074**	**105,0203**		3,60	2,10
27	12	South basin	**51,9233**	**105,4893**		2,40	1,70

Optical measurement N°	Location	Latitude N	Longitude E	SPM [mg/l]	acDOM (445) [1/m]	DOC [ppm] (Durham)	Chl-a [µg/l] (IGB)	Sum Caro [mg/l] (IGB)
1	MOORING S	**51 42.408**	**105 01.132**	1,1	0,18	0,22	0,90	0,45
no	Vydrino	**51 33.810**	**104 51.275**		0,21	1,98	1,00	0,70
no	Continent	**53 57.354**	**108 55.029**	1,6	0,16		0,70	0,34
2	SE of N-basin	**54 28.008**	**109 04.322**	0,6	0,21		0,60	0,27
3	SE of N-basin	**54 14.074**	**109 01.969**	0,4	0,08	< 0,1	0,71	0,35
4	SE of N-basin	**54 00.474**	**108 56.709**	0,9	0,06	< 0,1	0,70	0,30
5	MOORING N	**54 26.680**	**108 59.945**	0,3	0,08	0,57	0,67	0,27
6	Barguzin I	**53 25.836**	**108 58.191**	3,9	3,79	4,71	2,30	0,70
7	Barguzin II	**53 26.079**	**108 54.621**		0,70	1,40	2,10	0,90
8	Barguzin III	**53 26.363**	**108 50.270**	1,3	0,72	0,55	1,90	1,00
9	Barguzin IV	**53 25.541**	**108 45.884**	0,8	0,35		2,10	1,20
no	Barguzin V	**53 23.919**	**108 30.425**		0,22		2,30	1,90
no	Barguzin VI	**53 21.865**	**108 16.583**	0,8	0,13		0,70	0,40
10	Barguzin VII	**53 18.711**	**107 51.339**		0,04		1,40	0,90
13	Acad. Ridge	**53 30.045**	**108 14.902**		0,16	< 0,1	1,60	1,10
14	North basin	**53 53.007**	**108 18.774**	1,4	0,04	< 0,1	1,8	1,17
16	PEEPER II	**54 05.081**	**109 00.370**	0,3	0,13		0,56	0,25
17	Selenga N	**52 40.135**	**106 59.983**	1	0,60	0,76	3,40	2,5
18	Posolsky	**52 04.639**	**105 51.540**		0,30	9,26	1,50	1,00
19	Selenga I	**52 11.804**	**106 10.084**	1,1			2,60	1,20
20	Selenga II	**52 11.139**	**106 07.011**	0,6			2,80	1,90
21	Selenga III	**52 11.028**	**105 59.041**	0,7			2,30	1,70
22	Selenga V	**52 11.028**	**105 59.041**			2,00		

Table.4 a: Mean pigment concentrations, averaged over 30 m depth (Chl-*a*, sum of carotenoids and carotenoid/ Chl-*a* ratio), and contribution of the dominant phytoplankton groups to total Chl-*a* in July 2001 at Lake Baikal [pers., Fietz, IGB, Germany].

Location	**Code**	**N°**	**Lat**	**Long**	**Chl-*a****	**Caro***	**Caro/Chl-*a***	**Chl-*a* contribution***
Mooring North	5	1	**53.7878**	**108.4755**	0.66	0.40	0.61	Diatoms, (crypto)
Continent	4	2	**53.9581**	**108.9133**	1.10	0.60	0.55	Diatoms, (crypto)
Acad. Ridge	3	3	**53.2565**	**108.1909**	0.80	0.48	0.60	Diatoms, (crypto)
Central Basin	2	4	**52.9561**	**107.5926**	0.60	0.27	0.45	Diatoms, (crypto)
N' Selenga	1	5	**52.6667**	**107.0000**	0.90	0.45	0.50	Diatoms, (pico)
Selenga I	6	6	**52.4614**	**106.7233**	2.80	1.40	0.50	Pico, (diatoms, crypto)
Selenga II	7	7	**52.4112**	**106.4977**	2.10	1.00	0.48	Pico, (diatoms, green, crypto)
Selenga III	8	8	**52.3751**	**106.2707**	1.00	0.65	0.65	Pico, (diatoms, green)
Selenga IV	9	9	**52.1472**	**106.0950**	1.30	0.78	0.60	Pico, (green, crypto)
Posolsky	10	10	**52.0770**	**105.8557**	2.60	2.40	0.92	Pico, (diatoms, green)
South basin	12	11	**51.9233**	**105.4893**	2.40	1.70	0.71	Pico, (diatoms)
South basin	11	12	**51.7074**	**105.0203**	3.60	2.10	0.58	Pico,

chloro = chlorophyta, crypto = cryptophyta, diatoms, green = green algal, pico = cyanobacterial picoplankton

Table 4 b: Mean pigment concentrations, averaged over 30 m depth (Chl-*a*, sum of carotenoids and carotenoid/ Chl-*a* ratio), and contribution of the dominant phytoplankton groups to total Chl-*a* in July 2002 at Lake Baikal [pers., Fietz, IGB, Germany].

Location	**Code**	**N°**	**Lat**	**Long**	**Chl-*a****	**Caro***	**Caro/Chl-*a***	**Chl-*a* contribution***
Mooring North	5	1	**54.44467**	**108.8517**	0.67	0.27	**0.40**	Diatoms
N' Basin	2	2	**54.08351**	**109.0044**	0.6	0.27	**0.45**	Diatoms, crypto
N' Basin	3	3	**54.23457**	**109.0184**	0.71	0.35	**0.49**	Diatoms, crypto
N' Basin	16	4	**54.08493**	**109.0044**	0.56	0.25	**0.45**	Diatoms, crypto
N' Basin	4	5	**54.0075**	**108.9446**	0.7	0.3	**0.43**	Diatoms, crypto
Continent		6	**53.9547**	**108.9156**	0.7	0.34	**0.49**	Crypto, chloro, diatoms
N' Basin	14	7	**53.88703**	**108.3179**	1.8	1.17	**0.65**	Diatoms
Acad. Ridge	13	8	**53.50076**	**108.2484**	1.6	1.1	**0.69**	Diatoms, (crypto)
B1	6	9	**53.4306**	**108.9685**	2.3	0.7	**0.30**	Mixed
B2	7	10	**53.43452**	**108.9104**	2.1	0.9	**0.43**	Mixed
B3	8	11	**53.43938**	**108.8378**	1.9	1	**0.53**	Diatoms, pico
B4	9	12	**53.42568**	**108.7147**	2.1	1.2	**0.57**	Diatoms, pico
B5		13	**53.38507**	**108.5074**	2.3	1.9	**0.83**	Diatoms, pico
B6		14	**53.36277**	**108.2595**	0.7	0.4	**0.57**	Crypto, pico
B7	10	15	**53.31302**	**107.8561**	1.4	0.9	**0.64**	Crypto, pico
N' Selenga	17	16	**52.6649**	**107.0001**	3.4	2.5	**0.74**	Pico, diatoms
S1	20	17	**52.19673**	**106.1681**	2.6	1.2	**0.46**	Pico, diatoms
S1	21	18	**52.19418**	**106.119**	2.8	1.9	**0.68**	Pico, diatoms
S3	22	19	**52.1838**	**105.984**	2.3	1.7	**0.74**	Pico, diatoms
Posolsky	19	21	**52.07732**	**105.859**	1.5	1	**0.67**	Pico, diatoms
Mooring South	1	20	**51.70735**	**105.0194**	0.9	0.45	**0.50**	Chloro, green, diatoms
Vydrino		22	**51.5635**	**104.8543**	1	0.7	**0.70**	Diatoms, chloro

chloro = chlorophyta, crypto = cryptophyta, diatoms, green = green algal, pico = cyanobacterial picoplankton

Table 5: Comparison of in-situ Chl-*a* [pers., Fietz, IGB, Germany] in July 2001 to calculated SeaWiFS OC2 Chl-*a* from a wider range of time-near acquisition dates. Note that the shades of grey indicate spectral influence of terrigenous input (Case 2 waters)–the darker, the more intense.

HPLC	6/30	7/2	7/4	7/16	7/18	7/19	7/21	7/26
0,66		0,85			0,84	0,81	0,83	
1,10		0,96			0,96	0,72	0,99	
0,80		0,72	0,73	1,01	0,80	0,75	1,14	1,11
0,60	0,87		0,70			0,83	0,96	
0,90	0,90		0,96	1,68		1,20	2,22	2,28
2,80	3,07		4,30	3,98		4,25	14,98	12,67

HPLC	6/30	7/2	7/4	7/16	7/18	7/19	7/21	7/26
2,10	3,85	3,98	5,18	3,75		5,80		9,76
1,00	3,14			3,73		4,80		3,93
1,30	2,40			4,45	1,99	4,30		4,66
2,60		0,85	0,84	1,86	1,28	3,51		4,09
2,40	0,84		0,72	1,08	1,16	2,02		2,87
3,60	0,83	0,87	0,80	1,15	1,21	1,71		2,77

Table 6 a,b : Comparison of in-situ Chl-*a* [pers., Fietz, IGB, Germany] in July 2001 to calculated SeaWiFS OC2 and OC4 Chl-a from the five time-nearest selected dates. Note that the shades of grey indicate spectral influence of terrigenous input (Case 2 waters).

	OC2 Chl-*a*							HPLC	Date	Δ Chl-*a*	Δ Chl-*a*
N°	7/16	7/18	7/19	7/21	7/26	16-26	Date				%
1		0,84	0,81	0,83		0,84	**7/18**	0,66	7/18	0,18	27,3
2		0,96	0,72	0,99		0,96	**7/18**	1,10	7/17	-0,14	-12,7
3	1,01	0,80	0,75	1,14	1,11			0,80	7/16		
4			0,83	0,96		0,83	**7/19**	0,60	7/16	0,23	39,0
5	1,68		1,20	2,22	2,28			0,90	7/15		
6	3,98		4,25	14,98	12,67			2,80	7/21		
7	3,75		5,80		9,76			2,10	7/21		
8	3,73		4,80		3,93			1,00	7/21		
9	4,45	1,99	4,30		4,66			1,30	7/21		
10	1,86	1,28	3,51		4,09			2,60	7/21		
11	1,08	1,16	2,02		2,87	2,87	**7/26**	2,40	7/24	0,47	19,5
12	1,15	1,21	1,71		2,77	2,77	**7/26**	3,60	7/22	-0,83	-23,0

	OC4 Chl-*a*							HPLC	Date	Δ Chl-*a*	Δ Chl-*a*
N°	7/16	7/18	7/19	7/21	7/26	16-26	Date				%
1		0,79	0,83	0,86		0,79	**7/18**	0,66	7/18	0,13	19,0
2		1,01	0,73	1,04		1,01	**7/18**	1,10	7/17	-0,09	-8,3
3	1,06	0,83	0,77	1,22	1,19			0,80	7/16		
4			0,86	1,01		0,86	**7/19**	0,60	7/16	0,26	43,6
5	1,82		1,31	2,52	1,70			0,90	7/15		
6	4,04		3,61	11,20	10,78			2,80	7/21		
7	3,45		5,21		7,66			2,10	7/21		
8	4,34		4,82		3,49			1,00	7/21		
9	4,69	2,28	4,28		3,86			1,30	7/21		
10	1,82	1,22	2,79		3,31			2,60	7/21		
11	1,15	0,98	1,80		2,50	2,50	**7/26**	2,40	7/24	0,10	4,0
12	1,25	1,33	1,71		2,36	2,36	**7/26**	3,60	7/22	-1,24	-34,3

Table 7 a,b : Comparison of in-situ Chl-*a* (HPLC) in July 2002 to calculated SeaWiFS OC2 and OC4 Chl-*a* from the five time-nearest selected dates.

N°	OC2 Chl-*a* 7/2	7/12	7/13	7/20	02-13	Date	HPLC	Date	Δ Chl-*a*	Δ Chl-*a* %
1		0,70		0,72	0,70	**7/12**	0,67	**7/8**	0,03	4,9
2		0,75		0,74	0,75	**7/12**	0,6	**7/8**	0,15	25,3
3		0,67		0,77	0,67	**7/12**	0,71	**7/9**	-0,04	-5,0
4		0,75		0,74	0,75	**7/12**	0,56	**7/13**	0,19	34,3
5		0,72		0,84	0,72	**7/12**	0,7	**7/9**	0,02	2,9
6		0,71		0,98	0,71	**7/12**	0,7	**7/9**	0,01	1,1
7							1,8	**7/12**		
8		1,51	1,39	1,71	1,45	**mean**	1,6	**7/12**	-0,15	-9,2
9							2,3	**7/11**		
10			2,91	1,99	2,91		2,1	**7/11**	0,81	38,3
11		2,19	2,54	1,93	2,36	**mean**	1,9	**7/11**	0,46	24,5
12		1,96	2,01	1,48	1,99	**mean**	2,1	**7/11**	-0,11	-5,4
13		1,96		1,79	1,96	**7/12**	2,3	**7/11**	-0,34	-14,6
14			0,88	1,25	0,88	**7/13**	0,7	**7/11**	0,18	25,2
15				1,27			1,4	**7/12**		
16			1,67		1,67	**7/13**	3,4	**7/14**	-1,73	-50,7
17	2,46				2,46	**7/13**	2,6	**7/15**	-0,14	-5,5
18	2,90				2,90	**7/13**	2,8	**7/15**	0,10	3,6
19				1,35			2,3	**7/15**		
20	0,99			1,30	0,99	**7/13**	1,5	**7/14**	-0,51	-34,0
21	0,81			1,43	0,81	**7/2**	0,9	**7/5**	-0,09	-9,6
22	1,30			1,57	1,30	**7/13**	1	**7/15**	0,30	30,5

N°	OC4 Chl-*a* 7/2	7/12	7/13	7/20	02-13	Date	HPLC	Date	Δ Chl-*a*	Δ Chl-*a* %
1		0,72		0,70	0,72	**7/12**	0,67	**7/8**	0,05	6,8
2		0,77		0,76	0,77	**7/12**	0,6	**7/8**	0,17	28,2
3		0,68		0,76	0,68	**7/12**	0,71	**7/9**	-0,03	-3,5
4		0,77		0,76	0,77	**7/12**	0,56	**7/13**	0,21	37,3
5		0,73		0,87	0,73	**7/12**	0,7	**7/9**	0,03	4,9
6		0,72		1,04	0,72	**7/12**	0,7	**7/9**	0,02	2,9
7							1,8	**7/12**		
8		1,75	1,45	1,97	1,60	**mean**	1,6	**7/12**	0,00	0,0
9							2,3	**7/11**		
10			3,16	2,24	3,16		2,1	**7/11**	1,06	50,6
11		2,59	2,80	2,21	2,69	**mean**	1,9	**7/11**	0,79	41,8
12		2,43	2,14	1,70	2,28	**mean**	2,1	**7/11**	0,18	8,7
13		2,21		1,97	2,21	**7/12**	2,3	**7/11**	-0,09	-3,8
14			0,91	1,25	0,91	**7/13**	0,7	**7/11**	0,21	30,0
15				1,25			1,4	**7/12**		
16			1,78		1,78	**7/13**	3,4	**7/14**	-1,62	-47,7
17	2,60				2,60	**7/13**	2,6	**7/15**	0,00	0,0
18	3,45				3,45	**7/13**	2,8	**7/15**	0,65	23,3
19				1,21			2,3	**7/15**		
20	1,05			1,16	1,05	**7/13**	1,5	**7/14**	-0,45	-30,3
21	0,84			1,42	0,84	**7/2**	0,9	**7/5**	-0,06	-6,9
22	1,37			1,63	1,37	**7/13**	1	**7/15**	0,37	37,0

ANNEX B

BAIKAL WEB GIS

U.S. Geological Survey (USGS) stratigraphical map layers were reconstructed into a lithostratigraphical map in accordance with geological maps of the area [*Jansin et al.*, 1989; *Kalinin and Moiseeva*, 1981; *Mac et al.*, 2001].

Table 8: Description of the layer 'Lithostratigraphy of the Lake Baikal Catchment Area'

Lithological Assemblages	Lithostratigraphical Attribution Groups	Description
Sedimentary rocks	'Quaternary', 'Palaeogene/Neogene' 'Late Jurassic and Cretaceous' 'Permo-Triassic and Jurassic' 'Lower Palaeozoic'	Alluvial, lacustrine and glacio-fluvial sediments Clays, sands, conglomerates Clays with coals Sandstones, conglomerates, clays with coals, volcanoclastics Quartzose sandstones, quartzites, shales, and dolomites.
Volvano-clastica and volcanics	'Late Jurassic and Cretaceous' 'Permo-Triassic and Jurassic' 'Cenozoic extrusive rocks'	Both sedimentary attribution groups 'Late Jurassic and Cretaceous', and 'Permo-Triassic and Jurassic' contain a considerable proportion of volcanics and volcanoclastics. The explicitly named attribution group of 'Cenozoic extrusive rocks' represents provinces of mainly Tertiary basalts and various volcano-clastics.
Granitoid rocks	'Mesozoic intrusive rocks' 'Palaeozoic intrusive rocks' 'Archaic and Proterozoic intrusive rocks'	The Mongol-Okhotsk zone (MOZ) (first identified by Fersman [1926] as a geochemical province related to Mesozoic magmatism and mineralization) occurs as a wide belt from the Okhotsk Sea (China) into the Asian continent, and includes plutons of alkali granites and syenite in the Baikal region. Major formation was considered to take place continuously from early Permian to early Triassic. The Devonian to Early Carboniferous Sayan- regional volcanic-plutonic belt extends from the Altay-Sayan region and Northern Mongolia into Transbaikalia. All layers of intrusive rocks of the granitoid type of Precambrian (Achaen and Proterozoic) have been merged together.
Basic, ultra-basic and alkaline rocks	'Basic intrusive rocks'	Diabase, gabbro, basalt, and trachy basalts have been merged together with Proterozoic gabbroids, pyroxenites and peridotites (all stratigraphic ages).
Metamorphic rocks	'Precambrian'	Basement: Archean to Lower Proterozoic high-grade metamorphic rocks (gneiss, schistsm amphibolites, marbles)

Table 9: Areas and relative percentages of the lithology in the Selenga (SEL), Barguzin (BARG), and Upper Angara (U.AN) catchment areas.

	Quaternary	**Others (lakes, wide rivers)**	**Palaeogene/ Neogene (clays, sands, conglomerates)**	**Late Jurassic and Cretaceous (clays with coals)**	**Permo-Triassic and Jurassic (sandsto., congl., clays, volcanocl.)**	**Palaeozoic**	**Precambrian (gneiss, schists, amphibolites, marbles)**	**Mesozoic intrusive rocks**	**Palaeozoic intrusive rocks**	**Archaic and Proterozoic intrusive rocks**	**Basic intrusive rocks**	**Extrusive rocks, Pliocene and Quaternary**	***Total area: intrusive rocks***	***Toal catchment area***
SEL *[km^2]*	49959	2913	2802	12304	53434	32644	32375	22576	188711	38637	9020	4811	*249924*	***450185***
SEL *%*	**11**	**1**	**1**	**3**	**12**	**7**	**7**	**5**	**42**	**9**	**2**	**1**	***56***	
BARG *[km^2]*	6561	1					3553		445	10547	141		*10992*	***21248***
BARG *%*	**31**						**17**		**2**	**50**	**1**		***52***	
U.AN *[km^2]*	4201	43					5474		3457	9028	189		*12485*	***22391***
U.AN *%*	**19**						**24**		**15**	**40**	**1**		***56***	

Table 10: Operational Ocean Colour sensors

SENSOR	*AGENCY*	*SATELLITE*	*LAUNCH*	*RESOLUTION (m)*	*BANDS*	*SPECTRAL COVERAGE (nm)*
COCTS *http://www.ioccg.org/ sensors/cocts.html*	CNSA (China)	HaiYang-1 (China)	15/05/02	1100	10	402-12500
MERIS *http://www.ioccg.org/ sensors/meris.html*	ESA (Europe)	ENVISAT-1 (Europe)	01/03/02	300/1200	15	412-1050
MMRS *http://orbis.conae.gov.ar/sac-c/*	CONAE (Argentina)	SAC-C (Argentina)	21/11/00	175	5	480-1700
MODIS- Aqua *http://www.ioccg.org/ sensors/aqua.html*	NASA (USA)	Aqua (EOS-PM1)	04/05/02	1000	36	405-14385
MODIS-Terra *http://www.ioccg.org/ sensors/terra.html*	NASA (USA)	Terra (USA)	18/12/99	1000	36	405-14385
OCI *http://www.ioccg.org/ sensors/oci.html*	NEC (Japan)	ROCSAT-1 (Taiwan)	27/01/99	825	6	433-12500
OCM *http://www.ioccg.org/ sensors/ocm.html*	ISRO (India)	IRS-P4 (India)	26/05/99	350	8	402-885
OSMI *http://www.ioccg.org/ sensors/osmi.html*	KARI (Korea)	KOMPSAT (Korea)	20/12/99	850	6	400-900
SeaWiFS *http://www.ioccg.org/ sensors/seawifs.html*	NASA (USA)	OrbView-2 (USA)	01/08/97	1100	8	402-885

ANNEX C

GLOSSARY

absorbance The logarithm to the base 10 of the ratio of the radiant power at a given wavelength incident on a volume to the sum of the scattered and directly transmitted radiant powers; also called optical density (OD).

absorptance The fraction of the incident power at a given wavelength that is absorbed within a volume.

absorption coefficient The absorptance per unit distance in a medium, i.e., the limit of the ratio of the spectral absorptance to the distance [m^{-1}].

diffuse absorption coefficient for downwelling (upwelling) irradiance The ratio of the absorption coefficient to the mean cosine of the downward (upward) radiance.

specific absorption coefficient The absorption coefficient [m^{-1}] per unit mass of material, e.g., per unit chlorophyll *a* concentration [mg Chl-*a* m^{-3}]; in [m^2 mg Chl-*a*$^{-1}$].

albedo The ratio of plane irradiance leaving a water body to the plane irradiance incident on it; i.e., the upward irradiance to the downward irradiance just above the surface.

apparent optical property (AOP) A ratio of radiometric quantities that depends both on the IOP's and on the directional nature of the ambient light field and which is spatially and temporally stable enough to describe a water body; examples include the average cosine of the light field, the irradiance reflectance, the remote sensing reflectance, and the diffuse attenuation coefficients.

attenuation coefficient see beam attenuation coefficient and diffuse attenuation coefficient

backscattering coefficient The integral over the hemisphere of backward directions of the volume scattering function.

beam attenuation coefficient The limit of the ratio of the spectral absorptance plus spectral scatterance to the distance [m^{-1}]; equal to the sum of the absorption and scattering coefficients.

Beer's law Refers to any situation in which there is exponential attenuation of light in a specified direction.

benthos Bottom-dwelling marine organisms.

bidirectional reflection distribution function (BRDF) The ratio of the reflected radiance from a surface into a specific localized direction to the incident plane irradiance of a collimated beam in a specific direction [sr^{-1}].

biomass The amount of living matter per unit of water surface or water volume (i.e., in the water column) [kg m^{-2} or kg m^{-3}].

chlorophyll (Chl-*a*) lipophilic photosynthetic pigments occurring in phytoplankton that enable radiant energy to be converted to chemical energy in the process of photosynthesis; there are several chlorophyll pigment types with Chl-*a* the most present.

coloured dissolved organic matter (cDOM) High-molecular-weight organic compounds (humic and fluvic acids) formed from decomposition; they strongly absorb light in the short-wavelength range of the spectrum and can give water a yellowish to brownish colour at high concentrations.

cosine collector A radiant energy detector whose effective light collection area is proportional to the cosine of the angle between the incident light and the normal to the detector surface; used to measure plane irradiances.

depth

euphotic depth The depth to which significant phytoplankton photosynthesis can take place; typically taken to be the depth at which PAR falls to 1% of its value just below the surface [m].

optical depth The optical path length in the vertically downward direction.

detritus The particulate decomposition or disintegration products of plankton, including dead cells, cell fragments, fecal pellets, shells, and skeletons, and sometimes mineral particles in coastal waters.

diffuse absorption coefficient see absorption

diffuse attenuation coefficient of

downward (upward) irradiance The negative of the derivative with respect to depth of the natural logarithm of the downward (upward) plane irradiance.

downward (upward) scalar irradiance The negative of the derivative with respect to depth of the natural logarithm of the downward (upward) scalar irradiance.

diffuse scattering coefficient for downwelling (upwelling) irradiance The ratio of the scattering coefficient to the mean cosine of the downward (upward) radiance.

euphotic zone The water layer in which significant phytoplankton photosynthesis can take place; typically taken to be the layer down to which PAR falls to 1% of its value just below the sea surface.

fluorescence The inelastic scattering process in which a photon is absorbed by a molecule and shortly thereafter (10^{-11} to 10^{-8} s) another photon of greater wavelength is emitted; the emitted radiance is unpolarized.

Fresnel reflectance The fraction of radiant energy in a narrow beam that is reflected from a surface within mediums with different indexes of refraction.

gelbstoff see coloured dissolved organic matter

gilvin see coloured dissolved organic matter

inherent optical property (IOP) Any optical quantity that depends only on the properties of the water and is independent of the ambient light field; examples include the absorption coefficient, the scattering coefficient, and the beam attenuation coefficient; apparent optical properties become inherent optical properties if the radiance distribution is asymptotic.

intensity The radiant power in a given direction per unit solid angle per unit wavelength interval [W sr^{-1} nm^{-1}].

inverse problems A general classification for problems in which (ir)radiance measurements are used to infer inherent optical properties.

irradiance The radiant power per unit area per unit wavelength interval [W m^{-2} nm^{-1}].

> **downward** see downward plane irradiance
>
> **downward (upward) plane** The downward (upward) directed radiant power per unit area onto an upward (downward) facing horizontal surface [W m^{-2} nm^{-1}].
>
> **downward (upward) scalar** The downward (upward) directed radiant power per unit area onto a spherical collecting surface [W m^{-2} nm^{-1}].
>
> **ratio** The ratio of the upward plane irradiance to the downward plane irradiance.
>
> **reflectance** see irradiance ratio
>
> **scalar** The power per unit area incident from all directions onto a spherical collecting surface [W m^{-2} nm^{-1}]; it equals the downward scalar irradiance plus the upward scalar irradiance.
>
> **upward** see upward plane irradiance

Jerlov water type see water

K see diffuse attenuation coefficient

Lambertian surface A surface for which radiance is reflected or emitted equally in all directions over the hemisphere.

Mie scattering see scattering

nadir angle The angle between a given light ray and the downward vertical direction.

Ocean Colour A generic term referring to the spectral dependence of the radiance leaving a water body.

Ocean Colour sensor Any instrument for sensing of ocean colour, usually from aircraft or satellites.

optical density see absorbance

optical depth see depth

optical path length The integral of the dimensionless product of the beam attenuation coefficient [m^{-1}] multiplied by an infinitesimal unit of distance [m] along the direction of travel.

package effect The discrepancy between the spectral absorption coefficient of a particle suspension, consisting of a spatially nonuniform distribution of pigment molecules in cells, and the corresponding coefficient of a homogeneous solution containing the same amount of pigment.

PAR see photosynthetically available radiation

pelagic see water

phase function Describes the angular distribution of scattered radiation, as given by the ratio of the volume scattering function to the scattering coefficient [sr^{-1}]; the integral of the phase function over all directions is unity.

photoinhibition The decrease in photosynthetic rate with increasing irradiance that is caused by surpassing the photosynthetic capacity.

photosynthesis The manufacture of carbohydrates from carbon dioxide and water in the presence of chlorophyll, by utilizing radiant energy and releasing oxygen; the chemical change induced in chlorophyll by the absorption of a quantum of radiant energy.

photosynthetically available radiation (PAR) The integral over visible wavelengths (350-700 nm or sometimes 400-700 nm) of the number of photons available for photosynthesis [photons s^{-1} m^{-2}]; it can be computed by integrating the spectrally-dependent scalar irradiance divided by the photon energy at each wavelength.

photosynthetic pigment Molecules whose structures efficiently absorb light within the 400-700 nm range.

photosynthetic capacity The maximum photosynthetic rate per unit of biomass.

photosynthetic rate

> **gross** The total rate of carbon dioxide fixation with no allowance for the CO_2 simultaneously lost in respiration [e.g., in μmoles CO_2 (mg Chl-*a*)$^{-1}$ h^{-1} or mg C (carbon) (mg Chl-*a*)$^{-1}h^{-1}$].
>
> **net** The total rate of photosynthetic CO_2 fixation minus the rate of loss of CO_2 in respiration.
>
> **specific** Photosynthetic rate, net or gross, per unit biomass or per unit volume [e.g., μmoles CO_2 (mg Chl-*a*)$^{-1}$ h^{-1}].

phytoplankton see plankton

plankton Passively drifting or weakly swimming organisms.

> **plankton bloom** An unusually high concentration of phytoplankton.
>
> **phytoplankton** Plant forms of plankton, generally with sizes from less than 1 to several hundred μm.
>
> **zooplankton** Animal forms of plankton.

primary production The amount of organic matter produced from inorganic matter by photosynthesis, e.g., in [g C (Carbon) m^{-3}] or, for a water column, in [g C (Carbon) m^{-2}].

primary productivity The rate of production of organic matter from inorganic matter by photosynthesis, e.g., in [g C (Carbon) m^{-3} h^{-1}] or, for a water column, in [g C (Carbon) m^{-2} h^{-1}].

radiance The radiant power in a beam per unit solid angle per unit area perpendicular to the beam per unit wavelength interval [W m^{-2} sr^{-1} nm^{-1}].

radiative transfer equation The linear integrodifferential equation that describes the rate of change with distance of the radiance in a collimated beam at a specified location, direction, and wavelength; the equation accounts for all losses (e.g., due to absorption and scattering out of the beam) and gains (e.g., by emission or scattering into the beam).

radiometer An instrument used to measure radiant energy.

Raman scattering see scattering

Rayleigh scattering see scattering

reflectance

Fresnel see Fresnel reflectance

irradiance see irradiance ratio

remote sensing see remote sensing reflectance

refraction The change in direction of a photon when crossing an interface between two media that have different real indices of refraction.

refractive index The complex number for which the real part (typically about 1.34 for seawater and about 1.33 for fresh water) governs scattering at interfaces and the imaginary part governs absorption; the real part is the ratio of the velocity of light in vacuum to the phase velocity in the medium.

remote sensing reflectance The ratio of the water-leaving radiance in air to the downward plane irradiance incident onto the sea surface.

scatterance The fraction of the incident power at a prescribed wavelength that is scattered within a volume.

scattering

albedo see albedo for single scattering

angle The angle between the directions of the incident and scattered photons.

back Scattering through angles greater than 90°; see backscattering

coefficient The limit of the ratio of the incident power at a prescribed wavelength that is scattered within a small volume to the distance [m^{-1}].

Mie The exact solution for scattering of electromagnetic waves by homogeneous spheres of any size; the computations require knowledge of the complex index of refraction of the sphere relative to the surrounding medium and the ratio of the sphere circumference to the wavelength of the radiation.

Mie size parameter The ratio of a sphere's circumference to the wavelength.

Raman scattering Inelastic photon scattering in which the energy of the scattered photon equals the energy of the incident photon plus or minus energy determined by the vibrational and rotational frequencies of the molecule; it is characterized by a volume scattering function that has forward-backward directional symmetry.

Rayleigh scattering A mathematical model that describes scattering off very small particles (e.g., molecules); it is characterized by a volume scattering function that depends inversely with the fourth power of the wavelength and has forward-backward directional symmetry.

Secchi depth The depth at which a Secchi disk disappears from view as it is lowered in water [m].

Secchi disk A white disk of diameter 20-30 cm, used as a qualitative way of measuring water clarity.

Snell's law The law that describes the refraction of light at an interface between two media that have different real indices of refraction.

specific absorption coefficient see absorption

spectral Adjective used to denote either wavelength dependence or a radiometric quantity per unit wavelength interval.

spectroradiometer A radiometer that measures radiant energy as a function of wavelength.

two-flow equations The two coupled differential equations for irradiances obtained by integrating the radiative transfer equation over the hemispheres of downward and upward directions.

visible wavelengths Approximately 400 to 700 nm.

volume scattering function The ratio of the scattered intensity [W sr^{-1}] to the incident irradiance [W m^{-2}] per unit volume [m^3], given in [m^{-1} sr^{-1}]; the integral of the volume scattering function over all directions and all final wavelengths is the scattering coefficient so the VSF can be written as the product of the phase function [sr^{-1}] and the scattering coefficient [m^{-1}].

water

case 1 type Water whose optical properties are determined primarily by phytoplankton and co-varying cDOM and detritus.

case 2 type Water whose optical properties are significantly influenced by cDOM, detritus, minerogenic SPM, bubbles, or other substances whose concentrations do not co-vary with the phytoplankton concentration; not a synonym for coastal waters.

coastal Shallow water generally situated over continental shelves; often, but not always, case 2 waters.

eutrophic Waters with high phytoplankton biomass; Chl-*a* concentrations exceed 8 μg l^{-1}.

Jerlov type A water clarity classification scheme based on the downward diffuse attenuation coefficient just below the sea surface; the types are numbered I, IA, IB, II and III (ranging from clear to turbid pelagic waters) and 1 through 9 (ranging from clear to turbid coastal waters).

mesotrophic Waters with moderate concentrations of phytoplankton biomass; Chl-*a* concentrations range between approximately 3 to 8 μg l^{-1}.

oligotrophic Waters with low phytoplankton biomass, typical in many pelagic regions; Chl-*a* concentrations are below 4 μg l^{-1}.

pelagic Water seaward of the coasts; often, but not always, case 1 waters.

poly- to hypertrophic Waters with highest phytoplankton biomass; Chl-*a* concentrations exceed 50 μg l^{-1}.

ultra-oligotrophic Waters with lowest concentrations of phytoplankton biomass, Chl-*a* concentrations are below 1 μg l^{-1}.

yellow substance see coloured dissolved organic matter

zenith angle The angle between a given light ray and the upward direction.

zooplankton see plankton